DEVELOPMENT OF AN L-, C-, AND X-BAND RADAR FOR BACKSCATTERING STUDIES OVER VEGETATION

G. Lance Lockhart

Radar Systems and Remote Sensing Laboratory
Department of Electrical Engineering and Computer Science, University of Kansas
2291 Irving Hill Road, Lawrence, Kansas 66045-2969
TEL: 913/864-4835 * FAX: 913/864-7789 * E-MAIL: graham@ardneh.rsl.ukans.edu

RSL Technical Report 10290-1 and 10480-2

February 1995

Sponsored by:

NASA Headquarters, Washington DC 20546
Grant NGT-51021 (10290)

NASA Goddard Space Flight Center, Greenbelt MD 20771
Grant NAG 5-2344 (10480)

Table of Contents

Table of Contents (continued)

Table of Contents (continued)

List of Figures

List of Figures (continued)

List of Tables

Abstract

With the recent surge of interest in global change, the impact of different ecosystems on the Earth's carbon budget has become the focus of many scientific studies. Studies have been launched by NASA and other agencies to address this issue. One such study is the Boreal Ecosystem-Atmosphere Study (BOREAS). BOREAS focuses on the boreal ecosystem in Northern Canada.

As a part of the BOREAS study, we have developed a helicopter-borne three-band radar system for measuring the scattering coefficient of various stands within the boreal forest. During the summer of 1994 the radar was used at the southern study area (SSA) in Saskatchewan over the young jack pine (YJP), old jack pine (OJP), old black spruce (OBS) and old aspen (OA) sites. The data collected will be used to study the interaction of microwaves with forest canopy. By making use of three different frequency bands the contribution to the backscatter from each of the layers within the canopy can be determined. Using the knowledge gained from these studies, we will develop algorithms to enable more accurate interpretation of SAR images of the boreal region.

The following report describes in detail the development of the L-, C- and X-band radar system. The first section provides background information and explains the objectives of the boreal forest experiment. The second section describes the design and implementation of the radar system. All of the subsystems of the radar are explained in this section. Next, problems that were encountered during system testing and the summer experiments are discussed. System performance and results are then presented followed by a section on conclusions and further work.

Chapter 1 - Introduction

Remote sensing is the observation of a target from a distance. Remotely sensed data are used to provide information about a target that could not otherwise be obtained or is not easily obtained by in situ measurements. The primary advantage of remote sensing over direct sensing is the ability of remote sensing instruments to provide data from large areas on the Earth's surface in a small amount of time. In fact, many instruments that are in orbit today can provide global coverage within the span of a few days [Barbour, et al., 1987]. It is this ability that has propelled remote sensing to the forefront of global change studies. Remote sensing techniques provide scientists with spatially large data sets that can be used to test hypotheses on larger scales than previously possible [Ustin, et al., 1993]. Therefore, processes on a global scale can be studied in new and more insightful ways with remotely sensed data.

The wide-spread use of remotely sensed data has also spurred a new approach to Earth science studies. Data made available by remote sensing instruments have allowed scientists to study the Earth as a system for the first time. *Earth system science* has quickly become the catch phrase used within the scientific community to describe interdisciplinary studies of the Earth as a complex system of interacting components. An example of this type of interaction is the fact that many of the greenhouse gases responsible for global warming that originate on land may end up in the ocean. Understanding of processes such as these and their impact on the global climate requires interaction between atmospheric scientists and oceanographers. NASA's Mission to Planet Earth (MTPE) is an example of the new approach being taken to Earth system studies by organizations around the world. During the next decade, NASA will launch a series of satellites known as the Earth Observing System (EOS) to study the atmosphere, oceans, cryosphere, biosphere and solid Earth [EOS AM Spacecraft, 1994]. To utilize the data sets that will be collected by these sensors, scientists must learn to understand the sensors' interactions with

the Earth's surface and algorithms must be developed based on this knowledge to provide information that is useful for global change studies.

Before scientists can understand the Earth as a system on a global scale, they must first study the interaction of the various subsystems on a regional scale. Understanding the Earth's subsystems on a regional scale can be accomplished by performing a series of relatively small-scale ecosystem-atmosphere studies at various locations on the globe. Ideally, these studies should bring researchers from a wide variety of disciplines together at a single study area for extensive data collection. Measurements taken during the experiment should be analyzed and the results should be published or presented. The ground-based data sets collected during studies such as these allow scientists to understand the ecosystem's interaction with the atmosphere. The ground-based measurements also can be used to improve existing algorithms for interpreting the remotely sensed data that are collected during the study. NASA has sponsored experiments over the past several years aimed at accomplishing these objectives. Included in these studies are the First ISLSCP Field Experiment (FIFE) and, currently, the Boreal Ecosystem-Atmosphere Study (BOREAS).

BOREAS is an intensive three-year experiment taking place at two primary study areas in Canada. The study is a cooperative effort between the United States and Canadian agencies with NASA taking the lead. The Southern Study Area (SSA) is located in Prince Albert National Park, Saskatchewan, and the Northern Study Area (NSA) is located in Thompson, Manitoba. Each of the study areas is broken down into several smaller sites on the basis of the dominant tree type. Measurements are taken throughout the year with the main data collection effort taking place during the intensive field campaigns (IFCs). The boreal zone was chosen for this study because of the forest's importance in the global carbon cycle. A study by Tans, Fung and Takahashi presents evidence of a large terrestrial sink for carbon in the North Hemisphere [Tans, et al., 1990]. The study implies that the majority of the carbon is being stored in either living tissue or in the soil [Sellers, et al., 1994]. Therefore, any temperature

increase or change in soil moisture could create changes in nutrient cycling in the soils resulting in releases of CO_2, CH_4 and other trace gases. If this release of greenhouse gases were to occur on a large enough spatial scale, the chemistry of the atmosphere would be altered and surface temperature would again increase. Once this cycle of a surface temperature increase followed by a release of trace gases into the atmosphere is set into motion, it will continue to exist until a saturation point is reached. Saturation will occur when either the soil is depleted of nutrients or the atmosphere can no longer accommodate the release of more trace gases. At this point, no further warming would occur. However, if this saturation point is reached it could have catastrophic effects on the ecosystem. Although reactions such as this have serious implications in terms of global change, the boreal ecosystem's interaction with the atmosphere is not fully understood. As a result, further study is necessary to learn more about processes within the region to gain a more complete understanding of the carbon source/sink dynamics of the forest.

An accurate determination of the net carbon flux in the boreal forest region requires the measurement of many different parameters. Two parameters that affect the carbon fluxes within the forest canopy are the moisture of the soil and the biomass present in the forest. Soil moisture is important because of its role in supporting organic activity [Schlesinger, 1991]. Furthermore, by monitoring changes in soil moisture and atmospheric chemistry we can begin to understand the importance of soil moisture fluctuations in terms of the regional carbon budget. Monitoring biomass is also important because biomass estimates provide information about how much carbon is stored within the forest canopy. Additionally, accurate predictions of photosynthetic rate require knowledge of the amount of woody biomass present in the forest [Ranson and Sun, 1994]. In other words, monitoring of woody biomass can provide better estimates of the amount of carbon being utilized by the forest.

Parameters such as soil moisture and biomass need to be known on a large scale to determine their net effect on the boreal ecosystem. Therefore, if a

suitable sensor can be found, these two parameters are ideal candidates for being monitored using remote sensing techniques. A suitable sensor is one that is sensitive to the parameter of interest, is able to collect data on large scales at proper time intervals, and is able to provide the resolution necessary to make measurements on a logical spatial scale.

Although optical sensors have been used successfully for remote sensing studies of the forest [Sellers, 1985], they have two critical drawbacks that make them less desirable than microwave sensors for monitoring soil moisture and biomass. One drawback is the optical sensor's inability to measure the soil moisture within the canopy. The optical sensor's small wavelength does not allow penetration to the forest floor. Therefore, soil moisture measurements over the forest with an optical sensor are impossible. Second, optical wavelengths cannot penetrate clouds. This severely limits the utility of optical sensors in the boreal zone where cloud cover is common throughout the year. Optical data during periods of interest may be sparse or nonexistent because of clouds. Microwave sensors and, in particular, radars are sensitive to soil moisture over the forest at longer wavelengths. Additionally, microwaves can penetrate clouds and can operate at night, lending themselves to studies of diurnal change as well as providing uninterrupted data sets from season to season regardless of weather conditions. Space-borne microwave sensors such as synthetic-aperture radar can provide resolution that is comparable to that provided by space-borne optical sensors. For example, the ERS-1 SAR provides a resolution on the order of a few meters [Attema, 1991].

Currently, the First European Remote Sensing Satellite (ERS-1), the First Japanese Earth Resources Satellite (JERS-1) and the third Shuttle Imaging Radar (SIR-C) have been deployed and have collected radar images of the boreal region. Also, in the near future, more data will become available with the launch of the Second European Remote Sensing Satellite (ERS-2) and the Canadian Radar Satellite (RADARSAT). These satellites will make a large volume of SAR data available at several different frequencies for investigations of the boreal forest regions. To make this data useful for

global change studies, the microwave remote sensing community must develop reduction algorithms that can accurately transform the SAR data to useful geophysical products. Reduction of SAR data into useful geophysical information is essentially an inverse scattering problem. Problems of this nature are inherently non-unique and prior information about the target being observed is a necessity. Inversion of radar data for extracting geophysical parameters is currently in its infancy and satisfactory inverse scattering algorithms for the forest have yet to be developed.

We have proposed solving the inverse scattering problem by utilizing a short-range radar system that measures the scattering coefficient of the forest. Radars that measure the scattering coefficient are commonly known as scatterometers. The scatterometer used should measure the scattering coefficient of the forest at the same frequency, incidence angle and polarization as the SAR it is supporting. Measurements taken by the short-range radar system can provide insight into the sources of the scattering in the forest canopy because of the high resolution and large dynamic range that can be achieved using a short-range radar system. As a result, this type of system can provide useful knowledge for interpreting SAR data. Additionally, the short-range radar can take measurements at varying incidence angles and polarizations that provide further insight into the scattering characteristics of the forest.

At The University of Kansas Radar Systems and Remote Sensing Lab (RSL), we have developed a helicopter-based L- (1.5 GHz), C- (5.5 GHz) and X-band (10 GHz) radar operating at all four linear polarizations (VV,HH,VH,HV) with the ability to sweep through multiple incidence angles. This system is ideal for determining the scattering sources within the forest canopy. Microwave radiation at L band can penetrate to the forest floor and provide information about parameters such as surface roughness and soil moisture. The SAR on board JERS-1 operates at L band. C-band radiation interacts primarily with the secondary branches and stems of the trees and is attenuated more rapidly than the L-band

radiation. This frequency band is covered by the SAR on board ERS-1. The higher frequency radiation at X band provides information about scattering from the top layers of the canopy and does not penetrate to the forest floor. This frequency is used by the X-SAR that is part of the SIR-C mission. With measurements at these three frequencies as well as different combinations of polarization and incidence angle, we can obtain a more in-depth understanding of the forest canopy's scattering characteristics. The knowledge gained from the helicopter-based radar data can then be used to interpret more accurately the data collected by the SAR.

The radar we developed is a frequency-modulated continuous-wave (FM-CW) scatterometer that is mounted on a UH-1 helicopter provided by NASA. We have chosen to use an FM-CW radar rather than a pulse radar for two reasons. First, we can transmit less peak power using an FM-CW radar because transmission is continuous in time [Roddy, 1986]. Second, although we still require the same amount of bandwidth for a given range resolution, we can dictate the modulation frequency. This allows us to slowly sweep over a large bandwidth instead of having to use fast switches to produce a narrow pulse. The primary motivation for basing the radar on a helicopter is to provide easy access to the multiple sites being studied as a part of BOREAS and to allow for collection of data from above the canopy. In addition, the low altitudes that can be flown with a helicopter help to lower the transmit power requirements of the radar. Also, flying at low altitudes reduces the area illuminated by the antennas. When the helicopter is flying lines over the forest canopy, we can obtain multiple independent samples of the scattering coefficient in a relatively short period of time. These multiple samples are needed to provide a good estimate of the mean scattering coefficient of the canopy.

In addition to the previously mentioned reasons, the helicopter is also advantageous because overflights can be coordinated easily with ground truth measurements [Ulaby, et al., 1986]. Ground truth data are used to validate the scattering models developed and eventually to test the

accuracy of the inverse scattering algorithm. During IFC-2 and IFC-3 of the BOREAS experiment, ground truth data were collected by Dr. K. Jon Ranson, Dr. Roger Lang and Dr. Narinder Chuahan in conjunction with the helicopter overflights at the old jack pine (OJP) and young jack pine (YJP) sites in the SSA. We also took ground-based radar measurements during IFC-2 to gain a better understanding of the scattering response of the forest floor. Data collected during IFC-2 and IFC-3 by the helicopter radar are currently being processed. After the data have been properly reduced to scattering coefficients, the data will be analyzed and used in the development of scattering models. The scattering models will then be used to invert radar data taken by SAR to obtain large-scale estimates of parameters useful in global change studies such as soil moisture and forest biomass.

The following report describes the design and implementation of RSL's helicopter-based twelve-channel radar system. First, a system description is given and design equations are presented. Second, a description of the radar's evolution to its current state will be given using the problems encountered during the IFCs as background. In this section the eventual remedies to all of the problems encountered are given along with theoretical explanations of the solutions. The next section quantitatively describes the system's performance and presents radar measurements taken after the system problems were eliminated. The future work section offers suggestions for improving the radar performance and describes what needs to be done to prepare the radar for future experiments. Also, the possibility of future data collection is discussed. Conclusions are then made with suggestions regarding the usefulness of the radar in future scattering studies.

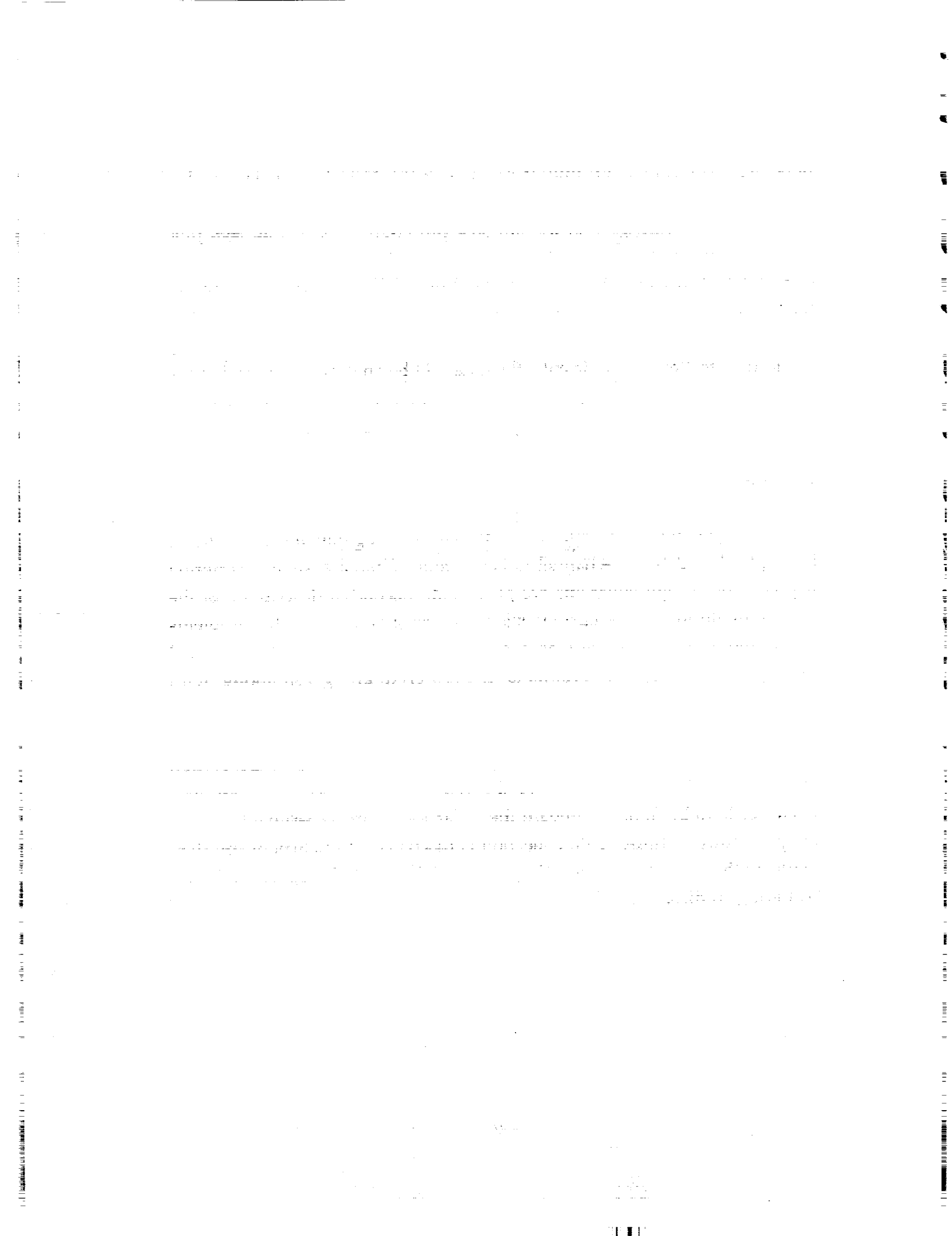

Chapter 2 - System Description

A radar can only provide information about the range to a target if it has bandwidth. Range measurement becomes more accurate as the system's bandwidth increases [Skolnik, 1980]. Bandwidth is acquired in a radar system by coding the transmit signal. Typically, a pulsed sinusoid is used as the transmit signal. For a pulsed waveform, the bandwidth increases with decreasing pulse width. The range to the target is measured by keeping track of the time between the transmission and reception of the pulse. Then, the transit time along with the velocity of propagation can be used to calculate the range to the target.

An FM-CW radar transmits a signal that is continuous in time but swept over a band of frequencies. Therefore, the beginning of the frequency sweep marks the time of transmission. The range to the target is measured by taking the difference between the return signal frequency and the transmit signal frequency. This technique of measuring range can best be understood by plotting the transmit and receive frequencies versus time (Figure 1).

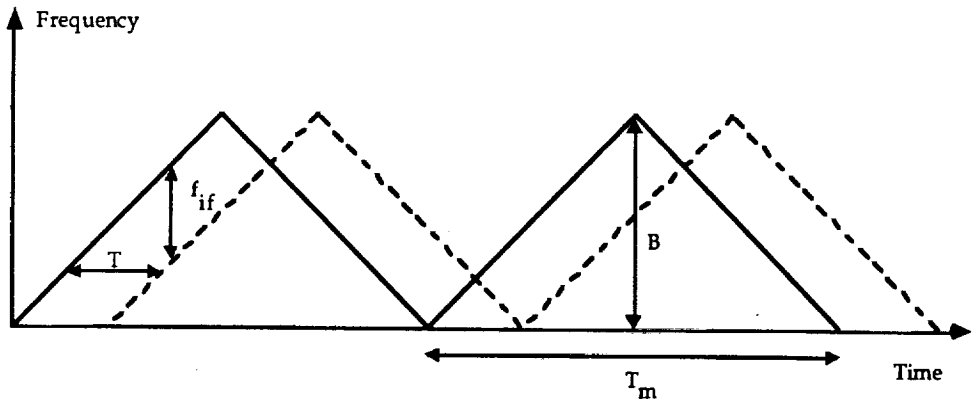

Figure 1. Transmit and Receive Frequency vs. Time for an FM-CW Radar

In this illustration, a triangle waveform is used to modulate the transmit frequency. When the radar is aimed toward a point target at a range R, the

return waveform will arrive at the receiver after a time T = 2R/c, where c is the speed of light in air. By mixing a portion of the transmit signal with the return signal, we obtain an intermediate frequency (IF) signal with a frequency f_{if}. This frequency is commonly referred to as the beat frequency. The beat frequency can be found in terms of the other FM-CW radar quantities in the following manner. Equating the slope of the modulation waveform to the change in frequency during the transit time, we obtain

$$\frac{f_{if}}{(2R/c)} = \frac{B}{(T_m/2)} \tag{2.1}$$

where B is the radio-frequency (RF) bandwidth in Hertz (Hz) and T_m is the period of the modulation waveform in seconds (s). After solving for the beat frequency, equation 2.1 becomes

$$f_{if} = \frac{4RBf_m}{c} \tag{2.2}$$

where $f_m = 1/T_m$ is the modulation frequency in Hz. From equation 2.2, we can see that the range to the target is directly proportional to the beat frequency. When multiple targets are present at different ranges, the principle of superposition can be applied to show that the return signal will consist of several different frequency components. The composition, size, and shape of the scatterers present will determine the magnitude and phase of the frequency components. Because the IF signal is the sum of several different frequency components we can take the Fourier transform to obtain a plot of the return versus frequency. Then, by converting the frequency axis to range using the system's parameters, we can acquire the return versus range.

The first step in designing an FM-CW radar is to determine the RF bandwidth, the modulation rate, the maximum unambiguous range

(R_{max}) required and the corresponding sampling frequency (f_s). The RF bandwidth dictates the range resolution (ΔR) according to the equation

$$\Delta R = \frac{c}{2B} \tag{2.3}$$

Therefore, if we want fine range resolution we must use a large RF bandwidth. However, a large RF bandwidth presents problems in terms of added system cost. We have chosen an RF bandwidth of 500 MHz for the L-, C-, and X-band sections. This provides a range resolution of .3 meters (m) in free space if the samples are uniformly weighted. Next, we consulted the helicopter crew and determined the lowest altitude that the helicopter could fly without disturbing the forest canopy. Then, we divided this number by the cosine of the largest incidence angle to obtain R_{max} = 60 m. By flying at the lowest possible altitude, we can minimize the area illuminated by the antennas, minimize spreading loss and reduce the sampling rate by lowering the bandwidth of the IF signal. The period of the modulation waveform must be large enough to allow for an acceptable sampling rate but small enough for the samples to be collected before the helicopter moves through the antenna's beamwidth. For our system, this can be achieved with a modulation frequency of 50 Hz. In this case the helicopter will move a distance of 20 cm during each sweep assuming a speed of 20 m/s. Plugging our system's parameters into equation 2.2 yields a maximum beat frequency of 20 kHz. Therefore, using the Nyquist criterion and assuming that the IF signal has been low pass filtered, we must sample at a frequency of 40 kHz. This means that during each upsweep or downsweep we will acquire

$$N = \frac{T_m}{2} f_s \tag{2.4}$$

samples of the return signal. Table 1 presents a summary of the FM-CW radar parameters used.

Parameter	Value	Units
RF Bandwidth	500	MHz
Range Resolution	30	cm
Max. IF Frequency	20	kHz
Sampling Frequency	40	kHz
Max. Unambiguous Range	60	m
Modulation Rate	50	Hz
Number of Samples for each Sweep	400	N/A

Table 1. FM-CW Radar Parameters

The signal at the output of the RF section is very small and must be amplified using an IF amplifier before it can be digitized. The exact level of the output signal from the RF section is unknown and we must estimate its value to determine the appropriate gain settings for the IF amplifier. The gain levels are determined so that they match the output voltage of the IF amplifier to the input voltage range of the A/D converter. By matching the gain settings in this manner, the system's dynamic range is maximized. We can determine the gain settings by using the radar equation to determine the power level out of the mixer and then determining the amount of gain needed to amplify this signal to the appropriate level. The radar equation relates the return power to the other radar system parameters as follows:

$$P_r = \frac{P_t G^2 \lambda^2 \sigma^o A_{ill}}{(4\Pi)^3 R^4 L_c} \qquad (2.5)$$

P_r = power received (W)
P_t = power transmitted (W)
G = antenna gain
λ = wavelength (m)
σ^o = scattering coefficient
A_{ill} = area illuminated (m^2)
R = range to target (m)
L_c = conversion loss of mixer

The minimum signal that can be digitized is equal to the input voltage range divided by the number of counts. For our case, this minimum voltage is .61 millivolts (mV). The maximum voltage for our A/D converter is 5 V.

We chose the same gain settings for C and X band for all the polarizations to eliminate the complexity of providing multiple gain settings. The L-band gain settings were chosen separately because of the larger signal level at L band. The L-band return is larger than that of C and X band because more power is transmitted, the wavelength is longer, a larger area is illuminated by the antenna and the L-band scattering coefficient is larger. The gain settings for the L-band amplifier were chosen in the following manner. The transmit power of the L-band RF portion is 13 dBm. We estimated the gain of the antenna to be 15 dB and the beamwidth of the antenna at L band to be 15°. This beamwidth yields an illuminated area of 112 m^2 (20 dB) at vertical incidence. Also, we assumed a maximum scattering coefficient value of -10 dB. Using the values λ^2 = -14 dB (λ = 20 cm) , $(4\pi)^3$ = 33 dB, R^4 = 66 dB (R = 45.72 m), and L_c = 10 dB along with the estimates of the system parameters, we find a received power of -55 dBm. When input into a 50 Ω load this results in a voltage level of -36.5 dBV. Since we want the maximum signal to be 5 V, we convert this value to a root-mean-square (rms) value and find that a 5.5 dBV signal is required at

the input of the A/D converter. Therefore, the voltage gain should be 42 dB and the current gain should be adjusted so that the amplifier can drive a 50-Ω load. To accommodate a wide range of input signal levels, we used a variable-gain amplifier with three different gain settings. This provides flexibility and allows us to adjust the radar's measurement range under varying conditions. For L band, we chose voltage gains of 20, 40 and 60 dB. Similar calculations were performed using the radar parameters at C and X band. After performing these calculations, we chose gains of 50, 70 and 90 dB for the C- and X-band IF amplifiers.

After specifying the general FM-CW radar parameters and the necessary gain levels for the IF amplifiers, we began the design and construction of the radar system. The radar system is divided into four subsystems. These are the antenna system, the RF section, the IF section and the data acquisition system. Each of the subsystems were designed, built and tested individually. Then, the entire system was integrated and tested. Figure 2 shows the interconnection of the radar's subsystems.

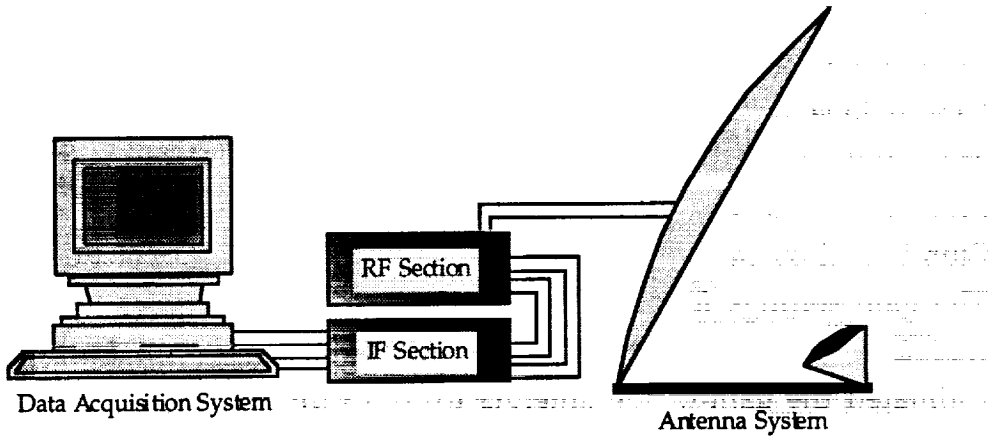

Figure 2. Radar System Block Diagram

The following sections describe the design and implementation of each of the radar's four subsystems. First, the antenna system is described. Then, the RF and IF sections are described followed by a discussion of the design of the data acquisition system.

2.1 Antenna System

The antenna used for the radar is an offset-fed parabolic reflector. In this configuration, the main reflector is fed from the focal point with the feed antenna pointing toward the center of the dish. The dish used is a cutout of a paraboloidal reflector. A paraboloidal reflector antenna was selected because of its capability to provide a high directivity. An offset feed configuration is advantageous because it eliminates aperture blockage [Balanis, 1982] and it allows us to measure backscatter at nadir without physically pointing the antenna straight down. Elimination of aperture blockage provides a higher antenna gain because scattering from the feed structure is eliminated. The latter advantage is convenient when operating from the helicopter because we can cover all incidence angles starting with nadir without lowering the antenna structure below the landing gear. The antenna system design consisted of choosing the main reflector dish, designing and fabricating the feeds and designing and building the mounting structure.

The main reflector dish for the antenna system is a satellite TV dish that is commercially available from Andersen Manufacturing Incorporated of Idaho Falls, Idaho. By using a commercially available dish we avoided the high cost of in-house design and fabrication. The dimensions of the dish that we chose are suitable for operation at C and X band. The dish diameter is 36" and the f/D ratio is .610. The manufacturer's data sheets are included in Appendix 1.

After choosing the main reflector dish, we designed three feeds to facilitate operation of the antenna at L, C and X bands. When designing a feed for a paraboloidal reflector, it is considered ideal to illuminate the reflector

uniformly over the solid angle of the aperture. If this is achieved, the taper efficiency is 100%. In addition, we would like provide a spillover efficiency of 100% by eliminating radiation from the feed that will not be intercepted by the reflector. Unfortunately, a feed that can simultaneously satisfy both of these requirements is not physically realizable. Therefore, in practical feed design, a tradeoff exists between taper and spillover efficiency. If taper efficiency is maximized then the feed pattern will radiate energy beyond the angle subtended by the reflector. Conversely, if a large amount of the feed radiation is intercepted by the reflector then the amount of radiated energy present at the reflector's edges will have decreased significantly resulting in a poor taper efficiency. Although these effects counteract each other, a point exists where optimal taper and spillover efficiency can be achieved. Typically, this occurs when the radiation from the feed at the reflector's edge is between 8 and 12 dB below that at the center [Skolnik, 1980]. We have chosen the patterns of our C- and X-band feeds using this design rule. This results in a first sidelobe level of 22 to 25 dB.

One problem that is present when using an offset-center fed parabolic reflector antenna is the high cross-polarized components that are generated. Superior cross-polar performance can be achieved by using conical horn feeds rather than pyramidal horn feeds [Rudge and Adatia, 1978]. For this reason, we decided to use conical horns as the C- and X-band feeds. We decided to provide a taper of 10 dB at the edges of the reflector. Therefore, the first step in designing these feeds is to determine the 10-dB beamwidth required. This is accomplished by using simple geometry. Figure 3 shows the geometry of the parabolic reflector antenna along with the corresponding dimensions.

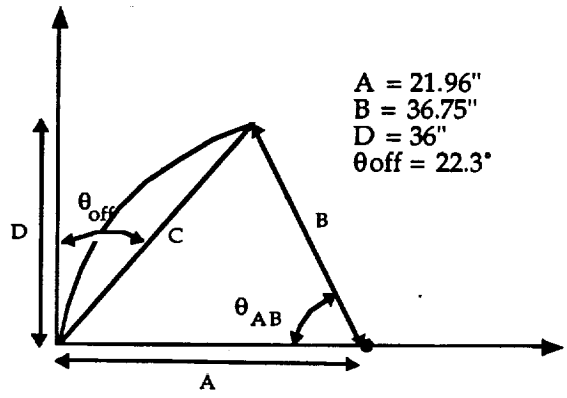

Figure 3. Geometry of the Offset-Fed Parabolic Dish

To determine the angle subtended by the reflector (θ_{AB}), we use the relation $\sin(\theta_{AB}) = D/B$. We know that B is 36.75" and D is 36". Using these values, we find $\theta_{AB} = 78.7°$. Therefore, we need to design conical horns that have a 10-dB beamwidth of approximately 78.7°.

While searching the literature, a conical horn with a 10-dB beamwidth of about 78.7° was located [Love, 1976]. The radiation pattern of the conical horn antenna from this paper is included in Appendix 1. Rather than go through the task of designing a new horn, we decided to use the design presented in the paper. Figure 4 is an illustration of the horn showing the dimensions specified in the paper.

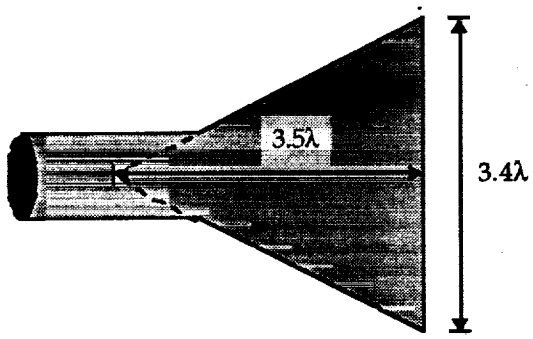

Figure 4. Dimensions of Conical Horn Antennas

After determining the dimensions of the conical horns, a section of waveguide must be designed to allow the desired frequencies to propagate. The waveguide design is accomplished as follows:

1. Choose the desired cutoff frequency for the waveguide.
2. Calculate the cutoff frequency for the next higher order mode.
3. Calculate the attenuation per meter over the desired frequency band.
4. If the attenuation is small enough over the desired band and the next mode does not begin to propagate, then the design is complete. Otherwise, steps 1 through 3 should be repeated or some bandwidth may have to be sacrificed.

The dominant mode in a circular waveguide is TE_{11}. For this mode, the cutoff frequency can be determined from the radius (a) of the waveguide [Collin, 1992] using

$$f_{c,11} = \frac{c}{3.41 \cdot a} \tag{2.6}$$

For the C-band waveguide, the cutoff frequency was initially chosen to be 4.75 GHz. This corresponds to a waveguide with a radius a = 1.85 cm. The cutoff frequency of the next higher order mode (TM_{01}) was calculated. For a radius of 1.85 cm, the cutoff frequency for the TM_{01} mode is 6.2 GHz.

Since this mode begins to propagate at a frequency very close to our desired band of 5 to 6 GHz, we decided to choose a new cutoff frequency. A cutoff frequency of 4.97 GHz (a = 1.77 cm) was chosen this time. The cutoff frequency for the next higher order mode is then 6.5 GHz. The next step is to insure that our signal will propagate in the waveguide. To determine this, we calculated the attenuation in the waveguide as a function of frequency using the equation given by Collin

$$\alpha = \frac{R_m}{a Z_0}\left[1-\frac{k_{c,11}^2}{k_0^2 a^2}\right]^{-1/2}\left[\frac{k_{c,11}^2}{k_0^2 a^2}+\frac{n^2}{\left(p'_{11}\right)^2-n^2}\right] \quad (2.7)$$

$$R_m = \left(\frac{\omega\mu}{\sigma}\right)^{1/2}$$

$\omega = 2\pi f$

μ = permeability of the waveguide material

σ = conductivity of the waveguide material

Z_0 = impedance of free space (Ω) = 120π

a = radius of the waveguide

$k_{c,11} = p'_{11}/a$

$p'_{11} = 3.832$

$k_0 = \omega(\mu_0\varepsilon_0)^{1/2}$

ε_0 = permittivity of free space

n = 1

We used these values along with the conductivity of aluminum (σ = $3.54*10^7$ S/m) [Cheng, 1989] in equation 2.7 to create a plot of attenuation in dB per meter versus frequency. This graph is included as Figure 5.

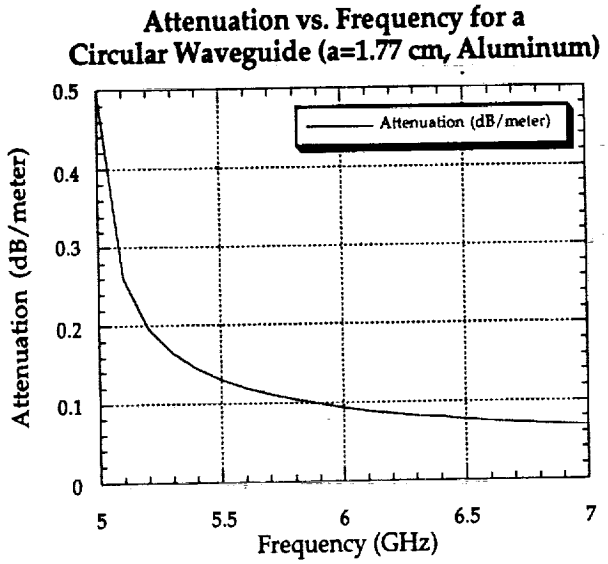

Figure 5. Attenuation versus Frequency for the C-band Waveguide

As is evident in the plot, this waveguide will allow a signal centered at 5.5 GHz with a bandwidth of 500 MHz to propagate with very little attenuation. Similar calculations were performed to determine the radius of the waveguide for the X-band horn. The radius used is a = 1 cm.

To provide the antennas with the capability to transmit and receive signals of both linear polarizations, we must excite the fields in the throat of the antenna using two separate launchers. These launchers should be orthogonal to one another and they should be positioned in a manner that provides minimal coupling between them. Therefore, the final step in the horn design is to find the dimensions of the waveguide necessary to provide appropriate spacing for the two separate launchers. Additionally, the distance between the launcher and the beginning of the flare should be large enough to provide adequate attenuation of the higher order modes that are introduced by the launchers. The center conductor of a coaxial cable is used as a launcher to excite the fields within the waveguide. The length of the center conductor determines the frequency of the wave that is produced. This length was adjusted until desirable return loss

characteristics were achieved over the bandwidth of interest. The two launchers are placed orthogonal to one another so that the antenna can transmit and receive both vertical and horizontal polarizations. The distance between the first launcher, the one that excites horizontally polarized waves, and the back plate of the waveguide is $\lambda_g/4$ so that the fields reflected from the back plate will add constructively with those produced by the launcher at its point of entry. The guide wavelength (λ_g) can be calculated using the following equation

$$\lambda_g = \frac{\lambda_o}{\sqrt{1 - f_c^2/f^2}} \quad . \tag{2.8}$$

For the C-band waveguide, the guide wavelength is 12.7 cm. A mode filter, which is simply a metal rod placed orthogonal to the horizontal launcher, is inserted at a distance $\lambda_g/4$ in front of the horizontal launcher. This mode filter attenuates any vertically polarized fields that are produced by the horizontal launcher. The rod is also used as a reflecting plate for the vertical launcher that is placed parallel to the mode filter at a distance $\lambda_g/4$. The rod performs the same function for the vertical launcher that the back plate performs for the horizontal launcher. The waveguide extends one guide wavelength past the vertical launcher to allow any higher order modes produced by the launchers to die out. Figure 6 is a drawing of the waveguide that feeds into the conical horn with the dimensions labeled in terms of guide wavelength.

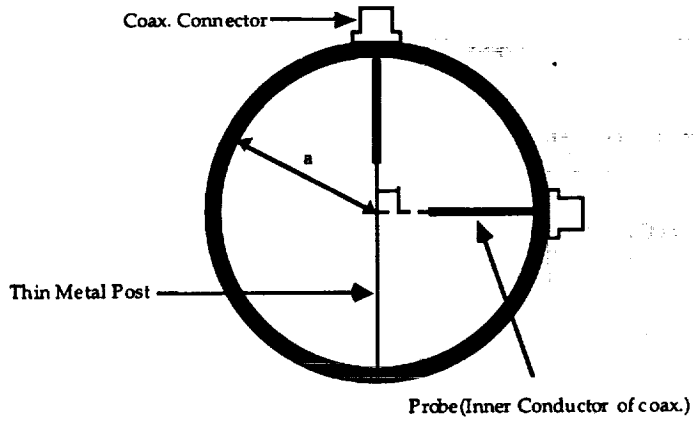

Rear View (without back plate)

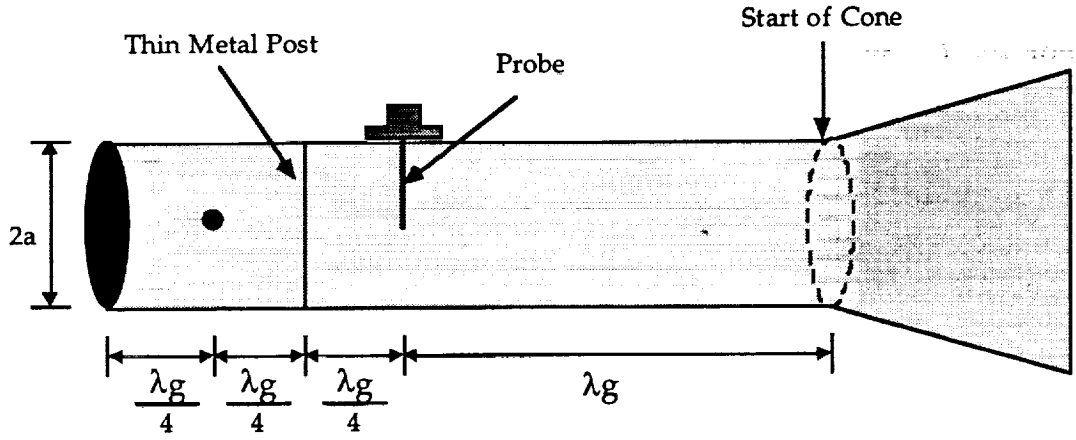

Side View

Figure 6. Drawing of Waveguide Design for Conical Horn Antennas

The dimensions were calculated for both the C- and X-band horns. Detailed calculations and the original drawings of the feeds are included in Appendix 1. The drawings of the conical horn antennas with the dimensions were taken to Nelson Machine and Tool of Lawrence, Kansas for fabrication.

Designing the feed for L band was a much harder task than we anticipated. First, we designed a conical horn that would operate at L band. However, we immediately realized that this design would not be practical for use on the helicopter because of its size. For example, the mouth of the horn would be 68 cm and the distance from the throat to the end of the horn would be 70 cm. Therefore, we were forced to sacrifice antenna performance and build the L-band feed using an open-ended rectangular waveguide. The open-ended waveguide provides a higher taper efficiency but a significantly lower spillover efficiency than the conical horn. Also, the sidelobe level will be much higher for this type of feed because of the uniform field distribution that the feed places on the surface of the reflector.

We initially specified a center frequency of 1.5 GHz with a 20% bandwidth (300 MHz) for the L-band feed antenna. We used a square waveguide to provide identical performance for both linear polarizations. For a square waveguide with sides of length a, the cutoff wavelength is given by

$$\lambda_c = \frac{2a}{\sqrt{m^2+n^2}} \tag{2.9}$$

Using equation 2.9, we can see that TE_{10} is the dominant mode for the square waveguide. The cutoff wavelength for this mode is $\lambda_c = 2a$ [Rizzi, 1988]. We used the same design procedure that was used for the C- and X-band circular waveguides to determine the dimensions of the L-band waveguide. We chose a length of a = 12 cm. The cutoff frequency for the next higher order mode (TM_{11}) is f_c = 1.77 GHz and the guide wavelength is 36.18 cm. The design calculations and drawings for the L-band feed are not included because this antenna was not used during the experiments.

The L-band waveguide antenna was fabricated by Nelson Machine and Tool in February 1994. Although the antenna was bulky, we decided to stick with our original design to save time and money. However, during

the flight test in May 1994, we were told that the L-band feed was too large for use on the helicopter. As a result, we had to redesign the L-band feed.

We decided to use a microstrip patch antenna as the new L-band feed. A microstrip antenna was chosen because it can be fabricated easily and it is lightweight. Also, the microstrip antenna provides performance characteristics similar to those of the open-ended waveguide. Microstrip antennas consist of a rectangular patch of conductor with dimensions dictated by the antenna's operating frequency. The rectangular patch is attached to the top of a dielectric substrate with a ground plane underneath as shown in figure 7.

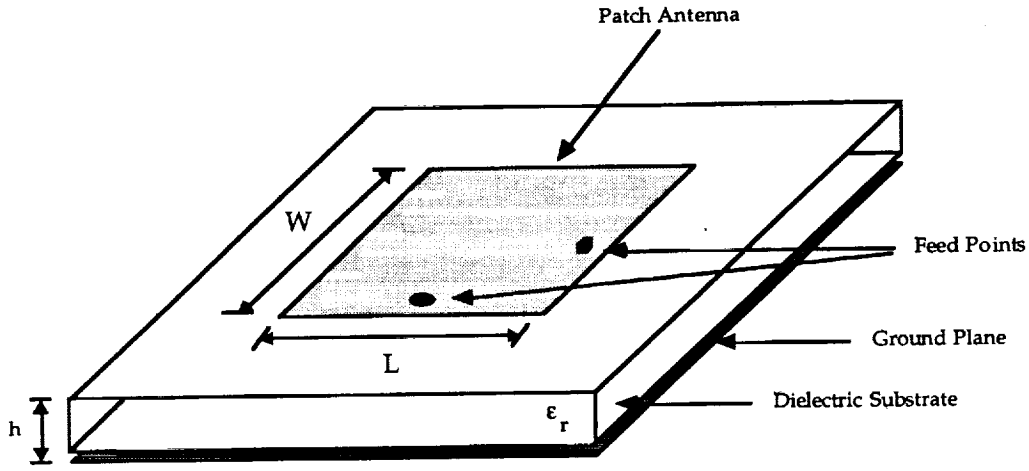

Figure 7. Geometry of the Rectangular Microstrip Antenna

The antenna is fed by inserting a coaxial probe from beneath the ground plane and soldering the end of the conductor to the patch antenna. We used two feed points as shown in figure 7 to provide dual polarization capability. Also, for identical performance at all polarizations, we used a square patch (L = W).

To find the dimensions for a rectangular microstrip patch antenna with a center frequency of 1.5 GHz and a 20% bandwidth, we used the design

procedure described in Bahl and Bhartia [Bahl and Bhartia, 1982]. The primary concern in the design of a microstrip patch is the bandwidth. Maximum bandwidth is achieved by using a thick substrate with a relative dielectric constant close to unity. We sampled a substrate (RT/5870) from Rogers Corporation of Chandler, Arizona with a thickness of 375 mils (1-mil=1/1000") and a relative dielectric constant of 2.33. Using this substrate, we can obtain a bandwidth of only 9.3%. Although this bandwidth does not satisfy the initial specifications, we sacrificed the bandwidth for the convenience of using a readily available material. The width W of the patch is calculated for a center frequency of f_r = 1.5 GHz and a relative dielectric constant of $\varepsilon_r = 2.33$ using

$$W = \frac{c}{2f_r}\left(\frac{\varepsilon_r+1}{2}\right)^{-1/2} \tag{2.10}$$

The width was found to be 3051 mils. Then, we calculated the effective dielectric constant (ε_e) using

$$\varepsilon_e = \frac{\varepsilon_r+1}{2} + \frac{\varepsilon_r-1}{2}\left(1+\frac{12h}{W}\right)^{-1/2} \tag{2.11}$$

The line extension was also calculated using

$$\frac{\Delta\ell}{h} = .412\left(\frac{(\varepsilon_e+.3)\left(W/h+.264\right)}{(\varepsilon_e-.258)\left(W/h+.8\right)}\right) \tag{2.12}$$

Next, the results from equation 2.11 and equation 2.12 were used to calculate the length L of the patch using

$$L = \frac{c}{2f_r\sqrt{\varepsilon_e}} - 2\Delta\ell \tag{2.13}$$

The length of the element was found to be 2346 mils. We wrote a MathCAD program to perform these calculations and it is included in Appendix 1.

Since we wanted the patch to be square, we used the largest of the two values as the length and width of the patch antenna. We etched the patch onto the substrate using the etching facility at the EE Shop. We tested the antenna using the Hewlett-Packard 8722C Network Analyzer by observing the return loss within the antenna's bandwidth. After testing the antenna and trying to tune it by changing the dimensions of the patch, we were unable to obtain satisfactory performance.

Therefore, after two failed attempts at designing and fabricating our own L-band feed, we decided to use two commercially available log-periodic array antennas. We mounted these antennas orthogonally to provide transmission and reception of both linear polarizations. The radiation pattern of the log-periodic antennas is down by 5 dB at the edges of the reflector. This provides a first sidelobe level of about 18 dB [Silver, 1984]. We used the log-periodic antennas during IFC-3. The log-periodic antenna specifications are included in Appendix I.

During February 1994 we designed a mounting structure to provide a rigid support for the three feeds. When the original mounting bar was designed, we were using the open-ended waveguide feed for the L-band radar. Because of the size and weight of the original L-band feed, we placed it at the center of the mounting bar. We used the original strut that was included with the reflector dish for supporting the center of the mounting bar and two additional struts to be attached to the ends of the mounting bar were built by Nelson Machine & Tool. These two struts are necessary to provide rotational stability.

We placed the L-band feed on the mounting bar so that the phase center is lined up with the focal point of the parabolic reflector at a distance of 21.96", which is the focal length of the reflector. We mounted the L-band

feed rigidly because the phase center of an open-ended waveguide remains at the center of the antenna's physical aperture regardless of a change in frequency. We designed a mounting bracket for the conical horns that allows the position of the horns' phase centers to be moved. This allows us to focus the conical horns. By focusing the conical horns, we can optimize the gain of the antenna. Figure 8 is a drawing of the mounting structure.

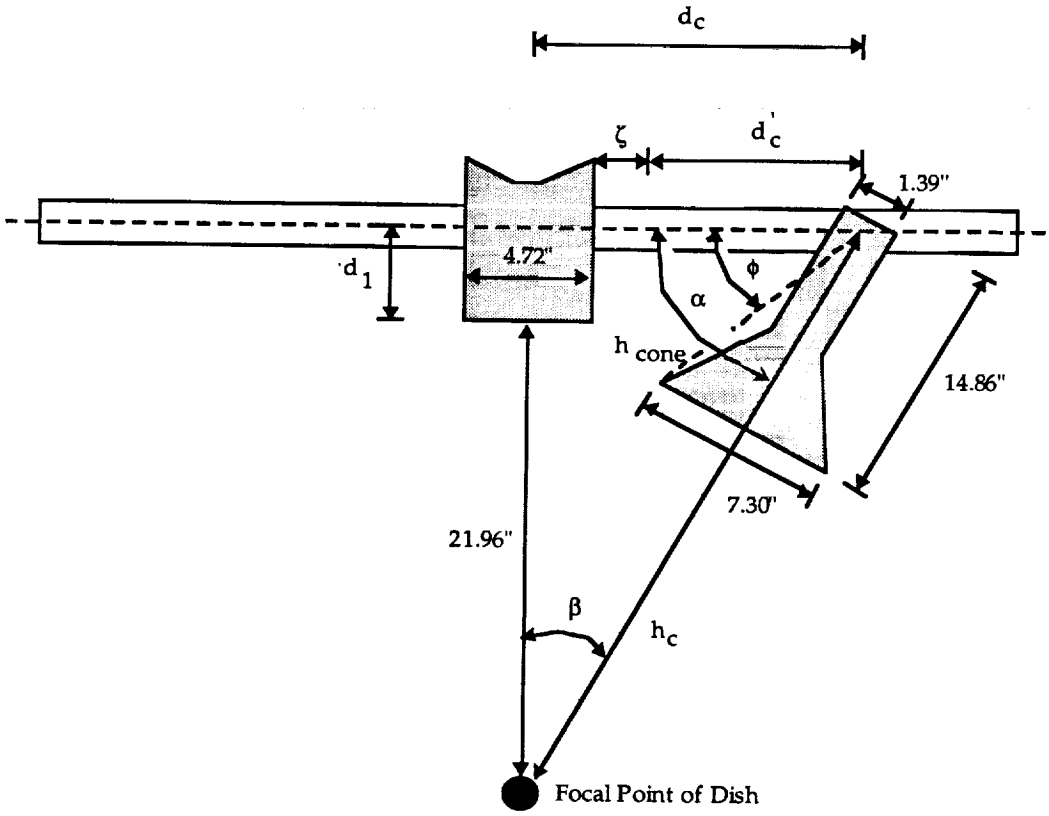

Figure 8. Geometry of the Antenna Mounting Structure

We determined the angle β such that the conical horn antennas are aimed at the focal point of the parabola. We also calculated d_c, ζ, and d_c' such that no interference exists between the C- and X-band feeds and the L-band feed. Appendix 1 includes the calculations performed to determine the dimensions of the mounting structure. After the mounting bar and struts were built, we mounted the feeds onto the supporting bar and the

positions of the conical horns were adjusted to obtain the desired antenna performance. Upon completion of the antenna system, we designed and built the L-, C-, and X-band RF sections.

2.2 RF Section

The RF section is the main subsystem of the radar. Its primary task is to transmit and receive the FM microwave signal. In the receiver, the receive signal is mixed with a portion of the transmit signal to form an IF signal. The IF signal's frequency is proportional to the range to the target. The C- and X-band RF sections are identical and Figure 9 shows a block diagram.

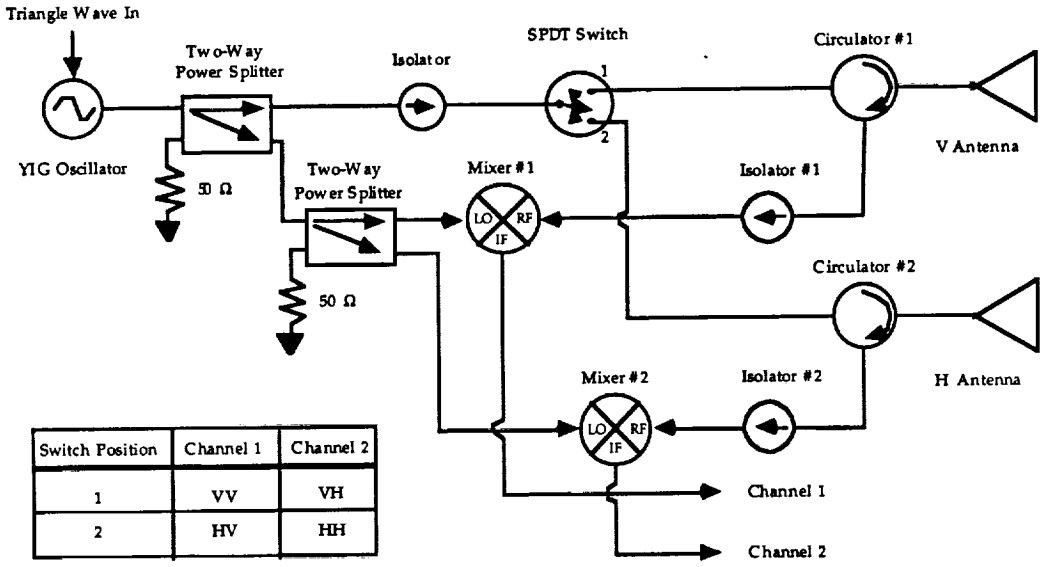

Switch Position	Channel 1	Channel 2
1	VV	VH
2	HV	HH

Figure 9. Block Diagram of RF Section for C and X Bands

We built the C- and X-band RF sections and housed them together in a Hoffman box. We used discrete components and flexible coaxial cable suitable for use at the desired frequencies for interconnecting the RF components. Yttrium-iron-garnet (YIG) oscillators are used to generate

the microwave signals. These oscillators are used because they can provide good tuning linearity over a wide bandwidth [Ulaby, et al., 1986]. The frequency of the YIG-tuned oscillator is determined by the magnetic field applied to the resonator according to the relation f = 2.8H where f is the resonant frequency in MHz and H is the field in gauss [Avantek Data Book, 1990]. The sensitivity of the oscillator is the change in frequency caused by a change in tuning current. This parameter is typically specified in units of MHz per milliamp (mA). For example, the C-band YIG oscillator that we used has a sensitivity of 15 MHz/mA. Therefore, to generate a FM waveform with a center frequency of 5.5 GHz and a bandwidth of 500 MHz, we must supply a triangular current waveform varying from 350 mA to 383.3 mA. We used an oscillator with a built in voltage-to-current converter and provided a triangular voltage waveform varying from 5.42 V to 6.25 V. The manufacturer's specifications for the C- and X-band YIGs are included in Appendix 2. We used a modulator board to generate the triangle wave. The modulator board was designed and built at RSL.

We designed the RF section in a manner that allows us to use a single antenna for both transmitting and receiving. A radar that operates in this fashion is known as monostatic. The RF section's design also allows us to collect data at two polarizations simultaneously while maintaining good polarization purity. Specifically, we have used a single-pull double-throw (SPDT) switch to determine the transmit polarization and we used circulators to isolate the transmit and receive paths. When the SPDT switch shown in Figure 9 is in position 1 the radar is transmitting a vertically-polarized signal and receiving both a vertically- and a horizontally-polarized signal. In other words, we are simultaneously measuring the VV and VH channels. Similarly, if the switch is in position 2, we are measuring the HH and HV channels.

The SPDT switches used in the C- and X-band RF sections are PIN diode switches manufactured by Narda Incorporated of Hauppauge, New York. We used these switches rather than mechanical ones to provide faster

switching times. Because these switches are built using PIN diodes they are current controlled. We designed a driver that converts a TTL control signal to the proper current levels for biasing the diodes in the switch. The design of the driver circuit is the subject of section 3.2 of this report. Appendix 2 contains the data sheet for the SPDT switches used in the radar. According to the specifications, these switches provide a minimum isolation of 55 dB in the OFF state and a maximum attenuation of 2.8 dB in the ON state.

We placed circulators before the antenna ports to enable the radar to transmit and receive signals simultaneously. Circulators are three-port devices that use ferrite technology to allow a wave incident in port 1 to be coupled into port 2 only and a wave incident in port 2 to be coupled into port 3 only, and so on. Signals can travel only in one direction so that a signal incident in port 2 will be isolated from port 1. Typical circulators have an insertion loss of less than 1 dB, isolation from 20 to 40 dB, and input reflection coefficients less than 0.2 [Collin, 1992]. We used isolators in the receive paths to prevent reflections at the mixers from being coupled to the circulators and back to the SPDT switch. Isolators also use the non-reciprocal transmission characteristics of ferrites to allow signals to travel in only one direction. Isolators can be constructed by matching one of the three ports of a circulator and the provide isolations from 20 to 40 dB.

We used a homodyne receiver in which a portion of the transmit signal is used as the local oscillator (LO) input of the mixer. We used mixers built by MITEQ, Incorporated of Hauppauge, New York that operate from 2 to 18 GHz. These are double-balanced mixers that require a LO power range of 7 to 13 dBm. The maximum specified conversion loss of the mixer is 8.5 dB for an IF frequency of 100 MHz but the conversion loss increases as the IF frequency decreases. We chose to use double-balanced mixers because they provide good isolation between the RF and LO ports, as well as between the IF and the RF and LO ports [Collin, 1992]. Double-balanced mixers also suppress the even harmonics of the RF and LO signals and therefore have

a lower level of intermodulation distortion than that of a single-balanced mixer. The data sheet for the mixers used is included in Appendix 2. The IF outputs of the mixers provide the input signal for the IF amplifiers that are discussed in section 2.3.

Ideally, we can isolate the transmit channels by 50 dB and the receive channels by 35 dB using the design shown in Figure 9. To understand how these values are determined, we must examine the paths where coupling between the channels is possible. For the transmit path, the only significant coupling that can occur is through the SPDT switch. Since this device has a typical isolation of 50 dB (see Appendix 2) at both C and X bands, we can see that if we wish to transmit a vertically-polarized signal a horizontally-polarized signal with 50 dB less power will also be transmitted. Although this seems like an insignificant amount of coupling, it may be important if the like-polarized scattering coefficient is much larger than the cross-polarized scattering coefficient. The receive channel provides less isolation than the transmit path. By examining the paths, we see that the most likely place for coupling to occur is in the path from the circulator to the isolator then to the mixer and the power splitter and, finally, to the LO port of the other channel's mixer. In the worst case, the RF to LO isolation is 20 dB and the power splitter isolation is 15 dB. This means that the worst case receive-path coupling is 20 dB + 15 dB = 35 dB.

During IFC-2 and IFC-3, a Hoffman box was used as the housing for the C- and X-band radars. A drawing of the Hoffman box that was sent to NASA Wallops is included in Appendix 2. Modifying the RF sections while they are in the Hoffman box is impractical because the box can only be opened from the top. As a result of this problem, we were unable to examine or repair the RF section during the field experiments. Therefore, after IFC-3, we repackaged the radar in a more convenient box. We designed a rack-mountable aluminum box with a sliding rack for mounting of the radar components. Figure 10 shows two views of the new RF box.

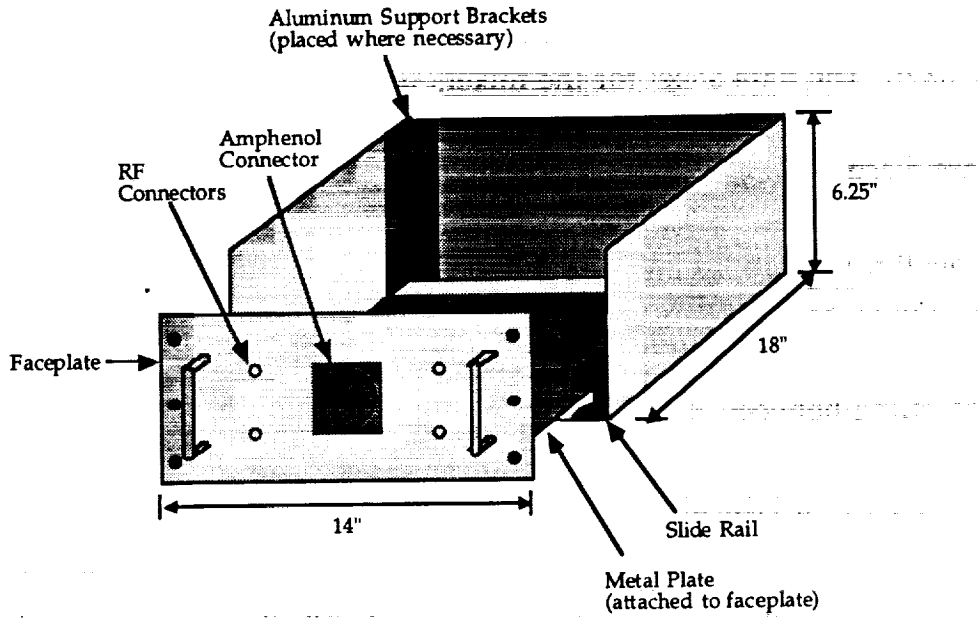

Three-Dimensional View of the Entire RF Box

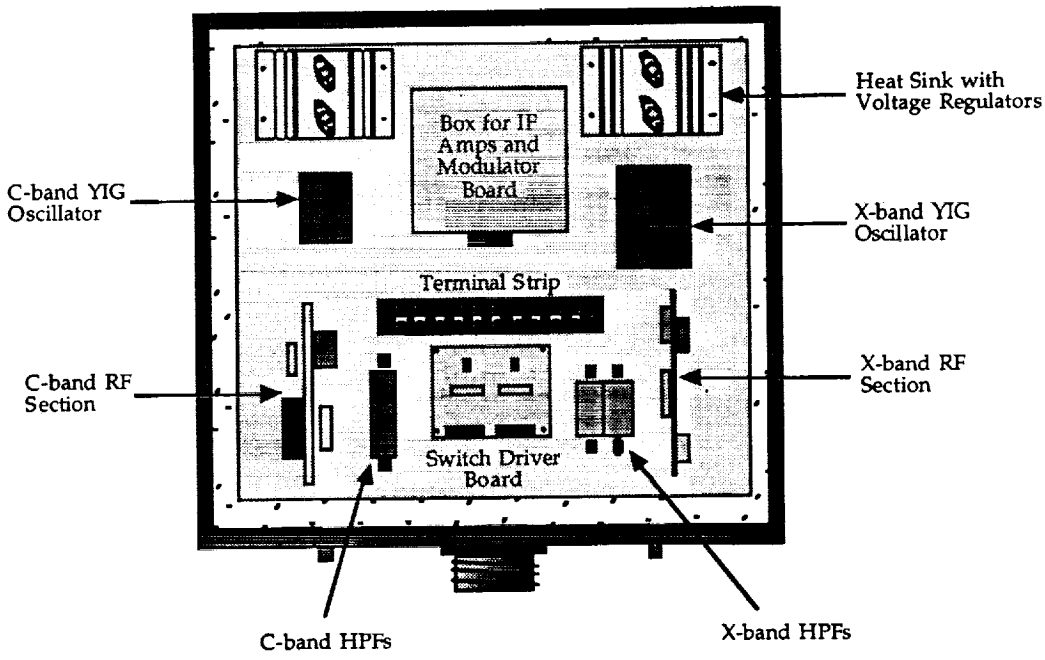

Top View of New RF Box Showing Component Layout

Figure 10. Design and Layout of the New RF Box

We went through several iterations in the design of the L-band radar because of logistics decisions made by the aircraft engineer at NASA Wallops. Initially, we had planned to house the L-band RF section in the same box as the C- and X-band sections. However, two external decisions forced us to change the original design of the L-band radar. First, during the test flight in May 1994, we were informed that the RF box could not be mounted on the outside of the helicopter near the feed antennas. Second, we were told that we would have to redesign the L-band feed antenna because the open-ended waveguide antenna was too big to be mounted on the helicopter.

Although we could not mount the RF box on the outside of the helicopter, we were allowed to mount the RF box on the side of the helicopter's rack to minimize the length of the coaxial cable running from the outputs of the RF box to the antenna ports. Even with this configuration, we still had to run about ten feet of RF cable from the RF box to the antennas. Although this did not cause us to change the design of the C- and X-band RF sections, we were forced to redesign the L-band radar. We did this because ten feet of cable between the circulators and the antenna ports will cause spikes in the IF spectrum that may drown out low-level return signals. These spikes are present as a result of mismatches at the input to the antenna that are not significantly attenuated by the RF cable. Therefore, to avoid this problem, we needed to come up with a design for the L-band radar that would allow us to mount the RF section closer to the feed antenna. Additionally, we had to design a new L-band feed antenna that would attach to the new RF section. The design of the L-band feed was discussed in section 2.1.

Initially, we designed the new L-band radar using surface-mount components. The block diagram of the radar is the same as that in Figure 9 but the SPDT switch and circulators are replaced by a transmit-receive (TR) switch and a directional coupler. We also built a driver circuit to convert a TTL control signal to the gate voltage needed to turn the FETs in

the TR switch ON or OFF. A diagram of the polarization switching for the L-band microstrip radar is shown in Figure 11.

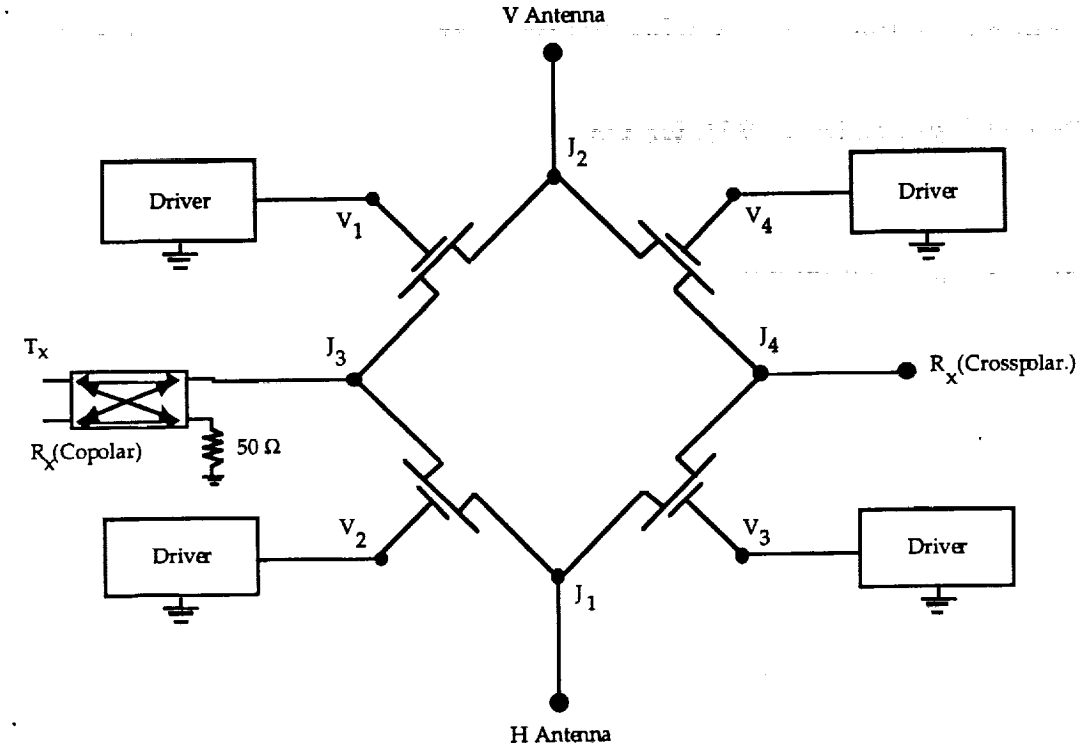

Control Inputs				ON Path	Transmit/Receive		
V_1	V_2	V_3	V_4	Other paths are OFF	T_X	R_X(CO)	R_X(CX)
0	-V	0	-V	J2 - J3 and J1 - J4	V	VV	VH
-V	0	-V	0	J1 - J3 and J2 - J4	H	HH	HV

Figure 11. Polarization Switching for the L-band Microstrip Radar

Six separate microstrip boards were designed and built. We fabricated the boards using PTFE substrates with one ounce of electrodeposited copper on both sides. We laid out the boards using Tango and printed the photoplots on a 600 dpi laser printer. Then, we transferred the patterns to the circuit boards and cut away the copper on top of the boards in the appropriate

regions. After the board patterns were completed, we soldered the components onto the circuit boards and the bare copper was tinned to prevent oxidation. We then tested the boards individually using the Hewlett-Packard 8722C Network Analyzer.

Once the boards were working, we designed a compartmentalized box to house the six boards. The box was milled out of a block of aluminum by Nelson Machine and Tool. The box is lightweight and it is designed to fit on the antenna mounting bar in the space previously occupied by the L-band waveguide feed. The microstrip radar block diagram and the RF box drawings are included in Appendix 3.

After the entire system was constructed, we connected the boards together using semi-rigid coaxial cable. We did this by soldering the center conductor of the coaxial cable to the 50-Ω microstrip line on the boards. These interconnects seriously degraded the VSWR characteristics of the radar resulting in undesirable system performance. As a result, we did not have a working L-band radar for IFC-2 in July 1994.

During the time between IFC-2 and IFC-3, we decided to build a new L-band radar using discrete components. We ordered small components manufactured by Mini-Circuits Incorporated of Brooklyn, New York. We also had the compartmentalized RF box completely hollowed out to accommodate the new RF section. The same design was used for the discrete L-band radar as was used for the C- and X-band radars except for the addition of an RF amplifier in the transmit path. The block diagram for the revised L-band radar design is included in Appendix 2. We used the RF amplifier to compensate for the loss in the RF cable that connects the L-band YIG in the radar control box to the input of the RF section. We managed to fit all of the discrete components inside of the small RF box. After the radar was completed, we ran delay-line tests using both the spectrum analyzer and the oscilloscope. Two log-periodic antennas were then fastened to the lid of the RF box and this L-band radar was used during IFC-3 in August 1994.

Because the output level of the mixer is small, an IF amplifier is needed to boost the received signal to a level that is useful for either display or digitization. We built an IF amplifier that provides three gain settings for amplifying the output of the RF portion of the receiver. The following section discusses the design and implementation of the IF amplifier.

2.3 IF Section

The IF section of the radar consists of a high-pass filter (HPF) and an IF amplifier followed by a low-pass filter (LPF). The LPF has a cutoff frequency of 22 kHz and is used to limit the bandwidth of the signal that is input to the data acquisition system. By limiting the bandwidth of the IF signal, we can avoid aliasing when the IF signal is sampled. The LPFs and HPFs are manufactured by TTE Incorporated of Los Angeles, California. The C- and X-band HPFs have a cutoff frequency of 10 kHz and the L-band HPFs have a cutoff frequency of 5 kHz. We use these filters to suppress the low-frequency components in the IF spectrum that are present due to the reflections at the antenna ports. All of the filters are passive and specifications are coded on the side of the filter.

The IF amplifier that we designed is a three-stage switchable-gain amplifier. The gain settings for the IF amplifier are determined as discussed in the beginning of section 2.0. The circuit diagram for one channel of the IF amplifier is shown in Figure 12.

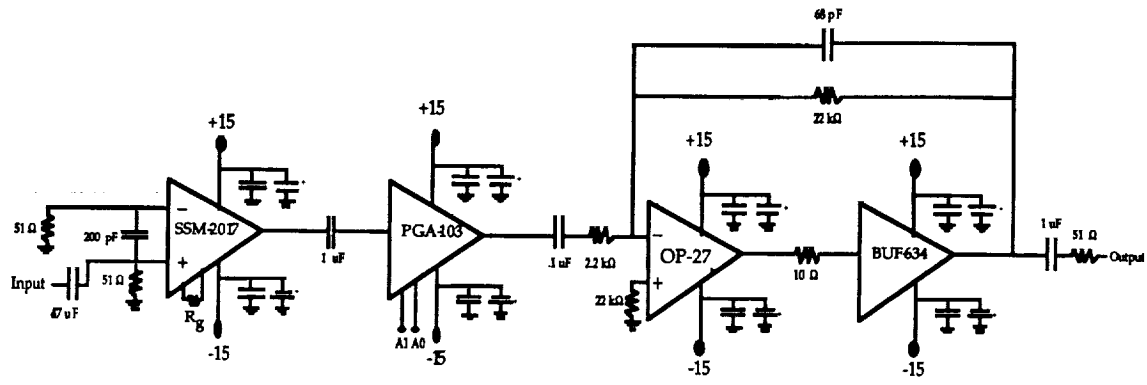

Figure 12. IF Amplifier Circuit Diagram

We used Tango to lay out the PCB and the board was fabricated at Colt Technology. The board layout and bill of materials are included in Appendix 4. We made three boards, one for each frequency, and each of them have two channels like the one shown in Figure 12.

We used three separate stages to provide the gain levels required. The first stage of the amplifier uses an SSM-2017 audio preamplifier manufactured by Analog Devices Incorporated of Norwood, Massachusetts. This is a fixed-gain amplifier that requires only one resistor to set the gain and provides good noise performance over the desired frequency range. The data sheet for this amplifier is included in Appendix 4. We designed the first stage of the C- and X-band amplifiers with a fixed gain of 30 dB ($R_g = 330\ \Omega$) and a gain of 0 dB ($R_g = \infty$) for the L-band amplifier. Ideally, the preamplifier should have a low noise figure and a large gain. If this is the case, the noise characteristics of the preamplifier will dominate. We can see this by examining the expression for the overall noise figure of a three -stage amplifier [Haykin, 1989]

$$F = F_1 + \frac{F_2 - 1}{G_1} + \frac{F_3 - 1}{G_1 G_2} \qquad (2.14)$$

Equation 2.14 tells us that the noise characteristics of the C- and X-band IF amplifiers are determined primarily by the first stage. The noise figure for the L-band amplifier is dominated by the noise figures of the first and second stage because of the low gain of the first stage. Therefore, the noise performance at L band will not be as good as the noise performance at the other two frequencies.

To provide the amplifier with three gain settings, we used a digitally-programmable amplifier with gains determined by two digital inputs (A_1 and A_0). Table 2 shows the digital inputs and the corresponding gain settings.

A_1	A_0	Gain	Gain (dB)
0	0	1	0
0	1	10	20
1	0	100	40
1	1	1000*	60*

* Only applies to new IF amplifier

Table 2. Gain Settings for the Second Stage of the IF Amplifier

The programmable-gain amplifier is a PGA-103 that is manufactured by Burr-Brown Corporation of Tucson, Arizona. The manufacturer's data sheet is included in Appendix 4. We chose this particular amplifier because it requires no external components for operation. The amplifier is also small and inexpensive.

We designed the third stage of the IF amplifier using two op amps to enable it to drive a 50-Ω load. We accomplished this by using a high-current buffer in the feedback loop of an OP-27 op amp to boost the output current. We used this configuration to provide the amplifier with the ability to drive loads requiring high current levels while remaining relatively immune to noise on the power supplies [Sedra and Smith, 1991].

The OP-27 is manufactured by Analog Devices and the buffer is a BUF-634 available from Burr-Brown. The data sheets for both of these integrated circuits are included in Appendix 4. Figure 12 shows the design of the output stage. The OP-27 is used in the inverting configuration with the BUF-634 in its feedback loop. This stage provides a fixed gain of 10 dB.

The output of the IF amplifier circuit is fed to a single-pole R-C high pass filter that provides a DC block. This HPF also provides a 50-Ω output impedance to match the 50-Ω input impedance of the A/D board.

We used a switching power supply to provide the DC voltages throughout the radar system. The power supply provides DC voltages of ± 24 V. Therefore, to provide the op amps with the proper supply voltages of ± 15, we used voltage regulators to convert the ± 24 V levels to ± 15 V levels. We used the LM-7815 and LM-7915 voltage regulators for this purpose. We decoupled the power inputs to all of the integrated circuits using a .1-μF monolithic ceramic capacitor. This prevents parasitic oscillations within the circuit [Analog Devices, 1992]. A 10-μF tantalum capacitor is also used on each power input to suppress low frequency spikes.

The IF amplifier was tested using a signal generator, a variable attenuator, and an oscilloscope. All of the gain levels were tested by using two voltage sources to provide the TTL control signals. The amplifier worked well on the test bench. However, when the IF amplifier is introduced into the radar system, we are unable to operate in the highest gain setting (90 dB) because of unwanted oscillations. At present, we have been unable to solve this problem and we have opted for a simpler design of the amplifiers. We feel that the problem with the amplifiers can be attributed to either the PCB layout or the wiring within the old RF box. However, we have been unable to isolate the cause.

After tests were run and significant progress was not made, we decided to build new amplifiers with separate channels for each polarization. This time we made six individual amplifier boards. The new IF amplifiers are

2.1" square and they consist of threes stages. The first stage is a high-gain preamplifier that is used for the same reasons as discussed earlier. The second stage is a programmable gain amplifier that has four different gain settings. We used a PGA-202 by Burr-Brown for this stage. This amplifier is similar to the PGA-103 and the gain settings for the new IF amplifier are included along with those for the old amplifier in Table 2. The third stage is a high-current op amp (BUF-634) that is used to drive a 50-Ω load.

We packaged the new amplifiers in a box with separate compartments for each channel. By placing each of the channels in a different compartment and by carefully managing the ground, we were able to achieve a much higher isolation between the channels. The new amplifier boards provide a 30-dB isolation between all channels in the highest gain setting. In the second gain setting the isolation between channels is 50 dB.

The first stage of the IF amplifier is constructed using an OP-37 op amp with an inverting gain of 20 dB. The maximum value of the noise spectral density for this IC is 3.8 nV/√Hz. Assuming that the noise characteristics of this stage dominate and that we are driving a 50-Ω load, we can distinguish a signal at a level of -100 dBm from the noise [Franco, 1988]. The circuit diagram for the new IF amplifier circuit is included in Appendix 4.

After the signal has been amplified, it is digitized using a high-speed A/D board. The design and implementation of the data acquisition system for the radar are the subject of the next section.

2.4 Data Acquisition System

The data acquisition system is used to digitally record the radar data. Recording the data in digital form is advantageous because it allows us to process the data after the experiment is completed. Therefore, we can make use of digital signal processing (DSP) techniques to eliminate unwanted signals and thereby improve the quality of the data. Each of the

twelve channels (CVV, CHH, CVH, CHV, XVV, XHH, XVH, XHV, LVV, LHH, LVH and LHV) of the radar are digitized during the helicopter overflights. We collect the data using a data acquisition board that is manufactured by Datel Incorporated of Mansfield, Massachusetts called the PC-414-B2. The specification sheet for this board is included in Appendix 5. We chose this board because of its ability to sample four channels simultaneously at 14 bits per sample (actually uses two bytes when storing) with sampling rates as high as 5 MHz. Also, the board has a built in first-in first-out memory (FIFO) for easy transfer of the data from the A/D board to the personal computer's memory.

We used the simultaneous four-channel sampling mode along with a switching scheme to collect data from all 12 channels during the flights. Channels 0 and 1 of the A/D board are dedicated to C-band V receive and C- band H receive respectively. Channel 2 switches between L-band V receive and X-band V receive and channel 3 switches between L-band H receive and X-band H receive. The switching between L and X band is performed once every four periods of the modulation waveform (a 50-Hz triangle wave). During the upsweeps of the modulation waveform , we keep the SPDT switch in position 1 (see Figure 9). This means that we collect CVV, CVH, LVV or XVV and LVH or XVH during the upsweeps. During the downsweeps, the computer switches the SPDT switch to position 2 and we collect CHV, CHH, LHV or XHV and LHH or XHH. Using this switching scheme, we obtain several independent samples of the backscatter for each frequency and polarization combination during each flight. Figure 13 illustrates the switching scheme and shows how all 12 channels are sampled multiple times during every flight line.

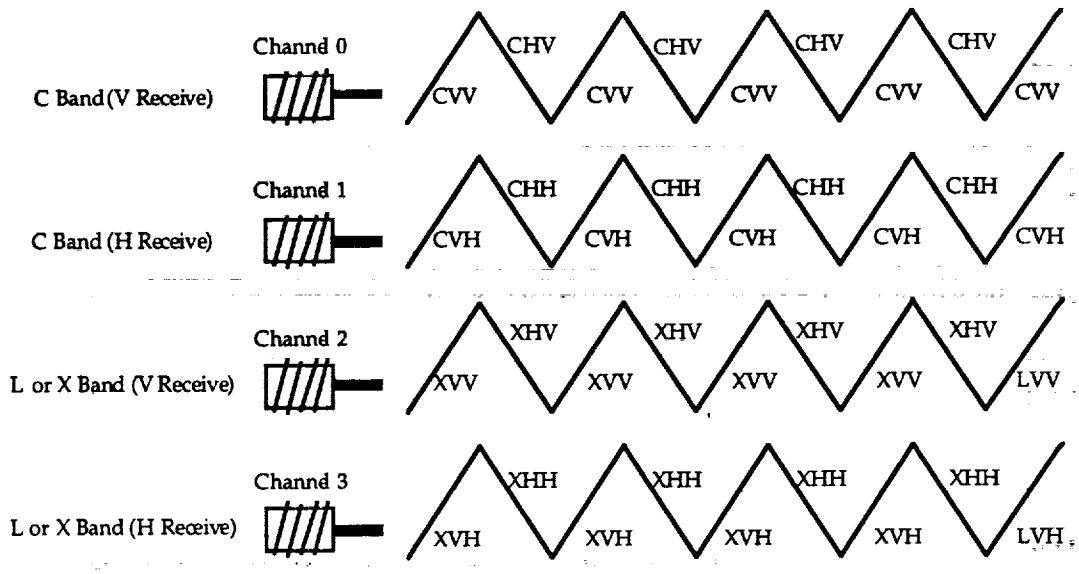

Figure 13. Data Acquisition Scheme for Digitizing 12 Channels

We chose a sampling rate of 160 kHz. This is four times the sampling rate required for a single channel. The sampling rate for an individual channel is determined based on the maximum unambiguous range desired as described in Section 2.0.

Each flight line is covered in a period of 40 seconds. Therefore, since 160 ksamples are taken each second and the sample length is two bytes, we collect approximately 12 Mbytes of data during each flight line. Additionally, each flight line must be flown six times for collection of backscatter data at varying incidence angles. This results in a minimum data volume of 72 Mbytes for each flight line.

The PC-414-B2 data acquisition board is designed to fit into a standard PC slot. The board is controlled using a program written in C. Basically, the program tells the board the sampling frequency, the mode of operation and the format of the data. The program also controls the acquisition of the data and the flow of the data to the PC. While the data are being sampled they are directed to the data acquisition board's FIFO and then to

the PC's memory. At the end of the flight line, the data are transferred from the memory to a 150-Mbyte Bernoulli disk.

We controlled the switching of the transmit polarization and the switching between L- and X-band data acquisition using waveforms generated by a digital input-output (I/O) board. The I/O board that we used is the CIO-DIO24 manufactured by Digital Boards, Incorporated of Mansfield. Massachusetts. The polarization switching is controlled using a 50-Hz TTL-level square wave. This square wave controls the position of the SPDT switch in the RF section. A 12.5-Hz TTL-level square wave is used to switch between the L- and X-band channels. This square wave controls the position of a switch on the L/X-band LPF board in the control box.

The details of the programs written for the data acquisition system are not included here because they are beyond the scope of this report. All of the programs were written by Simone Pinheiro during the spring and summer of 1994. They are the subject of an RSL Technical Report that is currently being written [Pinheiro, 1994].

2.5 Systems Integration

After all of the systems discussed in sections 2.1 - 2.4 were tested individually, we integrated the entire radar system. The radar system was powered up for the first time in the summer of 1994. However, several of the subsystems discussed were not functioning as well as they are at present. After several modifications, we packaged the radar system into three rack-mountable boxes. The first of these boxes is the rack-mountable PC that we obtained from Appro Incorporated of San Jose, California. The Bernoulli drive was attached to the top of the computer box for mounting in the helicopter. The second box is the RF box that has already been discussed in Section 2.2. The Hoffman box was mounted in the helicopter during IFC-2 and IFC-3 but a new RF box (see Figure 10) is currently being used. The third box is the control box. We used an old control box with a

linear power supply during IFC-2 but a new control box was built using a Vicor switching power supply for IFC-3. We designed the control box so that we could easily monitor the radar's output during the helicopter flights. A drawing of the front and back panel of the radar control box is shown in Figure 15a. Figure 15b shows the layout of the radar components within the control box.

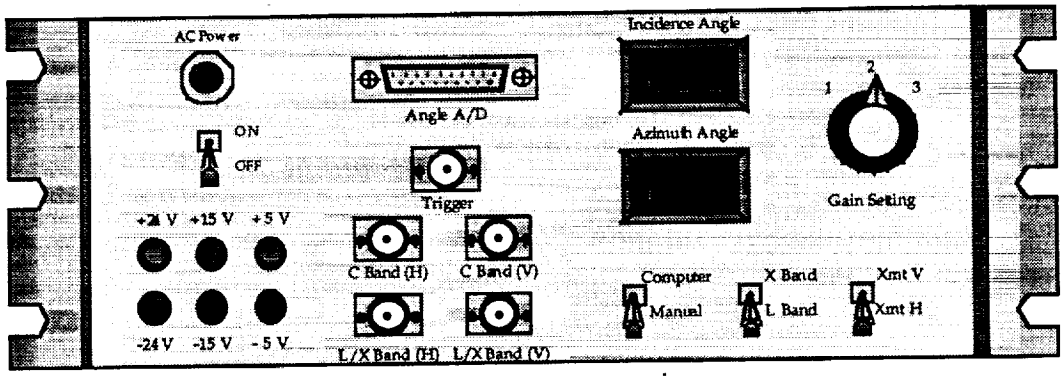

Front Panel

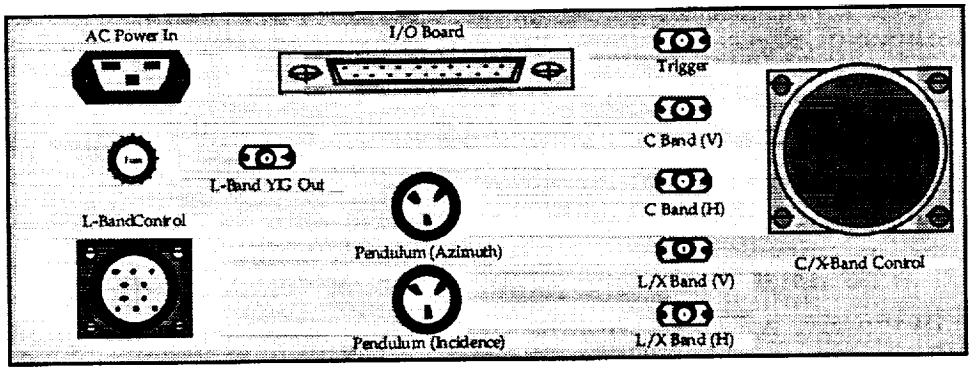

Back Panel

Figure 14a. Front and Back Panel of the Radar Control Box

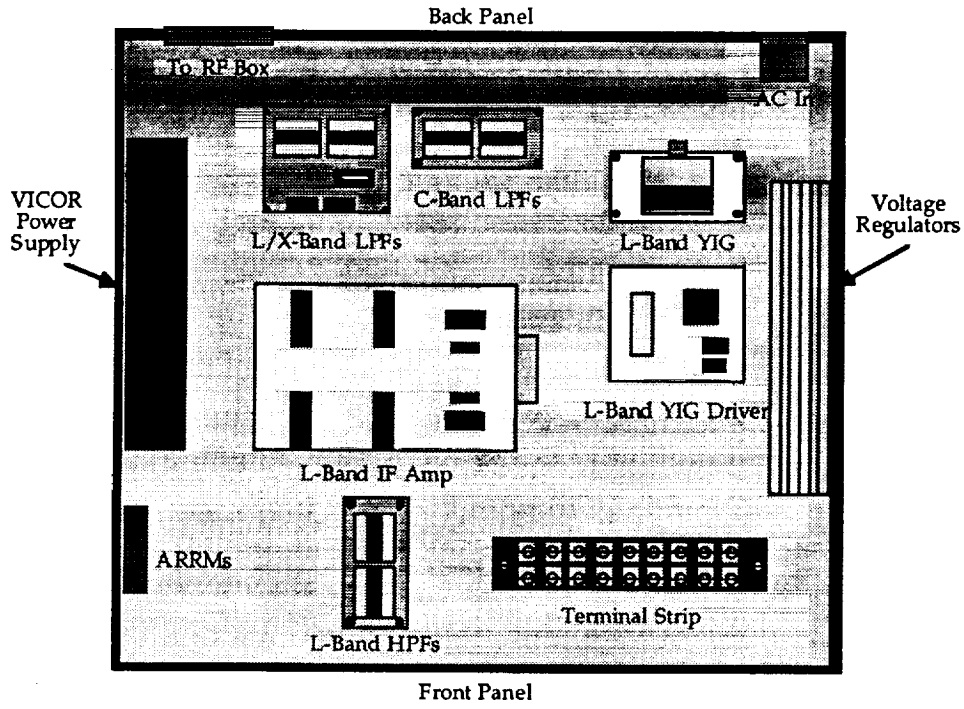

Figure 14b. Layout of the Components within the Radar Control Box

We mounted all of the boxes along with an HP digital oscilloscope inside the helicopter during both of the IFCs. Appendix 6 includes several photographs of the radar system.

As mentioned earlier, we operated the radar from the helicopter during IFC-2 in July 1994 and later during IFC-3 in September 1994. The following section describes the problems that we encountered during IFC-3 and provides detailed explanations of how we were able to overcome some of these problems.

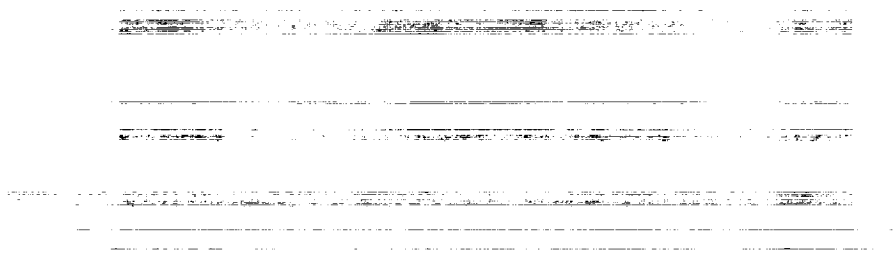

Chapter 3 - Problems with the Radar System During IFC-3

Although we experienced problems during IFC-2, they were not as interesting from an electrical engineering standpoint as the ones that we faced during IFC-3. Therefore, this section describes the actions we took to overcome the problems encountered during IFC-3. First, we will examine the problems caused by the long RF cables for the C- and X-band sections. We were forced to use long cables because the Hoffman box that houses the C- and X-band RF sections could not be mounted outside of the helicopter. We made changes to our original system design to counteract the effects of the long cable. Despite our efforts, the long cables still degraded the performance of the radar. After we have examined the problems with using long RF cables, we will discuss the mistakes made in the design of the switch driver board used to control the SPDT switches in the C- and X-band RF sections. Although the design of this circuit seemed to be simple, we made an error by overlooking a subtlety in the design when implementing the circuit. We did not detect this error until IFC-3 and we had to design and build a new circuit in the field. Then, we will discuss other problems that we faced during the field experiment. At present, we can not explain the causes of some of these problems. However, we will describe the tests that we have performed and discuss possible causes of the problems.

3.1 The Problems Caused by Long RF Cables

Using long RF cables causes problems because of the interference signals generated by multiple reflections and the loss of system sensitivity due to the lower transmit power at the antenna ports.

The worst-case scenario for multiple reflections occurs when we have long cables with very little loss and a poor match at the antenna port. For our case, this occurs at C band. We used ten feet of RF cable with loss of .4 dB/ft. The transmit power measured at the output of the circulator is 9 dBm. The C-band antenna has a 10-dB return loss at the edge of the

passband. Using these values and assuming a perfect match at the circulator port, we can calculate the power returned by the first reflection as 9 dBm - 10 dB (due to mismatch at antenna port) - 8 dB (due to cable loss) = -9 dBm. The mismatch at the inputs to the antennas and the long RF cables cause a spike in the IF spectrum with a magnitude that is 18 dB less than that present when the circulator port is shorted. The frequency at which this spike occurs can be calculated using equation 2.2 and is approximately 2 kHz. Additional spikes will be present at multiples 2 kHz and the magnitude of each of these spikes will be 18 dB lower than that of the previous spike.

Using this estimate, we chose to precede the IF amplifier with a HPF with a cutoff frequency of 10 kHz. This filter is used to attenuate the multiple reflections caused by the long cable and the antenna port mismatch. However, the HPF also attenuates the antenna feedthrough signal that we had planned to use in place of a delay line as our internal calibration signal. The RF sections were constructed before we learned that the RF box could not be mounted outside of the helicopter and we decided to use the attenuated version of the antenna feedthrough as our calibration signal.

Another more fundamental problem caused by the use of the long cables is the loss of transmit power at the antenna port. At X band, the radar's transmit power is lowered by 10 dB due to the loss in the cable. Lowering the transmit power of the radar will cause the system to be unable to detect small objects or large objects at longer ranges. Therefore, by introducing the long RF cables into the radar system, we have lost dynamic range. The only ways to remedy this situation are to either use a source with more output power or to somehow move the RF section closer to the feed antennas. Neither of these options were feasible and we had to sacrifice system performance.

3.2 The Switch-Driver Circuit

PIN-diode switches are used in the RF section rather than mechanical ones to provide faster switching times. We used switches that were readily available in the lab. However, these switches did not have a built-in driver circuit to convert the TTL control signal to the current levels necessary to properly bias the diodes. The switch-driver circuit controls these PIN-diode switches in the C- and X-band RF sections of the radar. We want to control the transmit polarization of the radar using TTL signals but the PIN-diode switches require two 30-mA currents of opposite polarity to control their position. Therefore, we needed to design a circuit to convert the TTL input signal into two 30-mA currents of opposite polarity.

We first designed the switch driver using a voltage-to-current converter commonly found in the literature [Sedra and Smith, 1991]. This circuit was used in conjunction with a comparator to produce the correct output current given the TTL input. The circuit diagram is shown in Figure 15.

Depending on the input voltage, the comparators hit either the positive or negative supply rail. Then, the rail voltage V is converted to a current ($I_{out} = V/R$) by the voltage-to-current converter. Therefore, by using two comparators and two voltage-to-current converters, we can produce the currents needed to control the switch. The original circuit was designed, built and tested by Steven LeBueof during the summer of 1994.

We used this circuit throughout IFC-2. After we returned from the field, we redesigned the switch driver board and fabricated it using the etching facility. We then tested the circuit in the lab and it was working properly.

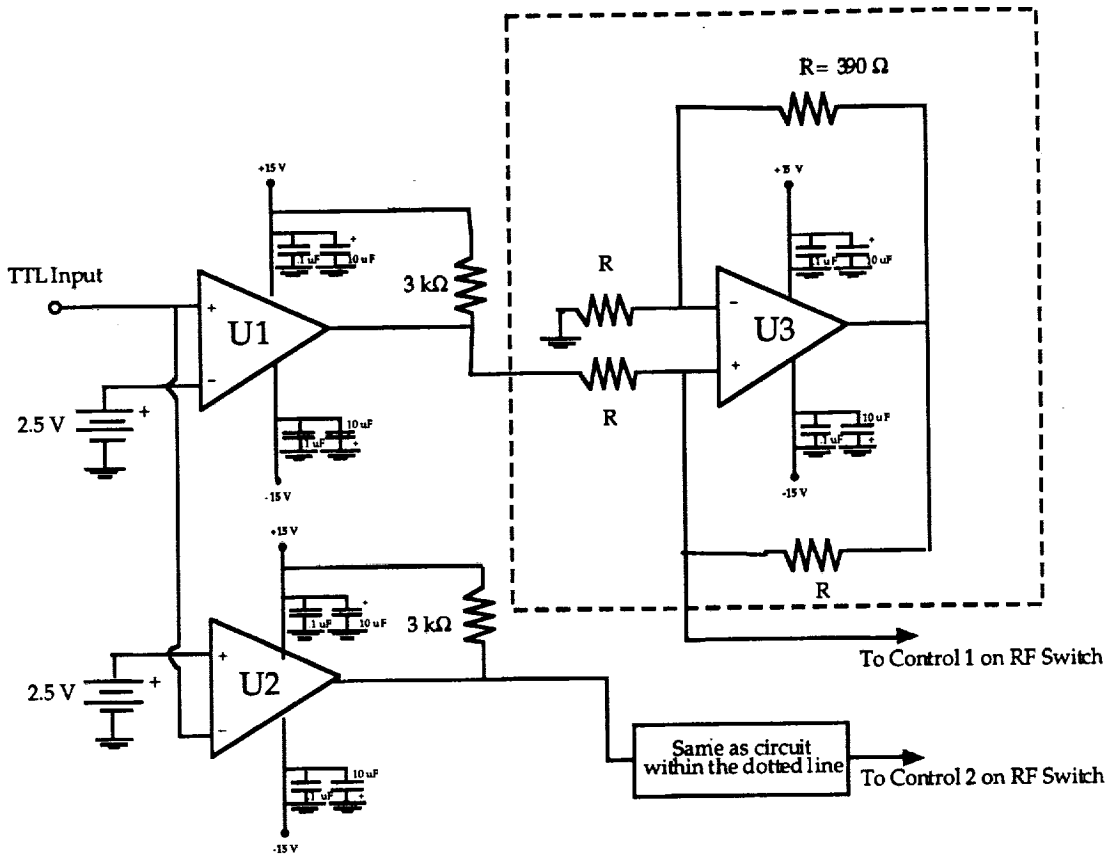

Figure 15. Original Switch Driver Circuit

When the radar was operating for longer periods of time during IFC-3, we observed that the comparator chips were abnormally hot. We then tested the circuit and found that it was not working. After taking a closer look at the circuit, we realized that the original design requires the comparator stage rather than the voltage-to-current stage to supply the current to the load.

Once we found the problem with the circuit, we came up with a new design for the switch driver. The new switch-driver circuit is not as complex as the original. A circuit diagram of the new switch driver is shown in Figure 16.

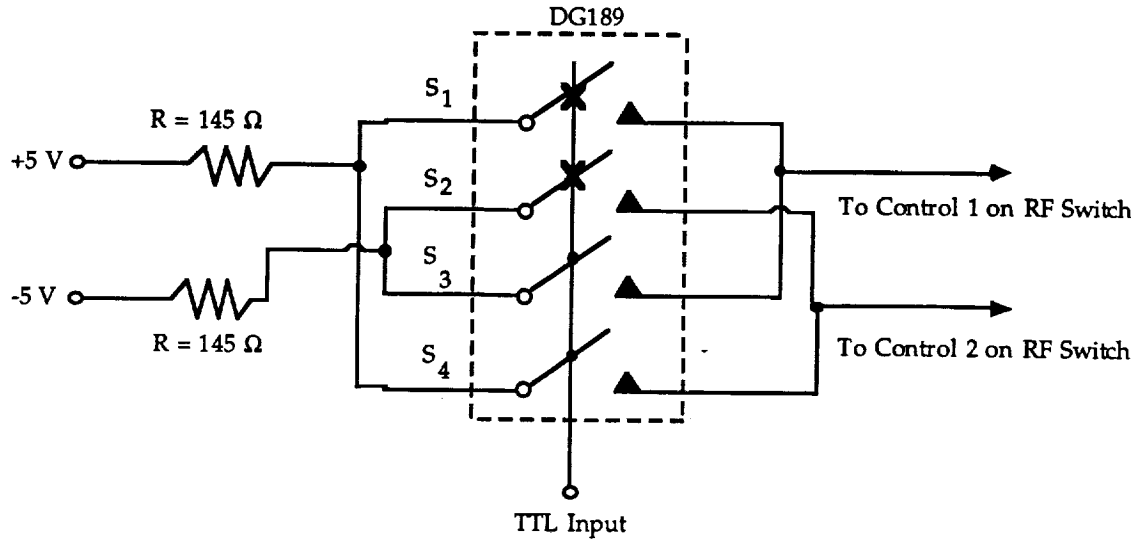

Figure 16. New Switch-Driver Circuit

We used this design because the parts needed to build the circuit were readily available. The voltages at the input are provided using 1-amp regulators (LM-7805 and LM-7905) and the switches are implemented using a DG-189 made by Siliconix Incorporated. The data sheet for the switch is included in Appendix 6.

The operation of this circuit is simple. The load current i_L is determined by the input voltage V_{in} and the series combination of the resistor R and the load resistance R_L as

$$i_L = \frac{V_{in}}{R + R_L} \tag{3.1}$$

Therefore, by choosing the proper value of R, we can adjust the amount of current supplied to the load. While designing this circuit, we made certain that the components possessed the ability to supply the current required by the load. The new switch-driver circuit was built in the field using a prototype board. This circuit was used successfully throughout

IFC-3. When we returned, we made a PCB version of the new switch-driver circuit.

3.3 Other Problems Encountered During the IFCs

In addition to the problems discussed above, we also solved a series of smaller problems during the field campaigns.

A new control box was constructed during the period between the second and third IFCs. One of the main reasons for building a new control box was to decrease the weight of the system by using a switching power supply rather than a bulky series supply. Although the switching power supply is very lightweight it has the disadvantage of being very noisy. Therefore, we used ripple attenuation modules inside the control box to filter the power supply noise. Initially, we did not obtain the performance that was specified by the manufacturer after installing the modules. After running several tests during IFC-3, we noticed that a mistake had been made in the wiring of the modules. We corrected the wiring error and this resulted in a drop in the noise floor of 20 dB.

The most mysterious problem that we encountered in the field was the appearance of a noise spike at 12 kHz when the system was mounted in the helicopter. The 12-kHz spike was not present during system testing and when we first saw the spike it was confused with the radar return. We realized that the spike was system induced after we started sweeping incidence angles and the spike did not move. Initially, we thought that the spike was being generated by the electronics on board the helicopter. However, when we landed, we tested the system using power from a nearby generator and the spike was still present. We then took the radar back to the lab to see if we could find out where the noise was coming from.

Once we figured out that the noise was not created by the helicopter, we began to suspect a grounding problem. After we returned to the lab with

the radar, we stacked the system as it was mounted in the helicopter and used grounding straps to interconnect the boxes. We were then able to see the 12-kHz spike in the lab. After testing the system, we discovered that an improper value resistor had been used on the input to the A/D board. We replaced the resistors and the 12-kHz spike disappeared leading us to believe that the problem was solved. However, when we remounted the radar in the helicopter for the next flight, the 12-kHz spike appeared once again.

To avoid interference with the 12 kHz spike, we took data at ranges corresponding to larger frequency values by flying at higher altitudes. Although this helped us to avoid interference between the radar return and the noise spike, the system sensitivity was lowered because of the larger area illuminated by the antennas and the increased spreading loss when flying at higher altitudes.

During the field experiment we could not find the source of this problem. We felt that the problem was either due to the wiring in the RF box or to the layout of the IF amplifier boards. Therefore, after we returned from the field, we repackaged the entire RF section and redesigned the IF section. We carefully wired the RF box making sure that we did not create any ground loops.

The following section describes the performance of the radar system at present. Also, results of test measurements are presented.

Chapter 4 - System Performance and Results

In this section we will discuss the performance of the radar system in its current state. First, the method used to calculate the antenna's beamwidth and gain at all three frequencies is discussed. This is followed by delay line measurement results with a table showing the isolation between channels. Delay line results are followed by lens measurements taken behind Nichols Hall. Using these results, we discuss the system's measurement capabilities and possible improvements that can be made. Several tree measurements are also presented. At the end of the section, we have included some of the initial results from the L-band radar data collected during IFC-3 over the YJP site.

4.1 Antenna Performance

Since we have not measured the antenna patterns to date, we estimated the antennas performance using basic equations [Ulaby, et al., 1986]. The L-, C- and X-band half-power beamwidths were calculated using

$$\beta_{1/2} = a\frac{\lambda}{d} \tag{4.1}$$

where λ is the wavelength, d is the diameter of the aperture and a is a factor based on the taper. We also calculated the gain of the antennas at each of the bands by first calculating the directivity using

$$D_0 = .78\frac{4\pi}{\beta_{1/2}^2} \tag{4.2}$$

Then, the gain is calculated using

$$G_0 = \eta D_0 \tag{4.3}$$

where η is the radiation efficiency of the antenna. The results of these calculations are presented in Table 3.

Freq. (GHz)	a	λ (cm)	d (m)	η	$\beta_{1/2}$ (°)	D_o (dB)	G_o (dB)
10	1.5	3.00	.9	.25	3.0	36	30
5.5	1.5	5.45	.9	.25	5.2	31	25
1.5	1.2	20.0	.9	.20	15	21	14

Table 3. L-, C- and X-Band Antenna Gain and Beamwidth

We measured the isolation between the V and H channels of the C- and X-band conical horns using the HP Network Analyzer. The isolation for each of the antennas is 20 to 25 dB.

4.2 Output Power Levels

The output power levels were measured for each of the transmit channels of the radar using a power meter. The results of these measurements are shown in Table 4.

Frequency Band	V-Channel Power Out (dBm)	H-Channel Power Out (dBm)
L	13.5	12.1
C	5.8	6.3
X	10.2	9.7

NOTE : The output power of the C- and X-band section is measured at the RF box rather than at the antenna ports so the loss in the RF cable must be taken into account before using these numbers in the radar equation.

Table 4. Output Power for the Transmit Channels

4.3 Delay Line Measurements

After the system was reconstructed, we ran a series of delay line tests to determine the amount of interference between the channels for the C- and X-band sections. Figures 17, 18, 19 and 20 show the delay line results for the all of the C- and X-band channels at gain setting 2 (40 dB) and gain setting 3 (60 dB). Gain setting 1 (20 dB) results are not included because no coupling between channels can be seen at this gain setting.

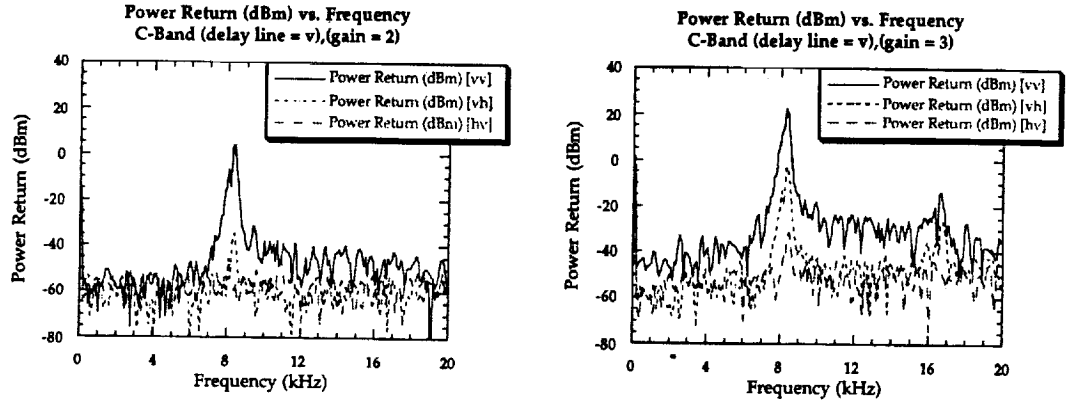

Figure 17. Delay Line Results for C-Band (V) at Gains Settings 2 and 3

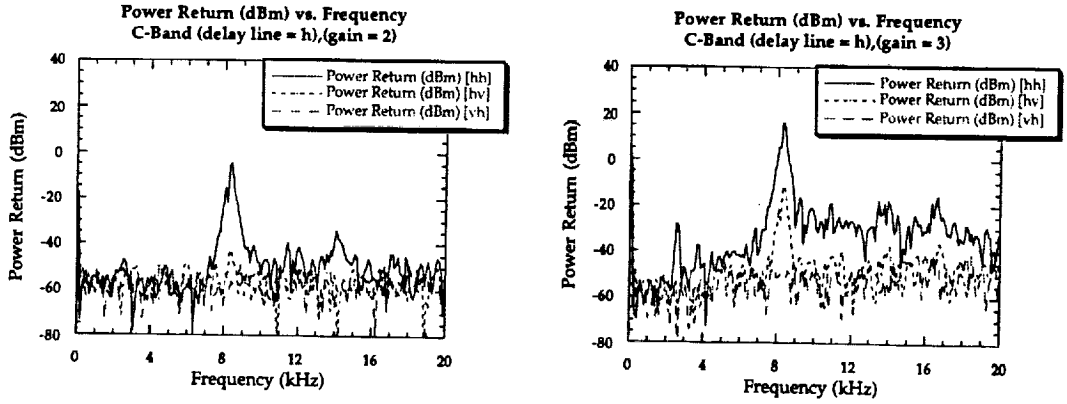

Figure 18. Delay Line Results for C-Band (H) at Gains Settings 2 and 3

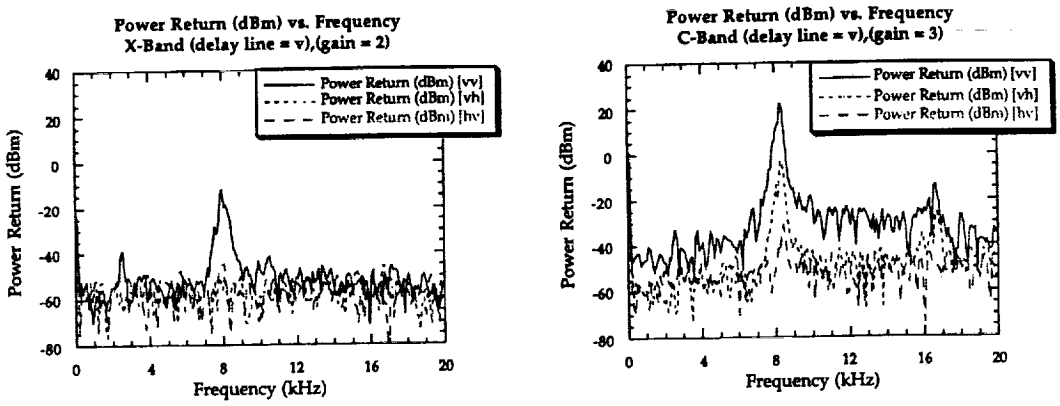

Figure 19. Delay Line Results for X-Band (V) at Gains Settings 2 and 3

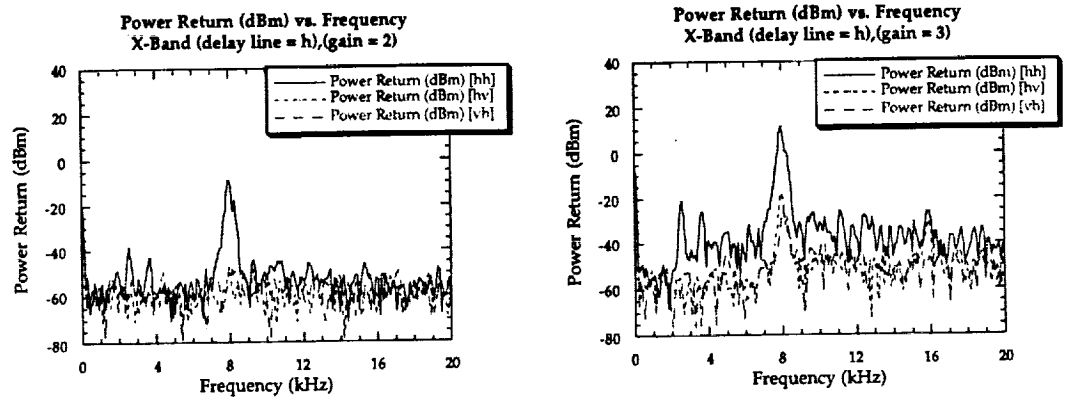

Figure 20. Delay Line Results for X-Band (H) at Gains Settings 2 and 3

Table 4 lists the isolation between channels obtained from the measurements displayed above for gain setting 3, which is the worst case.

Frequency Band	Delay Line Position	Transmit Switch Pos.	Channel Measured	Isolation from VV (dB)	Isolation from HH (dB)
C	V	V	H	26	N/A
C	V	H	V	53	N/A
C	H	H	V	N/A	27
C	H	V	H	N/A	65
X	V	V	H	29	N/A
X	V	H	V	33	N/A
X	H	H	V	N/A	29
X	H	V	H	N/A	39

Table 5. Isolation Between Channels for C and X bands

We also tested the functionality of all of the switches on the control box. Figure 21 shows the results of a test of the X/L switch. During this test the L-band radar was not connected and the delay line was connected to the X-band V channel.

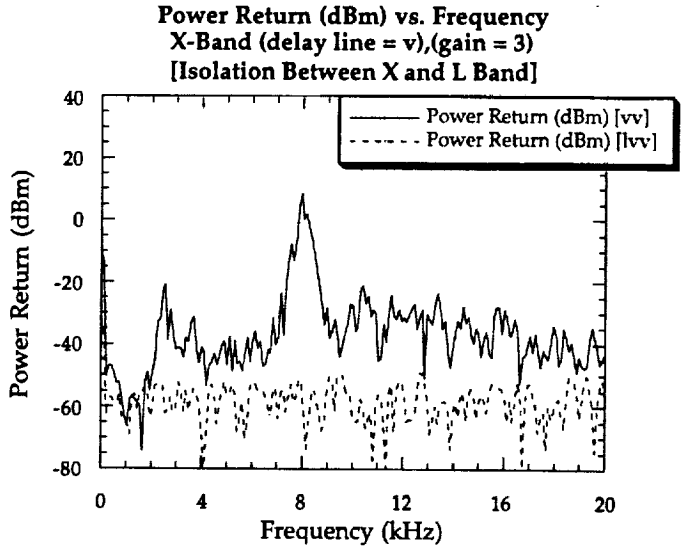

Figure 21. Functionality of the X-band/L-band Switch

Although the isolation provided by the amplifier is at worst 26 dB, this is not the limit of the system. The antennas provide only 25 dB isolation and this determines the isolation between the channels for the entire system. After the delay line tests were completed and we were satisfied with the system's performance, we connected the antenna and took the radar outside to perform lens measurements.

4.4 Lens Measurements

Lens measurements were collected in the field behind Nichols Hall using all three frequency bands and both VV and HH polarizations. We collected data at two different ranges for each of the bands' VV and HH channels. The ranges were chosen to represent typical ranges to targets present when taking data from the helicopter. The X-band returns exhibit a higher signal-to-noise ratio (SNR) than the returns at L and C bands. Figure 22 shows the X-band VV return from the lens at ranges of 100 feet and 157 feet. Figure 23 shows the X-band HH return from the lens at ranges of 100 feet and 160 feet.

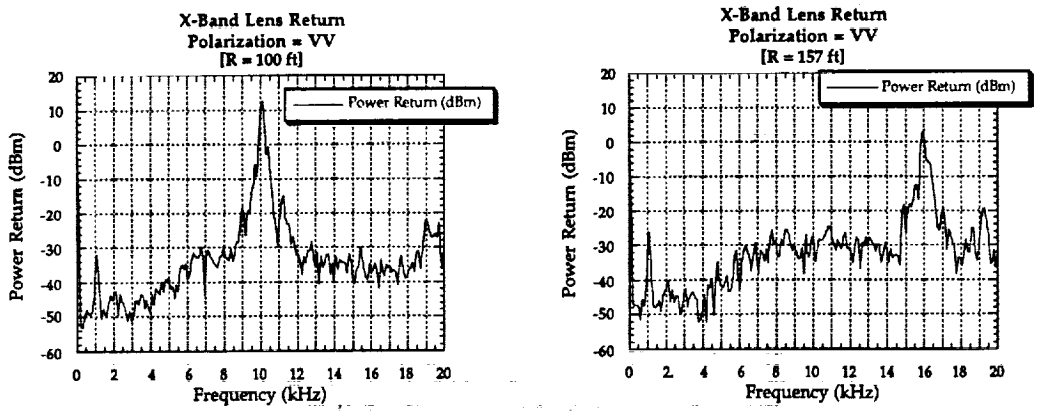

Figure 22. X-Band VV Lens Return at 100 and 157 feet

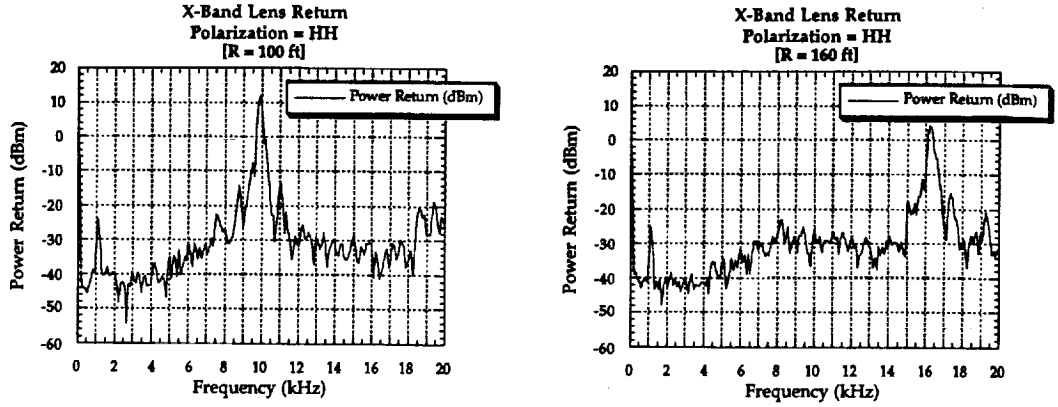

Figure 23. X-Band HH Lens Return at 100 and 160 feet

At R = 100 ft (30.5 m), the SNR is about 40 dB for both the VV and HH polarizations. Using this value for the SNR, we can determine the minimum detectable σ^o for the X-band radar at this range. The radar cross section of the lens is known to be 13 dB and we can calculate the area illuminated at nadir using

$$A_{ill} = \frac{\pi}{4} R^2 \beta_{1/2}^2 \tag{4.4}$$

Using the value for the half-power beamwidth for X band given in Table 3, we find that the area illuminated is 3 dB. Therefore the equivalent σ^o that we are measuring is the radar cross section of the lens divided by the area illuminated or 10 dB. This means that we can measure scattering coefficients as low as -25 dB with a SNR of 5 dB at a range of 100 feet with the X-band radar. Before we decide that the radar actually has the ability to detect a σ^o this low, we must calculate the power returned when σ^o = -25 dB and make sure that the IF amplifier can handle a signal this small. Using the radar equation and the values P_t = 5 dBm, G^2 = 60 dB, λ^2 = 30 dB, σ^o = -25 dB, A_{ill} = 3 dB, $(4\pi)^3$ = 33 dB, and R^4 = 60 dB, we find that the power returned is -80 dBm. Therefore, since the IF amplifier can accommodate signals as low as - 100 dBm (see Section 2.3), we can detect this signal.

By performing the same calculations for the return at 160 feet, we find that the X-band radar can measure scattering coefficients as low as -18.5 dB at this range. Since typical X-band scattering coefficients for vegetation are above this threshold, the radar provides sufficient dynamic range at X band for use in the forest.

Figures 24 and 25 show the C-band VV and HH lens returns at ranges of 100 feet and 160 feet.

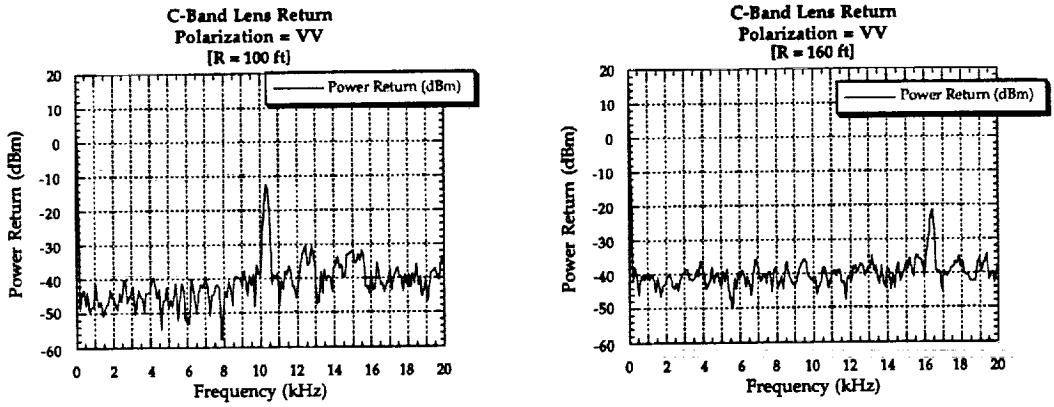

Figure 24. C-Band VV Lens Return at 100 and 160 feet

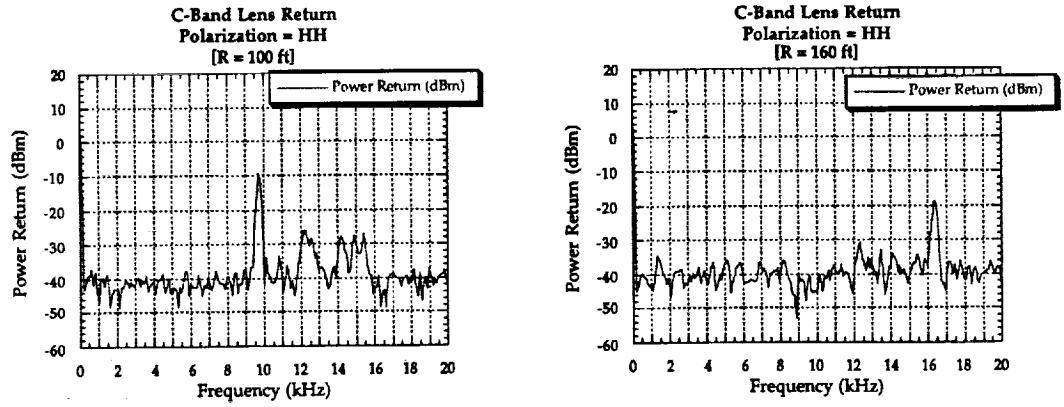

Figure 25. C-band HH Lens Return at 100 and 160 feet

The signal is lower at C band than X band because of the lower antenna gain and the smaller cross section of the lens at this frequency. Also, the

difference in the returns from the VV and HH channels can be attributed to differences in focusing of the antenna. Table 6 lists the results of calculations made to determine the minimum measurable scattering coefficient. We performed these calculations using the method described for the X-band radar.

Figures 26 and 27 show the lens return at L-band for the VV and HH channels at ranges of about 100 feet and 160 feet.

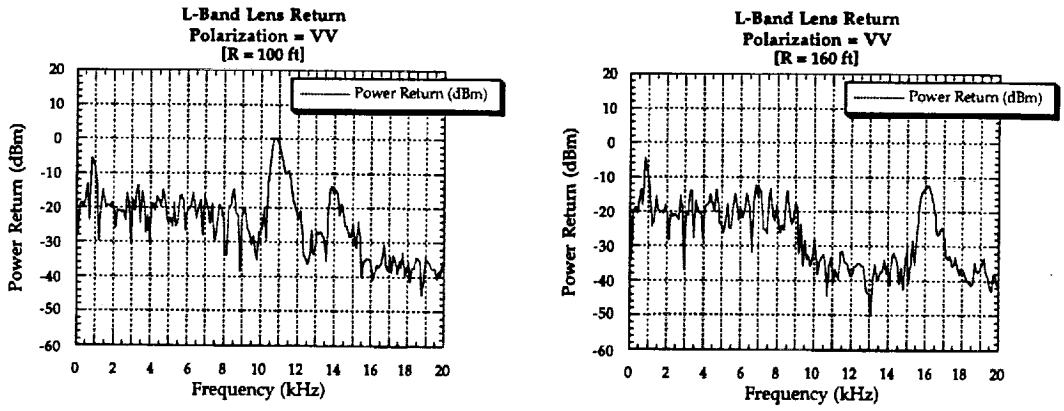

Figure 26. L-band VV Lens Return at 100 and 160 feet

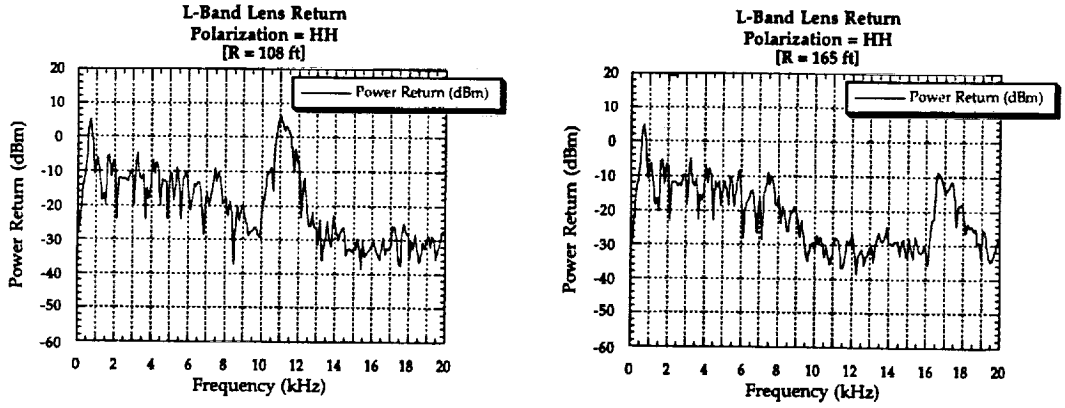

Figure 27. L-Band HH Lens Return at 108 and 165 feet

The L-band returns do not exhibit peaks at a single frequency because the ground is present in the area illuminated by the antenna. Also, the noise

floor is higher at lower IF frequencies because of the larger internal reflections in the L-band section. Table 6 shows results of calculations of the minimum measurable scattering coefficient at L band.

Frequency Band	Range (ft)	SNR (dB)	σ^{o}min (dB) with SNR = 5 dB
L	108	35	-36
L	165	20	-21
C	100	30	-27
C	160	20	-21
X	100	40	-25
X	160	30	-18.5

NOTE: Results are shown only for HH channel with but VV channel results are similar.

Table 6. Minimum Measurable Scattering Coefficients

The results from Table 6 indicate that the system gain is sufficient to measure the backscattering coefficient of vegetation at 150 feet. However, the helicopter often flies at an altitude of more than 150 feet. Also, larger incidence angles will increase the range to the target. Furthermore, the forest canopy will cause more attenuation than air. Therefore, we would still like to add an 80-dB gain setting to the system. This gain setting would be very useful for the C- and X-band portions of the radar.

Following the lens measurements, we performed measurements with the radar pointing at evergreen trees behind Nichols Hall.

4.5 Tree Measurements

We collected backscattering data from several evergreen trees behind Nichols Hall. We took these measurements to test the radar's ability to see trees with foliage present at ranges comparable to those that will be

encountered during field experiments. When taking the measurements we manually adjusted the antenna position to point at the trees. We made sure that the antenna was pointing in the right direction by placing the lens in front of one of the trees and validating that the tree was being seen by the radar. Linear plots of the X-band VV and HH returns are shown in Figure 28.

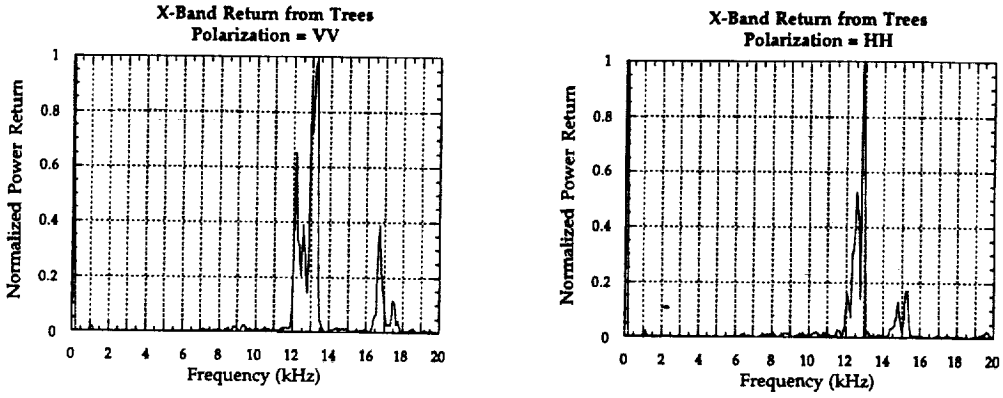

Figure 28. Linear Plots of X-Band VV and HH Tree Returns

The X-band antenna was aimed at three trees at ranges of about 130, 150 and 160 feet. The VV return from the second tree is not large but the third tree can be seen fairly well. The HH channel shows a large return from the second tree which shadows the return from the third tree.

Linear plots of the C-band VV and HH returns are shown in Figure 29.

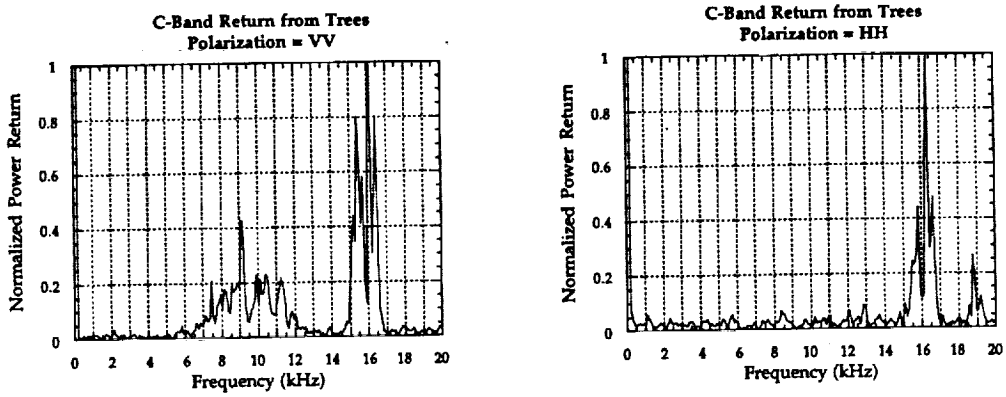

Figure 29. Linear Plots of C-Band VV and HH Tree Returns

The C-band antenna was looking at only two trees. The VV return in Figure 29 has some reflections from the ground in the lower frequency range and only one of the trees is present in the return. This is a result of the antenna's position. With the HH channel, we have no reflection from the ground and a second tree can be seen behind the first.

The L-band returns from the trees are broader than those at C and X band because of the larger antenna beam. The large beam also allows many reflections from the ground to be seen by the radar. Unfortunately, these ground reflections were dominant in the data that we collected. Figure 30 shows the L-band returns from the trees from both the VV and HH channels.

Although the ground return can be seen in these plots, it does not appear at the same range as the return from the trees. Therefore, by using filters, we can easily separate the return from the ground and the trees.

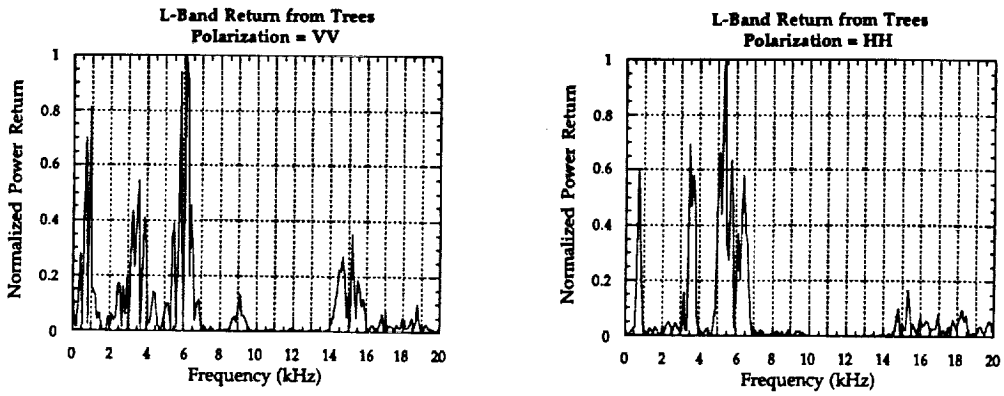

Figure 30. Linear Plots of L-Band VV and HH Tree Returns

4.6 IFC-3 Measurements

We collected data at all three frequencies during IFC-3. However, we have only processed the L-band spectra from the YJP site. Figure 31 shows normalized power return vs. range at incidence angles of 5° and 20°.

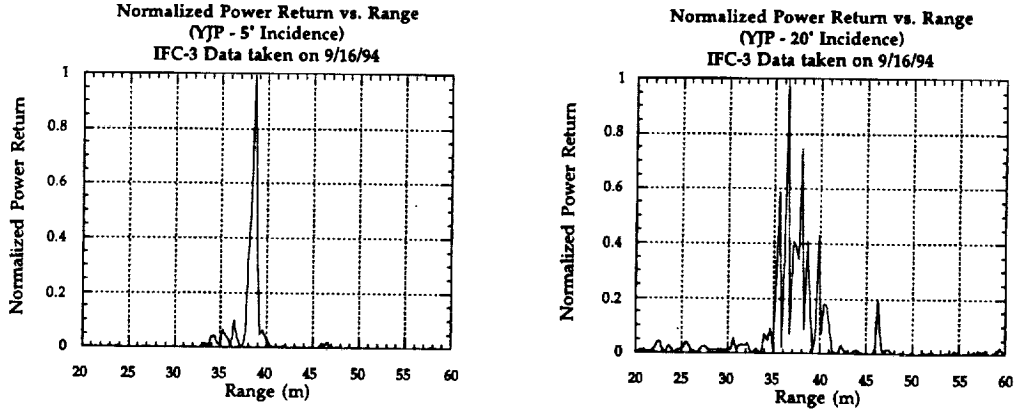

Figure 31. L-Band Normalized Power Return vs. Range at 5° and 20°

The data show a single spike at 5° incidence that is most likely the ground return preceded by smaller returns from the canopy. At 20° incidence, we see a spreading of the spectrum and the ground return no longer

dominates. Further processing is necessary before a more complete analysis of the IFC-3 data will be available.

Although the radar is currently working well, we have planned to make several additions to improve the system's ability to obtain a high quality data set. These additions along with conclusions are the subject of the next two sections.

Chapter 5 - Conclusions

Over the past year, we developed a three-frequency radar for use in backscattering studies over the boreal forest region in northern Canada. The radar is operated on board a UH-1 helicopter provided by NASA. During the summer of 1994, we participated in two IFCs as a part of the BOREAS project.

IFC-2 took place in July of 1994. The L-band portion of the radar was not operational during this experiment because of changes made in the design of the feed antenna. Therefore, we operated the radar at C and X band. We collected backscatter data in the SSA at the OJP, YJP, OA, and OBS sites. Although some of the data from this IFC are good, we experienced several system problems. As a result, we made improvements to the radar system in the time between IFC-2 and IFC-3.

The primary change that we made was to replace the IF amplifiers used in IFC-2 with higher gain amplifiers capable of driving a 50-Ω load. We also built a new control box that includes a switching power supply rather than the heavier series power supply that was used during IFC-2. We also built PCBs for the switch driver and the filters used in the system.

During IFC-3, we once again took measurements in the SSA. The L-band portion of the radar was operational at this time. We repeated the flight lines from IFC-2 paying special attention to the YJP site. The data taken during IFC-3 are good with the exception of those data sets taken when the amplifier was set to the highest gain.

Although the system was improved greatly for IFC-3, we still experienced some problems because of the long RF cables used to connect the RF box to the feed antennas. Also, the noise spike present at 12 kHz and the inability to operate the radar at the highest gain setting decreased the sensitivity of the radar during IFC-3. At present, we have rewired the RF

section of the radar and made further improvements to the IF amplifiers. As a result, the radar is performing better than ever before.

We plan to take the new radar system to the field in the summer of 1995. We will once again perform measurements at the SSA over the previously mentioned sites. The improvements that we have made to the radar over the past year will allow us to collect a superior data set for use in studying the canopy's interaction with microwave radiation. By using the data collected with this radar, we plan to develop scattering models that will allow us to estimate important geophysical parameters. These parameters include soil moisture and biomass.

Although the radar is fully functional at this point in time, we plan to make several additions to the system that will improve its functionality during the 1995 experiments.

Chapter 6 - Future Work

We collected data using the helicopter-borne radar during IFC-2 and IFC-3. The IFC-2 data are very difficult to interpret because of the numerous system problems that were present. Also, during IFC-2, the L-band RF section was not operational. After IFC-2, we repaired the radar and improved the data acquisition system. We also built a new L-band radar during this time. Therefore, the IFC-3 data set is easier to interpret and more complete. Although we did experience some problems during IFC-3, we feel that the data collected will be useful.

After IFC-3, we made further improvements to the radar system. As a result, the radar is now working better than it was during either of the IFCs. It is for this reason that we are attempting to organize another set of flights during the summer of 1995. Since the radar system is performing well and time still remains for system testing, we believe that a better data set can be collected. If our proposal is accepted, we will repeat the measurements made during IFC-3 using the radar in its improved state.

6.1 Improvements to the Radar System

Although the radar is fully functional at this point in time, we still would like to add several features to the system. These features will improve the radar's ability to provide accurate backscattering coefficient measurements. The following is a list of the improvements that we would like to make to the radar system. The list is not in the order of priority.

1. Use of a differential-mode GPS to determine the position of the helicopter
2. Add another inclinometer to the mount outside of the helicopter to provide information about the azimuth angle or build a more advanced antenna mount for this purpose
3. Add a delay line to the system for more accurate internal calibration
4. Temperature stabilize the RF box using a Minsco heater

5. Add gain setting switches so that each band can be controlled separately
6. Improve the data acquisition program
   a) Add the capability to sample at any frequency
   b) Real-time display of time domain data for all bands
   c) Faster transfer of data to storage medium
   d) Ability to process data in the field
7. Mount a video camera on the antenna structure and synchronize the clock with the GPS
8. Cut the antenna pattern for all three frequencies
9. Add two more BNC connectors to the front of the control box for monitoring X-band signals
10. Calibrate the digital panel meters (DPM) properly so that angle calibration does not have to be performed before flights
11. Purchase sturdy low-loss RF cables for the connecting RF box to the antennas
12. Calibrate the radar system using corner reflectors to allow for application of vector correction techniques to the data set
13. Put new IF amplifiers in the L-band section
14. Figure out why the highest gain setting of the IF amplifier will not work and repair the problem

References

[1] E. P. W. Attema, "The Active Microwave Instrument On-Board the ERS-1 Satellite," *Proceedings of the IEEE*, vol.79, no. 6, pp. 791-799, June 1991.

[2] *Avantek Data Book: Modular and Oscillator Components*, 2nd ed., pp. 14.62-14.64, 1990.

[3] I. J. Bahl and P. Bhartia, *Microstrip Antennas*, Dedham, MA: Artech House, Inc., pp. 31-80, 1982.

[4] C. A. Balanis, *Antenna Theory: Analysis and Design*, New York: Harper and Row, Publishers, Inc., pp. 604-605, 1982.

[5] M. G. Barbour, J. H. Burk, and W. D. Pitts, *Terrestrial Plant Ecology*, Menlo Park, CA.: Benjamin/Cummings Publishing Company, Inc, p. 221, 1987.

[6] D. K. Cheng, *Field and Wave Electromagnetics*, Norwood, MA: Addison-Wesley Publishing Co., p. 675, 1989.

[7] R. E. Collin, *Foundations for Microwave Engineering*, New York: McGraw-Hill, Inc., pp. 194-200, 1992.

[8] *EOS AM Spacecraft: A Key Component of the U. S. Global Change Research Program*, Washington, D.C.: U. S. Government Printing Office, 1994.

[9] S. Franco, *Design with Operational Amplifiers and Analog Integrated Circuits*, New York: McGraw-Hill, Inc., pp. 592-621, 1988.

[10] S. Haykin, *An Introduction to Analog and Digital Communications*, New York: John Wiley & Sons, Inc., pp. 603-622, 1989.

[11] A. W. Love (ed.), *Electromagnetic Horn Antennas*, New York: IEEE Press, pp. 88-89, 1976.

[12] K. J. Ranson and G. Sun, "Mapping Biomass of a Northern Forest Using Multifrequency SAR Data," *IEEE Trans. on Geoscience and Remote Sensing* vol. 32, no. 2, pp. 388-396, March 1994.

[13] P. A. Rizzi, *Microwave Engineering: Passive Circuits*, Englewood Cliffs, New Jersey: Prentice-Hall, Inc., pp. 201-206, 1988.

[14] D. Roddy, *Microwave Technology*, Englewood Cliffs, New Jersey: Prentice-Hall Inc., pp. 499-503, 1986.

[15] A. W. Rudge and N. A. Adatia, "Offset-Parabolic-Reflector Antennas: A Review," *Proceedings of the IEEE*, vol. 66, no. 12, pp.1592-1618, December 1978.

[16] W. H. Schlesinger, *Biogeochemistry: An Analysis of Global Change*, New York: Academic Press, pp. 135-137, 1991.

[17] A. S. Sedra and K. C. Smith, *Microelectronic Circuits*, Chicago, IL: Holt, Rhinehart and Winston, pp. 646-697, 1991.

[18] P. J. Sellers, "Canopy Reflectance, Photosynthesis, and Transpiration," *International Journal of Remote Sensing*, vol. 6, pp. 1335-1372, 1985.

[19] P. J. Sellars, F. G. Hall, D. Baldocchi, J. Cihlar, P. Crill, J. Den Hartog, B. Goodison, R. D. Kelly, D. Lettenmeier, H. Margolis, J. Ranson and M. Ryan, *Experiment Plan: Boreal Ecosystem-Atmosphere Study*, NASA-GSFC, pp. 1-3, 1994.

[20] S. Silver (ed.), *Microwave Antenna Theory and Design*, London, UK: Peter Peregrinus, Ltd., p. 195-Table 6.2, 1984.

[21] M. I. Skolnik, *Introduction to Radar Systems*, New York: McGraw-Hill, Inc., pp. 82-92, 1980.

[22] P. P. Tans, I. Y. Fung. and T. Takahashi, "Observational Constraints on the Global Atmospheric CO_2 Budget," *Science*, vol. 247, pp. 1431-1438, 1990.

[23] F. T. Ulaby, R. K. Moore, and A. K. Fung, *Microwave Remote Sensing: Active and Passive* , Vol. III, Norwood, MA.: Artech House, pp. 1262-1263, 1986.

[24] S. L. Ustin, M. O. Smith, and J. B. Adams, "Remote Sensing of Ecological Processes: A Strategy for Developing and Testing Ecological Models Using Spectral Mixture Analysis," Chapter 19 in *Scaling Physiological Processes: Leaf to Globe*, J. R. Ehleringer and C.B.Fields,eds., New York: Academic Press, pp. 339-357, 1993.

Appendix 1

Antenna System Information

TRUE FOCUS OFFSET REFLECTOR SPECIFICATIONS

DISH DIAMETER	DIMENSION "A"	DIMENSION "B"
(.75 M) 30.0 IN	18.3 IN	30.5 IN
(.90 M) 36.0 IN.	21.96 IN.	36.75 IN.
(1.0 M) 42.0 IN.	25.62 IN.	42.31 IN.
(1.2 M) 48.0 IN.	29.28 IN.	48.87 IN.

PARENT DISH F/D .305
OFFSET REFLECTOR F/D .610

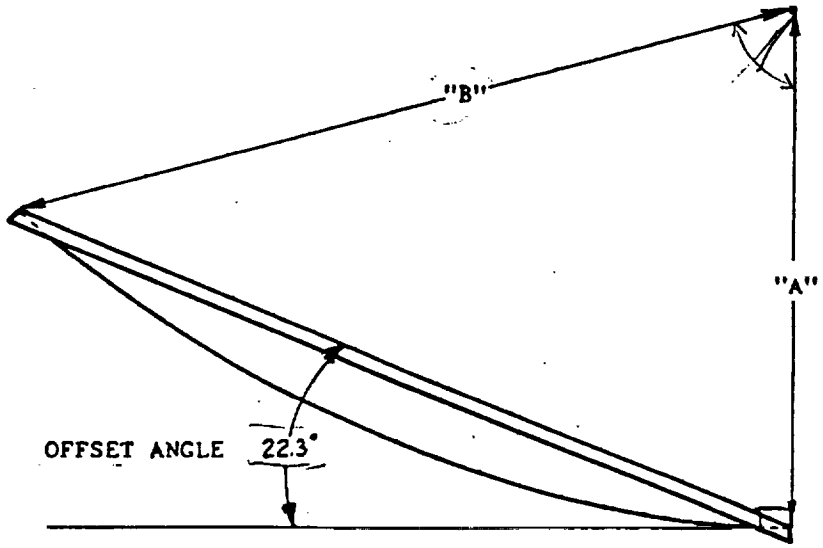

REPORT 9116-710

SUMMARY OF TEST DATA

ANDERSEN MANUFACTURING
36" (.9M) KU-BAND OFFSET ANTENNA

FREQUENCY:	11.7	11.95	12.2	GHz
PEAK GAIN:	39.1	39.65	39.75	dBi
EFFICIENCY, NET (*):	65	70	69	%
BEAMWIDTHS (3dB):				
AZIMUTH	1.9	1.9	1.8	( )
ELEVATION	1.9	1.9	1.8	( )
CROSSPOLARIZATION: MAXIMUM WITH 1 dB CO-POLAR BEAMWIDTH	24.2	21.3	22.1	dB
SIDELOBES: MAXIMUM IN AZ. OR EL.	24.0	24.5	24.6	dB

(*) NET EFFICIENCY IS BASED ON ACTUAL REFLECTOR DIAMETER USING THE GAIN MEASURED AT THE WR-75 FEEDHORN WAVEGUIDE FLANGE.

NOISE TEMPERATURE AND G/T:

ELEVATION ANGLE ( )	ANTENNA NOISE TEMPERATURE	G/T dB/K
30	28K	18.3
40	26	18.3
50	24	18.4

G/T ASSUMES A LNA WITH A 1.4 dB NOISE FIGURE, AMBIENT OF 290K AND CLEAR SKY CONDITIONS.

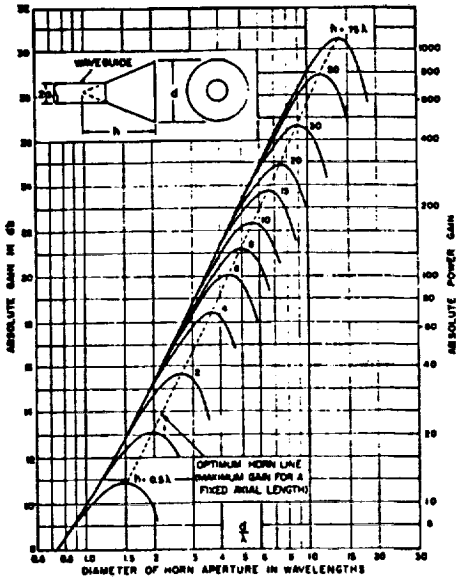

Fig. 6. Absolute gain of a conical horn as a function of physical dimensions.

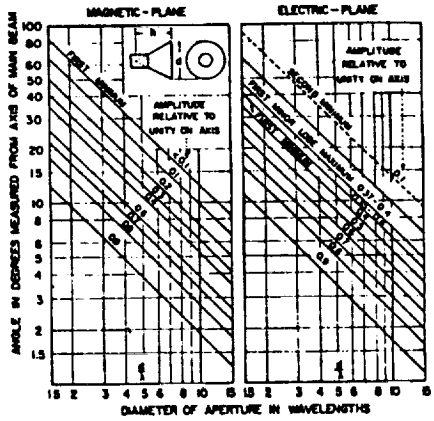

Fig. 8. Monograph for plotting the radiation characteristics for conical horns of optimum design.

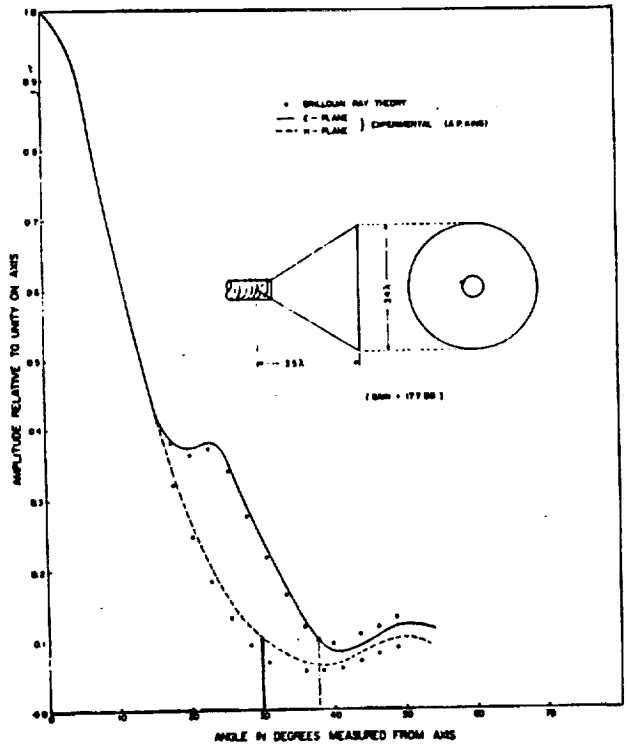

Fig. 7. Radiation pattern of a conical horn.

Compute θ_o & θ^* :

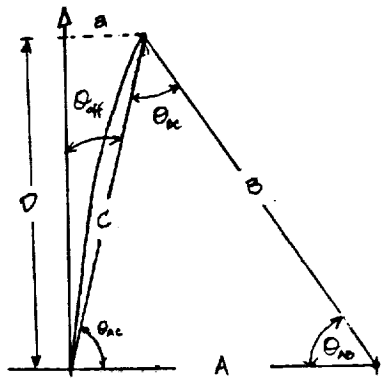

A = 21.96"

B = 96.75"

D = 36"

θ_{off} = 22.3°

A/D = .61ϕ ✓

[for "parent" $f/D_p = .345$
$\therefore D_{p/2} = A$ & we have half of the dish]

① Find a

$\tan\theta_{off} = a/D$

a = 14.76"

② Find θ_{AB}

$\sin\theta_{AB} = D/B$ $\quad \theta_{AB} = 78.7°$

Using A&P Magazine (Stutzman & Terada) notation ....

$\psi_L = \phi°$

$\psi_s = 78.7°/2 = 39.35°$

$\psi_B = 39.35°$ (choose $\psi_f = \psi_B$)

X-band (10 GHz) $\lambda = 3\text{ cm} = 1.181''$

$\left(\frac{36''}{1.181''} = \underline{30.5}\right)$

For our case $(h/D) = \phi$ (b/c $h = \phi$)

$D \cong 30.48\lambda$

$F/D_p = .305$

$$\Delta F_T = 10 \log \left\{ \frac{\cos(0°)}{\cos(39.35°)} \right\} + \Delta F_I \quad \text{(choose } \phi\text{)}$$

$\Delta F_T = 1.47\text{ dB}$

$2\psi_s = (78.7° - \phi°) = 78.7°$

Now, find feed pattern .... ⇒ [This applies to finding optimal pointing angle ψ_f.]

★ Conical Horn w/ 10 dB Beamwidth of 78.7°

(FEB) "Electromagnetic Horn Antennas"

⇓

Fig 7.

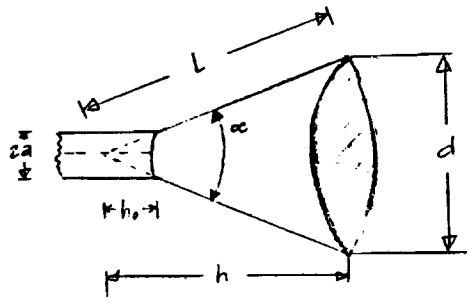

$h_o = 2.058\,cm$

$$\begin{bmatrix} d = 3.4\lambda \\ h = 3.5\lambda \end{bmatrix}$$

for X-band

$d = 3.4\,(3.0\,cm) = 10.2\,cm = 4.016"$ ✓

$h = 3.5\,(3.0\,cm) = 10.5\,cm = 4.134"$ ✓

$\alpha = ?$ $\quad \tan(\alpha/2) = \frac{d/2}{h} \rightarrow \alpha = 51.8°$

$L = ?$ $\quad \sin(\alpha/2) = \frac{d/2}{L} \rightarrow L = 11.67\,cm = 4.596"$

• 9.5 GHz to 10.5 GHz
(3.158 cm to 2.859 cm)

$\lambda_{c,11} = 3.41a$ (TE_{11})

$$f_{c,11} = \frac{c}{3.41a} = \frac{299792539.5894}{a} = 9.3\times10^{9}\,GHz$$

$a = 9.4598\times10^{-3}\,m$

$2a = 1.892\,cm$ ✓ ⟶ (1st Try)

$$k_{c,11}(TE_{11}) = 1.841/a = 1.841/9.4598\times10^{-3}\,m$$

$$k_{c,11} = 194.613$$

Attenuation

$$\alpha = \frac{R_M}{a Z_0}\left[1 - \frac{1.841^2}{k_0^2 a^2}\right]^{-1/2}\left(\frac{1.841^2}{k_0^2 a^2} + 0.4165\right)$$

$$k_0 = \omega\sqrt{\mu_0\varepsilon_0} = 2\pi f\sqrt{\mu_0\varepsilon_0}$$

$$= 2\pi f\,(3.3356) \quad \text{(Chang)}$$

$$\sigma_{brass} = 1.57\times10^{7}$$

(in GHz)

$$R_M(brass) = \left(\omega\mu/\sigma\right)^{1/2} = \left(\frac{2\pi f[4\pi\times10^{-7}\,H/m]}{1.57\times10^{7}}\right)^{1/2}$$

$$= \sqrt{f}\,[2.243\times10^{-2}]$$

↳ f in GHz

α ⇒ attenuation

[Plug in Matlab] ⟹ 2 Hached as 4a w/ a = 1 cm

$$\alpha = \frac{(2.243\times10^{-2})\sqrt{f}}{1.892\times10^{-2}/2}\left[1 - \frac{1.841^2}{\left[2\pi f(3.3356)(1.892\times10^{-2}/2)\right]^2}\right]^{-1/2}\left[\frac{1.841^2}{[2\pi f\ldots]^2} + 0.4165\right]$$

(120π) = Z_0

★ f in GHz

$$\lambda_{c,01}(TM_{01}) = \frac{2\pi(1.892\times10^{-2})}{(2.405)2} = \frac{4.943\times10^{-2}}{2} \Rightarrow$$

$f_{c,01}(TM_{01}) = 12.14$ GHz ✓ ⟹ [Next higher order Mode]

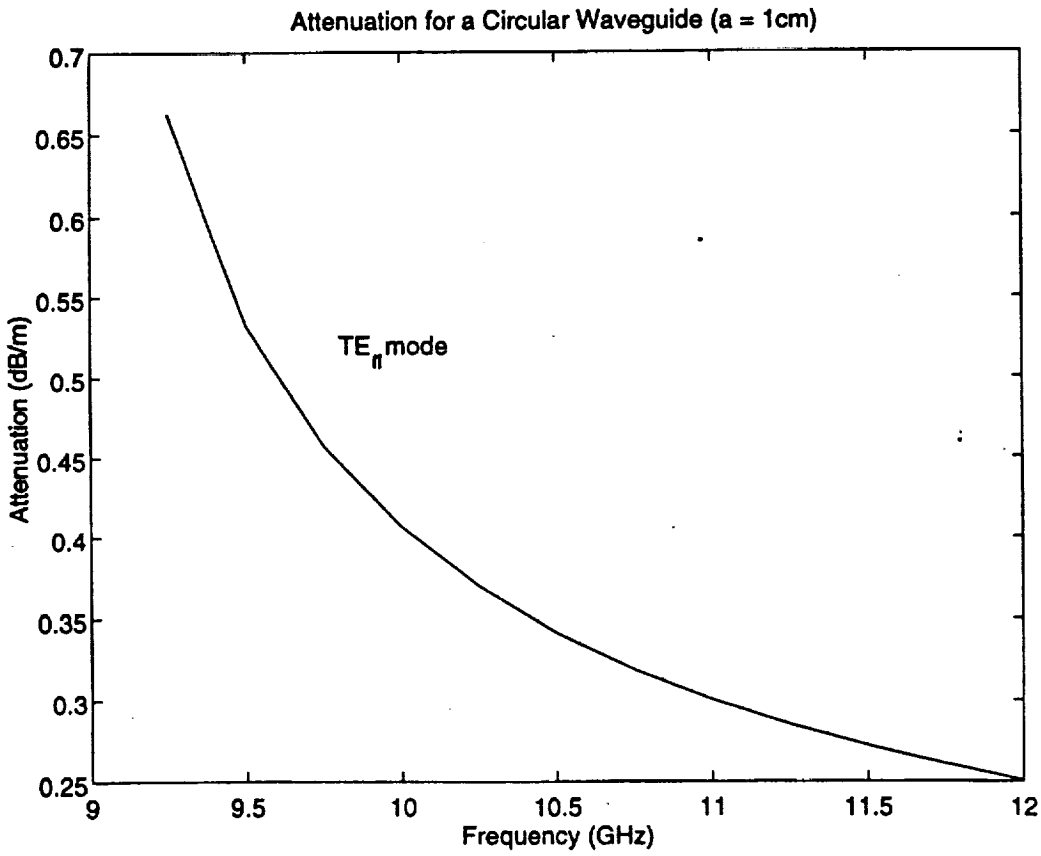
Attenuation for a Circular Waveguide (a = 1cm)
Attenuation (dB/m)
0.7
0.65
0.6
0.55
0.5
0.45
0.4
0.35
0.3
0.25
TE11 mode
9
9.5
10
10.5
11
11.5
12
Frequency (GHz)

$$\left\{ \begin{array}{l} 2\pi f\,(3.3356)(9.4598\times10^{-3}) = 1.841 \\ \quad f = 1.841/(2\pi\cdot 3.3356\cdot 9.4598\times10^{-3}) \\ \quad \langle f = 9.206 \rangle \end{array} \right\} \text{ ASIDE}$$

$a = 9.4598\times10^{-3}$ M gives too much atten. @ 9.5 GHz for Bross

Try $a = 10\times10^{-3}$ M = 1cm (page 4a)

Gives ⇒ $\alpha = .5327$ dB/M @ 9.5 GHz

$\alpha = .3419$ dB/M @ 10.5 GHz

$$\lambda_{c,01}(TM_{01}) = \frac{2\pi(1\times10^{-2}M)}{2.405} = 2.613\times10^{-2}M$$

$$f_{c,01}(TM_{01}) = \underline{11.48\ GHz}\ \checkmark\ (\underline{good})$$

(10.25GHz) $$\lambda_g = \frac{\lambda_0}{\sqrt{1 - f_c^2/f^2}}$$

$$f_{c,11} = \frac{3\times10^8\ M/s}{3.41(1\times10^{-2}M)} = 8.80\ GHz$$

$$\lambda_g(10.25\ GHz) = \frac{2.927\times10^{-2}M}{\sqrt{1 - (8.8/10.25)^2}} = 5.708\ cm\ \checkmark$$

For C-band

Same dimension horn...

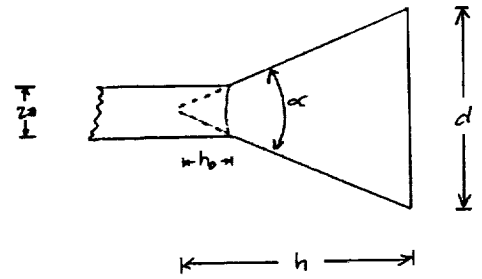

$d = 3.4\lambda$
$h = 3.5\lambda$
} dimensions from p. EE "Electromagnetic Horn Antennas" {included as p. 38}

$f_c = 5.5$ GHz

$$\lambda = \frac{3\times10^8}{5.5\times10^9} = 5.455\times10^{-2}\ m$$

$d = 3.4\lambda = 18.55$ cm $= 7.301$"

$h = 3.5\lambda = 19.09$ cm $= 7.516$"

$\alpha = 51.8°$

$h_0 = ?$ → depends on a

$h_0 = \frac{a}{\tan(\alpha/2)}$ → $a = 3.644$ cm $= 1.4349$"

- Circular Waveguide (5.0 GHz to 6.0 GHz)

$\lambda_{c,11}(TE_{11}) = 3.41a$ → from Collins

$$f_{c,11} = \frac{3\times10^8}{3.41a} = 4.75\ GHz$$

$a = 1.852$ cm ⇒ 1st try

$$\alpha = \frac{R_M}{a Z_0}\left[1 - \frac{1.841^2}{k_0^2 a^2}\right]^{-1/2}\left[\frac{1.841^2}{k_0^2 a^2} + \phi.4185\right]$$

for TE_{11} from Collin

$$k_0 = 2\pi f (3.3356) \quad [f \text{ in GHz}]$$

$$R_M(\text{brass}) = \left(\frac{\omega\mu}{\sigma}\right)^{1/2} = \sqrt{f}\,(2.243\times 10^{-2}) \quad [f \text{ in GHz}]$$

(1.57×10^7) Brass

$$\alpha = \frac{(2.243\times 10^{-2})\sqrt{f}}{a\,(12\phi\pi)}\left[1 - \frac{1.841^2}{[2\pi f(3.3356)a]^2}\right]^{-1/2}\left[\frac{1.841^2}{[\,\cdot\,]^2} + .4185\right]$$

- Put in MATLAB → α looks OK (check for $f_{c,01}$)

α (5 GHz) = .2644 dB/M ✓

α (6 GHz) = .1164 dB/M ✓

Find next mode (1st higher order mode) [TM_{01}]

$\lambda_{c,01} = \frac{2\pi(1.852\text{ cm})}{2.405} = 4.838\text{ cm}$ $\quad f_{c,01} = 6.2$ GHz

$\lambda_{c,01} = 4.615$ cm

Too low !!

2nd try $a = 1.77$ cm → $f_{c,11} = 4.97$ GHz, $f_{c,01} = 6.5$ GHz } α on 7a

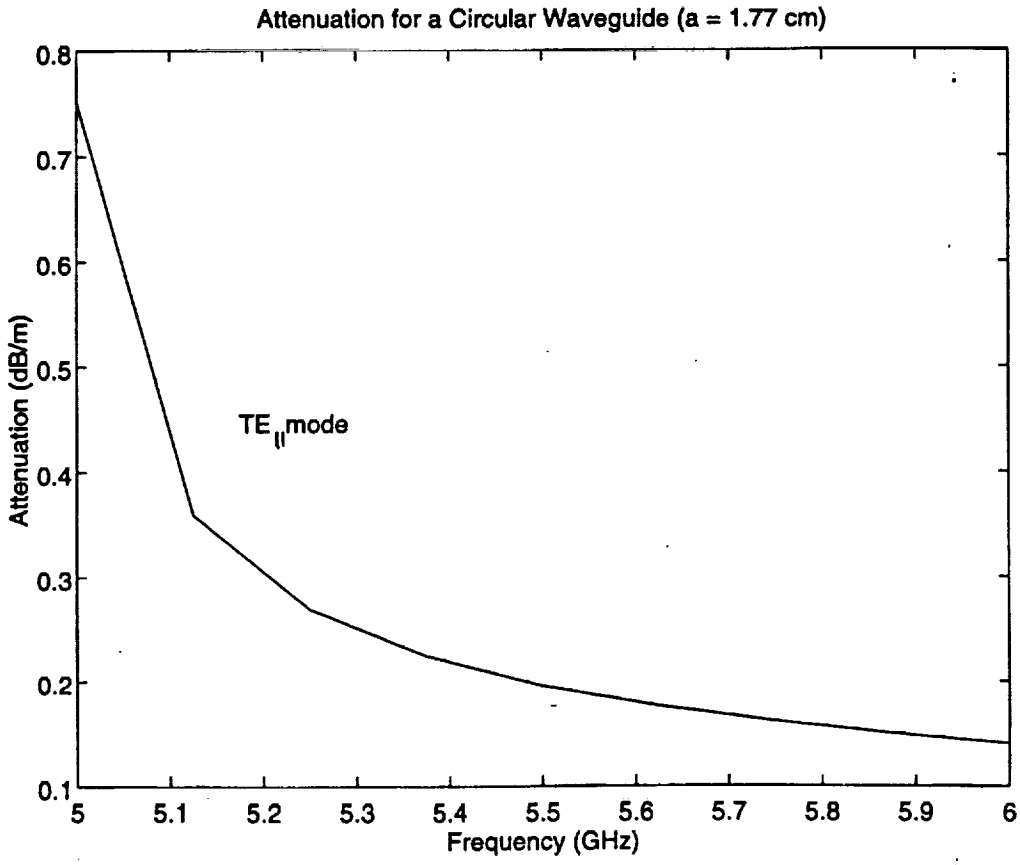
Attenuation for a Circular Waveguide (a = 1.77 cm)
Attenuation (dB/m)
Frequency (GHz)
TE11 mode
0.8
0.7
0.6
0.5
0.4
0.3
0.2
0.1
5
5.1
5.2
5.3
5.4
5.5
5.6
5.7
5.8
5.9
6

For $\lambda = 1.77$ cm

$$\alpha\,(5\text{GHz}) = .7527 \text{ dB/M}$$
$$\alpha\,(6\text{GHz}) = .1443 \text{ dB/M}$$

The guide wavelength is ...

$$\lambda_g = \frac{\lambda_0}{\sqrt{1 - f_c^2/f^2}}$$

$$\lambda_g(5.5\text{GHz}) = \frac{5.455 \times 10^{-2}\,\text{M}}{\sqrt{1 - \frac{(4.97)^2}{(5.5)^2}}}$$

$$\lambda_g = 12.736 \text{ cm} = 5.0143''$$

The next step is to calculate the bandwidth that we can get .

$$\varepsilon_o := 8.854 \cdot 10^{-12} \qquad \mu_o := 4 \cdot \pi \cdot 10^{-7} \qquad \lambda_o := \frac{c}{f_r} \qquad loss\_tan := .0005$$

$$k_o := 2 \cdot \pi \cdot f_r \cdot \sqrt{\varepsilon_o \cdot \mu_o} \qquad k_o = 31.437$$

$$I_1 := \int_0^{\pi} \left(\sin\left(\frac{k_o \cdot W\_calc \cdot \cos(\theta)}{2} \right) \right)^2 \cdot (\tan(\theta))^2 \cdot \sin(\theta)\, d\theta$$

$$I_1 = 1.798511$$

$$Q_r := \frac{c \cdot \sqrt{\varepsilon_e}}{4 \cdot f_r \cdot h} \qquad Q_r = 7.585$$

$$R_c := .00027 \cdot \sqrt{\frac{f_r}{10^9}} \cdot \frac{L}{W\_calc} \cdot Q_r^2 \qquad R_c = 0.014625$$

$$R_d := \frac{30 \cdot loss\_tan}{\varepsilon_r} \cdot h \cdot \frac{\lambda_o}{L \cdot W\_calc} \cdot Q_r^2 \qquad R_d = 0.152794$$

$$R_r := \frac{120 \cdot \pi^2}{I_1^2} \qquad R_r = 366.146$$

$$Rr\_prime := \frac{R_r}{2}$$

$$Q_T := \frac{Q_r \cdot (Rr\_prime + R_d)}{Rr\_prime} \qquad Q_T = 7.591$$

$$s := 2$$

$$BW := \frac{s - 1}{Q_T \cdot \sqrt{s}} \qquad BW = 0.093$$

This shows that we can only get a 3% bandwidth with the thickest substrate that we can get from Rogers (meaning a standard thickness). To obtain the desired bandwidth we would need to use a substrate with a 410 mil thickness. As of June 19, 1994, three substrates have been obtained (125,125,93) and they will be stacked to obtain better bandwidth than the 125 mil slab alone (about 8.7% can be obtained ideally).

$\varepsilon_r := 2.33$ $f_r := 1500 \cdot 10^6$ $c := 3 \cdot 10^8$

$$W\_calc := \frac{c}{(2 \cdot f_r)} \cdot \frac{1}{\sqrt{\frac{\varepsilon_r + 1}{2}}}$$ *Equation 2.66 in Bahl and Bhartia (page 57)

W_calc = 0.077

This width is given in meters and needs to be converted to mils

con_factor := 39370.0787402 *Conversion factor (meters to mils)

W_mil := W_calc · con_factor

$W\_mil = 3.051 \cdot 10^3$

h_mil := 375

$$h := \frac{h\_mil}{con\_factor}$$

h = 0.009525

The effective dielectric constant is calculated using equation 2.31 (page 46)

$$\varepsilon_e := \left[\frac{\varepsilon_r + 1}{2} + \frac{\varepsilon_r - 1}{2} \cdot \left(\frac{1}{\sqrt{1 + 12 \cdot \frac{h}{W\_calc}}} \right) \right]$$ $\varepsilon_e = 2.088$

Now, calculate the line extension using equation 2.32 (page 46)

$$\Delta l := \frac{.412 \cdot h \cdot (\varepsilon_e + .3) \cdot \left(\frac{W\_calc}{h} + .264 \right)}{(\varepsilon_e - .258) \cdot \left(\frac{W\_calc}{h} + .8 \right)}$$ $\Delta l = 0.004814$

Using the effective dielectric constant and the line extension, we can calculate the length of the resonant element using equation 2.67 (page 57)

$$L := \frac{c}{2 \cdot f_r \cdot \sqrt{\varepsilon_e}} - 2 \cdot \Delta l$$ $L = 0.059581$

Next...convert the length of the element to mils

L_mil := L · con_factor $L\_mil = 2.346 \cdot 10^3$

Linearly Polarized Log-Periodic Antennas

- 20 MHz TO 18 GHz FREQUENCY COVERAGE
- BROADBAND
- NEAR CONSTANT GAIN AND BEAMWIDTH

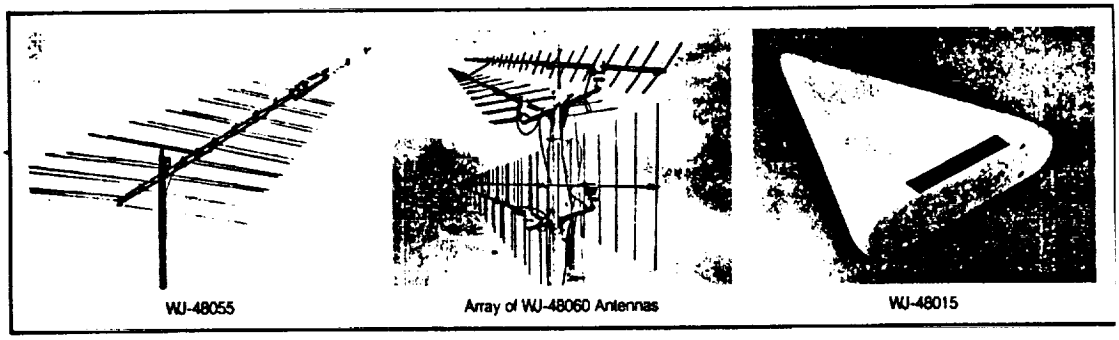

WJ-48055 | Array of WJ-48060 Antennas | WJ-48015

WJ-48050 and WJ-48100 Series. These standard log-periodic antennas cover the frequency range from 20 MHz up to 1100 MHz. All models are linearly polarized and matched to 50 ohms. These antennas are designed for receiving applications, and are capable of handling moderate transmitter power.

All the antennas in this series are constructed with stainless-steel spars and stainless-steel radiators, the longer of which are threaded for easy assembly and disassembly. Such construction makes them equally practical for portable uses as well as fixed installations. Log-periodic design results in electrical properties that are nearly independent of frequency. The WJ-48075 demonstrates the low VSWR of these log-periodics; its VSWR never exceeds 2:1 as measured from 225 to 1100 MHz. Uniformity of the pattern characteristics of the WJ-48050 Series antennas is illustrated by the radiation patterns for the WJ-48055 which are taken at 30, 100, 500, and 1000 MHz. Gain for all antennas in this series also remains near a constant value of 8 dB.

WJ-48000 Series. The WJ-48000 Series consists of four linearly polarized antennas: the WJ-48005 for the frequency range from 1 to 12.4 GHz, the WJ-48010 from 0.5 to 12.4 GHz, the WJ-48015 from 1 to 18 GHz and the WJ-48020 from 0.5 to 18 GHz. These antennas are specifically designed to illuminate parabolic reflectors. They are fabricated by high-precision techniques and are completely enclosed by foam-filled outer fiberglass housings.

The radiating structure of the WJ-48000 Series of antennas has been painstakingly adjusted to obtain outstanding electrical performance. Radiation patterns remain nearly constant from 1 to 18 GHz, yielding an average illumination taper of 10 dB for reflectors with F/D ratios of approximately 0.4.

PHYSICAL SPECIFICATIONS

Model Number	"A" in. (cm)	"B" in. (cm)	"C" in. (cm)	"D" in. (cm)	"E" in. (cm)	Weight lb. (kg.)	MTG Hdw	Connector Type
WJ-48005	9 (23)	7 (18)	4.875 (12.38)	1.250 (3.18)	1.78 (4.52)	0.6 (0.3)	8-32	N Female
WJ-48010	17 (43.1)	13.75 (35.9)	12 (30.48)	2 (5.08)	3 (7.62)	2.7 (1.2)	¼-28	N Female
WJ-48015	9.6 (24.4)	7.7 (19.6)	4.875 (12.38)	1.250 (3.18)	1.95 (4.95)	0.7 (.32)	8-32	3mm Female
WJ-48020	17 (43.1)	13.75 (35.9)	12 (30.48)	2 (5.08)	3 (7.62)	2.7 (1.2)	¼-28	3mm Female
WJ-48055	245 (622)	204 (518)				93 (42)	*	N Female
WJ-48060	78 (198)	67 (169)				20 (9)	*	N Female
WJ-48065	31 (79)	24 (62)				4 (2)	*	N Female
WJ-48070	156 (396)	130 (331)				60 (27)	*	N Female
WJ-48075	37 (94)	28 (71)				5 (2.3)	*	N Female
WJ-48105	244 (620)	205 (520)				132 (60)	*	N Female

*Outline drawings furnished on request.

OUTLINE DRAWINGS

WJ-48000 Series

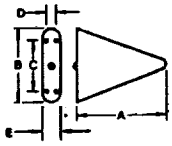

WJ-48050 and WJ-48100 Series

PERFORMANCE SPECIFICATIONS

Model Number	Frequency Range	VSWR (Max.)	Gain (Nom.)	Polarization	F-to-B Ratio	Cross Polarization (Min.)	CW Power*
WJ-48005	1.0-12.4 GHz	2.5:1	8 dB	Linear	18 dB	15 dB (1-8 GHz)	30w
WJ-48010	0.5-12.4 GHz	2.5:1	8 dB	Linear	18 dB	15 dB (0.5-8 GHz)	30w
WJ-48015	1.0-18.0 GHz	2.5:1	8 dB	Linear	18 dB	10 dB	5w
WJ-48020	0.5-18.0 GHz	2.5:1	8 dB	Linear	18 dB	10 dB	5w
WJ-48055	30-1100 MHz	2.25:1	8 dB	Linear	20 dB Above 35 MHz	15 dB	400w
WJ-48060	90-1100 MHz	2.25:1	8 dB	Linear	20 dB Above 110 MHz	15 dB	400w
WJ-48065	250-1100 MHz	2:1	8 dB	Linear	20 dB Above 300 MHz	15 dB	400w
WJ-48070	50-1100 MHz	2.25:1	8 dB	Linear	20 dB Above 60 MHz	15 dB	400w
WJ-48075	225-1100 MHz	2:1	8 dB	Linear	20 dB Above 250 MHz	15 dB	400w
WJ-48105	20-1000 MHz	2.5:1	6 dB	Linear	15 dB	12 dB	200w

*The CW power rating specified is the feeder power rating reduced 6 dB for safety factor and taken at the highest operating frequency. Conditions assumed are sea level and +40°C ambient operation. Antennas with higher power ratings are available.

RADIATION PATTERNS

WJ-48055 (Scale: 0 to 100% Voltage)

WJ-48005 (Scale: 10 dB/Division)

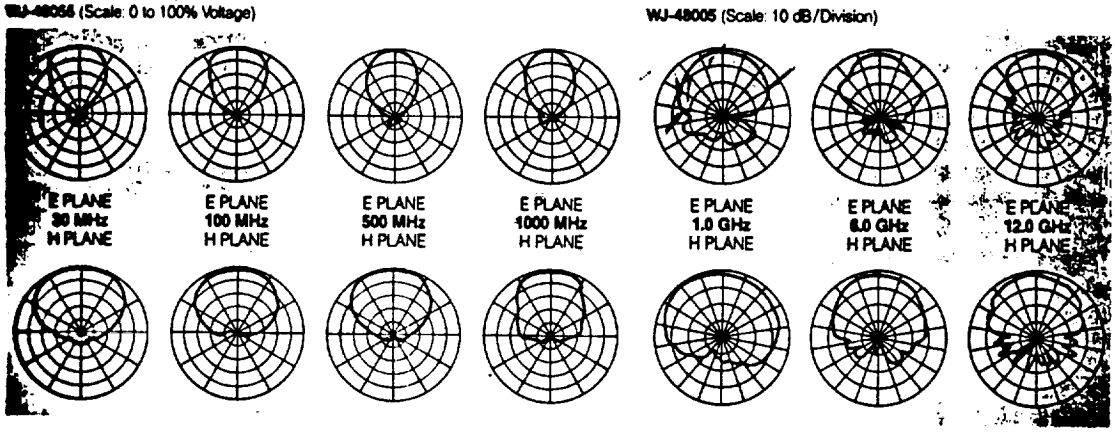

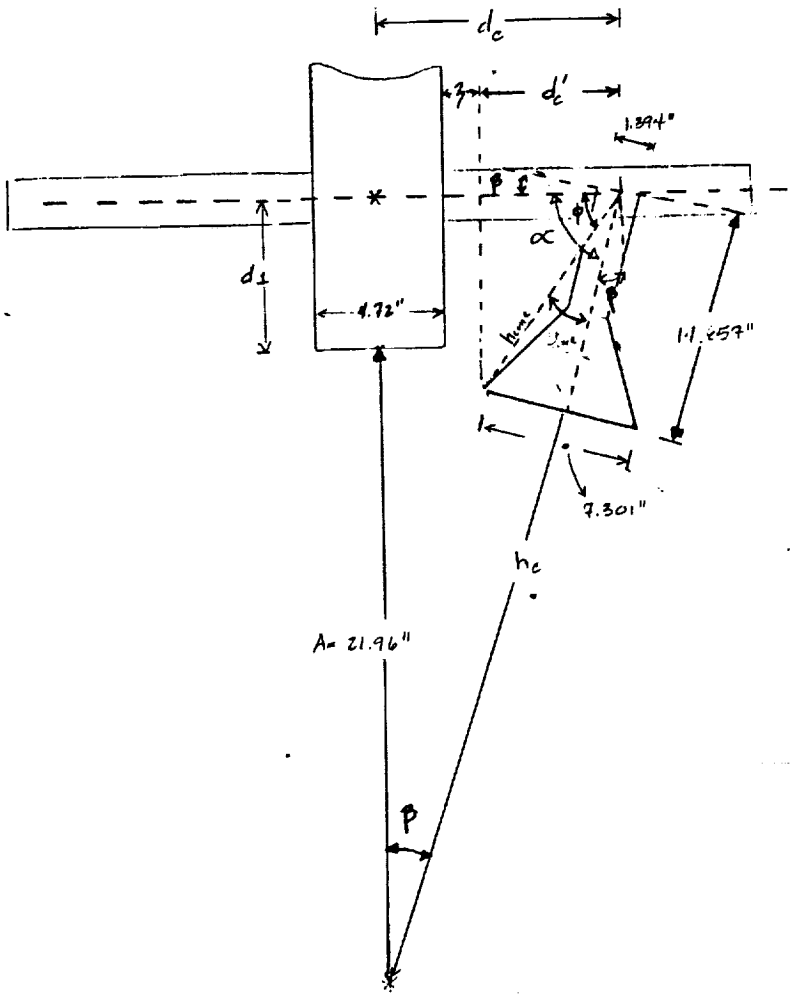

$d_c = 2.36" + \eta + d_c'$

① Choose d_1

② Choose d_c which causes η to be small (iterate)

1ST iteration

$d_1 = 6''$

$d_c = 10''$

$$\tan\alpha = \frac{d_1 + A}{d_c} = \frac{27.96''}{10''} \Rightarrow \alpha = 70.32°$$

$$\beta = 19.68°$$

$$\tan\Theta_{cone} = \left(\frac{7.301''}{2}\right) / 14.857''$$

$$\Theta_{cone} = 13.805°$$

$$\phi = 56.52°$$

$$\sin\Theta_{cone} = \left(\frac{7.301''}{2}\right) / h_{cone}$$

$$h_{cone} = \left(\frac{7.301''}{2}\right) / \sin(13.805°)$$

$$h_{cone} = 15.298''$$

$$\cos\phi = d_c' / h_{cone} \quad ; \quad d_c' = 15.298''\,(\cos(56.52°))$$

$$d_c' = 8.44''$$

$$\therefore d_c = 2.36'' + \eta + 8.44'' = 10.8'' > 10''$$

$\therefore$ We must increase our initial guess of d_c

2nd iteration

$d_1 = 6''$

$d_c = 10.75''$

⇨ put on MATLAB & did iterations

FINAL VALUES: $d_c' = 8.955''$

$\beta = 22.0236°$

$\alpha = 67.9764°$

* see note on next page

- d_1 can now be independently adjusted so that the horns can be adjusted throughout the possible range of phase center values
  (apex for large flare, aperture for small flare)

- I chose $d_1 = 3.65''$ so the X-band (most critical) can be adjusted throughout the range of possible phase center values

  L-band is rigidly mounted & X and C band have brackets for phase center adjustments

* actually used
  d_c new = 11.9689
  $\alpha = 64.89°$
  $\beta = 25.10°$
  $\phi = 51.09°$

Appendix 2
RF Section Information

Installation

Bias voltage should be within ± 0.2 volts of the correct value to obtain specified operation. At 2 or 3 volts above the correct value the Zener diode, placed in the bias circuit to provide protection, will begin to draw excess current.

CAUTION: If the bias current exceeds the maximum bias current shown on the data sheet by as much as 50 milliamperes, the protective Zener will be endangered. For GaAs oscillators, a current peak up to 200 mA higher than the value recorded on the data sheet may be observed at low (-2 to -4V dc) negative bias levels, however.

If excess current is drawn, check for high bias voltage or reversed bias polarity.

Heaters

Heaters are often included in the oscillator to minimize such temperature effects as frequency drift and power output variation. These heaters are self-regulating and may be operated from an unregulated voltage within the range of 22 to 30 volts. Transients of up to 80 volts in accordance with Figure 6 of MIL-STD-704-A will not normally damage the heater.

Mounting

The oscillator may be mounted in any orientation. The unit (particularly units that tune above 4 GHz) should be mounted to a smooth heat sink capable of dissipating up to 10 watts without raising the temperature at the base of the unit adjacent to the heat sink above the specified operating temperature range. (Use of heat sink compound (e.g., Dow Corning 340) is recommended on mounting surface).

YIG-TUNED GaAs OSCILLATOR

Type No.: 5157-3000 Serial No.: 1027 (ER)

Operating Conditions:

Heater Voltage:	+28.0 Vdc	Current:	180 mA at -54° C
Bias Voltage:	±18.00 Vdc	Current:	1050/500 mA

Test Data:

Tuning Vdc	Calculated Frequency (GHz)	Δ Frequency (MHz) +25° C	Power Output (mw) +25° C
0	8.00	0	30
1	9.00	-10	58
2	10.00	-13	62
3	11.00	-10	68
4	12.00	- 6	64
5	13.00	- 3	46
6	14.00	- 2	49
7	15.00	+ 1	41
8	16.00	+ 2	29
9	17.00	+ 1	21
10	18.00	-3	19

Hysteresis: 11 MHz

YIG-TUNED GaAs OSCILLATOR

Type No: 5157-300 DF Serial No: 1092

Operating Conditions:

Heater Voltage:	+28.0 Vdc	Current:	170 mA
Bias Voltage:	+18.00 Vdc	Current:	500 mA

Test Data:

Tuning Vdc	Calculated Frequency (GHz)	Δ Frequency (MHz) +25° C	Power Output (mw) +25° C
0	8.00	0	24.0
1	9.00	+ 1	38.0
2	10.00	+ 9	38.0
3	11.00	+ 7	54.0
4	12.00	+ 9	54.0
5	13.00	+13	44.0
6	14.00	+ 9	48.0
7	15.00	+16	35.0
8	16.00	+10	31.0
9	17.00	+ 5	28.0
10	18.00	0	19.0

Hysteresis: 8.0 MHz

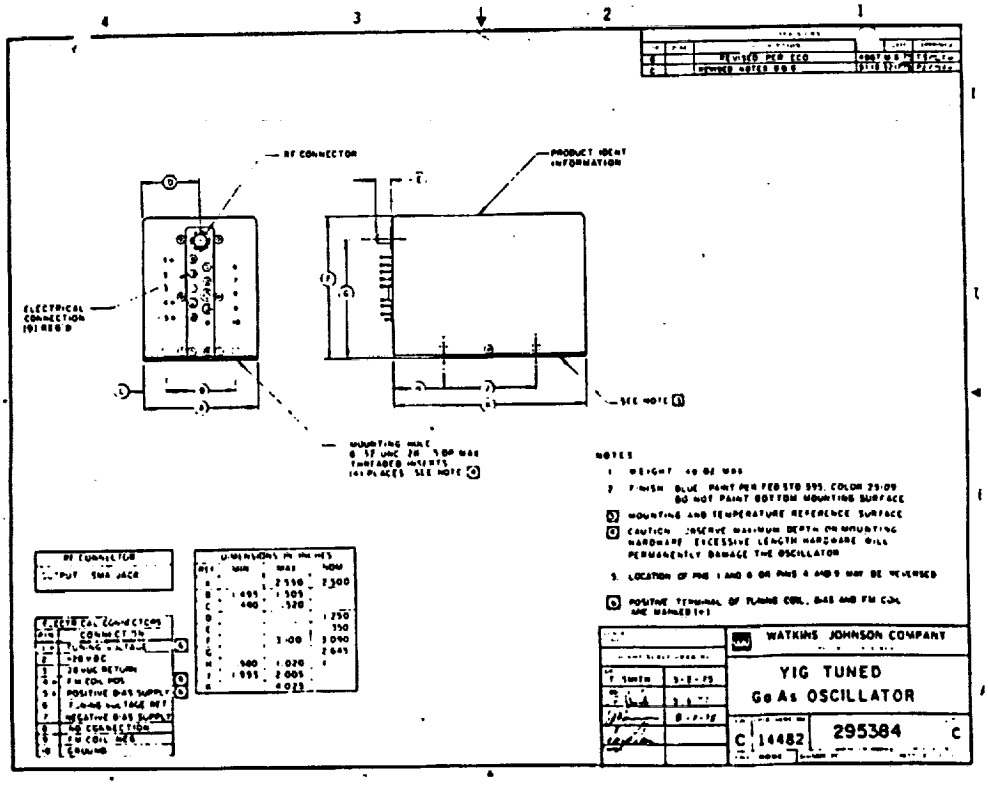

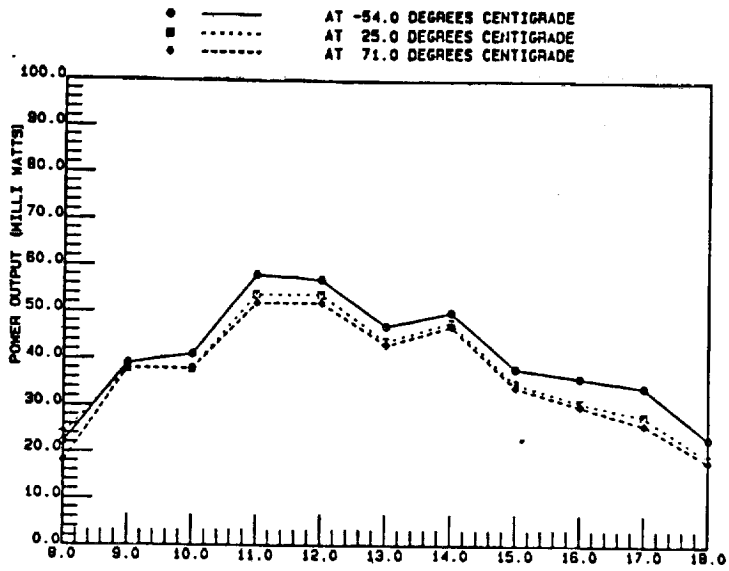

POWER OUTPUT, YIG-OSCILLATOR MODEL# 5157-3000F

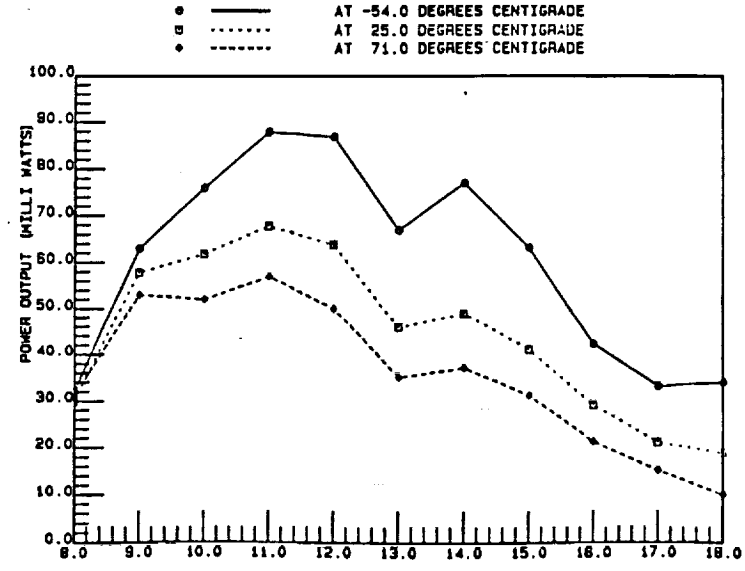

POWER OUTPUT, YIG-OSCILLATOR MODEL# 5157-3000

YIG-TUNED TRANSISTOR OSCILLATOR

Type No.: 6708-304F Serial No.: 1094 (Catalog Item)

Operating Conditions:

Heater Voltage:	28 Vdc	Current:	26 mA
Transistor Voltage:	+15 Vdc; -15 Vdc	Current:	643 mA; 44 mA

Tuning Voltage (V)	Calculated Frequency (GHz)	Frequency Deviation (MHz) 25° C	Power Output (mW) 25° C
0	2.0	0	35
1	2.6	- .8	53
2	3.2	- .3	46
3	3.8	+1.4	60
4	4.4	+2.1	73
5	5.0	+4.8	40
6	5.6	+7.2	55
7	6.2	+7.1	54
8	6.8	+9.0	50
9	7.4	+9.5	54
10	8.0	- .2	65

Drift: 7.7 MHz (max) Hysteresis: 8 MHz

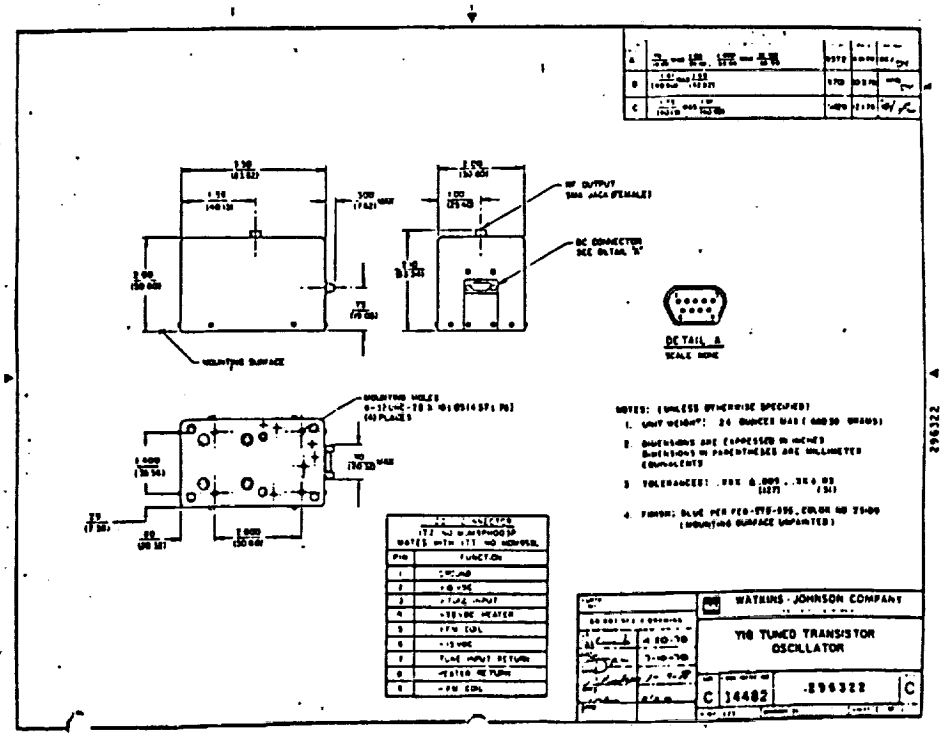

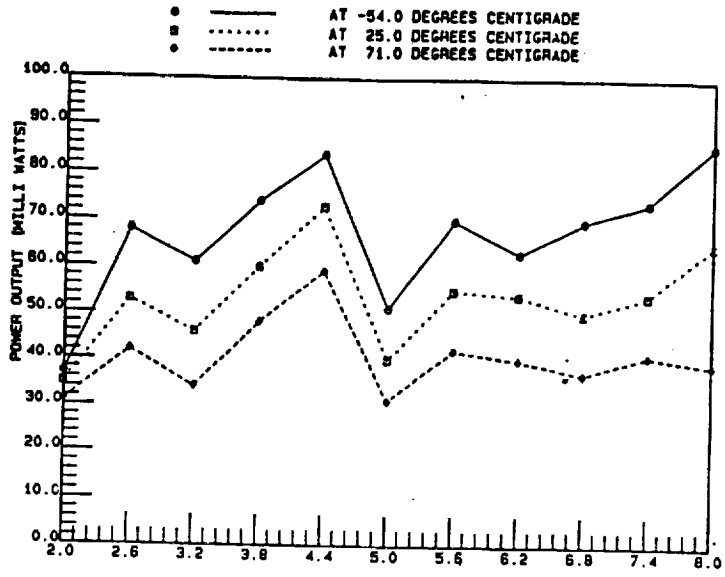

POWER OUTPUT AT DIFFERENT TEMP

2-18 GHz

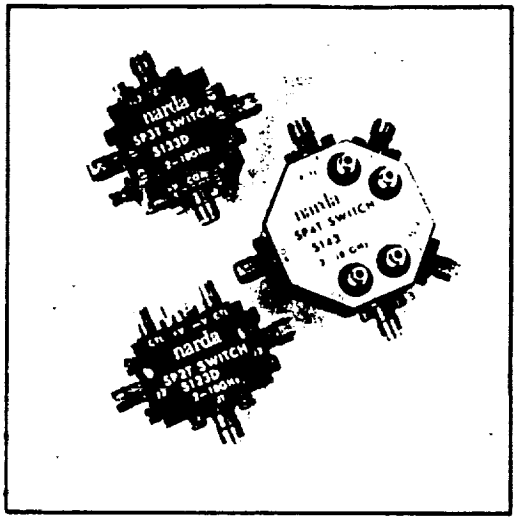

MEDIUM SPEED MULTI-THROW

Models S123, S123D, S133, S133D, S143, S143D, S123S, S123DS, S133S, S133DS, S143S, S143DS

DESCRIPTION

These SP2T, SP3T, SP4T switches are medium speed multithrow PIN switches employing a series/shunt diode configuration to provide high isolation and low insertion loss with moderate switching speeds. These switches are available in hermetic and non-hermetic versions, with and without TTL compatible drivers.

Custom configurations are available. These configurations can include filtering, phase matched arms, amplitude matched arms, optimization of performance over narrower frequency bands, drop-in packages, and ruggedized construction.

In order to insure the availability of custom configurations, consult the factory with your specific requirements.

FEATURES

- **Laser Welded, Hermetically Sealed***
- **Low VSWR**
- **Low Insertion Loss**
- **High Isolation**
- **Small Size**
- **With or Without Drivers**

SPECIFICATIONS

MODEL NO.*	TYPE	FREQUENCY RANGE 2-18 GHz	INSERTION LOSS dB (Max)	VSWR (Max)	ISOLATION dB (Min)	SWITCHING SPEED[1]	OUTLINE DRAWING
S123 S123D	SP2T	2-4 4-8 8-12 12-18	1.5 1.7 2.0 2.5	1.75:1 1.75:1 1.75:1 2.0:1	60 60 60 55	50 nsec 50 nsec 50 nsec 50 nsec	3/4
S123S S123DS	SP2T	2-4 4-8 8-12 12-18	1.8 2.0 2.3 2.8	1.75:1 1.75:1 1.9:1 2.0:1	60 60 60 55	50 nsec 50 nsec 50 nsec 50 nsec	3/4
S133 S133D	SP3T	2-4 4-8 8-12 12-18	1.5 1.7 2.0 2.5	1.75:1 1.75:1 1.75:1 2.0:1	60 60 60 55	50 nsec 50 nsec 50 nsec 50 nsec	5/6

narda

*"S" Suffix denotes Hermetic as in Model S123S. Typical

SPECIFICATIONS

MODEL NO.*	TYPE	FREQUENCY RANGE 2-18 GHz	INSERTION LOSS dB (Max)	VSWR (Max)	ISOLATION dB (Min)	SWITCHING SPEED[1]	OUTLINE DRAWING
S133S S133DS	SP3T	2-4 4-8 8-12 12-18	1.8 2.0 2.3 2.8	1.75:1 1.75:1 1.75:1 2.0:1	60 60 60 55	50 nsec 50 nsec 50 nsec 50 nsec	5/6
S143 S143D	SP4T	2-4 4-8 8-12 12-18	1.5 1.7 2.1 2.7	1.75:1 1.75:1 1.75:1 2.0:1	60 60 60 55	50 nsec 50 nsec 50 nsec 50 nsec	7/10
S143S S143DS	SP4T	2-4 4-8 8-12 12-18	1.8 2.0 2.3 2.8	1.75:1 1.75:1 1.75:1 2.0:1	60 60 60 55	50 nsec 50 nsec 50 nsec 50 nsec	7/10

[1]Rise/Fall Times (See Switching Definitions)

POWER SUPPLY REQUIREMENTS
(ONE (1) PORT "ON")

S123/S123S, S133/S133S, S143/S143S	Port "Off" Port "On"	+30 mA −30 mA
S123D S123DS	+5V ± 2% −5 to −15V	100 mA −50 mA
S133D S133DS	+5V ± 2% −5 to −15V	150 mA −100 mA
S143D S143DS	+5V ± 2% −5 to −15V	220 mA −110 mA

NOTE: Data Shown is Typical for S123/S123D.

CONTROL INPUT CHARACTERISTICS

TTL 2 UNIT LOADS
(A unit load is 1.6 mA sink current and 40μA source current)

CONTROL LOGIC

LOGIC—Non-Inverting TTL
Logic "0" (-0.3 to +0.8V) for port ON
Logic "1" (+2.4 to +5.0V) for port OFF

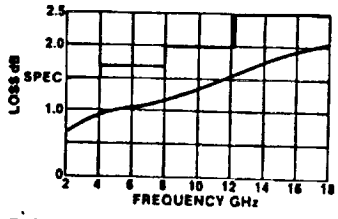

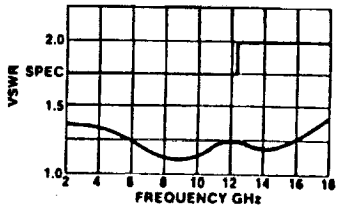

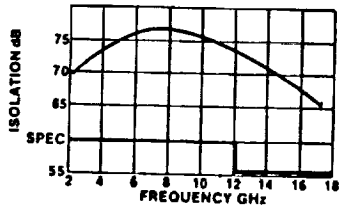

SCHEMATIC

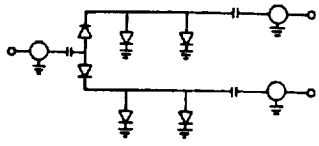

SP2T

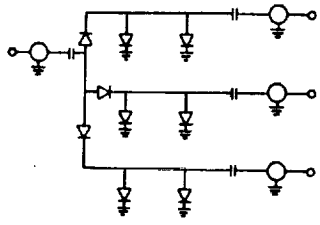

SP3T

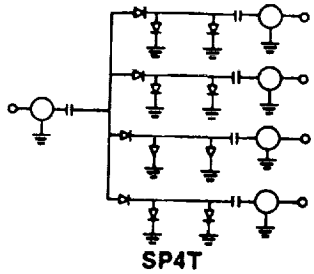

SP4T

narda

2 to 18 GHz DOUBLE BALANCED MIXER
MODELS: DB0218LW2 and DB0218LA1

FEATURES:

- RF/LO COVERAGE: 2 to 20 GHz
- IF OPERATION: DC to 750 MHz
- LO POWER RANGE: +7 to +13 dBm
- 6.5 dB TYPICAL CONVERSION LOSS
- HERMETICALLY SEALED PACKAGE

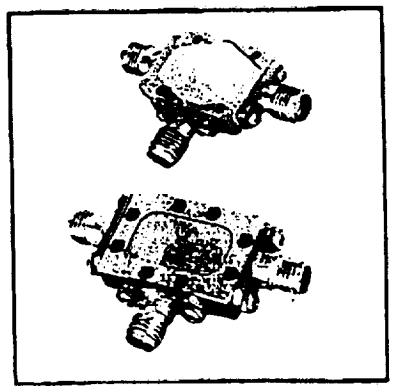

MITEQ's DB0218LW2 mixer is constructed of a balanced diode quad fed by microstrip RF and LO baluns and a DC coupled IF structure. The construction, coupled with the hermetic packaging, provide for high inherent reliability and performance over an extremely broad frequency range. This device performs as an up or down converter covering most EW bands, utility testing and breadboard applications.

ELECTRICAL SPECIFICATIONS

INPUT PARAMETERS		UNITS	MIN	TYP	MAX
RF FREQUENCY RANGE		GHz	2.0		18.0
RF VSWR (RF = -10 dBm, LO = +10 dBm)	(2 to 18 GHz)	RATIO		1.5:1	
	(2 to 20 GHz)	RATIO		2.5:1	
LO FREQUENCY RANGE		GHz	2.0		18.0
LO POWER RANGE		dBm	+7	+10	+13
LO VSWR (RF = -10 dBm, LO = +10 dBm)	(2 to 18 GHz)	RATIO		1.5:1	
	(2 to 20 GHz)	RATIO		2.0:1	

TRANSFER CHARACTERISTICS		UNITS	MIN	TYP	MAX
CONVERSION LOSS (IF = 100 MHz)	(2 to 18 GHz)	dB		6.5	8.5
	(2 to 22 GHz)	dB		7.5	10.0
SINGLE SIDEBAND NOISE FIGURE	(2 to 18 GHz)	dB			9.0
ISOLATION - LO TO RF	(2 to 18 GHz)	dB	22	30	
ISOLATION - LO TO IF	(2 to 18 GHz)	dB		20	
ISOLATION - RF TO IF	(2 to 18 GHz)	dB		20	
INPUT POWER AT 1 dB COMPRESSION	(LO = +10 dBm)	dBm		+5	
INPUT TWO-TONE 3RD ORDER INTERCEPT POINT	(LO = +10 dBm)	dBm		+15	

OUTPUT PARAMETERS		UNITS	MIN	TYP	MAX
IF FREQUENCY RANGE	(3 dB bandwidth)	MHz	DC		750.0
IF VSWR (RF = -10 dBm, LO = +10 dBm)		RATIO		1.5:1	

030618

MITEQ SPECIAL MIXER PRODUCTS DEPARTMENT
100 Davids Drive, Hauppauge, NY 11788

MITEQ MODEL: DB0218LW2/A1

TYPICAL TEST DATA

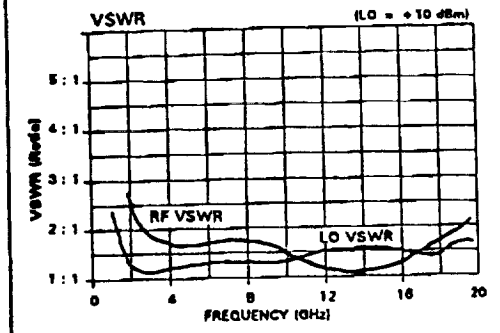

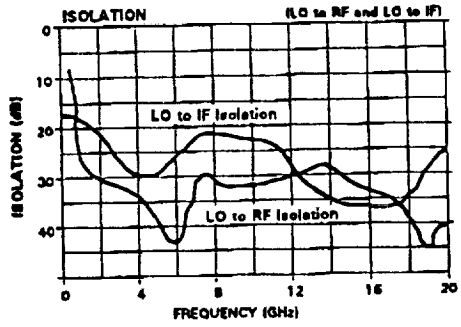

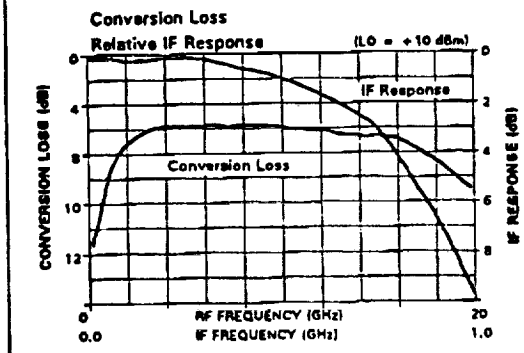

Single Tone (m) RF +/- (n) LO Spur Level
Relative (dBc) to REF (RF = -10 dBm, LO = +10 dBm)

RF Harmonic	1	2	3	4	5
5	>85	>85	>85	>85	>85
4	75	75	80	85	80
3	45	60	55	65	55
2	43	49	50	50	60
1	REF	30	11	33	20

LO Harmonic

MAXIMUM RATINGS

Specifications at +25 Deg C.

Operating Temperature	-54 to +85 Deg C
Storage Temperature	-65 to +125 Deg C

GENERAL NOTES:

Available Options:
- High dynamic range operation
- Custom Microstrip Packaging

OUTLINE DRAWING

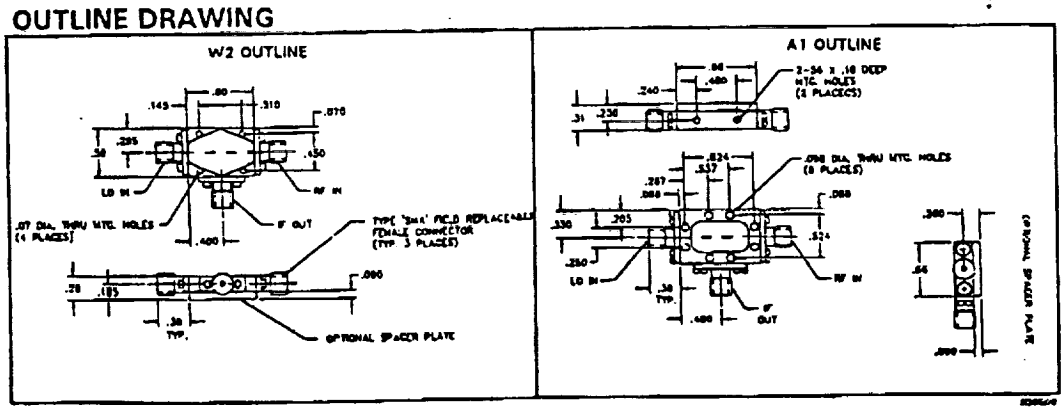

MITEQ SPECIAL MIXER PRODUCTS DEPARTMENT
100 Davids Drive, Hauppauge, NY 11788

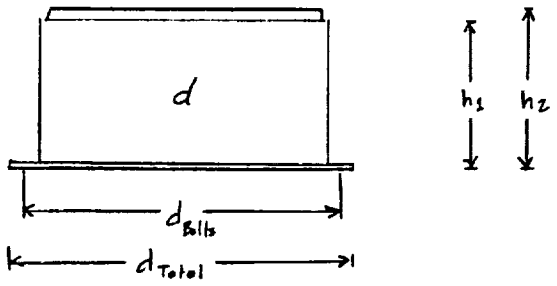

d_{bolts} [distance from center of bolt holes]
d_{total} [total distance]
h_1 [height without top] ; h_2 [height with top]

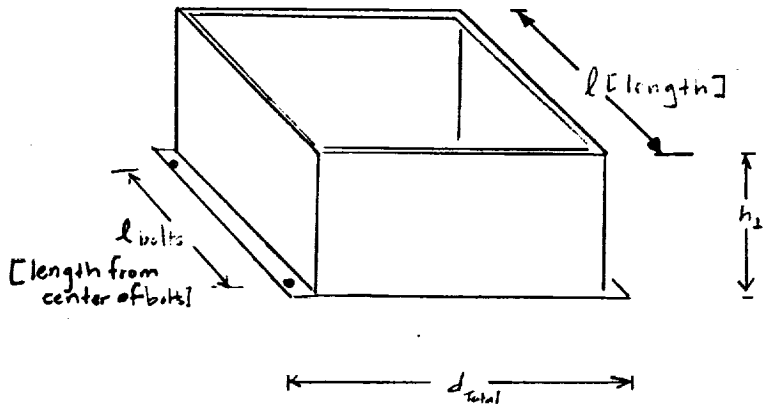

Dimensions: $d_{bolts} = 15\frac{3}{4}"$; $d_{Total} = 15\frac{5}{16}"$; $h_1 = 6\frac{1}{8}"$;
$h_2 = 6\frac{1}{4}"$; $l = 11.9"$; $l_{bolts} = 10"$; $d = 13\frac{15}{16}"$

Weight ⇨ No more than 25 lbs.

★ To be mounted on outside of helicopter as close to the antennas as possible

★ The diameter of the bolt holes is 5/16"

Revised L-band Block Diagram

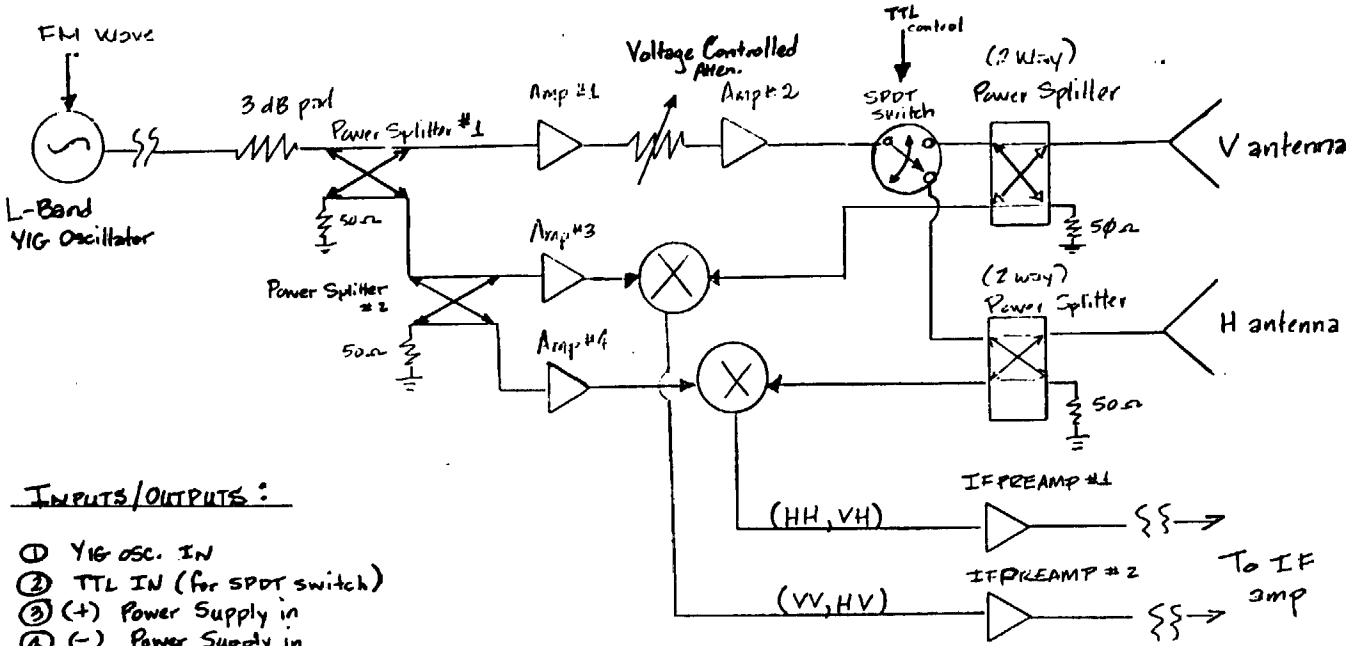

Inputs/Outputs:

1. YIG osc. IN
2. TTL IN (for SPDT switch)
3. (+) Power Supply in
4. (-) Power Supply in
5. Ground
6. Control Voltage IN (for VCA)
7. IFOUT (RCV H path)
8. IFOUT (RCV V path)

* All components to be put together on one board

* Voltage Reg. Board w/ LM7805, 7905, 7815, 7915 is also to be part of the radar system

Appendix 3
L-Band Microstrip Radar

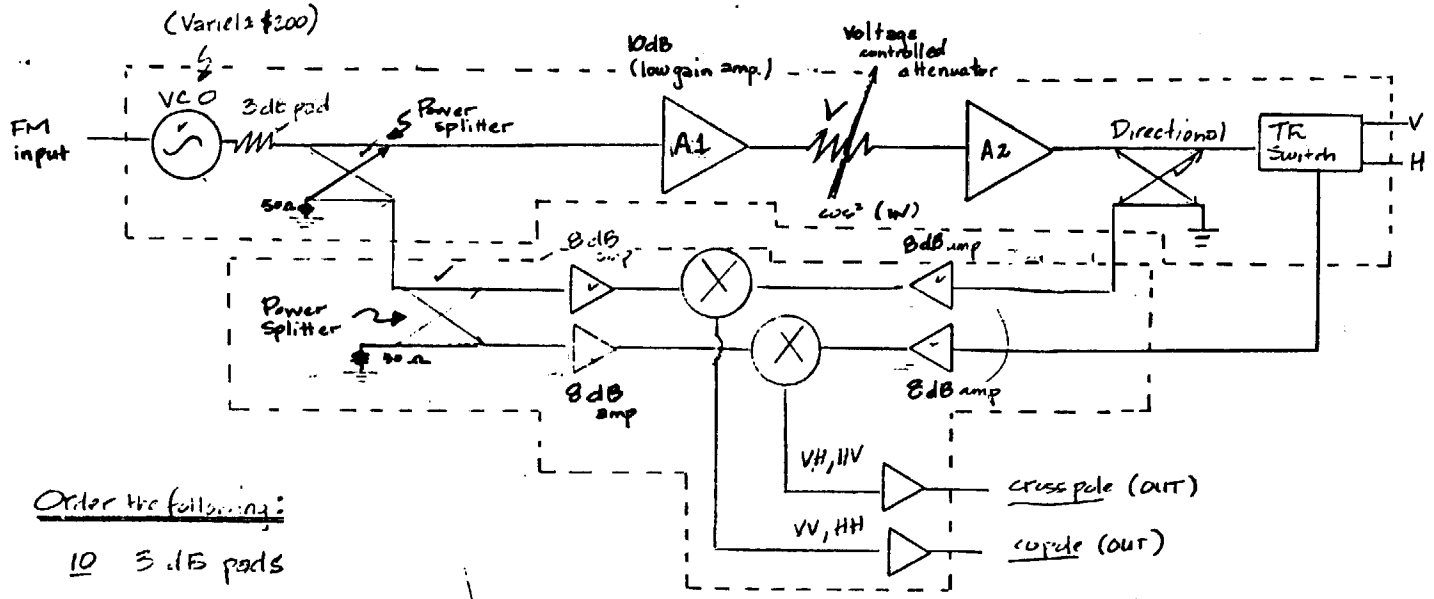

Order the following:

10 3 dB pads

4 3 dB hybrids

2 6 dB power divider (high directivity)

2 variable attenuator

10 low-gain, high-isolation amp

4 Mixers

PINS:

① gnd (2 pins ⑤ req'd)

✓② +/- power supply

X ③ FM waveform

✓④ cos^2 waveform

✓⑤ switch controls

✓⑥ output (co & cross)

L-Band Microstrip Radar

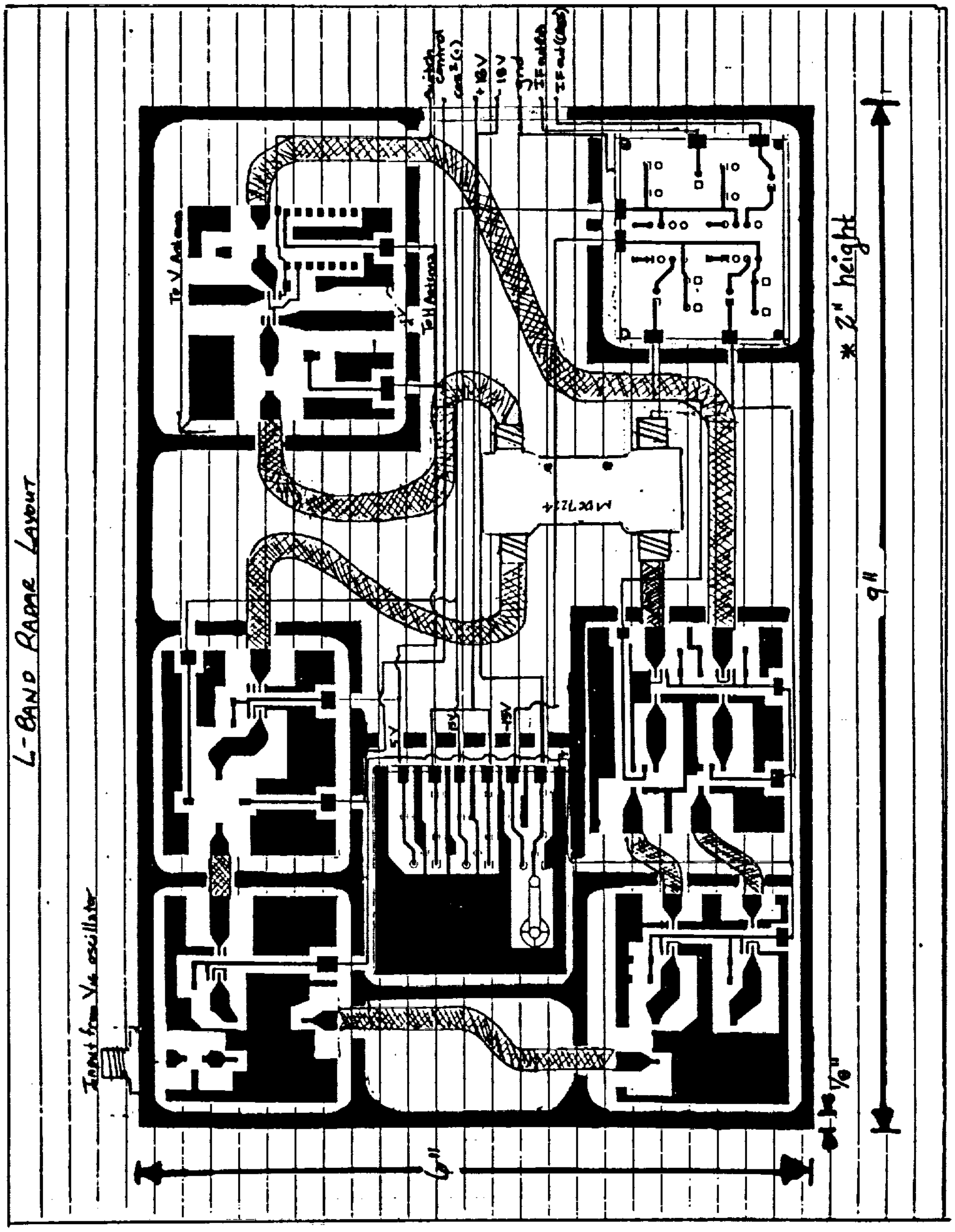
L-BAND RADAR LAYOUT
To V Antenna
To H Antenna
* 2" height
9"
6"

Appendix 4

IF Section Information

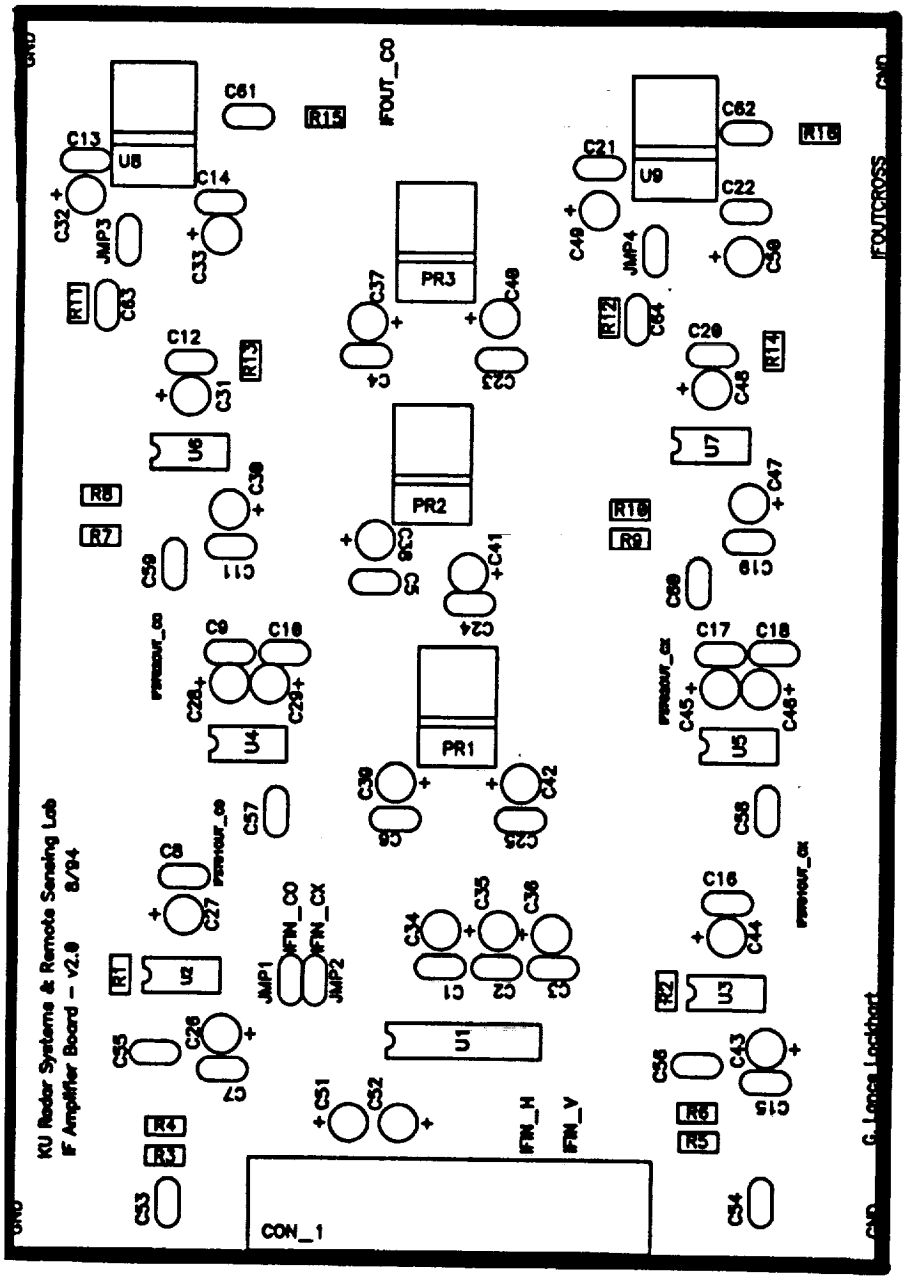

Bill of Materials IFAMPRV2.PCB

IF Amplifier Board v2.0

Quantity	Type	Value	Ref Designators
1	25 Pin D-type		CON_1
2	ADOP07		U6,U7
2	BUF634		U8,U9
31	Capacitor	.1 uF	C1,C2,C3,C4,C5,C6,C7,C8, C9,C10,C11,C12,C13,C14, C15,C16,C17,C18,C19,C20, C21,C22,C23,C24,C25,C57, C58,C59,C60,C61,C62
2	Capacitor	.47 uF	C53,C54
27	Capacitor	10 uF	C26,C27,C28,C29,C30,C31, C32,C33,C34,C35,C36,C37, C38,C39,C40,C41,C42,C43, C44,C45,C46,C47,C48,C49, C50,C51,C52
2	Capacitor	68 pF	C63,C64
2	Capacitor	220 pF	C55,C56
1	DG-189		U1
4	JUMPER		JMP1,JMP2,JMP3,JMP4
1	LM7805		PR3
2	LM7815		PR1,PR2
2	PGA103		U4,U5
4	Resistor	2.2 kohm	R7,R8,R9,R10
4	Resistor	10 ohm	R13,R14,R15,R16
2	Resistor	22 kohm	R11,R12
4	Resistor	51 ohm	R3,R4,R5,R6
2	Resistor	330 ohm	R1,R2
2	SSM-2017		U2,U3

ANALOG DEVICES

Self-Contained Audio Preamplifier

SSM-2017

FEATURES

- Excellent Noise Performance: 950 pV/$\sqrt{\text{Hz}}$ or 1.5 dB Noise Figure
- Ultralow THD: <0.01% @ G = 100 Over the Full Audio Band
- Wide Bandwidth: 1 MHz @ G = 100
- High Slew Rate: 17 V/μs typ
- Unity Gain Stable
- True Differential Inputs
- Subaudio 1/f Noise Corner
- 8-Pin Mini-DIP with Only One External Component Required
- Very Low Cost
- Extended Temperature Range: −40°C to +85°C

APPLICATIONS

- Audio Mix Consoles
- Intercom/Paging Systems
- Two-Way Radio
- Sonar
- Digital Audio Systems

GENERAL DESCRIPTION

The SSM-2017 is a latest generation audio preamplifier combining SSM preamplifier design expertise with advanced processing. The result is excellent audio performance from a self-contained 8-pin mini-DIP device, requiring only one external gain set resistor or potentiometer. The SSM-2017 is further enhanced by its unity gain stability.

Key specifications include ultralow noise (1.5 dB noise figure) and THD (<0.01% at G = 100), complemented by wide bandwidth and high slew rate.

Applications for this low cost device include microphone preamplifiers and bus summing amplifiers in professional and consumer audio equipment, sonar, and other applications requiring a low noise instrumentation amplifier with high gain capability.

FUNCTIONAL BLOCK DIAGRAM

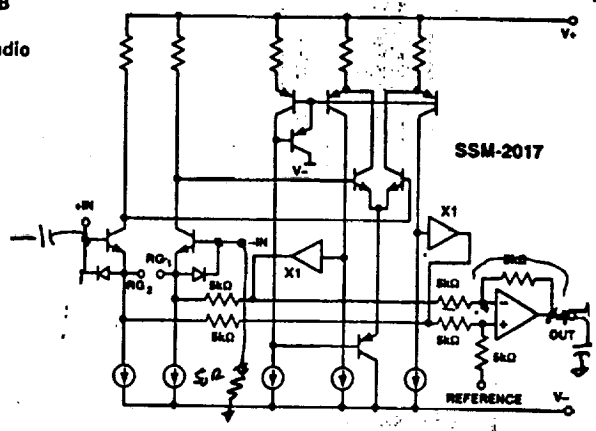

PIN CONNECTIONS

Epoxy Mini-DIP (P Suffix)
and
Hermetic DIP (Z Suffix)

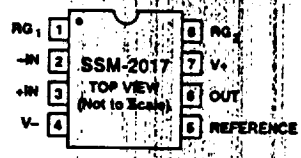

16-Pin SOIC (S Suffix)

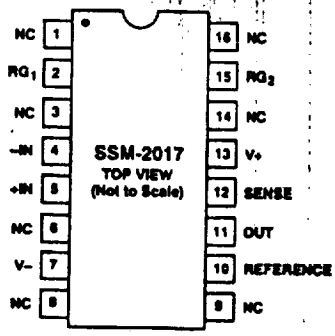

NC = NO CONNECT

REV. A

One Technology Way, P.O. Box 9106, Norwood, MA 02062-9106, U.S.A.
Tel: 617/329-4700 Fax: 617/326-8703 Twx: 710/394-6577
Telex: 924491 Cable: ANALOG NORWOODMASS

SSM-2017—SPECIFICATIONS (V_S = ±15 V and −40°C ≤ T_A ≤ +85°C, unless otherwise specified. Typical specifications apply at T_A = +25°C.)

Parameter	Symbol	Conditions	Min	Typ	Max	Units
DISTORTION PERFORMANCE		T_A = +25°C V_O = 7 V_{RMS} R_L = 5 kΩ				
Total Harmonic Distortion Plus Noise	THD+N	G = 1000, f = 1 kHz		0.012		%
		G = 100, f = 1 kHz		0.005		%
		G = 10, f = 1 kHz		0.004		%
		G = 1, f = 1 kHz		0.008		%
NOISE PERFORMANCE						
Input Referred Voltage Noise Density	e_n	f = 1 kHz, G = 1000		0.95		nV/√Hz
		f = 1 kHz; G = 100		1.95		nV/√Hz
		f = 1 kHz; G = 10		11.83		nV/√Hz
		f = 1 kHz; G = 1		107.14		nV/√Hz
Input Current Noise Density	i_n	f = 1 kHz, G = 1000		2		pA/√Hz
DYNAMIC RESPONSE						
Slew Rate	SR	G = 10 R_L = 4.7 kΩ C_L = 50 pF T_A = +25°C	10	17		V/μs
Small Signal Bandwidth	$BW_{-3\,dB}$	G = 1000		200		kHz
		G = 100		1000		kHz
		G = 10		2000		kHz
		G = 1		4000		kHz
INPUT						
Input Offset Voltage	V_{IOS}			0.1	1.2	mV
Input Bias Current	I_B	V_{CM} = 0 V		6	25	μA
Input Offset Current	I_{OS}	V_{CM} = 0 V		±0.002	±2.5	μA
Common-Mode Rejection	CMR	V_{CM} = ±8 V				
		G = 1000	80	112		dB
		G = 100	60	92		dB
		G = 10	40	74		dB
		G = 1, T_A = +25°C	26	54		dB
		G = 1, T_A = −40°C to +85°C	20	54		dB
Power Supply Rejection	PSR	V_S = ±6 V to ±18 V				
		G = 1000	80	124		dB
		G = 100	60	118		dB
		G = 10	40	101		dB
		G = 1	26	82		dB
Input Voltage Range	IVR		±8			V
Input Resistance	R_{IN}	Differential, G = 1000		1		MΩ
		G = 1		30		MΩ
		Common Mode, G = 1000		5.3		MΩ
		G = 1		7.1		MΩ
OUTPUT						
Output Voltage Swing	V_O	R_L = 2 kΩ; T_A = +25°C	±11.0	±12.3		V
Output Offset Voltage	V_{OOS}			−40	500	mV
Minimum Resistive Load Drive		T_A = +25°C		2		kΩ
		T_A = −40°C to +85°C		4.7		kΩ
Maximum Capacitive Load Drive				50		pF
Short Circuit Current Limit	I_{SC}	Output-to-Ground Short		±50		mA
Output Short Circuit Duration					10	sec
GAIN						
Gain Accuracy	$R_G = \frac{10\,k\Omega}{G-1}$	T_A = +25°C				
		R_G = 10 Ω, G = 1000		0.25	1	dB
		R_G = 101 Ω, G = 100		0.20	1	dB
		R_G = 1.1 kΩ, G = 10		0.20	1	dB
		R_G = ∞, G = 1		0.05	0.5	dB
Maximum Gain	G			70		dB

Parameter	Symbol	Conditions	Min	Typ	Max	Unit
REFERENCE INPUT						
Input Resistance				10		kΩ
Voltage Range				±8		V
Gain to Output				1		V/V
POWER SUPPLY						
Supply Voltage Range	V_S		±6		±22	V
Supply Current	I_{SY}	V_{CM} = 0 V, R_L = ∞		±10.6	±14.0	mA

Specifications subject to change without notice.

ABSOLUTE MAXIMUM RATINGS

Supply Voltage . . . . . ±22 V
Input Voltage . . . . . Supply Voltage
Output Short Circuit Duration . . . . . 10 sec
Storage Temperature Range (P, Z Packages) . −65°C to +150°C
Junction Temperature (T_J) . . . . . −65°C to +150°C
Lead Temperature Range (Soldering, 60 sec) . . . . . 300°C
Operating Temperature Range . . . . . −40°C to +85°C
Thermal Resistance[1]
8-Pin Hermetic DIP (Z): θ_{JA} = 134; θ_{JC} = 12 . . . . . °C/W
8-Pin Plastic DIP (P): θ_{JA} = 96; θ_{JC} = 37 . . . . . °C/W
16-Pin SOIC (S): θ_{JA} = 92; θ_{JC} = 27 . . . . . °C/W

NOTE
[1]θ_{JA} is specified for worst case mounting conditions, i.e., θ_{JA} is specified for device in socket for cerdip and plastic DIP; θ_{JA} is specified for device soldered to printed circuit board for SOIC package.

ORDERING GUIDE

Model	Operating Temperature Range*	Package
SSM-2017P	−40°C to +85°C	8-Pin Plastic DIP
SSM-2017Z	−40°C to +85°C	8-Pin Hermetic DIP
SSM-2017S	−40°C to +85°C	16-Lead SOIC

*XIND = −40°C to +85°C.

Typical Performance Characteristics

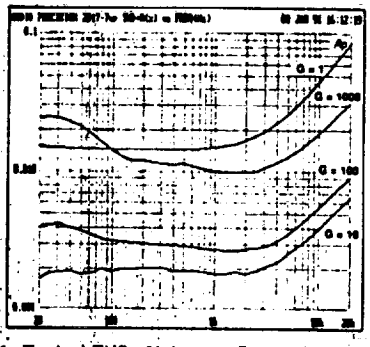

Figure 1. Typical THD+Noise at G = 1, 10, 100, 1000; V_O = 7 V_{RMS}, V_S = ±15 V, R_L = 5 kΩ; T_A = +25°C*

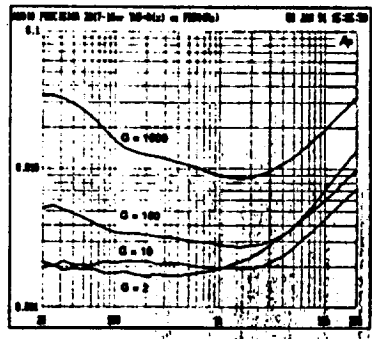

Figure 2. Typical THD+Noise at G = 2, 10, 100, 1000; V_O = 10 V_{RMS}, V_S = ±18 V, R_L = 5 kΩ; T_A = +25°C*

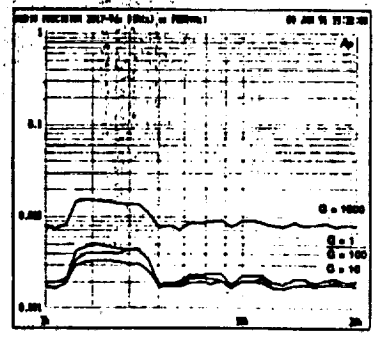

Figure 3. Typical DIM at G = 1, 10, 100, 1000; V_O = 7 V_{RMS}, V_S = ±15 V, R_L = 5 kΩ; T_A = +25°C

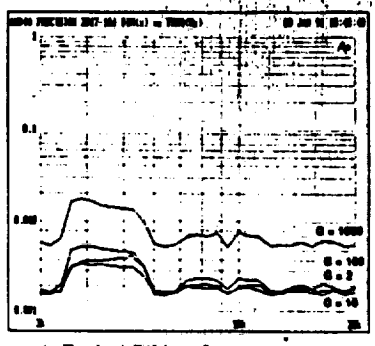

Figure 4. Typical DIM at G = 2, 10, 100, 1000; V_O = 10 V_{RMS}, V_S = ±18 V, R_L = 5 kΩ; T_A = +25°C

*80 kHz low-pass filter used for Figures 1–2.

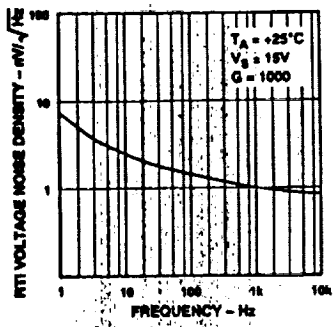

Figure 5. Voltage Noise Density vs. Frequency

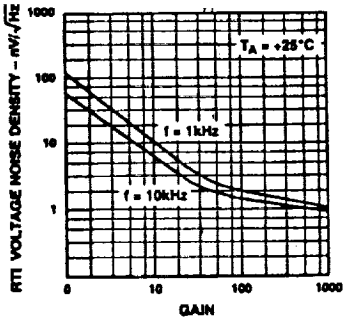

Figure 6. RTI Voltage Noise Density vs. Gain

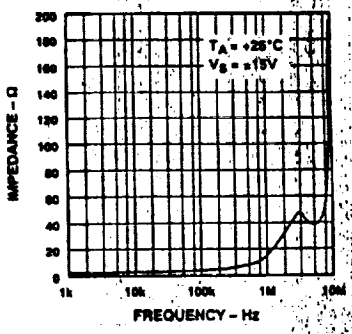

Figure 7. Output Impedance vs. Frequency

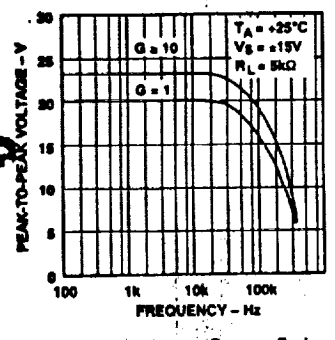

Figure 8. Maximum Output Swing vs. Frequency

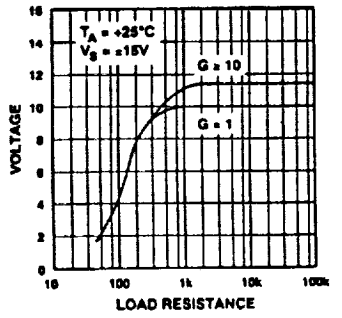

Figure 9. Maximum Output Voltage vs. Load Resistance

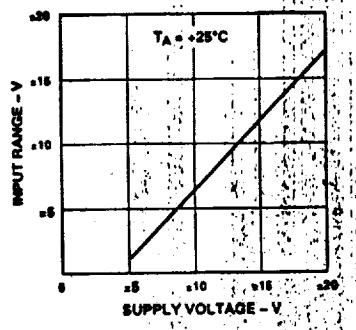

Figure 10. Input Voltage Range vs. Supply Voltage

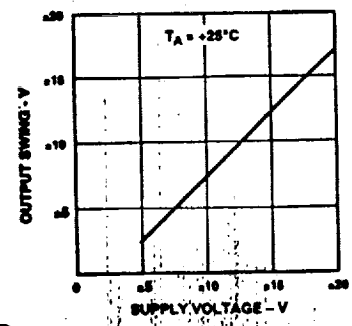

Figure 11. Output Voltage Range vs. Supply Voltage

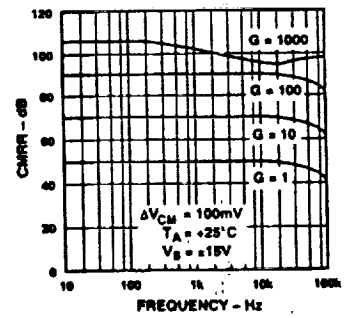

Figure 12. CMRR vs. Frequency

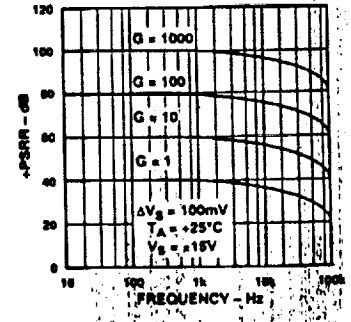

Figure 13. +PSRR vs. Frequency

Typical Performance Characteristics—SSM-2017

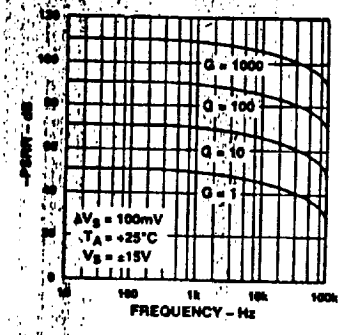

Figure 14. –PSRR vs. Frequency

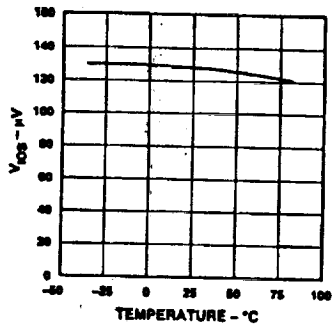

Figure 15. V_{IOS} vs. Temperature

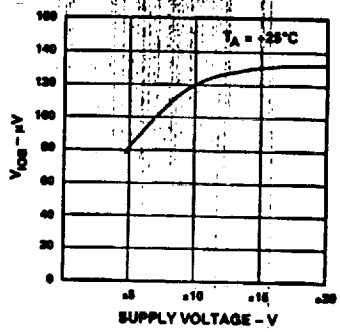

Figure 16. V_{IOS} vs. Supply Voltage

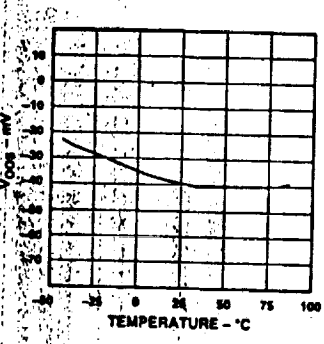

Figure 17. V_{OOS} vs. Temperature

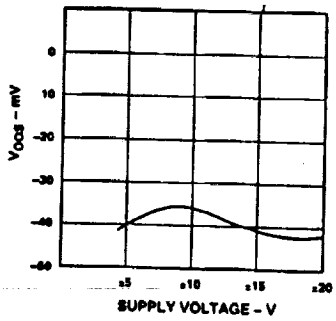

Figure 18. V_{OOS} vs. Supply Voltage

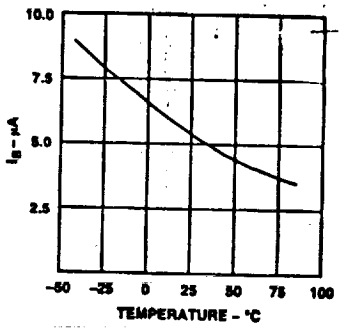

Figure 19. I_B vs. Temperature

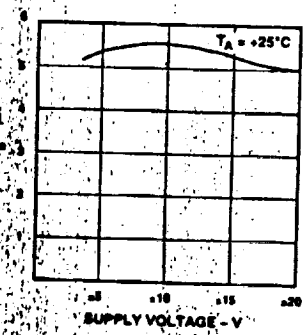

Figure 20. I_B vs. Supply Voltage

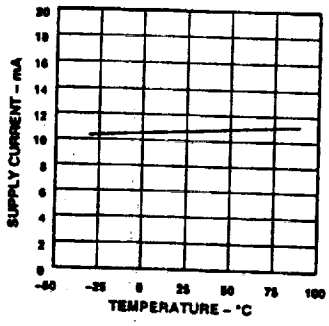

Figure 21. I_{SY} vs. Temperature

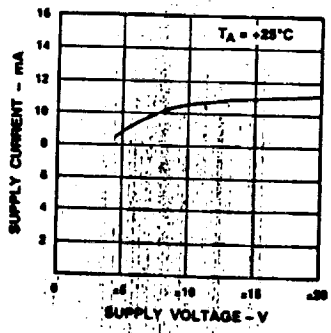

Figure 22. I_{SY} vs.Supply Voltage

SSM-2017—Applications Information

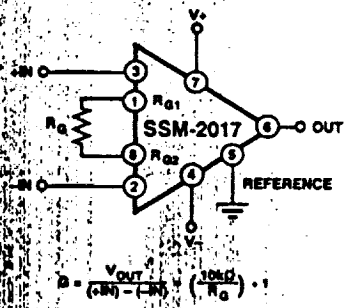

Basic Circuit Connections

GAIN

The SSM-2017 only requires a single external resistor to set the voltage gain. The voltage gain, G, is:

$$G = \frac{10\ k\Omega}{R_G} + 1$$

and

$$R_G = \frac{10\ k\Omega}{G - 1}$$

For convenience, Table I lists various values of R_G for common gain levels.

Table I. Values of R_G for Various Gain Levels

A_V	dB	R_G
1	0	NC
3.2	10	4.7k
10	20	1.1k
31.3	30	330
100	40	100
314	50	32
1000	60	10

The voltage gain can range from 1 to 3500. A gain set resistor is not required for unity gain applications. Metal-film or wire-wound resistors are recommended for best results.

The total gain accuracy of the SSM-2017 is determined by the tolerance of the external gain set resistor, R_G, combined with the gain equation accuracy of the SSM-2017. Total gain drift combines the mismatch of the external gain set resistor drift with that of the internal resistors (20 ppm/°C typ).

Bandwidth of the SSM-2017 is relatively independent of gain as shown in Figure 23. For a voltage gain of 1000, the SSM-2017 has a small-signal bandwidth of 200 kHz. At unity gain, the bandwidth of the SSM-2017 exceeds 4 MHz.

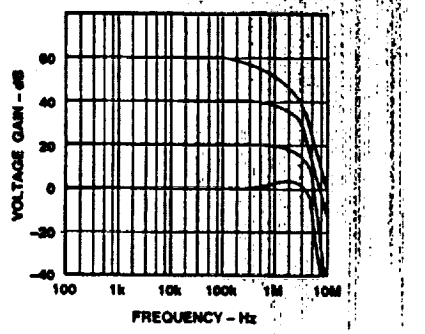

Figure 23. Bandwidth of the SSM-2017 for Various Values of Gain

NOISE PERFORMANCE

The SSM-2017 is a very low noise audio preamplifier exhibiting a typical voltage noise density of only 1 nV/√Hz at 1 kHz. The exceptionally low noise characteristics of the SSM-2017 are in part achieved by operating the input transistors at high collector currents since the voltage noise is inversely proportional to the square root of the collector current. Current noise, however, is directly proportional to the square root of the collector current. As a result, the outstanding voltage noise performance of the SSM-2017 is obtained at the expense of current noise performance. At low preamplifier gains, the effect of the SSM-2017's voltage and current noise is insignificant.

The total noise of an audio preamplifier channel can be calculated by:

$$E_n = \sqrt{e_n^2 + (i_n R_s)^2 + e_t^2}$$

where:

E_n = total input referred noise

e_n = amplifier voltage noise

i_n = amplifier current noise

R_s = source resistance

e_t = source resistance thermal noise.

For a microphone preamplifier, using a typical microphone impedance of 150 Ω the total input referred noise is:

e_n = 1 $nV/\sqrt{Hz}$ @ 1 kHz, SSM-2017 e_n

i_n = 2 $pA/\sqrt{Hz}$ @ 1 kHz, SSM-2017 i_n

R_S = 150 Ω, *microphone source impedance*

e_t = 1.6 $nV/\sqrt{Hz}$ @ 1 kHz, *microphone thermal noise*

$E_n = \sqrt{(1\ nV/\sqrt{Hz})^2 + 2(2\ pA/\sqrt{Hz} \times 150\ \Omega)^2 + (1.6\ nV/\sqrt{Hz})^2} = 1.93\ nV/\sqrt{Hz}$ @ 1 kHz.

This total noise is extremely low and makes the SSM-2017 virtually transparent to the user.

INPUTS

The SSM-2017 has protection diodes across the base emitter junctions of the input transistors. These prevent accidental avalanche breakdown which could seriously degrade noise performance. Additional clamp diodes are also provided to prevent the inputs from being forced too far beyond the supplies.

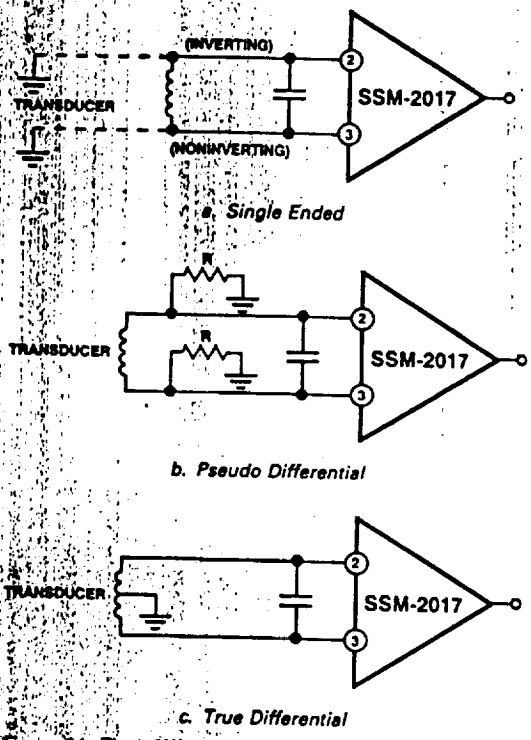

Figure 24. Three Ways of Interfacing Transducers for High Noise Immunity

Although the SSM-2017's inputs are fully floating, care must be exercised to ensure that both inputs have a dc bias connection capable of maintaining them within the input common-mode range. The usual method of achieving this is to ground one side of the transducer as in Figure 24a, but an alternative way is to float the transducer and use two resistors to set the bias point as in Figure 24b. The value of these resistors can be up to 10 kΩ, but they should be kept as small as possible to limit common-mode pickup. Noise contribution by resistors themselves is negligible since it is attenuated by the transducer's impedance. Balanced transducers give the best noise immunity and interface directly as in Figure 24c.

REFERENCE TERMINAL

The output signal is specified with respect to the reference terminal, which is normally connected to analog ground. The reference may also be used for offset correction or level shifting. A reference source resistance will reduce the common-mode rejection by the ratio of 5 kΩ/R_{REF}. If the reference source resistance is 1 Ω, then the CMR will be reduced to 74 dB (5 kΩ/1 Ω = 74 dB).

COMMON-MODE REJECTION

Ideally, a microphone preamplifier responds only to the difference between the two input signals and rejects common-mode voltages and noise. In practice, there is a small change in output voltage when both inputs experience the same common-mode voltage change; the ratio of these voltages is called the common-mode gain. Common-mode rejection (CMR) is the logarithm of the ratio of differential-mode gain to common-mode gain, expressed in dB.

PHANTOM POWERING

A typical phantom microphone powering circuit is shown in Figure 25. Z_1 through Z_4 provide transient overvoltage protection for the SSM-2017 whenever microphones are plugged in or unplugged.

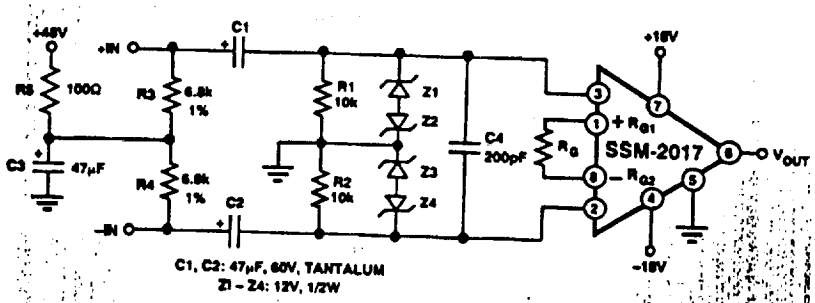

Figure 25. SSM-2017 in Phantom Powered Microphone Circuit

BUS SUMMING AMPLIFIER

In addition to is use as a microphone preamplifier, the SSM-2017 can be used as a very low noise summing amplifier. Such a circuit is particularly useful when many medium impedance outputs are summed together to produce a high effective noise gain.

The principle of the summing amplifier is to ground the SSM-2017 inputs. Under these conditions, Pins 1 and 8 are ac virtual grounds sitting about 0.55 V below ground.

To remove the 0.55 V offset, the circuit of Figure 26 is recommended.

A_2 forms a "servo" amplifier feeding the SSM-2017's inputs. This places Pins 1 and 8 at a true dc virtual ground. R4 in conjunction with C2 remove the voltage noise of A_2, and in fact just about any operational amplifier will work well here since it is removed from the signal path. If the dc offset at Pins 1 and 8 is not too critical, then the servo loop can be replaced by the diode biasing scheme of Figure 26. If ac coupling is used throughout, then Pins 2 and 3 may be directly grounded.

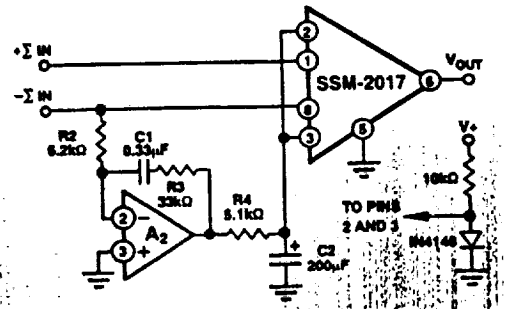

Figure 26. Bus Summing Amplifier

OUTLINE DIMENSIONS

Dimensions shown in inches and (mm).

8-Pin Plastic DIP (P) Package

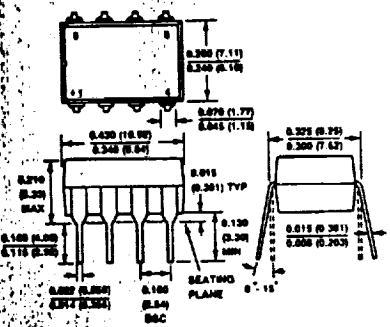

8-Pin Hermetic DIP (Z) Package

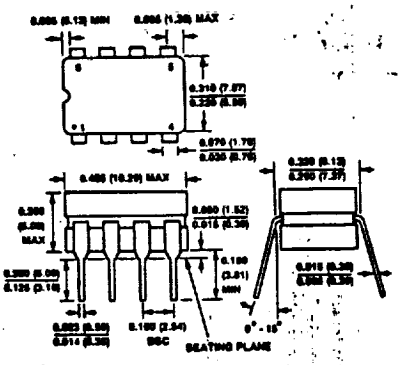

16-Pin SOIC (S) Package

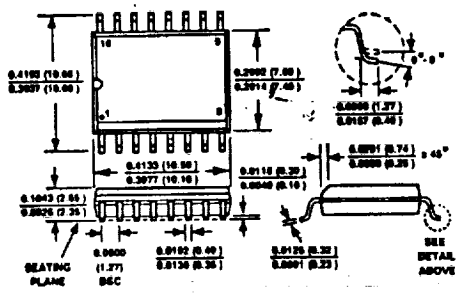

BURR-BROWN®

PGA103

**ADVANCED INFORMATION
SUBJECT TO CHANGE**

Programmable Gain AMPLIFIER

FEATURES

- DIGITALLY PROGRAMED GAINS: G=1, 10, 100
- CMOS/TTL-COMPATIBLE INPUTS
- LOW GAIN ERROR: ±0.05% max
- LOW OFFSET VOLTAGE DRIFT: 2μV/°C
- LOW QUIESCENT CURRENT: 2.4mA
- LOW COST
- 8-PIN PLASTIC DIP, SO-8 PACKAGES

APPLICATIONS

- DATA ACQUISITION SYSTEM
- GENERAL PURPOSE ANALOG BOARDS
- MEDICAL INSTRUMENTATION

DESCRIPTION

The PGA103 is a programmable-gain amplifier for general purpose applications. Gains of 1, 10 or 100 are digitally selected by two CMOS/TTL-compatible address lines. The PGA103 is ideal for systems that must handle wide dynamic range signals.

The PGA103's high speed circuitry provides fast settling time, even at G=100 (8.2μs to 0.01%). Bandwidth is 250kHz at G=100, yet quiescent current is only 2.4mA from ±15V power supplies. It operates from ±5V to ±18V power supplies.

The PGA103 is available in 8-pin plastic DIP and SO-8 surface-mount packages, specified for the –40°C to +85°C temperature range. Dice are also available.

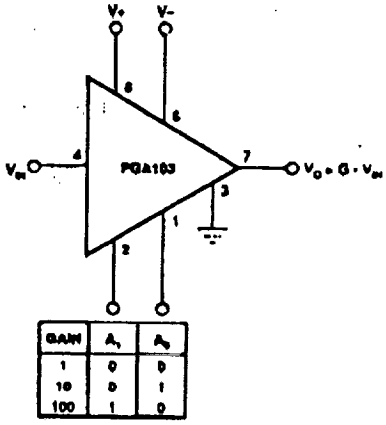

GAIN	A_1	A_0
1	0	0
10	0	1
100	1	0

International Airport Industrial Park • Mailing Address: PO Box 11400 • Tucson, AZ 85734 • Street Address: 6730 S. Tucson Blvd. • Tucson, AZ 85706
Tel: (602) 746-1111 • Twx: 910-952-1111 • Cable: BBRCORP • Telex: 066-6491 • FAX: (602) 889-1510 • Immediate Product Info: (800) 548-6132

SPECIFICATIONS

ELECTRICAL

T_A = +25°C, V_S = ±15V, R_L = 2kΩ unless otherwise specified.

PARAMETER	CONDITIONS	PGA103P, U MIN	PGA103P, U TYP	PGA103P, U MAX	UNITS
INPUT					
Offset Voltage, RTI					
G=1	T_A = +25°C			±1500	µV
G=10				±500	µV
G=100				±400	µV
vs Temperature	T_A = T_{min} to T_{max}				
G=1			±7		µV/°C
G=10			±3		µV/°C
G=100			±2		µV/°C
vs Power Supply	V_S = ±5V to ±18V		6 + 22/G	30 + 40/G	µV/V
Impedance			10^9 ‖ 2		Ω ‖ pF
Bias Current			±20	±100	nA
vs Temperature			±100		pA/°C
Noise Voltage, RTI	G=100, R_S = 0Ω				
f=10Hz			20		nV/√Hz
f=100Hz			18		nV/√Hz
f=1kHz			18		nV/√Hz
f_B=0.1Hz to 10Hz			0.6		µVp-p
Noise Voltage	G=10, R_S = 0Ω				
f=10Hz					nV/√Hz
f=100Hz					nV/√Hz
f=1kHz					nV/√Hz
f_B=0.1Hz to 10Hz					µVp-p
Noise Voltage	G=1, R_S = 0Ω				
f=10Hz			155		nV/√Hz
f=100Hz			93		nV/√Hz
f=1kHz			79		nV/√Hz
f_B=0.1Hz to 10Hz			4.5		µVp-p
Noise Current					
f=10Hz			2.8		pA/√Hz
f=1kHz			0.43		pA/√Hz
f_B=0.1Hz to 10Hz			76		pAp-p
GAIN					
Gain Error	G=1		±0.01	±0.02	%
	G=10		±0.01	±0.05	%
	G=100		±0.02	±0.1	%
Gain vs Temperature	G=1, 10, 100		±2.5	±20	ppm/°C
Nonlinearity	G=1		±0.001	±0.003	% of FSR
	G=10		±0.002	±0.008	% of FSR
	G=100		±0.004	±0.01	% of FSR
OUTPUT					
Voltage, Positive	I_O = 5mA	(V+) –6	(V+) –2.6		V
Negative	I_O = –5mA	(V–) +5	(V–) +2.6		V
Load Capacitance max			1000		pF
Short Circuit Current			±25		mA
FREQUENCY RESPONSE					
Bandwidth, -3dB	G=1		1.5		MHz
	G=10		750		kHz
	G=100		250		kHz
Slew Rate	V_O = ±10V		9		V/µs
Settling Time, 0.1%	G=1		1.6		µs
	G=10		2.2		µs
	G=100		5.2		µs
0.01%	G=1		2.8		µs
	G=10		2.8		µs
	G=100		8.7		µs
Overload Recovery	50% Overdrive		2.5		µs
DIGITAL LOGIC INPUTS					
Digital Low Voltage		V–		0.8	V
Digital Low Current			1		µA
Digital High Voltage		2		V_+	V
POWER SUPPLY					
Voltage Range		±5	±15	±18	V
Current	V_{IN} = 0V		±2.4	±3.3	mA
TEMPERATURE RANGE					
Specification		-40		+85	°C
Operating		-40		+125	°C
θ_{JA}: P or U Package			100		°C/W

ANALOG DEVICES

Low-Noise Precision High-Speed Operational Amplifier ($A_{VCL} \geq 5$)

OP-37

FEATURES

- Low Noise ..... 80nV p-p (0.1Hz to 10Hz)
  ..... $3nV/\sqrt{Hz}$ at 1kHz
- Low Drift ..... 0.2μV/°C
- High Speed ..... 17V/μs Slew Rate
  ..... 63MHz Gain Bandwidth
- Low Input Offset Voltage 10μV
- Excellent CMRR ... 126dB (Common-Voltage of ±11V)
- High Open-Loop Gain ..... 1.8 Million
- Replaces 725, OP-05, OP-06, OP-07, AD510, AD517, SE5534 in Gains >5
- Available in Die Form

ORDERING INFORMATION †

T_A = +25°C V_{OS} MAX (μV)	PACKAGE TO-99	CERDIP 8-PIN	PLASTIC 8-PIN	LCC 20-CONTACT	OPERATING TEMPERATURE RANGE
25	OP37AJ*	OP37AZ*	–	–	MIL
25	OP37EJ	OP37EZ	OP37EP	–	IND/COM
60	OP37BJ*	OP37BZ*	–	OP37BRC/883	MIL
60	OP37FJ	OP37FZ	OP37FP	–	IND/COM
100	OP37CJ*	OP37CZ	–	–	MIL
100	OP37GJ	OP37GZ	OP37GP	–	XIND
100	–	–	OP37GS††	–	XIND

* For devices processed in total compliance to MIL-STD-883, add /883 after part number. Consult factory for 883 data sheet.

† Burn-in is available on commercial and industrial temperature range parts in CerDIP, plastic DIP, and TO-can packages.

†† For availability and burn-in information on SO package, contact your local sales office.

GENERAL DESCRIPTION

The OP-37 provides the same high performance as the OP-27, but the design is optimized for circuits with gains greater than five. This design change increases slew rate to 17V/μsec and gain-bandwidth product to 63MHz.

The OP-37 provides the low offset and drift of the OP-07 plus higher speed and lower noise. Offsets down to 25μV and drift of 0.6μV/°C maximum make the OP-37 ideal for precision instrumentation applications. Exceptionally low noise (e_n = 3.5nV/$\sqrt{Hz}$ at 10Hz), a low 1/f noise corner frequency of 2.7Hz, and the high gain of 1.8 million, allow accurate high-gain amplification of low-level signals.

The low input bias current of ± 10nA and offset current of 7nA are achieved by using a bias-current-cancellation circuit. Over the military temperature range this typically holds I_B and I_{OS} to ±20nA and 15nA respectively.

The output stage has good load driving capability. A guaranteed swing of ± 10V into 600Ω and low output distortion make the OP-37 an excellent choice for professional audio applications.

PIN CONNECTIONS

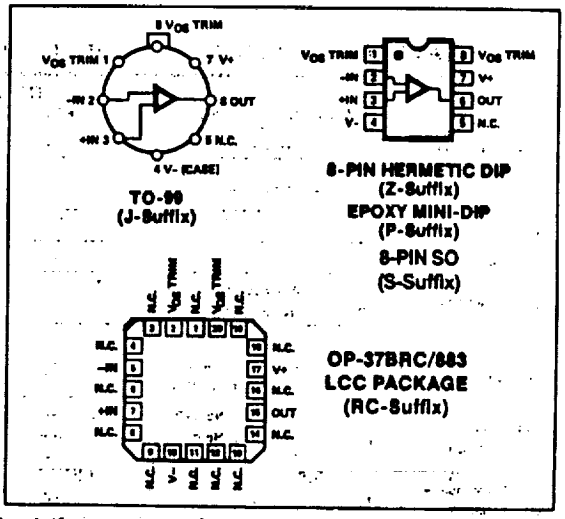

SIMPLIFIED SCHEMATIC

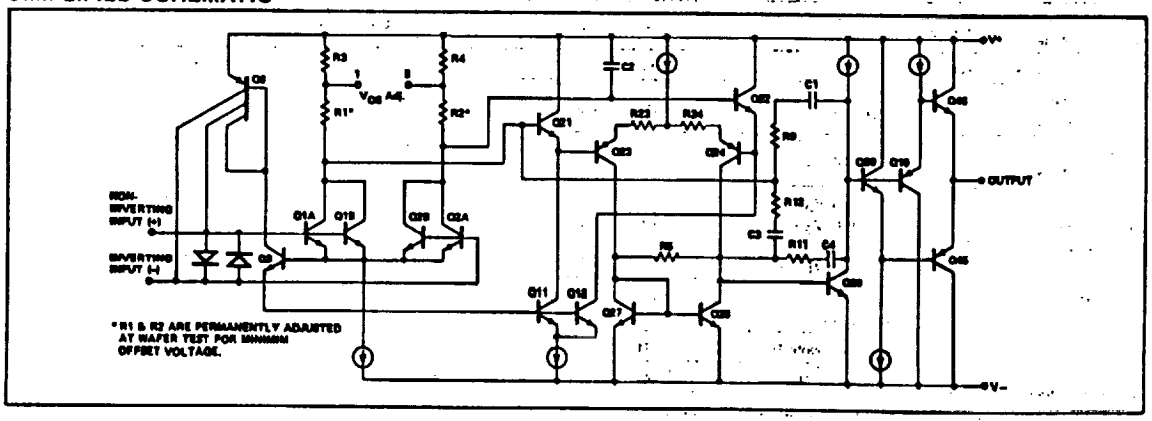

DICE CHARACTERISTICS

DIE SIZE 0.096 × 0.056 inch, 5488 sq. mils
(2.49 × 1.42 mm, 3.54 sq. mm)

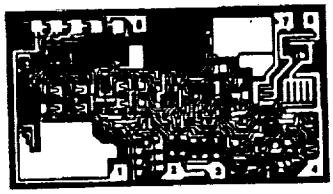

1. NULL
2. (–) INPUT
3. (+) INPUT
4. V–
6. OUTPUT
7. V+
8. NULL

WAFER TEST LIMITS at $V_S = \pm 15V$, $T_A = 25°C$ for OP-37N, OP-37G and OP-37GR devices; $T_A = 125°C$ for OP-37NT and OP-37GT devices, unless otherwise noted.

PARAMETER	SYMBOL	CONDITIONS	OP-37NT LIMIT	OP-37N LIMIT	OP-37GT LIMIT	OP-37G LIMIT	OP-37GR LIMIT	UNITS
Input Offset Voltage	V_{OS}	(Note 1)	60	35	200	60	100	μV MAX
Input Offset Current	I_{OS}		50	35	85	50	75	nA MAX
Input Bias Current	I_B		±60	±40	±95	±55	±80	nA MAX
Input Voltage Range	IVR		±10.3	±11	±10.3	±11	±11	V MIN
Common-Mode Rejection Ratio	CMRR	$V_{CM} = \pm 11V$	108	114	100	106	100	dB MIN
Power Supply Rejection Ratio	PSRR	$T_A = 25°C$, $V_S = \pm 4V$ to $\pm 18V$ $T_A = 125°C$, $V_S = \pm 4.5V$ to $\pm 18V$	10 16	10 —	10 20	10 —	20 —	μV/V MAX
Large-Signal Voltage Gain	A_{VO}	$R_L \geq 2k\Omega$, $V_O = \pm 10V$ $R_L \geq 1k\Omega$, $V_O = \pm 10V$	600 —	1000 800	500 —	1000 800	700 —	V/mV MIN
Output Voltage Swing	V_O	$R_L \geq 2k\Omega$ $R_L \geq 600\Omega$	±11.5 —	±12.0 ±10.0	±11.0 —	±12.0 ±10.0	±11.5 ±10.0	V MIN
Power Consumption	P_d	$V_O = 0$	—	140	—	140	170	mW MAX

NOTES:
For 25°C characteristics of OP-37NT and OP-37GT devices, see OP-37N and OP-37G characteristics, respectively.

Electrical tests are performed at wafer probe to the limits shown. Due to variations in assembly methods and normal yield loss, yield after packaging is not guaranteed for standard product dice. Consult factory to negotiate specifications based on dice lot qualification through sample lot assembly and testing.

TYPICAL ELECTRICAL CHARACTERISTICS at $V_S = \pm 15V$, $T_A = +25°C$, unless otherwise noted.

PARAMETER	SYMBOL	CONDITIONS	OP-37NT TYPICAL	OP-37N TYPICAL	OP-37GT TYPICAL	OP-37G TYPICAL	OP-37GR TYPICAL	UNITS
Average Input Offset Voltage Drift	TCV_{OS} or TCV_{OSn}	Nulled or Unnulled $R_P = 8k\Omega$ to $20k\Omega$	0.2	0.2	0.3	0.3	0.4	μV/°C
Average Input Offset Current Drift	TCI_{OS}		80	80	130	130	180	pA/°C
Average Input Bias Current Drift	TCI_B		100	100	160	160	200	pA/°C
Input Noise Voltage Density	e_n	$f_O = 10Hz$ $f_O = 30Hz$ $f_O = 1000Hz$	3.5 3.1 3.0	3.5 3.1 3.0	3.5 3.1 3.0	3.5 3.1 3.0	3.8 3.3 3.2	$nV/\sqrt{Hz}$
Input Noise Current Density	I_n	$f_O = 10Hz$ $f_O = 30Hz$ $f_O = 1000Hz$	1.7 1.0 0.4	1.7 1.0 0.4	1.7 1.0 0.4	1.7 1.0 0.4	1.7 1.0 0.4	$pA/\sqrt{Hz}$
Input Noise Voltage	e_{np-p}	0.1Hz to 10Hz	0.08	0.08	0.08	0.08	0.09	μV_{p-p}
Slew Rate	SR	$R_L \geq 2k\Omega$	17	17	17	17	17	V/μs
Gain Bandwidth Product	GBW	$f_O = 10kHz$	63	63	63	63	63	MHz

NOTE:
1. Input offset voltage measurements are performed by automated test equipment approximately 0.5 seconds after application of power.

TYPICAL PERFORMANCE CHARACTERISTICS

NOISE-TESTER FREQUENCY RESPONSE (0.1Hz TO 10Hz)

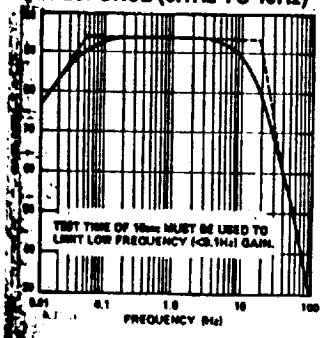

VOLTAGE NOISE DENSITY vs FREQUENCY

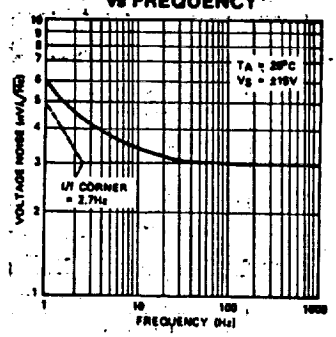

A COMPARISON OF OP AMP VOLTAGE NOISE SPECTRA

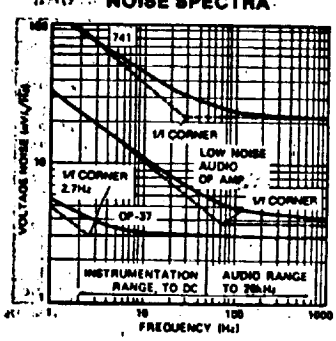

2

INPUT WIDEBAND VOLTAGE NOISE vs BANDWIDTH (0.1Hz TO FREQUENCY INDICATED)

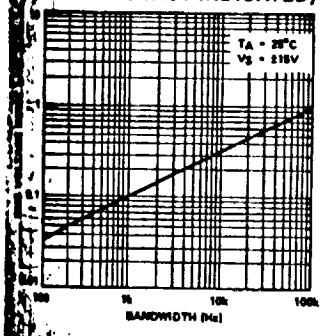

TOTAL NOISE vs SOURCE RESISTANCE

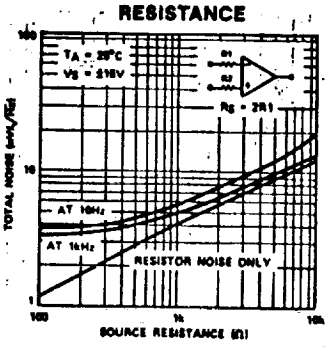

VOLTAGE NOISE DENSITY vs TEMPERATURE

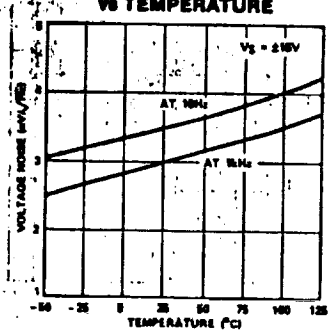

VOLTAGE NOISE DENSITY vs SUPPLY VOLTAGE

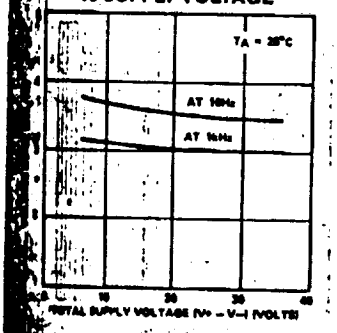

CURRENT NOISE DENSITY vs FREQUENCY

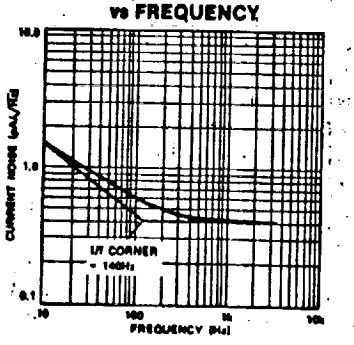

SUPPLY CURRENT vs SUPPLY VOLTAGE

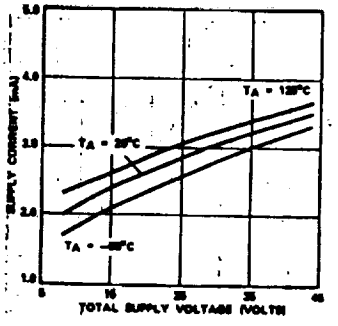

TYPICAL PERFORMANCE CHARACTERISTICS

OFFSET VOLTAGE DRIFT OF EIGHT REPRESENTATIVE UNITS vs TEMPERATURE

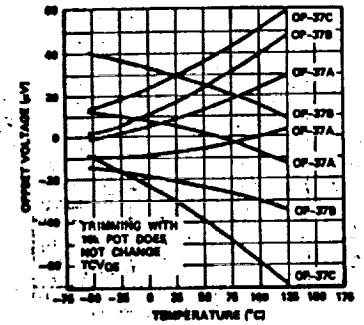

LONG-TERM OFFSET VOLTAGE DRIFT OF SIX REPRESENTATIVE UNITS

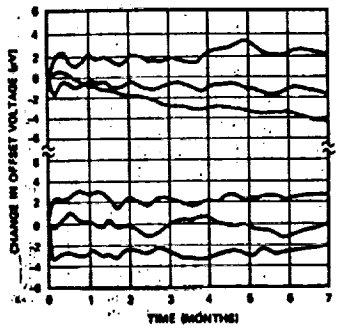

WARM-UP OFFSET VOLTAGE DRIFT

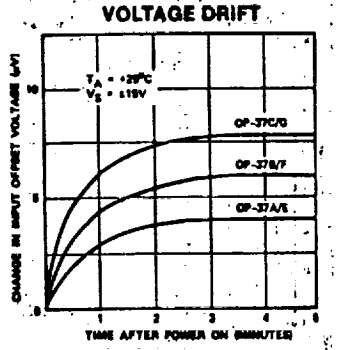

OFFSET VOLTAGE CHANGE DUE TO THERMAL SHOCK

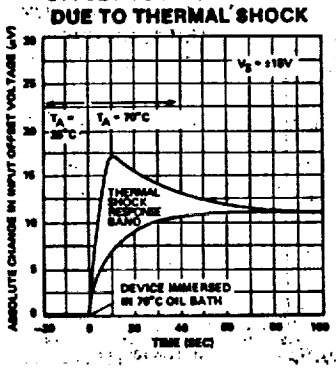

INPUT BIAS CURRENT vs TEMPERATURE

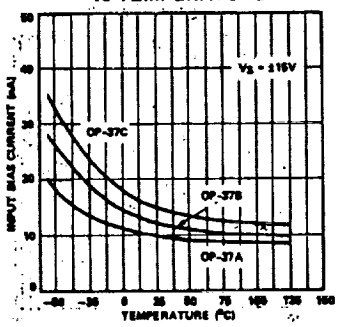

INPUT OFFSET CURRENT vs TEMPERATURE

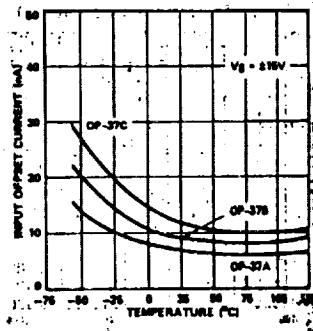

OPEN-LOOP GAIN vs FREQUENCY

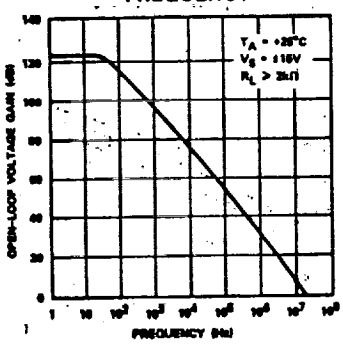

SLEW RATE, GAIN BANDWIDTH PRODUCT, PHASE MARGIN vs TEMPERATURE

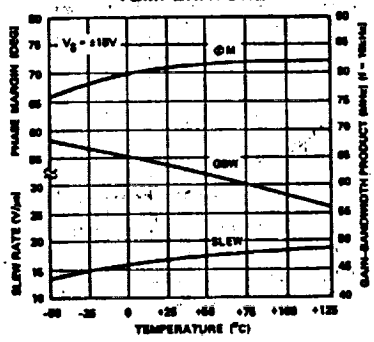

GAIN, PHASE SHIFT vs FREQUENCY

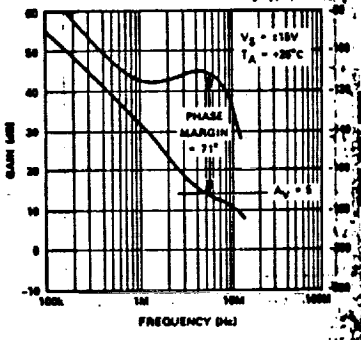

TYPICAL PERFORMANCE CHARACTERISTICS

OPEN-LOOP VOLTAGE GAIN vs SUPPLY VOLTAGE

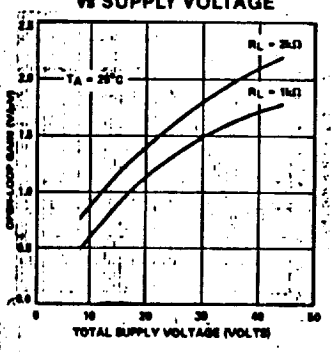

MAXIMUM OUTPUT SWING vs FREQUENCY

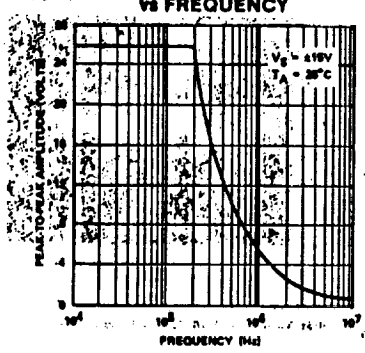

MAXIMUM OUTPUT VOLTAGE vs LOAD RESISTANCE

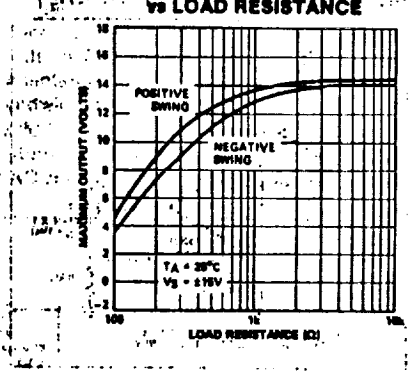

SMALL-SIGNAL OVERSHOOT vs CAPACITIVE LOAD

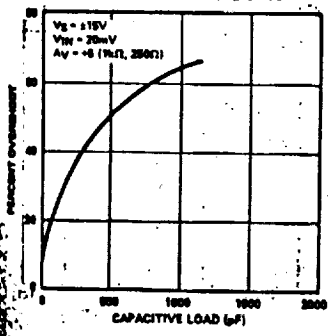

LARGE-SIGNAL TRANSIENT RESPONSE

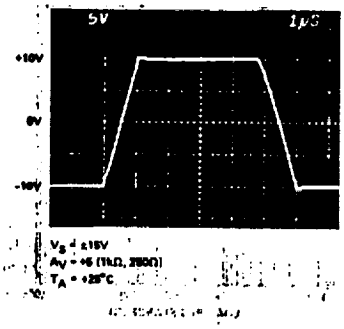

SMALL-SIGNAL TRANSIENT RESPONSE

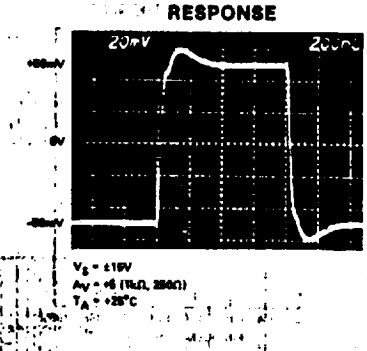

SHORT-CIRCUIT CURRENT vs TIME

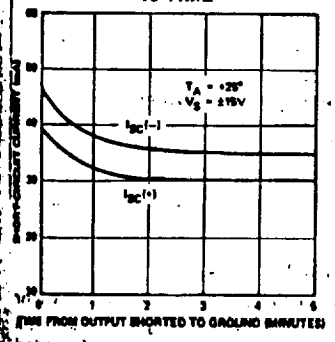

CMRR vs FREQUENCY

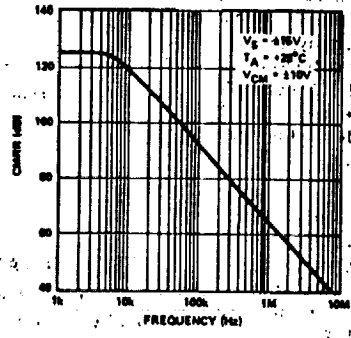

COMMON-MODE INPUT RANGE vs SUPPLY VOLTAGE

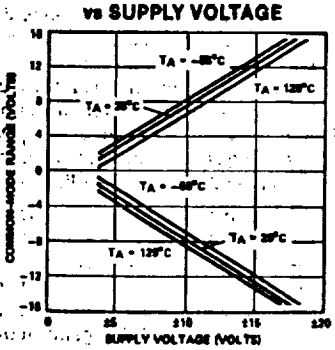

TYPICAL PERFORMANCE CHARACTERISTICS

NOISE TEST CIRCUIT (0.1Hz TO 10Hz)

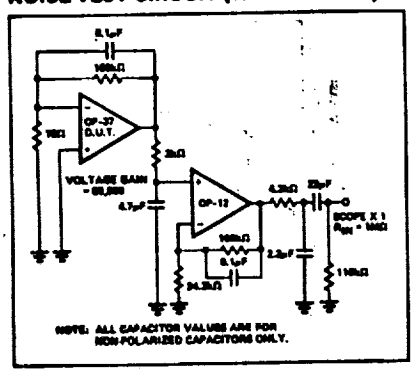

LOW-FREQUENCY NOISE

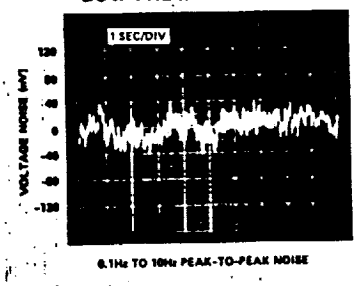

NOTE:
Observation time limited to 10 seconds.

OPEN-LOOP VOLTAGE GAIN vs LOAD RESISTANCE

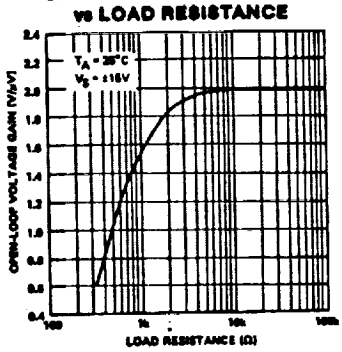

PSRR vs FREQUENCY

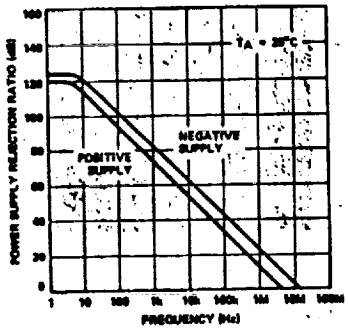

SLEW RATE vs LOAD

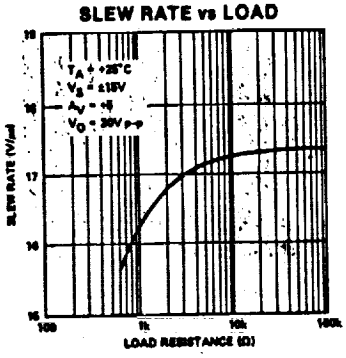

SLEW RATE vs SUPPLY VOLTAGE

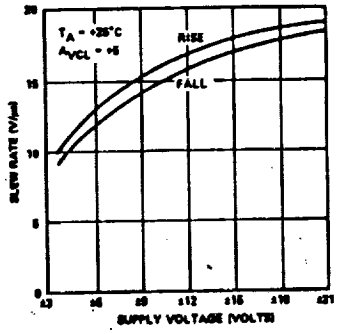

APPLICATIONS INFORMATION

OP-37 Series units may be inserted directly into 725, OP-06, OP-07, and OP-05 sockets with or without removal of external compensation or nulling components. Additionally, the OP-37 may be fitted to unnulled 741-type sockets; however, if conventional 741 nulling circuitry is in use, it should be modified or removed to ensure correct OP-37 operation. OP-37 offset voltage may be nulled to zero (or other desired setting) using a potentiometer (see offset nulling circuit).

The OP-37 provides stable operation with load capacitances of up to 1000pF and ±10V swings; larger capacitances should be decoupled with a 50Ω resistor inside the feedback loop. Closed-loop gain must be at least five. For closed-loop gain between five to ten, the designer should consider both the OP-27 and the OP-37. For gains above ten, the OP-37 has a clear advantage over the unity-gain-stable OP-27.

Thermoelectric voltages generated by dissimilar metals at the input terminal contacts can degrade the drift performance. Best operation will be obtained when both input contacts are maintained at the same temperature.

OFFSET NULLING CIRCUIT

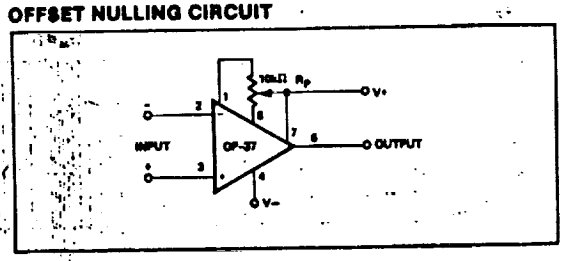

OFFSET VOLTAGE ADJUSTMENT

The input offset voltage of the OP-37 is trimmed at wafer level. However, if further adjustment of V_{OS} is necessary, a 10kΩ trim potentiometer may be used. TCV_{OS} is not degraded (see offset nulling circuit). Other potentiometer values from 1kΩ to 1MΩ can be used with a slight degradation (0.1 to 0.2μV/° C) of TCV_{OS}. Trimming to a value other than zero creates a drift of approximately (V_{OS}/300) μV/° C. For exam-

ple, the change in TCV_{OS} will be 0.33μV/° C if V_{OS} is adjusted to 100μV. The offset-voltage adjustment range with a 10kΩ potentiometer is ±4mV. If smaller adjustment range is required, the nulling sensitivity can be reduced by using a smaller pot in conjunction with fixed resistors. For example, the network below will have a ±280μV adjustment range.

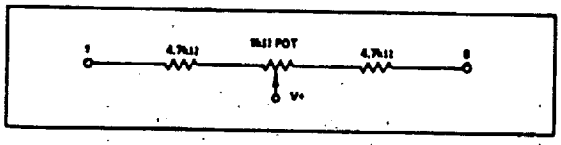

BURN-IN CIRCUIT

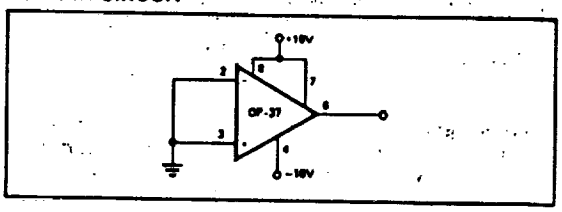

NOISE MEASUREMENTS

To measure the 80nV peak-to-peak noise specification of the OP-37 in the 0.1Hz to 10Hz range, the following precautions must be observed:

(1) The device has to be warmed-up for at least five minutes. As shown in the warm-up drift curve, the offset voltage typically changes 4μV due to increasing chip temperature after power-up. In the 10 second measurement interval, these temperature-induced effects can exceed tens-of- nanovolts.

(2) For similar reasons, the device has to be well-shielded from air currents. Shielding minimizes thermocouple effects.

(3) Sudden motion in the vicinity of the device can also "feed-through" to increase the observed noise.

(4) The test time to measure 0.1Hz-to-10Hz noise should not exceed 10 seconds. As shown in the noise-tester frequency response curve, the 0.1Hz corner is defined by only one zero. The test time of 10 seconds acts as an additional zero to eliminate noise contributions from the frequency band below 0.1Hz.

(5) A noise-voltage-density test is recommended when measuring noise on a large number of units. A 10Hz noise-voltage-density measurement will correlate well with a 0.1Hz-to-10Hz peak-to-peak noise reading, since both results are determined by the white noise and the location of the 1/f corner frequency.

OPTIMIZING LINEARITY

Best linearity will be obtained by designing for the minimum output current required for the application. High gain and excellent linearity can be achieved by operating the op amp with a peak output current of less than ±10mA.

INSTRUMENTATION AMPLIFIER

A three-op-amp instrumentation amplifier provides high gain and wide bandwidth. The input noise of the circuit below is $4.9nV/\sqrt{Hz}$. The gain of the input stage is set at 25 and the gain of the second stage is 40; overall gain is 1000. The amplifier bandwidth of 800kHz is extraordinarily good for a precision instrumentation amplifier. Set to a gain of 1000, this yields a gain-bandwidth product of 800MHz. The full-power bandwidth for a $20V_{p-p}$ output is 250kHz. Potentiometer R7 provides quadrature trimming to optimize the instrumentation amplifier's AC common-mode rejection.

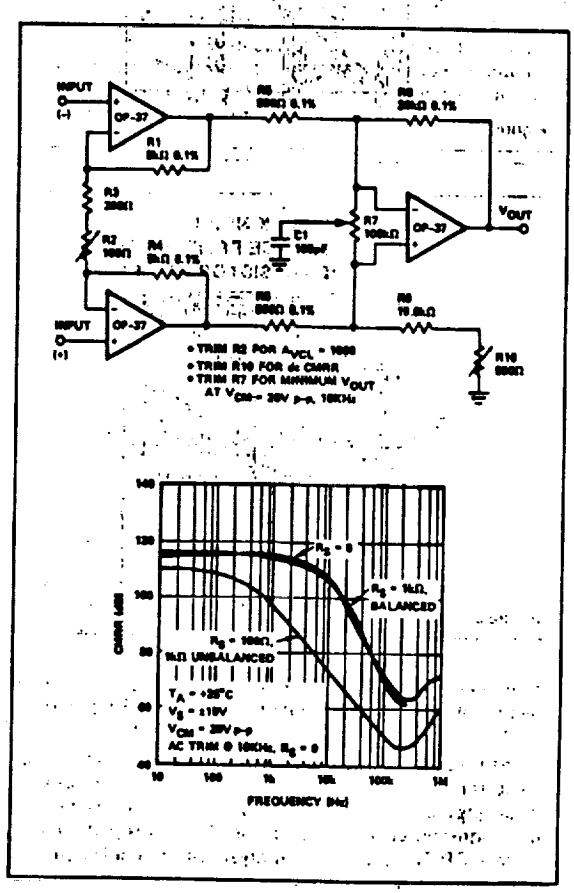

COMMENTS ON NOISE

The OP-37 is a very low-noise monolithic op amp. The outstanding input voltage noise characteristics of the OP-37 are achieved mainly by operating the input stage at a high quiescent current. The input bias and offset currents, which would normally increase, are held to reasonable values by the input-bias-current cancellation circuit. The OP-37A/E has I_B and I_{OS} of only ±40nA and 35nA respectively at 25° C. This is particularly important when the input has a high source-resistance. In addition, many audio amplifier designers

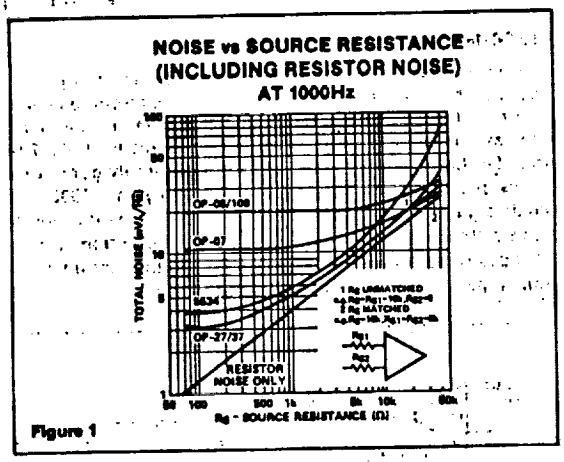

Figure 1

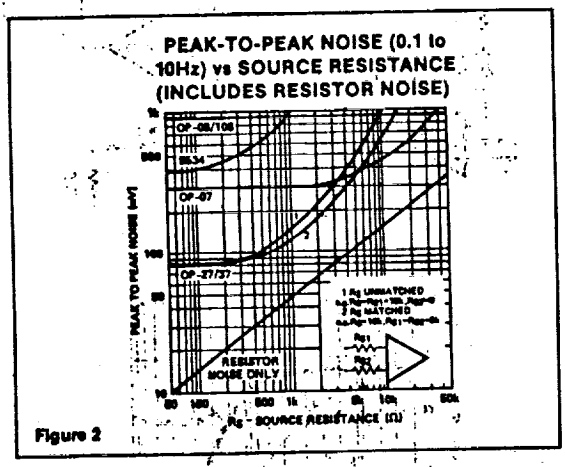

Figure 2

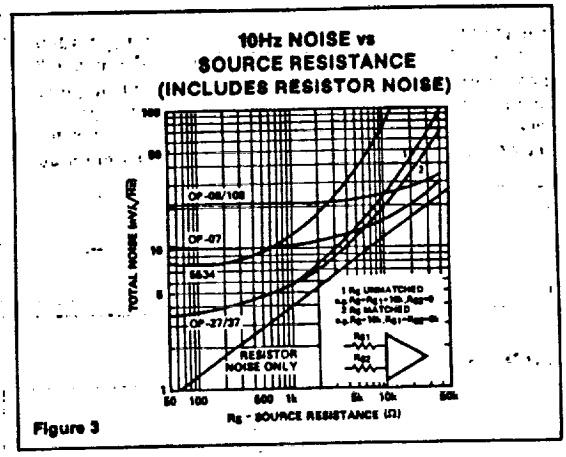

Figure 3

prefer to use direct coupling. The high I_B, TCV_{OS} of previous designs have made direct coupling difficult, if not impossible, to use.

Voltage noise is inversely proportional to the square-root of bias current, but current noise is proportional to the square-root of bias current. The OP-37's noise advantage disappears when high source-resistors are used. Figures 1, 2, and 3 compare OP-37 observed total noise with the noise performance of other devices in different circuit applications.

Total noise = $[(\text{Voltage noise})^2 + (\text{current noise} \times R_S)^2 + (\text{resistor noise}^2)]^{1/2}$

Figure 1 shows noise-versus-source-resistance at 1000Hz. The same plot applies to wideband noise. To use this plot, just multiply the vertical scale by the square-root of the bandwidth.

At R_S<1kΩ, the OP-37's low voltage noise is maintained. With R_S< 1kΩ, total noise increases, but is dominated by the resistor noise rather than current or voltage noise. It is only beyond R_S of 20kΩ that current noise starts to dominate. The argument can be made that current noise is not important for applications with low-to-moderate source resistances. The crossover between the OP-37 and OP-07 and OP-08 noise occurs in the 15-to-40kΩ region.

Figure 2 shows the 0.1Hz-to-10Hz peak-to-peak noise. Here the picture is less favorable; resistor noise is negligible, current noise becomes important because it is inversely proportional to the square-root of frequency. The crossover with the OP-07 occurs in the 3-to 5kΩ range depending on whether balanced or unbalanced source resistors are used (at 3kΩ the I_B, I_{OS} error also can be three times the V_{OS} spec.).

Therefore, for low-frequency applications, the OP-07 is better than the OP-27/37 when R_S > 3kΩ. The only exception is when gain error is important. Figure 3 illustrates the 10Hz noise. As expected, the results are between the previous two figures.

For reference, typical source resistances of some signal sources are listed in Table 1.

Table 1

DEVICE	SOURCE IMPEDANCE	COMMENTS
Strain gauge	<500Ω	Typically used in low-frequency applications.
Magnetic tapehead	<1500Ω	Low I_B very important to reduce self-magnetization problems when direct coupling is used. OP-37 I_B can be neglected.
Magnetic phonograph cartridges	<1500Ω	Similar need for low I_B in direct coupled applications. OP-37 will not introduce any self-magnetization problem.
Linear variable differential transformer	<1500Ω	Used in rugged servo-feedback applications. Bandwidth of interest is 400Hz to 5kHz.

AUDIO APPLICATIONS

The following applications information has been abstracted from a PMI article in the 12/20/80 issue of Electronic Design magazine and updated.

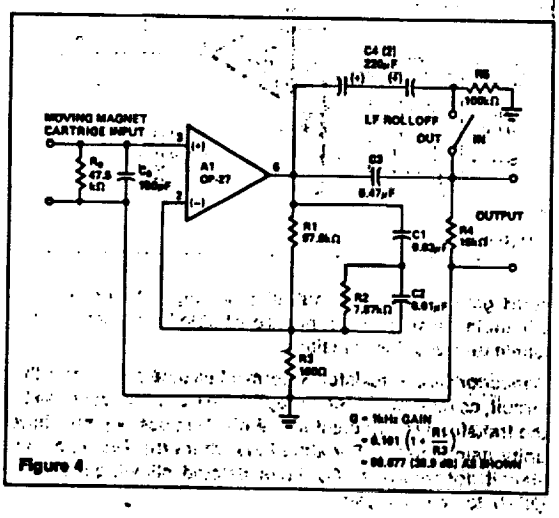

Figure 4

Figure 4 is an example of a phono pre-amplifier circuit using the OP-27 for A_1; R_1-R_2-C_1-C_2 form a very accurate RIAA network with standard component values. The popular method to accomplish RIAA phono equalization is to employ frequency-dependent feedback around a high-quality gain block. Properly chosen, an RC network can provide the three necessary time constants of 3180, 318, and 75μs.[1]

For initial equalization accuracy and stability, precision metal-film resistors and film capacitors of polystyrene or polypropylene are recommended since they have low voltage coefficients, dissipation factors, and dielectric absorption.[4] (High-K ceramic capacitors should be avoided here, though low-K ceramics—such as NPO types, which have excellent dissipation factors, and somewhat lower dielectric absorption — can be considered for small values or where space is at a premium.)

The OP-27 brings a $3.2nV/\sqrt{Hz}$ voltage noise and 0.45 $pA/\sqrt{Hz}$ current noise to this circuit. To minimize noise from other sources, R_3 is set to a value of 100Ω, which generates a voltage noise of $1.3nV/\sqrt{Hz}$. The noise increases the $3.2nV/\sqrt{Hz}$ of the amplifier by only 0.7dB. With a 1kΩ source, the circuit noise measures 63dB below a 1mV reference level, unweighted, in a 20kHz noise bandwidth.

Gain (G) of the circuit at 1kHz can be calculated by the expression:

$$G = 0.101\ (1 + \frac{R_1}{R_3})$$

For the values shown, the gain is just under 100 (or 40dB). Lower gains can be accommodated by increasing R_3, but gains higher than 40dB will show more equalization errors because of the 8MHz gain-bandwidth of the OP-27.

This circuit is capable of very low distortion over its entire range, generally below 0.01% at levels up to 7V rms. At 3V output levels, it will produce less than 0.03% total harmonic distortion at frequencies up to 20kHz.

Capacitor C_3 and resistor R_4 form a simple 6dB-per-octave rumble filter, with a corner at 22Hz. As an option, the switch-selected shunt capacitor C_4, a nonpolarized electrolytic, bypasses the low-frequency rolloff. Placing the rumble filter's high-pass action after the preamp has the desirable result of discriminating against the RIAA-amplified low-frequency noise components and pickup-produced low-frequency disturbances.

A preamplifier for NAB tape playback is similar to an RIAA phono preamp, though more gain is typically demanded, along with equalization requiring a heavy low-frequency boost. The circuit in Fig. 4 can be readily modified for tape use, as shown by Fig. 5.

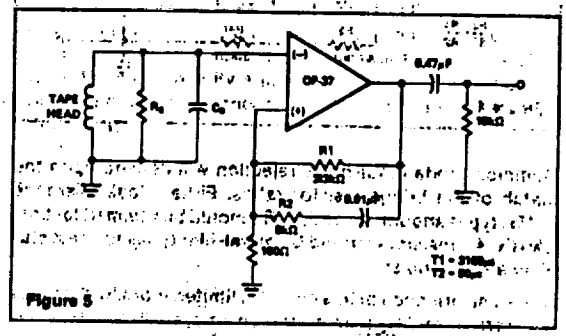

Figure 5

While the tape-equalization requirement has a flat high-frequency gain above 3kHz ($T_2 = 50\mu s$), the amplifier need not be stabilized for unity gain. The decompensated OP-37 provides a greater bandwidth and slew rate. For many applications, the idealized time constants shown may require trimming of R_1 and R_2 to optimize frequency response for nonideal tape-head performance and other factors.[5]

The network values of the configuration yield a 50dB gain at 1kHz, and the dc gain is greater than 70dB. Thus, the worst-case output offset is just over 500mV. A single 0.47μF output capacitor can block this level without affecting the dynamic range.

The tape head can be coupled directly to the amplifier input, since the worst-case bias current of 85nA with a 400mH, 100 μin. head (such as the PRB2H7K) will not be troublesome.

One potential tape-head problem is presented by amplifier bias-current transients which can magnetize a head. The OP-27 and OP-37 are free of bias-current transients upon power up or power down. However, it is always advantageous to control the speed of power supply rise and fall, to eliminate transients.

In addition, the dc resistance of the head should be carefully controlled, and preferably below 1kΩ. For this configuration, the bias-current-induced offset voltage can be greater than the 170μV maximum offset if the head resistance is not sufficiently controlled.

A simple, but effective, fixed-gain transformerless microphone preamp (Fig. 6) amplifies differential signals from low-impedance microphones by 50dB, and has an input impedance of 2kΩ. Because of the high working gain of the circuit, an OP-37 helps to preserve bandwidth, which will be 110kHz. As the OP-37 is a decompensated device (minimum stable gain of 5), a dummy resistor, R_p, may be necessary, if the microphone is to be unplugged. Otherwise the 100% feedback from the open input may cause the amplifier to oscillate.

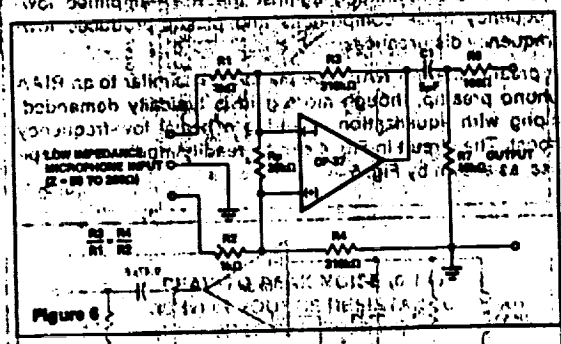

Figure 6

Common-mode input-noise rejection will depend upon the match of the bridge-resistor ratios. Either close-tolerance (0.1%) types should be used, or R_4 should be trimmed for best CMRR. All resistors should be metal-film types for best stability and low noise.

Noise performance of this circuit is limited more by the input resistors R_1 and R_2 than by the op amp, as R_1 and R_2 each generate a $4nV/\sqrt{Hz}$ noise, while the op amp generates a $3.2nV/\sqrt{Hz}$ noise. The rms sum of these predominant noise sources will be about $6nV/\sqrt{Hz}$, equivalent to 0.9μV in a 20kHz noise bandwidth, or nearly 61dB below a 1mV input signal. Measurements confirm this predicted performance.

For applications demanding appreciably lower noise, a high-quality microphone-transformer-coupled preamp (Fig. 7) incorporates the internally compensated OP-27. T_1 is a JE-115K-E 150Ω/15kΩ transformer which provides an optimum source resistance for the OP-27 device. The circuit has an overall gain of 40dB, the product of the transformer's voltage setup and the op amp's voltage gain.

Gain may be trimmed to other levels, if desired, by adjusting R_2 or R_3. Because of the low offset voltage of the OP-27, the output offset of this circuit will be very low, 1.7mV or less, for a

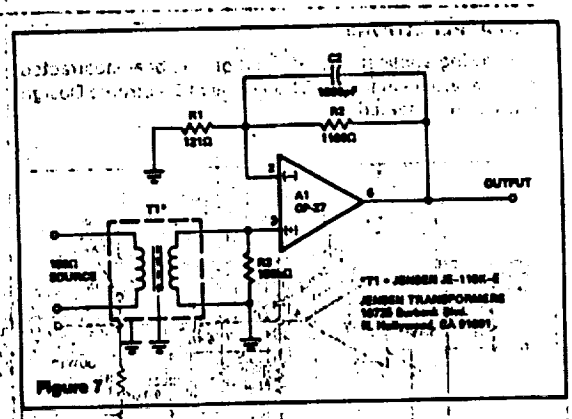

Figure 7

40dB gain. The typical output blocking capacitor can be eliminated in such cases, but is desirable for higher gains to eliminate switching transients.

Capacitor C_2 and resistor R_2 form a 2μs time constant in this circuit, as recommended for optimum transient response by the transformer manufacturer. With C_2 in use, A_1 must have unity-gain stability. For situations where the 2μs time constant is not necessary, C_2 can be deleted, allowing the faster OP-37 to be employed.

Some comment on noise is appropriate to understand the capability of this circuit. A 150Ω resistor and R_1 and R_2 gain resistors connected to a noiseless amplifier will generate 220 nV of noise in a 20kHz bandwidth, or 73dB below a 1mV reference level. Any practical amplifier can only approach this noise level; it can never exceed it. With the OP-27 and T_1 specified, the additional noise degradation will be close to 3.6dB (or −69.5 referenced to 1mV).

References

1. Lipshitz, S.P., "On RIAA Equalization Networks," JAES, Vol. 27, June 1979, p. 458-481.
2. Jung, W.G., IC Op Amp Cookbook, 2nd Ed., H.W. Sams and Company, 1980.
3. Jung, W.G., Audio IC Op Amp Applications, 2nd Ed., H.W. Sams and Company, 1978.
4. Jung, W.G., and Marsh, R.M., "Picking Capacitors," Audio, February & March, 1980.
5. Otala, M., "Feedback-Generated Phase Nonlinearity in Audio Amplifiers," London AES Convention, March 1980, preprint 1578.
6. Stata, D.F., and Kaufman, M., Handbook of Operational Amplifier Circuit Design, New York, McGraw Hill, 1976.

BURR-BROWN®

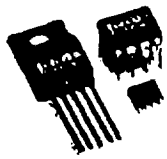

BUF634

AVAILABLE IN DIE

250mA HIGH-SPEED BUFFER

FEATURES

- HIGH OUTPUT CURRENT: 250mA
- SLEW RATE: 2000V/µs
- PIN-SELECTED BANDWIDTH: 30MHz/180MHz
- LOW QUIESCENT CURRENT: 1.5mA (30MHz BW)
- WIDE SUPPLY RANGE: ±2.25 to ±18V
- INTERNAL CURRENT LIMIT
- THERMAL SHUT-DOWN
- 8-PIN DIP, SO-8, 5-PIN TO-220 PACKAGES, DICE

APPLICATIONS

- VALVE DRIVER
- SOLENOID DRIVER
- OP AMP CURRENT BOOSTER
- LINE DRIVER
- HEADPHONE DRIVER
- VIDEO DRIVER
- MOTOR DRIVER
- TEST EQUIPMENT
- ATE PIN DRIVER

DESCRIPTION

The BUF634 is a high speed unity-gain open-loop buffer recommended for a wide range of applications. It can be used inside the feedback loop of op amps to increase output current, eliminate thermal feedback and improve capacitive load drive.

For low power applications, the BUF634 operates on 1.5mA quiescent current with 250mA output and 2000V/µs slew rate. Bandwidth is increased from 30MHz to 180MHz by connecting pin 1 to V–.

Output circuitry is fully protected by internal current limit and thermal shut-down making it rugged and easy to use.

The BUF634 is available in a variety of packages to suit mechanical and power dissipation requirements. Types include 8-pin DIP, SO-8 surface-mount and 5-pin TO-220. Dice are also available.

8-Pin DIP Package
SO-8 Surface-Mount Package

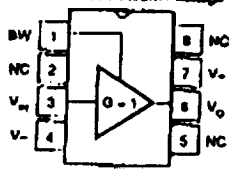

5-Pin TO-220

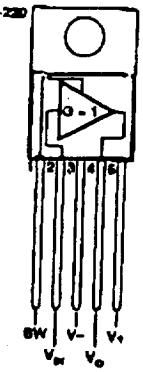

Tel: (602) 746-1111 • Twx: 910-952-1111 • Telex: 066-6491 • FAX: (602) 889-1510

SPECIFICATIONS

ELECTRICAL

T_A = +25°C, V_S = ±15V unless otherwise noted

PARAMETER	CONDITION	BUF634F, U, T						UNITS
		LOW QUIESCENT CURRENT MODE			WIDE BANDWIDTH MODE			
		MIN	TYP	MAX	MIN	TYP	MAX	
INPUT								
Offset Voltage	Specified Temperature Range		±30	±100		•	•	mV
vs Temperature	V_S = ±2.25V[1] to ±18V		±100			•		µV/°C
vs Power Supply	V_{IN} = 0V		0.1	1		•		mV/V
Input Bias Current	R_L = 100Ω		±0.5	±2		45	±20	µA
Input Impedance	f = 10kHz		60 ‖ 8			8 ‖ 8		MΩ ‖ pF
Noise Voltage			4			•		nV/√Hz
GAIN	R_L = 1kΩ, V_O = ±10V	0.95	0.99		•	•		V/V
	R_L = 100Ω, V_O = ±10V	0.85	0.93		•	•		V/V
	R_L = 67Ω, V_O = ±10V	0.8	0.9		•	•		V/V
OUTPUT								
Current Output, Continuous			±250			•		mA
Voltage Output, Positive	I_O = 10mA	(V+) –2.1	(V+) –1.7		•	•		V
Negative	I_O = –10mA	(V–) +2.1	(V–) +1.8		•	•		V
Positive	I_O = 100mA	(V+) –3	(V+) –2.4		•	•		V
Negative	I_O = –100mA	(V–) +4	(V–) +3.6		•	•		V
Positive	I_O = 150mA	(V+) –4	(V+) –3.6		•	•		V
Negative	I_O = –150mA	(V–) +5	(V–) +4		•	•		V
Short-Circuit Current			±350	±550		±400		mA
DYNAMIC RESPONSE								
Bandwidth, –3dB	R_L = 1kΩ		30			180		MHz
	R_L = 100Ω		80			160	•	MHz
Slew Rate	20Vp-p, R_L = 100Ω		2000			•		V/µs
Settling Time, 0.1%	20V Step, R_L = 100Ω		200			•		ns
1%	20V Step, R_L = 100Ω		50			•		ns
Differential Gain	3.58MHz, V_O = 0.7V, R_L = 150Ω		4			0.4		%
Differential Phase	3.58MHz, V_O = 0.7V, R_L = 150Ω		7.5			0.1		°
POWER SUPPLY								
Specified Operating Voltage			±15			•	•	V
Operating Voltage Range		±2.25[1]		±18	•		•	V
Quiescent Current, I_O	I_O = 0		±1.5	±2		±15	±20	mA
TEMPERATURE RANGE								
Specification		–40		+85	•		•	°C
Operating		–40		+125	•		•	°C
Storage		–40		+125	•		•	°C
Thermal Shutdown Temperature, T_J			175			•		°C
Thermal Resistance, θ_{JA}	"P" Package[3]		100			•		°C/W
θ_{JA}	"U" Package[3]		150			•		°C/W
θ_{JC}	"T" Package[3]		65			•		°C/W
θ_{JC}	"T" Package		8			•		°C/W

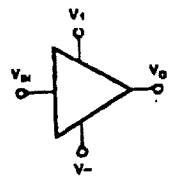

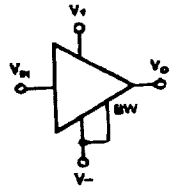

NOTES: (1) Tests are performed on high speed automatic test equipment, at approximately 25°C junction temperature. The power dissipation of this product will cause some parameters to shift when warmed up. See typical performance curves for over-temperature performance. (2) Limited output swing available at low supply voltage. See Output voltage specifications. (3) Typical when all leads are soldered to a circuit board. See text for recommendations.

PIN CONFIGURATION

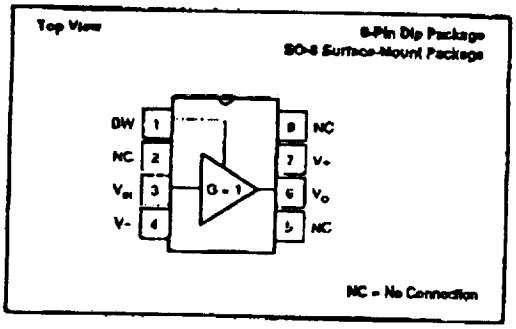

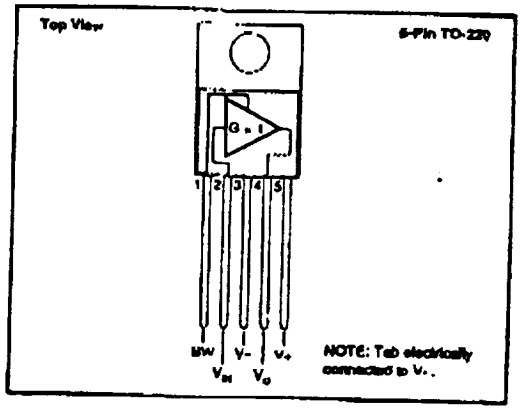

ABSOLUTE MAXIMUM RATINGS

Supply Voltage	±18V
Input Voltage Range	$±V_s$
Output Short-Circuit (to ground)	Continuous
Operating Temperature	-40°C to +125°C
Storage Temperature	-40°C to +125°C
Junction Temperature	+150°C
Lead Temperature (soldering,10s)	+300°C

PACKAGE INFORMATION[1]

MODEL	PACKAGE	PACKAGE DRAWING NUMBER
BUF634P	8-Pin PDIP	006
BUF634U	SO-8 Surface Mount	182
BUF634T	5-Pin TO-220	315

NOTE: (1) For detailed drawing and dimension table, please see end of data sheet, or Appendix D of Burr-Brown IC Data Book.

ELECTROSTATIC DISCHARGE SENSITIVITY

Any integrated circuit can be damaged by ESD. Burr-Brown recommends that all integrated circuits be handled with appropriate precautions. Failure to observe proper handling and installation procedures can cause damage.

ESD damage can range from subtle performance degradation to complete device failure. Precision integrated circuits may be more susceptible to damage because very small parametric changes could cause the device not to meet published specifications.

ORDERING INFORMATION

MODEL	PACKAGE	TEMPERATURE RANGE	PACKAGE NUMBER
BUF634P	8-Pin Plastic DIP	-40 to +85°C	006
BUF634U	SO-8 Surface Mount	-40 to +85°C	182
BUF634T	5-Pin TO-220	-40 to +85°C	315
BUF634D	Dice	-40 to +85°C	--

DICE INFORMATION

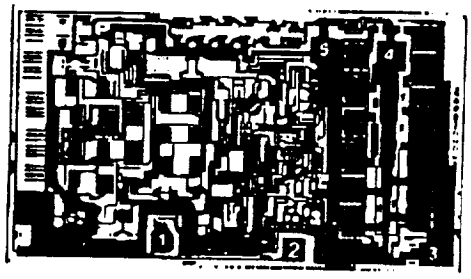

BUF634 DIE TOPOGRAPHY

PAD	FUNCTION
1	BW
2	V_{IN}
3	V-
4	V_O
5	V_+

Substrate Bias: Internally connected to V- power supply.

MECHANICAL INFORMATION

	MILS (0.001")	MILLIMETERS
Die Size	120 x 70 ±5	3.05 x 1.78 ±0.13
Die Thickness	20 ±3	0.51 ±0.08
Min. Pad Size	4 x 4	0.1 x 0.1
Backing		Chromium-Silver

See "DICE PRODUCTS" Appendix C in Burr-Brown IC Data Book, or contact factory for current information.

TYPICAL PERFORMANCE CURVES

T_A = +25°C, V_S = ±15V unless otherwise noted.

GAIN and PHASE vs FREQUENCY vs QUIESCENT CURRENT

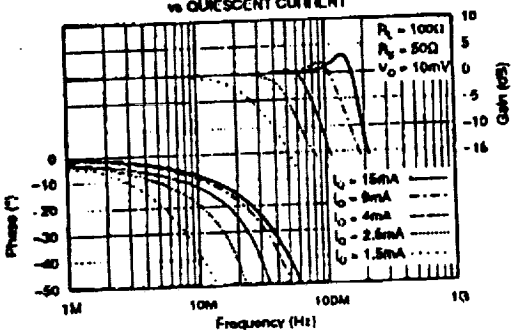

GAIN and PHASE vs FREQUENCY vs TEMPERATURE

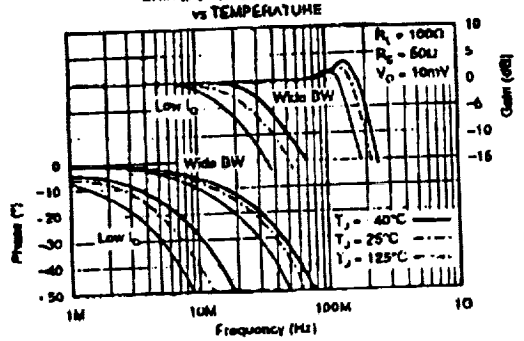

GAIN and PHASE vs FREQUENCY vs SOURCE RESISTANCE

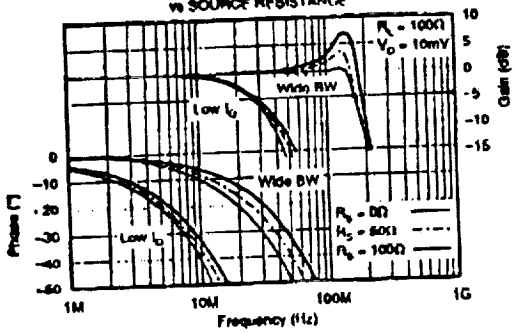

GAIN and PHASE vs FREQUENCY vs LOAD RESISTANCE

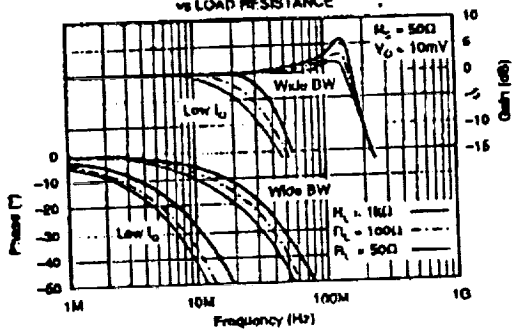

GAIN and PHASE vs FREQUENCY vs LOAD CAPACITANCE

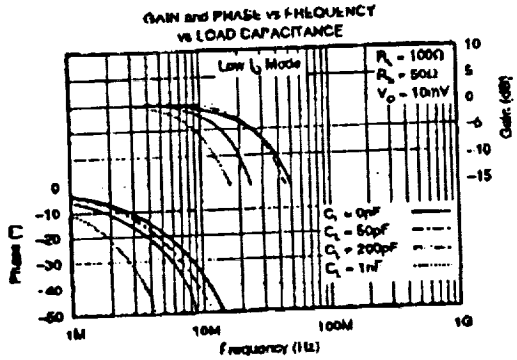

GAIN and PHASE vs FREQUENCY vs LOAD CAPACITANCE

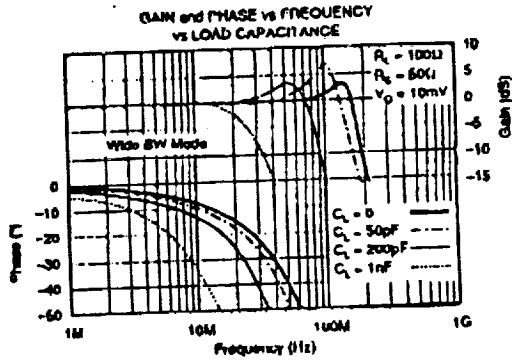

TYPICAL PERFORMANCE CURVES (CONT)

T_A = +25°C, V_S = ±15V unless otherwise noted

GAIN and PHASE vs FREQUENCY vs POWER SUPPLY VOLTAGE

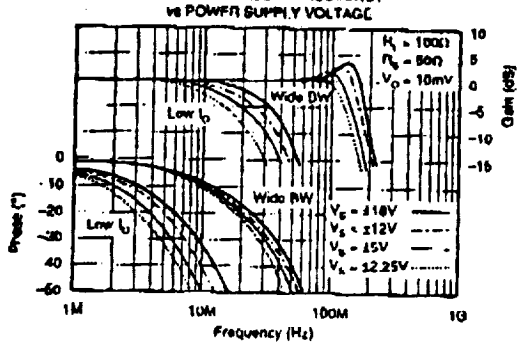

POWER SUPPLY REJECTION vs FREQUENCY

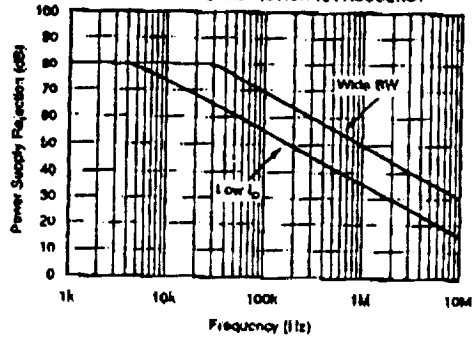

QUIESCENT CURRENT vs RESISTANCE

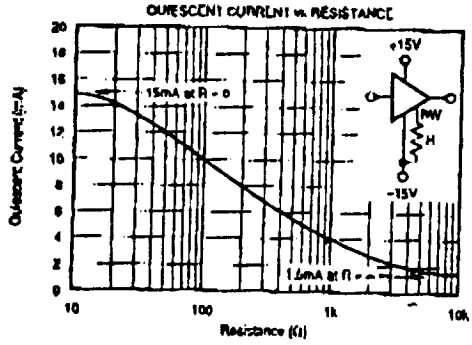

SHORT CIRCUIT CURRENT vs TEMPERATURE

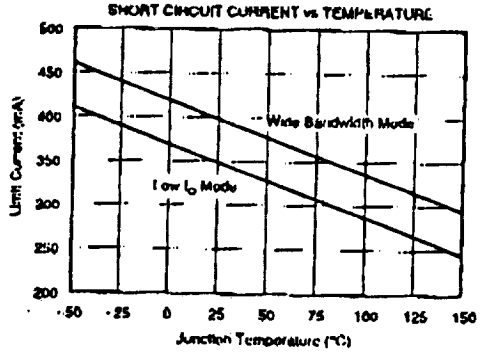

QUIESCENT CURRENT vs TEMPERATURE

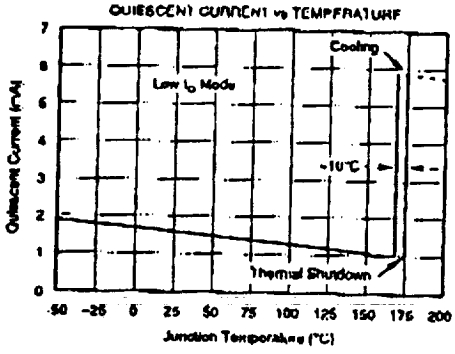

QUIESCENT CURRENT vs TEMPERATURE

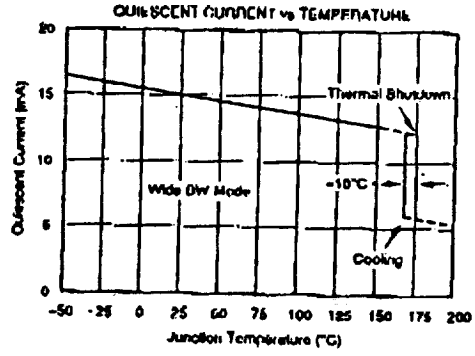

TYPICAL PERFORMANCE CURVES (CONT)

T_A = +25°C, V_S = ±15V unless otherwise noted.

OUTPUT VOLTAGE SWING vs OUTPUT CURRENT

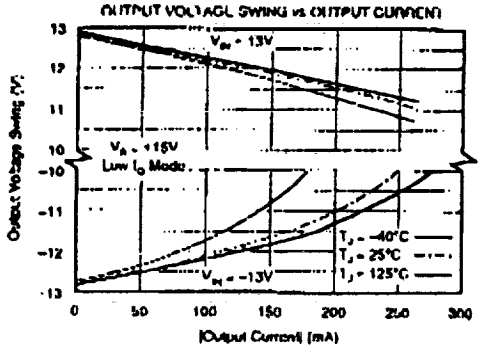

OUTPUT VOLTAGE SWING vs OUTPUT CURRENT

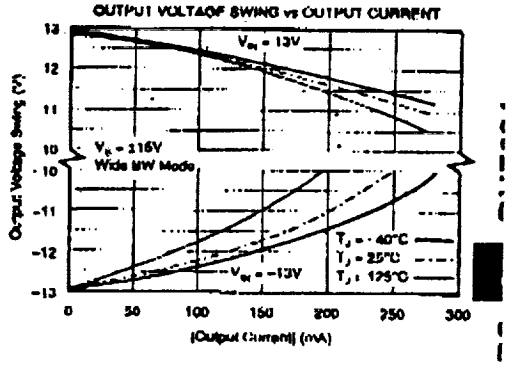

MAXIMUM POWER DISSIPATION vs TEMPERATURE

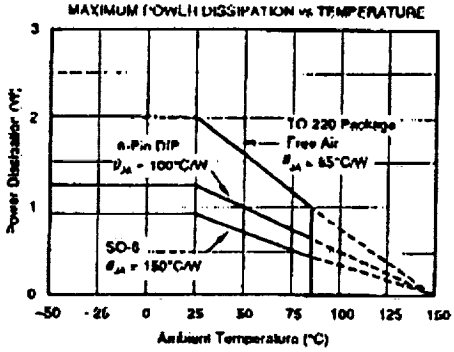

MAXIMUM POWER DISSIPATION vs TEMPERATURE

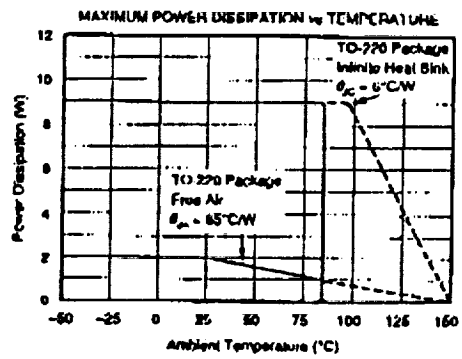

SMALL SIGNAL RESPONSE

R_L = 50Ω, R_f = 100Ω

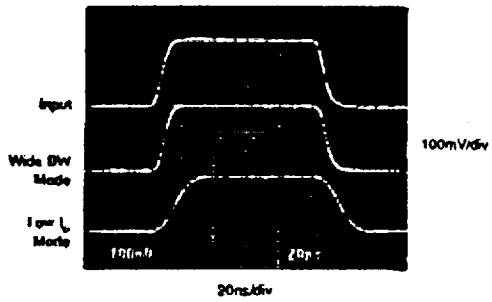

LARGE-SIGNAL RESPONSE

R_L = 50Ω, R_f = 100Ω

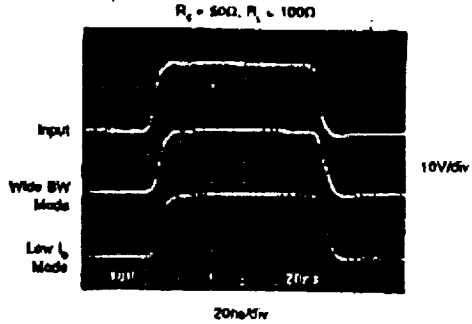

APPLICATION INFORMATION

Figure 1 is a simplified circuit diagram of the BUF634 showing its open-loop complementary follower design.

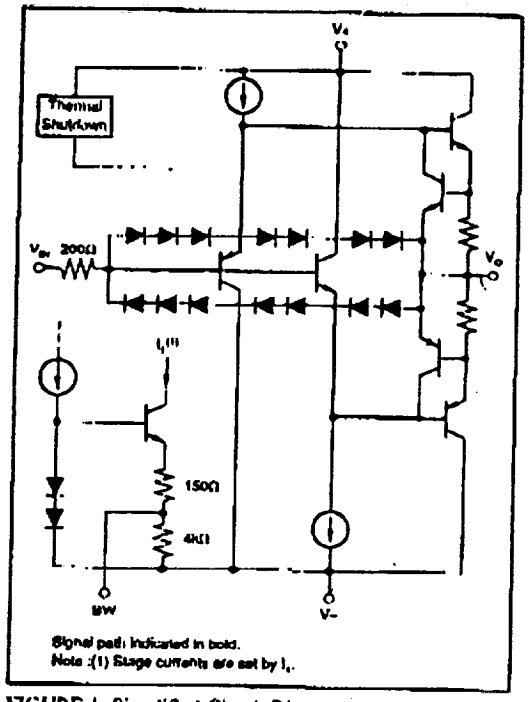

FIGURE 1. Simplified Circuit Diagram.

Figure 2 shows the BUF634 connected as an open-loop buffer. The source impedance and optional input resistor, R_S, influence frequency response—see typical curves. Power supplies should be bypassed with capacitors connected close to the device pins. Capacitor values as low as 0.1µF will assure stable operation in most applications, but high output current and fast output slewing can demand large current transients from the power supplies. Solid tantalum 10µF capacitors are recommended.

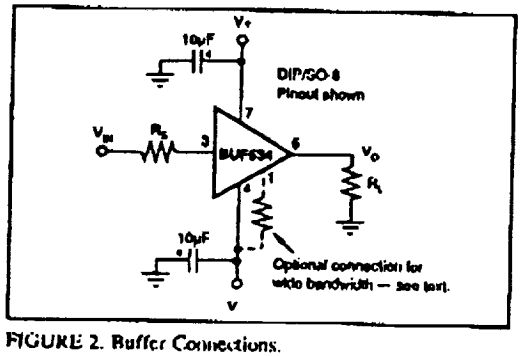

FIGURE 2. Buffer Connections.

High frequency open-loop applications may benefit from special bypassing and layout considerations- see "High Frequency Applications" at end of applications discussion.

OUTPUT CURRENT

The BUF634 can deliver up to ±250mA continuous output current. Internal circuitry limits output current to approximately ±350mA—see typical performance curve "Short Circuit Current vs Temperature". For many applications, however, the continuous output current will be limited by thermal effects.

The output voltage swing capability varies with junction temperature and output current- see typical curves "Output Voltage Swing vs Output Current." Although all three package types are tested for the same output performance using a high speed test, the higher junction temperatures with the DIP and SO-8 package types will often provide less output voltage swing. The TO-220 package can be used with a heat sink to reduce junction temperature, allowing maximum possible output swing.

THERMAL PROTECTION

Power dissipated in the BUF634 will cause the junction temperature to rise. A thermal protection circuit in the BUF634 will disable the output when the junction temperature reaches approximately 175°C. When the thermal protection is activated, the output stage is disabled, allowing the device to cool. Quiescent current is approximately 6mA during thermal shutdown. When the junction temperature cools to approximately 165°C the output circuitry is again enabled. This can cause the protection circuit to cycle on and off with a period ranging from a fraction of a second to several minutes or more, depending on package type, signal, load and thermal environment.

The thermal protection circuit is designed to prevent damage during abnormal conditions. Any tendency to activate the thermal protection circuit during normal operation is a sign of an inadequate heat sink or excessive power dissipation for the package type.

The 5-pin TO-220 package provides best thermal performance. When used with a properly sized heat sink, output of the TO-220 version is not limited by thermal performance. See Application Bulletin AB-037 for details on heat sink calculations. The mounting tab of the TO-220 package is electrically connected to the V– power supply.

The DIP and SO-8 surface-mount packages are excellent for applications requiring high output current with low average power dissipation.

To achieve the best possible thermal performance with the DIP or SO-8 packages, solder the device directly to a circuit board. Since much of the heat is dissipated by conduction through the package pins, sockets will degrade thermal performance. Use wide circuit board traces on all the device pins, including pins that are not connected. With the DIP package, use traces on both sides of the printed circuit board if possible.

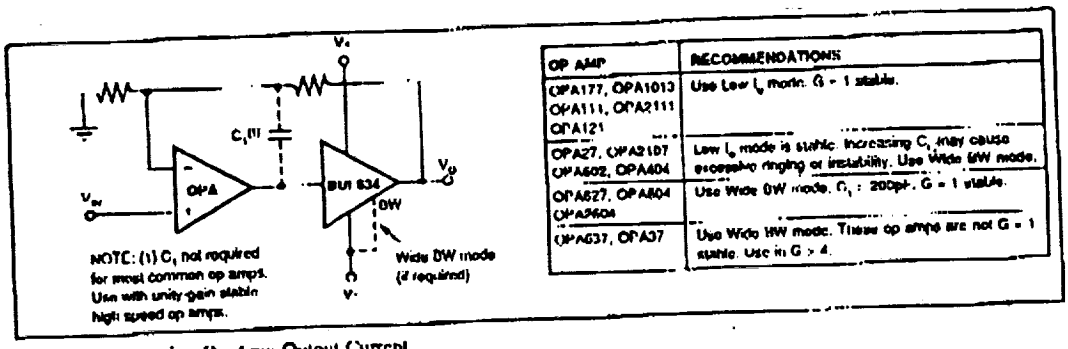

OP AMP	RECOMMENDATIONS
OPA177, OPA1013 OPA111, OPA2111 OPA121	Use Low I_Q mode. G = 1 stable.
OPA27, OPA2107 OPA602, OPA404	Low I_Q mode is stable. Increasing C_1 may cause excessive ringing or instability. Use Wide BW mode.
OPA627, OPA604 OPA2604	Use Wide 0W mode. C_1 = 200pF, G = 1 stable.
OPA637, OPA37	Use Wide BW mode. These op amps are not G = 1 stable. Use in G > 4.

FIGURE 3. Boosting Op Amp Output Current.

POWER DISSIPATION

Power dissipation depends on power supply voltage, signal and load conditions. With dc signals, power dissipation is equal to the product of output current times the voltage across the conducting output transistor. Power dissipation can be minimized by using the lowest possible power supply voltage necessary to assure the required output voltage swing.

For resistive loads, the maximum power dissipation occurs at a dc output voltage of one-half the power supply voltage. Dissipation with ac signals is lower. Application Bulletin AB-039 explains how to calculate or measure power dissipation with unusual signals and loads.

Any tendency to activate the thermal protection circuit indicates excessive power dissipation or an inadequate heat sink. For reliable operation, junction temperature should be limited to 150°C, maximum. To estimate the margin of safety in a complete design, increase the ambient temperature until the thermal protection is triggered. The thermal protection should trigger more than 45°C above the maximum expected ambient condition of your application.

INPUT CHARACTERISTICS

Internal circuitry is protected with a diode clamp connected from the input to output of the BUF634 (see Figure 1). If the output is unable to follow the input within approximately 3V (such as with an output short-circuit), the input will conduct increased current from the input source. This is limited by the internal 200Ω resistor. If the input source can be damaged by this increase in load current, an additional resistor can be connected in series with the input.

BANDWIDTH CONTROL PIN

The -3dB bandwidth of the BUF634 is approximately 30MHz in the low quiescent current mode (1.5mA typical). To select this mode, leave the bandwidth control pin open (no connection).

Bandwidth can be extended to approximately 180MHz by connecting the bandwidth control pin to V–. This increases the quiescent current to approximately 15mA. Intermediate bandwidths can be set by connecting a resistor in series with the bandwidth control pin (see typical curve "Quiescent Current vs Resistance" for resistor selection. Characteristics of the bandwidth control pin can be seen in the simplified circuit diagram, Figure 1.

The rated output current and slew rate are not affected by the bandwidth control, but the current limit value changes slightly. Output voltage swing is somewhat improved in the wide bandwidth mode. The increased quiescent current when in wide bandwidth mode produces greater power dissipation during low output current conditions. This quiescent power is equal to the total supply voltage, (V+)+|V–|, times the quiescent current.

BOOSTING OP AMP OUTPUT CURRENT

The BUF634 can be connected inside the feedback loop of most op amps to increase output current—see Figure 3. When connected inside the feedback loop, the BUF634's offset voltage and other errors are corrected by the feedback of the op amp.

To assure that the op amp remains stable, the BUF634's phase shift must remain small throughout the loop gain of the circuit. For a G=+1 op amp circuit, the BUF634 must contribute little additional phase shift (approximately 20° or less) at the unity-gain frequency of the op amp. Phase shift is affected by various operating conditions that may affect stability of the op amp—see typical Gain and Phase curves.

Most general-purpose or precision op amps remain unity-gain stable with the BUF634 connected inside the feedback loop as shown. Large capacitive loads may require the BUF634 to be connected for wide bandwidth for stable operation. High speed or fast-settling op amps generally require the wide bandwidth mode to remain stable and to assure good dynamic performance. To check for stability with an op amp, look for oscillations or excessive ringing on signal pulses with the intended load and worst case conditions that affect phase response of the buffer.

HIGH FREQUENCY APPLICATIONS

The BUF634's excellent bandwidth and fast slew rate make it useful in a variety of high frequency open-loop applications. When operated open-loop, circuit board layout and bypassing technique can affect dynamic performance.

For best results, use a ground plane type circuit board layout and bypass the power supplies with 0.1µF ceramic chip

capacitors at the device pins. Source resistance will affect high-frequency peaking and step response overshoot and ringing. Best response is usually achieved with a series input resistor of 25Ω to 200Ω, depending on the signal source. Response with some loads (especially capacitive) can be improved with a resistor of 10Ω to 150Ω in series with the output.

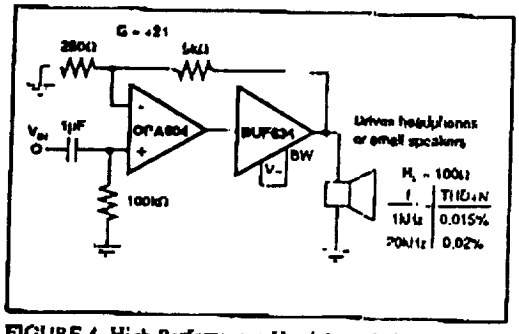

FIGURE 4. High Performance Headphone Driver.

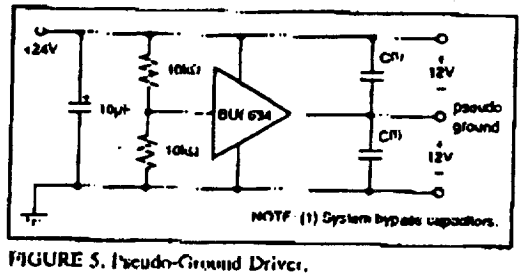

FIGURE 5. Pseudo-Ground Driver.

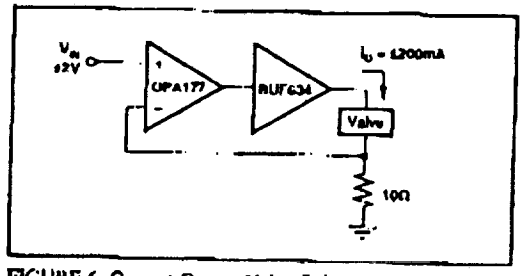

FIGURE 6. Current-Output Valve Driver.

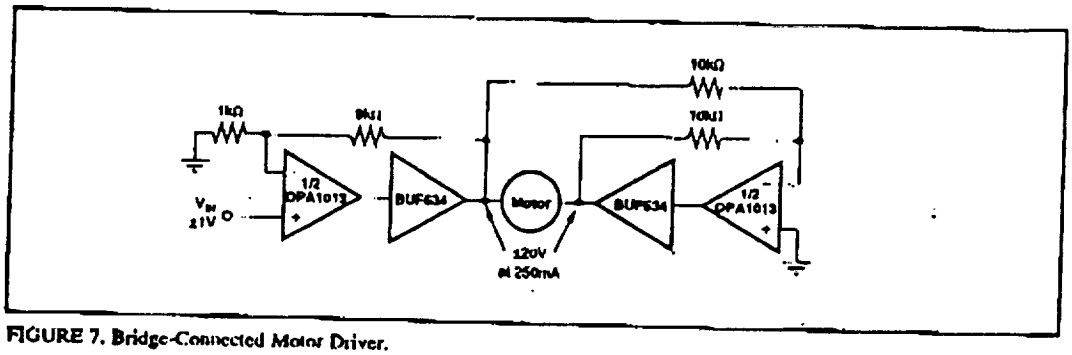

FIGURE 7. Bridge-Connected Motor Driver.

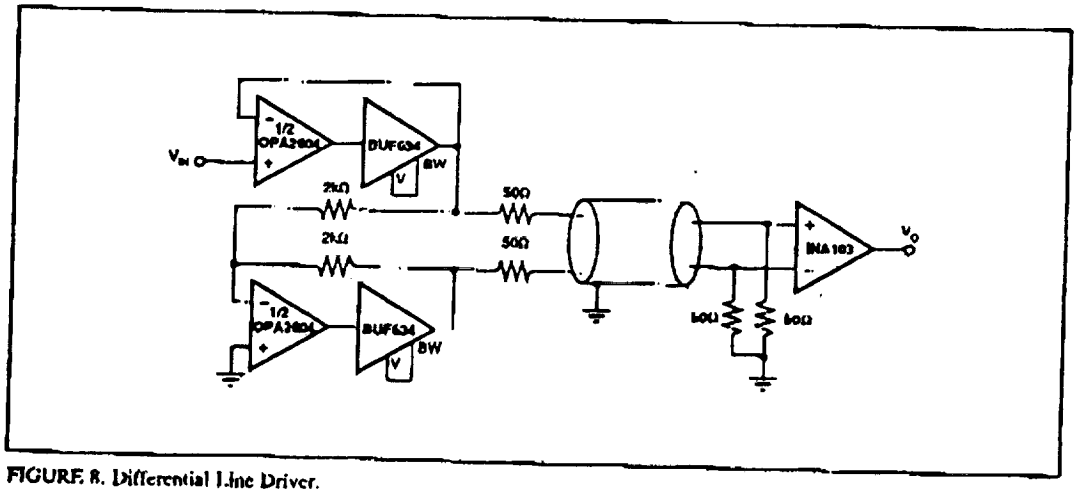

FIGURE 8. Differential Line Driver.

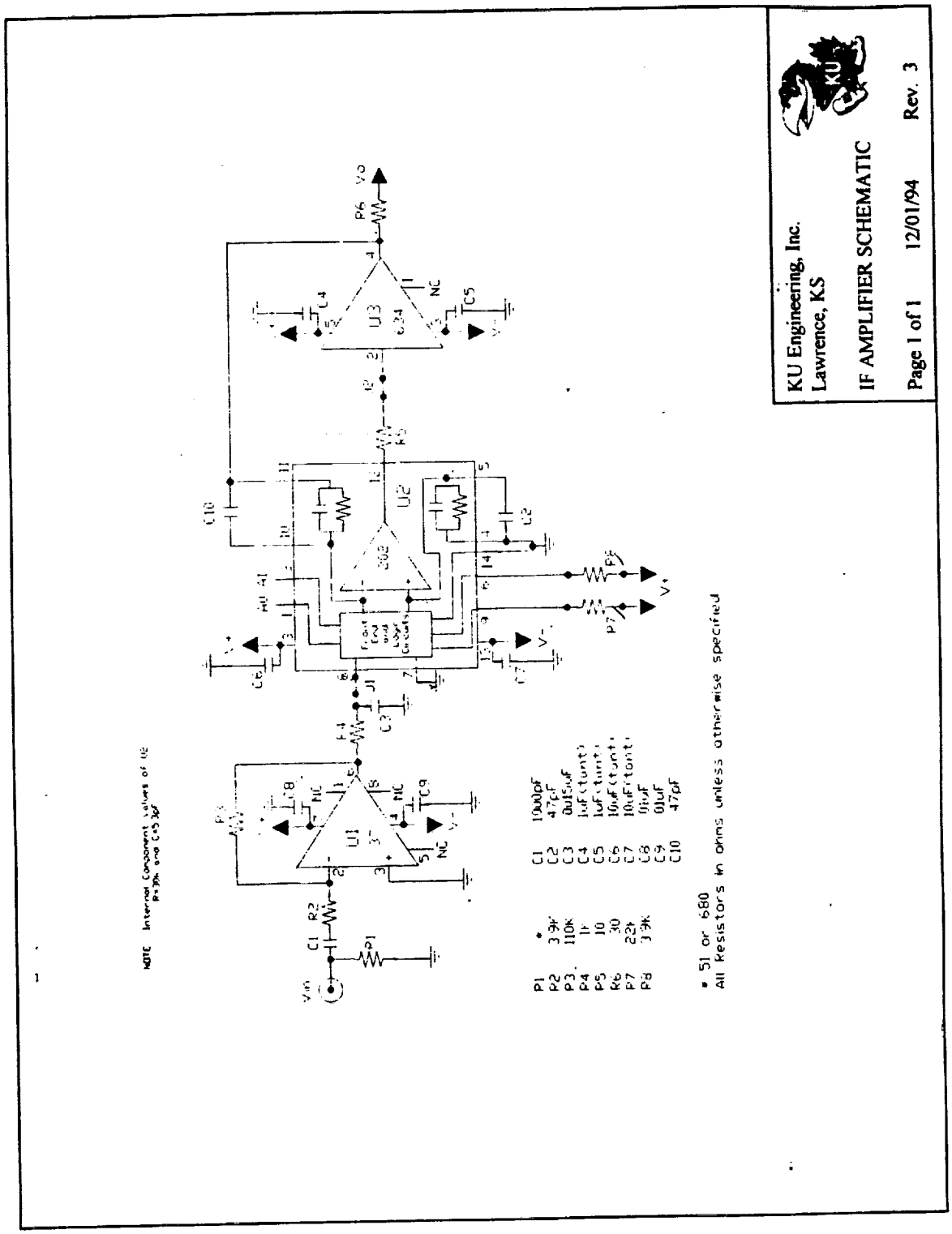

BURR-BROWN®

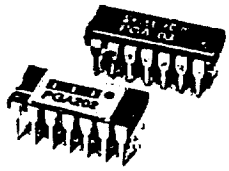

PGA202/203

Digitally Controlled Programmable-Gain INSTRUMENTATION AMPLIFIER

FEATURES

- DIGITALLY PROGRAMMABLE GAINS:
  DECADE MODEL—PGA202
  GAINS OF 1, 10, 100, 1000
  BINARY MODEL—PGA203
  GAINS OF 1, 2, 4, 8
- LOW BIAS CURRENT: 50pA max
- FAST SETTLING: 2µs to 0.01%
- LOW NON-LINEARITY: 0.012% max
- HIGH CMRR: 80dB min
- NEW TRANSCONDUCTANCE CIRCUITRY
- LOW COST

APPLICATIONS

- DATA ACQUISITION SYSTEMS
- AUTO-RANGING CIRCUITS
- DYNAMIC RANGE EXPANSION
- REMOTE INSTRUMENTATION
- TEST EQUIPMENT

DESCRIPTION

The PGA202 is a monolithic instrumentation amplifier with digitally controlled gains of 1, 10, 100 and 1000. The PGA203 provides gains of 1, 2, 4, and 8. Both have TTL or CMOS-compatible inputs for easy microprocessor interface. Both have FET inputs and a new transconductance circuitry that keeps the bandwidth nearly constant with gain. Gain and offsets are laser trimmed to allow use without any external components. Both amplifiers are available in ceramic or plastic packages. The ceramic package is specified over the full industrial temperature range while the plastic package covers the commercial range.

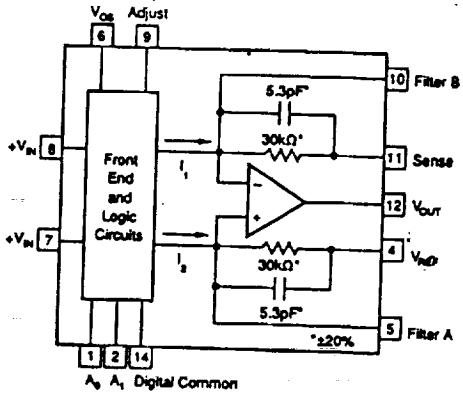

International Airport Industrial Park • Mailing Address: PO Box 11400 • Tucson, AZ 85734 • Street Address: 6730 S. Tucson Blvd. • Tucson, AZ 85706
Tel: (602) 746-1111 • Twx: 910-952-1111 • Cable: BBRCORP • Telex: 066-6491 • FAX: (602) 889-1510 • Immediate Product Info: (800) 548-6132

SPECIFICATIONS

ELECTRICAL

At +25°C, V_{cc} = ±15V unless otherwise noted.

PARAMETER	CONDITION	PGA202/203AG[1]			PGA202/203BG[1]			PGA202/203KP[1]			U
		MIN	TYP	MAX	MIN	TYP	MAX	MIN	TYP	MAX	
GAIN											
Error[2]	G < 1000		0.05	0.25		•	0.15		•	•	
	G = 1000		0.1	1		0.08	0.5		•	•	
Nonlinearity	G < 1000		0.002	0.015		•	0.012		•	•	
	G = 1000		0.02	0.06		•	0.04		•	•	
Gain vs Temperature	G < 100		3	25		•	15		•		ppm
	G = 100		40	120		•	60		•		ppm
	G = 1000		100	300		•	150		•		ppm
RATED OUTPUT											
Voltage	$\|I_{out}\| \le 5mA$	±10	±12		•	•		•	•		
Over Specified Temperature	See Typical Perf. Curve		±9			•			±10		
Current	$\|V_{out}\| \le 10V$	±5	±10		•	•		•	•		m
Impedance			0.5			•			•		Ω
ANALOG INPUTS											
Common-Mode Range		±10	±13		•	•		•	•		V
Absolute Max Voltage[3]	No Damage			$\pm V_{cc}$			•			•	V
Impedance, Differential			10 ‖ 3			•			•		GΩ
Common-Mode			10 ‖ 1			•			•		GΩ
OFFSET VOLTAGE (RTI)											
Initial Offset at 25°C[4]			±(0.5 + 5/G)	±(2 + 24/G)		•	±(1 + 12/G)		•	•	m
vs Temperature			±(3 + 50/G)	±(24 + 240/G)		•	±(12 + 120/G)		•		µV/
Offset vs Time			50			•			•		µV/M
Offset vs Supply	$10 \le V_{cc} \le 15$		10 + 250/G	100 + 900/G		•	50 + 450/G		•	•	µV
INPUT BIAS CURRENT											
Initial Bias Current: at 25°C			10	50		•	•		•	•	p
at 85°C			640	3200		•	•		•	•	p
Initial Offset Current: at 25°C			5	25		•	•		•	•	p
at 85°C			320	1600		•	•		•	•	p
COMMON MODE REJECTION RATIO											
	G = 1	80	100		•	•		•	•		dB
	G = 10	86	110		•	•		•	•		dB
	G = 100	92	120		•	•		•	•		dB
	G = 1000	94	120		•	•		•	•		dB
INPUT NOISE											
Noise Voltage 0.1 to 10Hz			1.7			•			•		µVp
Noise Density at 10kHz[5]			12			•			•		nV/√
OUTPUT NOISE											
Noise Voltage 0.1 to 10Hz			32			•			•		µVp
Density at 1kHz[5]			400			•			•		nV/√
DYNAMIC RESPONSE											
Frequency Response	G < 1000		1000			•			•		kH
	G = 1000		250			•			•		kH
Full Power Bandwidth	G < 1000		400			•			•		kH
	G = 1000		100			•			•		kH
Slew Rate		10	20		15	•		•	•		V/µ
Settling Time (0.01%)[7]	G < 1000		2			•			•		µs
	G = 1000		10			•			•		µs
Overload Recovery Time[7]	G < 1000		5			•			•		µs
	G = 1000		10			•			•		µs
DIGITAL INPUTS											
Digital Common Range		$-V_{cc}$		$V_{cc} - 8$	•		•	•		•	V
Input Low Threshold[6]				0.8			•			•	V
Input Low Current				10			•			•	µA
Input High Voltage		2.4			•			•			V
Input High Current				10			•			•	µA
POWER SUPPLY											
Rated Voltage			±15			•			•		V
Voltage Range		±6		±18	•		•	•		•	V
Quiescent Current			6.5			•			•		mA
TEMPERATURE RANGE											
Specification		–25		85	•		•	0		70	°C
Operating		–55		125	•		•	–55		85	°C
Storage		–65		150	•		•	–40		100	°C
θ_{ja}			100			•			•		°C/W

[1] Same as the PGA202/203AG

NOTES: (1) All specifications apply to both the PGA202 and the PGA203. Values given for a gain of 10 are the same for a gain of 8 and other values may be interpolated. (2) Measured with a 10k load. (3) The analog inputs are internally diode clamped. (4) Adjustable to zero. (5) $V_{noise,rms} = \sqrt{(V_{n,amp})^2 + (V_{n,output}/Gain)^2}$. (6) Threshold voltages are referenced to Digital Common. (7) From input change or gain change.

PIN CONFIGURATION

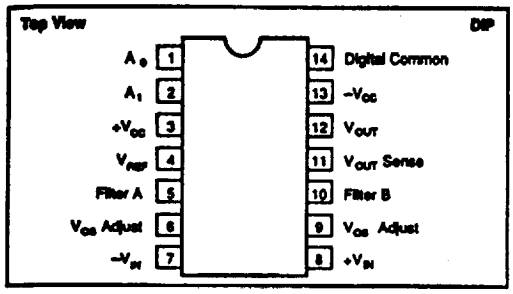

ABSOLUTE MAXIMUM RATINGS

Supply Voltage	±18V
Internal Power Dissipation	750mW
Analog and Digital Inputs	±(V_{CC} + 0.5V)
Operating Temperature Range:	
G Package	–55°C to +125°C
P Package	–40°C to +100°C
Lead Temperature (soldering, 10s)	300°C
Output Short Circuit Duration	Continuous
Junction Temperature	175°C

PACKAGE INFORMATION[1]

MODEL	PACKAGE	PACKAGE DRAWING NUMBER
PGA202KP	14-Pin Plastic DIP	010
PGA202AG	14-Pin Ceramic DIP	169
PGA202BG	14-Pin Ceramic DIP	169
PGA203KP	14-Pin Plastic DIP	010
PGA203AG	14-Pin Ceramic DIP	169
PGA203BG	14-Pin Ceramic DIP	169

NOTE: (1) For detailed drawing and dimension table, please see end of data sheet, or Appendix D of Burr-Brown IC Data Book.

ORDERING INFORMATION

MODEL	GAINS	PACKAGE	TEMPERATURE RANGE	OFFSET VOLTAGE MAX (mV)
PGA202KP	1, 10, 100, 1000	Plastic DIP	0°C to +70°C	±(2 + 24/G)
PGA202AG	1, 10, 100, 1000	Ceramic DIP	–25°C to +85°C	±(2 + 24/G)
PGA202BG	1, 10, 100, 1000	Ceramic DIP	–25°C to +85°C	±(1 + 12/G)
PGA203KP	1, 2, 4, 8	Plastic DIP	0°C to +70°C	±(2 + 24/G)
PGA203AG	1, 2, 4, 8	Ceramic DIP	–25°C to +85°C	±(2 + 24/G)
PGA203BG	1, 2, 4, 8	Ceramic DIP	–25°C to +85°C	±(1 + 12/G)

TYPICAL PERFORMANCE CURVES

T_A = +25°C, V_S = ±15V unless otherwise noted.

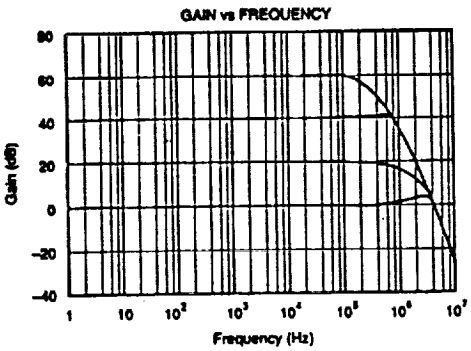

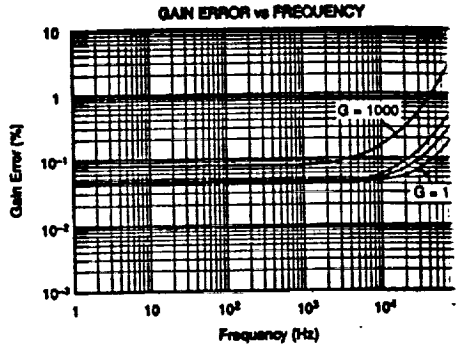

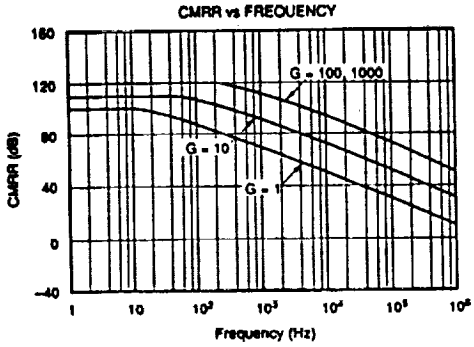

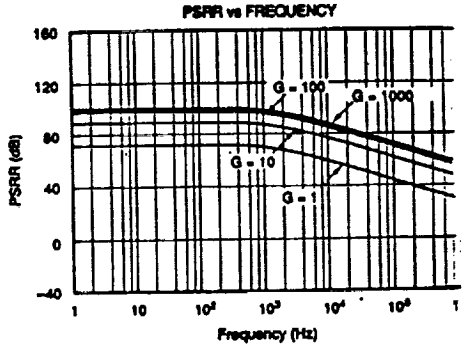

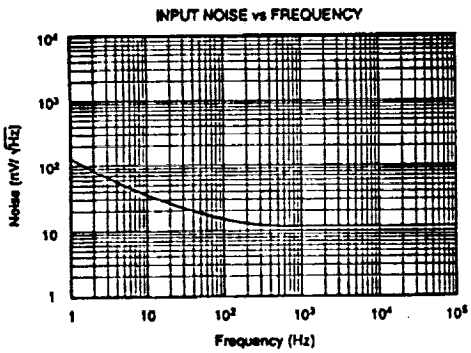

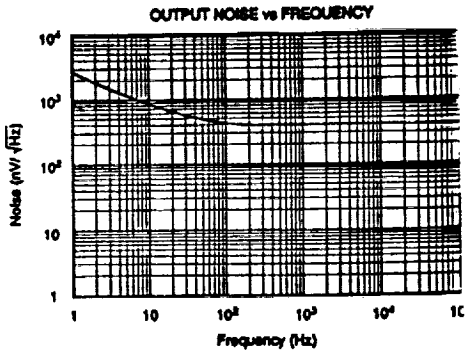

TYPICAL PERFORMANCE CURVES (CONT)

T_A = +25°C, V_S = ±15V unless otherwise noted.

QUIESCENT CURRENT vs POWER SUPPLY

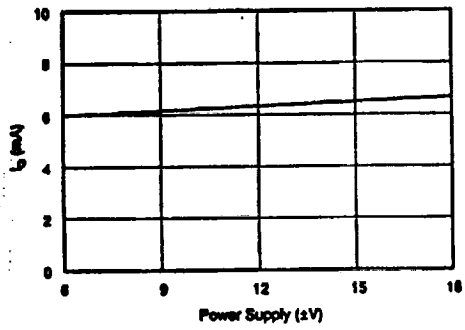

INPUT BIAS CURRENT vs POWER SUPPLY

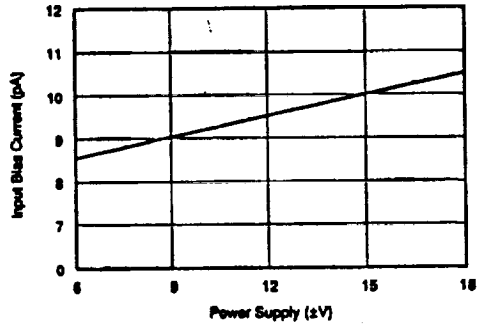

INPUT RANGE vs POWER SUPPLY

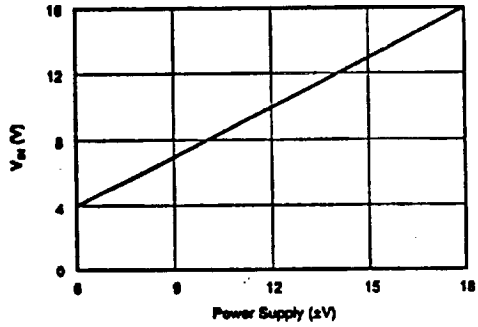

OUTPUT SWING vs POWER SUPPLY

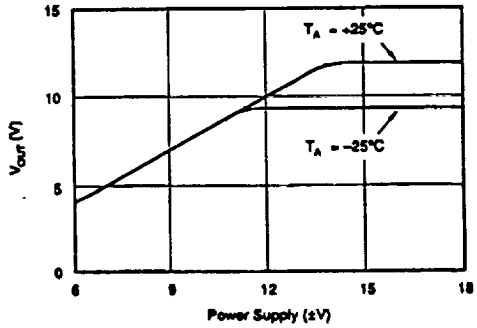

OUTPUT SWING vs LOAD

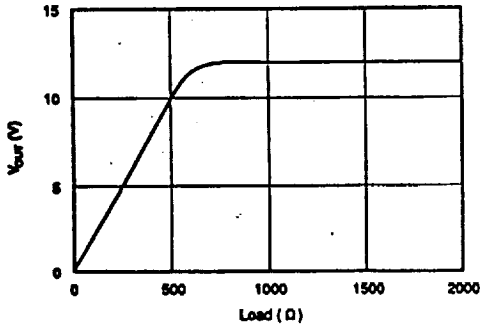

SETTLING TIME vs FILTER CAPACITOR

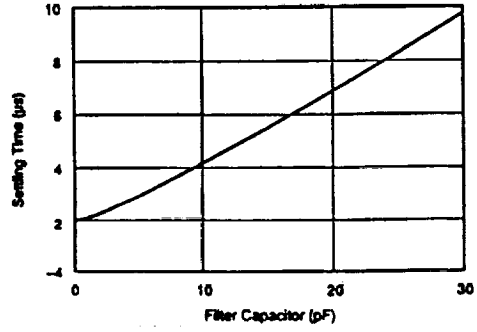

TYPICAL PERFORMANCE CURVES (CONT)

T_A = +25°C, V_S = ±15V unless otherwise noted.

QUIESCENT CURRENT vs TEMPERATURE

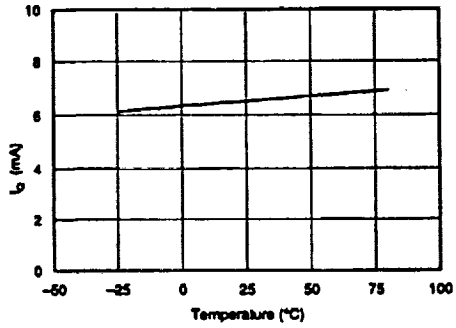

INPUT BIAS CURRENT vs TEMPERA

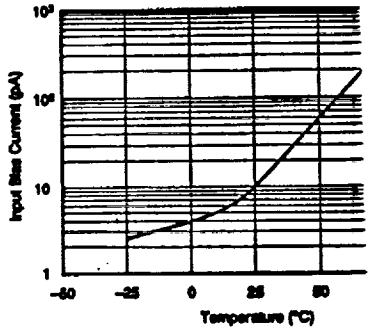

CURRENT LIMIT vs TEMPERATURE

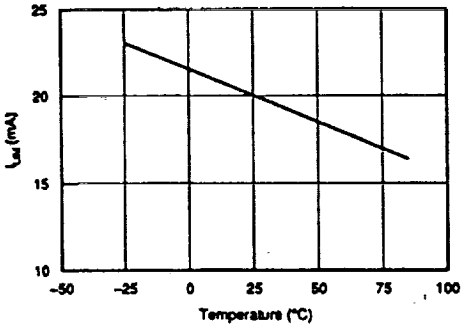

SLEW RATE vs TEMPERATURE

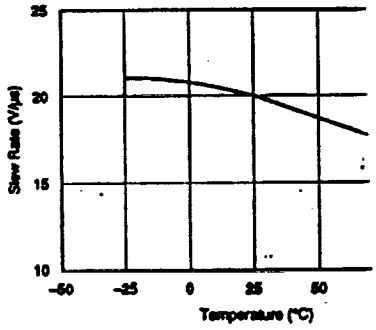

OUTPUT SWING vs TEMPERATURE

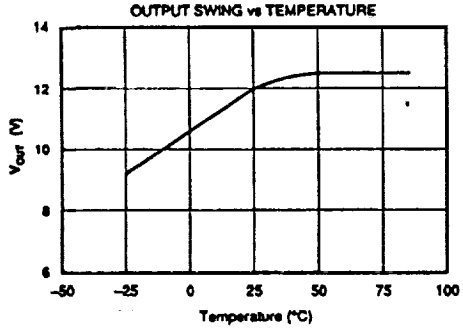

LARGE SIGNAL RESPONSE

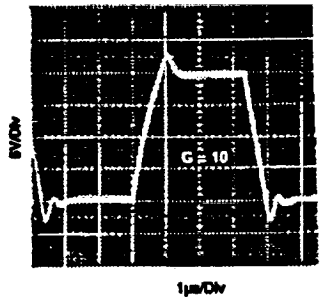

TYPICAL PERFORMANCE CURVES (CONT)

T_A = +25°C, V_{cc} = ±15V unless otherwise noted.

SMALL SIGNAL RESPONSE

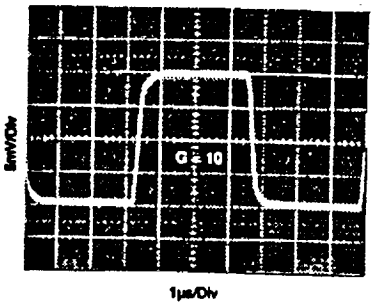

DISCUSSION OF PERFORMANCE

A simplified diagram of the PGA202/203 is shown on the first page. The design consists of a digitally controlled, differential transconductance front end stage using precision FET buffers and the classical transimpedance output stage. Gain switching is accomplished with a novel current steering technique that allows for fast settling when changing gains. The result is a high performance, programmable instrumentation amplifier with excellent speed and gain accuracy.

The input stage uses a new circuit topology that includes FET buffers to give extremely low input bias currents. The differential input voltage is converted into a differential output current with the transconductance gain selected by steering the input stage bias current between four identical input stages differing only in the value of the gain setting resistor. Each input stage is individually laser-trimmed for input offset, offset drift and gain.

The output stage is a differential transimpedance amplifier. Unlike the classical difference amplifier output stage, the common mode rejection is not limited by the resistor matching. However, the output resistors are laser-trimmed to help minimize the output offset and drift.

BASIC CONNECTIONS

Figure 1 shows the proper connections for power supply and signal. The power supplies should be decoupled with 1µF tantalum capacitors placed as close to the amplifier as possible for maximum performance. To avoid gain and CMR errors introduced by the external components, you should connect the grounds as indicated. Any resistance in the sense line (pin 11) or the V_{REF} line (pin 4) will lead to a gain error, so these lines should be kept as short as possible. Also to maintain stability, avoid capacitance from the output to the input or the offset adjust pins.

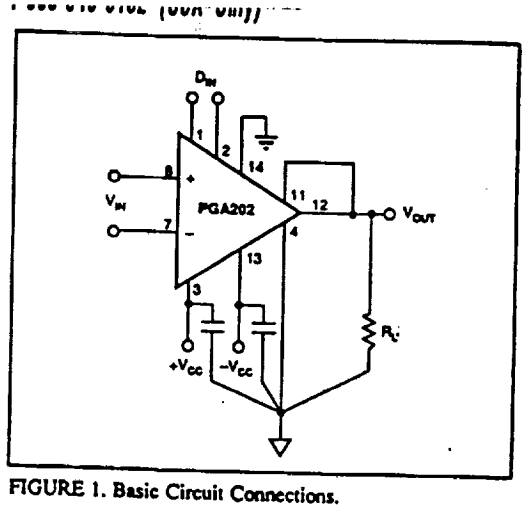

FIGURE 1. Basic Circuit Connections.

OFFSET ADJUSTMENT

Figure 2 shows the offset adjustment circuits for the PGA202/203. The input offset and the output offset are both separately adjustable. Notice that because the PGA202/203 change between four different input stages to change gain, the input offset voltage will change slightly with gain. For systems using computer autozeroing techniques, neither offset nor drift is a major concern, but it should be noted that since the input offset does change with gain, these systems should perform an autozero cycle after each gain change for optimum performance.

In the output offset adjustment circuit, the choice of the buffering op amp is very important. The op amp needs to have low output impedance and a wide bandwidth to maintain full accuracy over the entire frequency range of the PGA202/203. For these reasons we recommend the OPA602 as an excellent choice for this application.

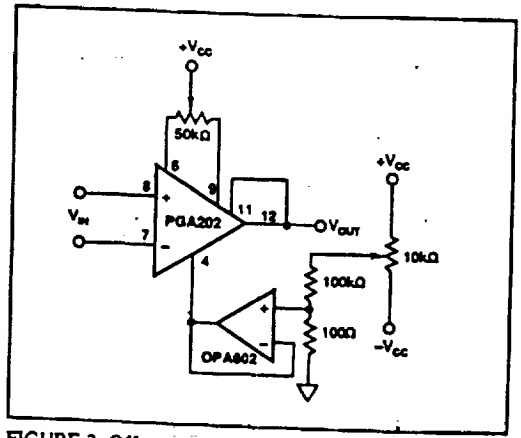

FIGURE 2. Offset Adjustment Circuits.

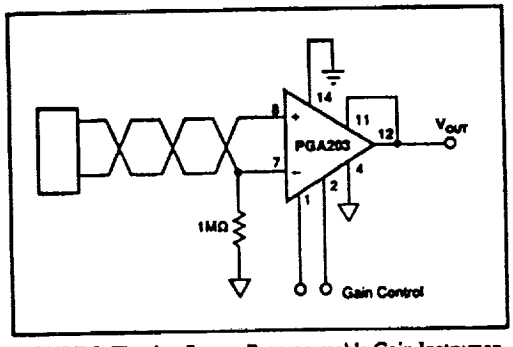

FIGURE 9. Floating Source Programmable Gain Instrumentation Amplifier.

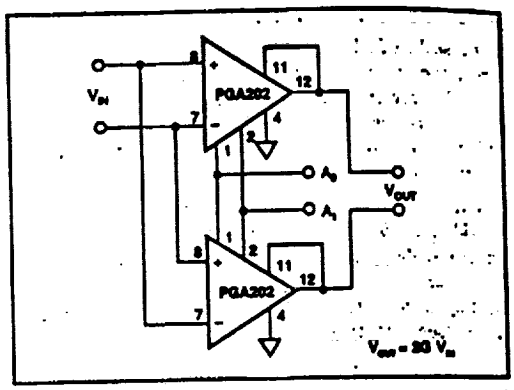

FIGURE 11. Programable Differential In/Differential Out Amplifier.

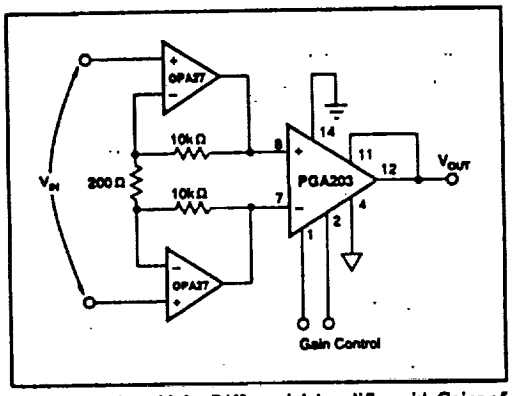

FIGURE 10. Low Noise Differential Amplifier with Gains of 100, 200, 400, 800.

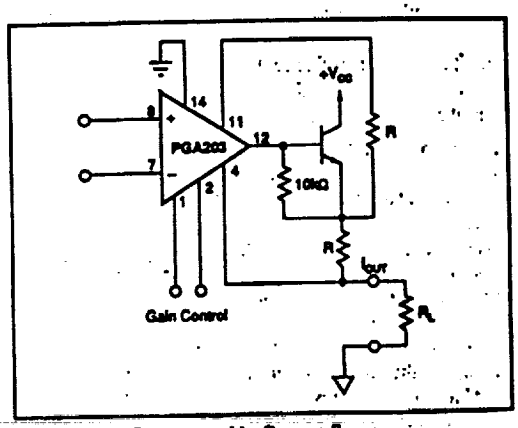

FIGURE 12. Programmable Current Source.

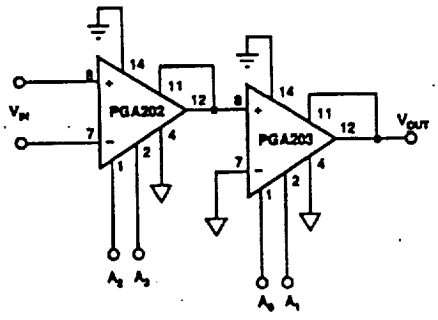

A_3	A_2	A_1	A_0	GAIN
0	0	0	0	1
0	0	0	1	2
0	0	1	0	4
0	0	1	1	8
0	1	0	0	10
0	1	0	1	20
0	1	1	0	40
0	1	1	1	80
1	0	0	0	100
1	0	0	1	200
1	0	1	0	400
1	0	1	1	800
1	1	0	0	1000
1	1	0	1	2000
1	1	1	0	4000
1	1	1	1	8000

FIGURE 13. Cascaded Amplifiers.

Appendix 5

Data Acquisition System Information

DATEL
INNOVATION and EXCELLENCE

PC-414
High Speed Analog Input Board for IBM-PC/AT™, PS-30, or EISA Computers

FEATURES

- Up to 5MHz A/D sample rate
- Very low harmonic distortion
- Analog input comparator trigger
- Choice of 12 or 14 bit A/D resolution
- Optional 2 or 4 channel simultaneous sampling
- On-board FIFO memory up to 16,384 samples
- Ideal for FFT's, DSP or array processor "front ends"
- Non-bus burst parallel port for seamless recording

GENERAL DESCRIPTION

Offering very high system speed, the PC-414 is a multi-channel analog input board for the IBM-PC/AT, PS-30, EISA and compatible computers. Full power input bandwidth is available up to 2.5MHz and may be sampled at up to 5MHz. A common motherboard is used, with the analog section contained in a pluggable 2" by 4" module. This allows for a family of several different Sample/Hold - A/D Converter speed and resolution options by exchanging analog modules.

The analog input ranges of the A/D converter are selectable as unipolar 0 to +10V, or bipolar ±5V, or ±10V depending on model. The gain on the PC-414A may be user-selected times one or times ten for two channels. This offers one-volt input ranges for receiver signal measurement. The input configuration is excellent for analyzing wide band communications signals. Model PC-414E offers 16 single-ended or 8 differential high speed channels.

Models PC-414A, F, and G use a Simultaneous Sampling section. This function acquires signals on parallel channels at the same time. This provides phase correction and deskewing of multichannel correlated signals. Applications include high speed cross-channel computation, beam-former coherency for sonar or acoustics, telemetry, multiple carrier demodulation, and highly concurrent system testing.

A/D data passes to an on-board First-In, First-Out (FIFO) data memory and then to the host computer bus interface under software control. The FIFO acts to decouple the precise timing of the A/D section with the block-oriented data transfers on the bus. The design can continuously collect analog data with non-stop converter triggering while data is simultaneously read from the FIFO. This allows the collection of "seamless" wide-bandwidth signals of millions of samples or greater. Functions such as FFT sampling cannot tolerate lost samples without increases in "arithmetic" noise during computation processing.

Data may be transferred to mass storage peripherals such as disk or magnetic tape. Applications include long-baseline studies in astrophysics, component life testing, and anomalous pattern search.

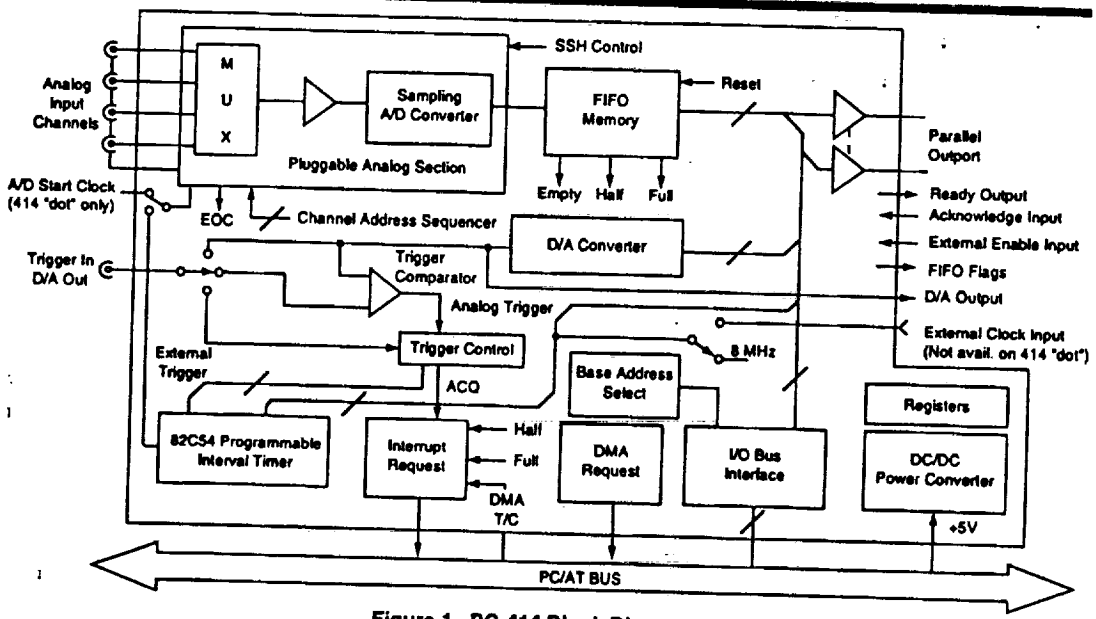

Figure 1. PC-414 Block Diagram

The FIFO data output may also be routed under host software control to an on-board parallel data port instead of being sent to the computer bus. This parallel burst channel data may be read by an external processor at very high speeds and avoids possible speed restrictions of the computer bus. The outport uses a very simple ready/acknowledge transfer handshake which is adaptable to any remote parallel port including DT Connect®.

The analog section of the PC-414 is optimized for high signal quality and very low dynamic noise. The PC-414 is ideal as an FFT "front end" or DSP quantizer for array processors.

The A/D conversion timing section is designed for accurate multi-scan data acquisition. Software programmable timers control the interval between each conversion and each multi-channel scan. A programmable sample counter will allow sample blocks of specified length independent of FIFO length. The timer/counter section uses a precision on-board crystal clock. Timeout and sample count activities may be monitored using I/O status registers and/or programmable interrupts. The interrupt method may be fully synchronized with software programmable DMA transfers directly to host computer memory.

S/H-A/D triggering may use several sources under software control. The internal timebase is the normal trigger source although single conversions or scans may be directly commanded by host I/O register writes. An external trigger clock may also be used to precisely synchronize sampling with external events. This external trigger may start a single multi-channel scan or "N" multiple scans separated by programmable delays.

Analog sampling may also be level-triggered using an on-board analog comparator and an external level input. The reference trigger level to the comparator is derived from an on-board 12-bit D/A converter. If preferred, the D/A converter may also be used as an analog output channel for any purpose.

The PC-414 A thru G contains five signal connectors. Four connectors are for the sampled analog channels. The fifth connector is for a choice of the external timebase clock input, the external analog trigger reference level or for the D/A output. The PC-414E accepts 16S/8D input channels plus trigger.

The computer interface for control and status uses 16-bit I/O addressing. A/D data uses 16-bit transfers under program or host DMA control. A single interrupt is generated for a variety of conditions. These include A/D data ready, DMA terminal count, sample count reached, FIFO half-full or FIFO full.

A/D output data coding is right-justified two's complement with sign extension. This format is excellent for integer data typing with high level computer languages such as "C", FORTRAN, Pascal or Ada. It is also directly compatible with very fast arithmetic instructions for all microprocessor assembly languages and math coprocessors. Straight binary coding may also be selected.

A high-efficiency, low noise DC/DC converter provides quiet power to linear sections. PC-414A - G analog inputs use rear SMA coaxial threaded connectors (DB-25 for 414E). The burst channel parallel output port uses an internal header connector.

Software

A menu-driven windowed setup and configuration program is optionally available on both 5.25" or 3.5" MS-DOS disks. The program automatically adapts to the display type and mouse. The program sets the I/O base address, interrupt and DMA systems, loads registers and D/A converter data, starts timers and saves data to disk or memory. The entire hardware configuration may be saved to disk. The software also includes A/D-D/A calibration procedures.

A/D data may be sent to base memory (below 640K) either by DMA, program transfer, or extended memory (above 1Mb). Disk data formats include binary integer, IEEE-754 binary floating point, and ASCII floating point (Lotus PRN format). The setup program is also available in source language format and includes fast assembly language modules which may be linked to user-written programs. Both WINDOWS and MS-DOS versions are available.

Users have three methods of implementing PC-414 software; the optional setup/configuration program, third party software or user-written code. Third party display and processing software offers graphic outputs, DSP functions such as FFT's and statistical analysis of data files. Third party packages will accept data by file transfer. A QuickBASIC disk is available at no charge for user modification.

Simultaneous Sampling

In Figure 2, four input signals are sampled at the same time using the PC-414A's Simultaneous Sample/Hold (SSH) option. Once the signals are acquired, they are rapidly digitized sequentially by the A/D converter. For correlation of phase-related signals, SSH removes skew delay errors from conventional sequential multiplexer scanning. The PC-414F or G offers the same function at a higher speed using two simultaneous A/D's.

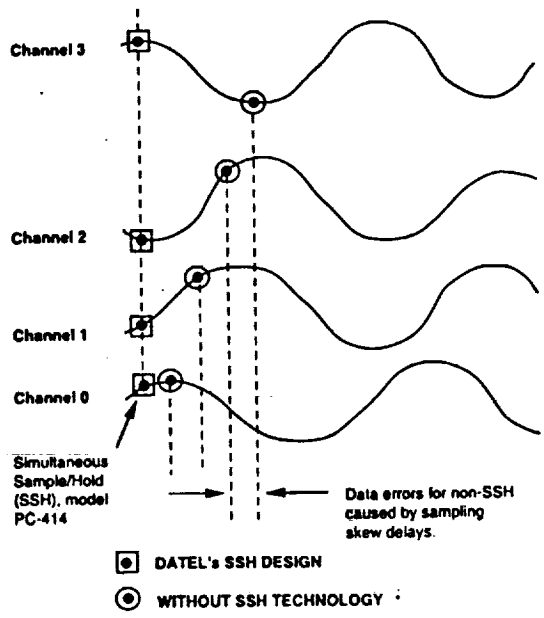

Figure 2. PC-414 Simultaneous Sampling

FUNCTIONAL SPECIFICATIONS

(Typical at +25°C, dynamic conditions, gain = 1, unless noted.)

ANALOG INPUTS	414A	414B	414C	414D	414E	414F	414G
Number of channels	4 simul.	4	4	1	16S/8D	2 simul.	2 simul.
Input Configuration (non-isolated)	SE	SE	SE	Diff.	SE or Diff.	SE	SE
Full Scale Input Ranges (user-selectable) (gain = 1)	0 to 10V ±10V [Note 1]	0 to 10V ±10V ±5V	0 to 10V ±10V ±5V	±5V	0 to 10V ±10V ±5V [Note 1]	0 to 10V ±5V	±5V 0 to 10V (special)
Input Bias Current	±1nA	±1nA	±1nA	±1nA	±1nA	±1nA	±1nA
Input Overvoltage (no damage)	±15V	±15V	±15V	±15V	±15V	±15V	±15V
Overvoltage Recovery Time, maximum	2µs	2µs	2µs	2µs	2µs	2µs	2µs
Common Mode Voltage Range, maximum	—	—	—	±1V	±10V	—	—
Input Impedance [Notes 6 and 10]	10MΩ	10MΩ	10MΩ	2kΩ	100MΩ	1kΩ	1kΩ
SAMPLE/HOLD							
Acquisition Time (FSR step) to 0.01% of FSR, max.	900ns	750ns	200ns	50ns	750ns	165ns	350ns [Note 11]
Aperture Delay	±15ns	±20ns	±20ns	±10ns	±20ns	±20ns	±20ns
A/D CONVERTER							
Resolution	12 bits	14 bits	12 bits	12 bits	12 bits	12 bits	14 bits
Conversion Period	500ns	1.6µs	500ns	200ns	500ns	400ns	500ns
SYSTEM DC CHARACTERISTICS							
Integral Non-linearity LSB of FSR	±1	±1.5	±1	±2	±1	±1	±1.5
Differential Non-linearity LSB of FSR	±0.75	±1	±0.75	±1	±0.75	±1	±1
Full Scale Temperature Coefficient (LSB per °C)	±0.1	±0.3	±0.1	±0.1	±0.1	±0.1	±0.3
Zero or Offset Temperature Coefficient (LSB per °C)	±0.1	±0.3	±0.1	±0.3	±0.1	±0.1	±0.3
SYSTEM DYNAMIC PERFORMANCE [Note 2]							
System Bandwidth (single channel, FSR input)	1MHz	200kHz	1MHz	2.5MHz	200kHz	1MHz	500kHz
Throughput to FIFO (single channel, gain = 1)	700ns	2µs	625ns	200ns [Note 9]	500ns	500ns	1µs
Throughput to FIFO (sequential channels, gain = 1) [Note 4]	1µs	3µs	2µs	—	2µs	250ns (2 chans.)	500ns (2 chans.)
Total Harmonic Distortion FS Input [Note 3]	–72dB	–75dB	–72dB	–68dB	–72dB	–70dB	–80dB

ANALOG INPUTS	
Programmable Gains	See Note 1
Common Mode Rejection (DC - 60Hz)	-80dB (g = 100) (414E)
Addressing Modes	1. Single channel 2. Simultaneous sampling 3. Sequential with autosequenced addressing 4. Random addressing by host software

A/D CONVERTER	
Output Coding	Positive-true right-justified straight bin. (unipolar) or right-justified 2's comp. (bipolar) with sign extension thru bit 15.
Trigger Sources (Software selectable)	1. Local Pacer frame clock 2. External TTL frame clock 3. Analog threshold comp.
A/D Sample Clock	1. Internal programmable 82C54 timer 2. Ext. TTL input, active high (PC-414 "dot" only)

A/D MEMORY	
Architecture	First-In, First-Out (FIFO)
Memory Capacity	1024, 4096, or 16,384 A/D samples

TRIGGER CONTROL	
Programmable Interval Timer Type	82C54
Functions	1. A/D sample count reached 2. A/D start rate (16 bit divisor) 3. SSH sample counter (414A)
Pacer Sample Counter	3 to 65,536 samples. Drives the Acquire flag/interrupt gate for A/D start pulses.
82C54 Clock Source	1. Internal 8MHz crystal clock 2. External TTL input, 10MHz max. On PC-414 "dot" models only, the 82C54 is clocked only by the internal 8MHz source.
Scan Trigger Clock	125, 250, or 500kHz
Analog Trigger Input Range [Note 5]	±10 Volts (not avail. 414D)
Analog Trigger Response	2µs to set status flag
Analog Trigger Hysteresis	40mV

ANALOG OUTPUT (not available PC-414D)	
Number of Channels	One channel
Function (user-selectable)	1. General purpose analog output 2. Threshold comparator for A/D trigger.
Resolution	12 bits
Output Voltage Range (user-selectable)	0 to +10V, ± 5V and ±10V at 5mA max.
Linearity	± 0.05% of FSR
Settling time (10V step)	5 microseconds to 0.05%
Input Coding (user-selectable)	Same as A/D section

PC/AT BUS INTERFACE	
Architecture	I/O mapped, pluggable to IBM-PC/AT, PS-30, EISA bus and compatibles. Decodes eight 16-bit I/O registers.
I/O Mapping	Decodes I/O address lines A9-A0.
Data Transfer	I/O transfer or host DMA, software selectable.
Data Bus	16 bits.
Direct Memory Access	1 channel, selectable on channels 5, 6, or 7, set by software.
DMA Request Conditions (software selectable)	FIFO full, half full, not empty, scan acquire flag (sample count reached).
Control/Status Functions	Board reset, FIFO flags, interrupt select and status, DMA select and status, trigger source, timer control and period, sample count load, parallel outport enable, A/D enable, MUX auto-sequence.
Number of Interrupts [Note 14]	1 interrupt, selectable on level 7, 9 thru 12, or 15. The interrupt level is set by software.
Bus Interrupt Sources	Scan acquire flag (sample count), FIFO full or half full, DMA terminal count from bus.

PARALLEL DATA PORT	
Outport Type	16 data output lines, TTL levels from A/D FIFO. Includes handshake signals and FIFO flags. The outport does not provide addressing.
Operating Modes	Asynchronous master to external slave receiver. On PC-414 "dot" models, 4 modes are included, offering internal/external clocking (to 10MHz), synchronous/asynchronous handshaking. Sequencing is adaptable to DT Connect®.
Parallel Port Loading	24mA out, 1.6mA in. On PC-414 "dot" models, the data outputs may be 3-stated for shared bus connection.
Parallel Port Connector	2-row 26-pin header type mounted on board interior. 0.100" pin spacing suitable for flat cable. Scramble pads are included to reconfigure the pinout order on PC-414 "dot" versions. Pinout is adaptable to DT Connect®.
Port Data Rate	4MHz maximum. On PC-414 "dot" models, data may be transferred up to 10MHz with external clocking

DIGITAL I/O PORT (PC-414 "dot" models only)	
Connector	Dual row, 26-pin header mounted on board interior. Uses 0.100" pin spacing suitable for flat cable. Includes +5V dc and digital ground connections.
Configuration	8 digital outputs, 8 digital inputs (unlatched)
Levels	All lines are buffered, TTL levels. 10 output loads.
Outport Settling Time	50ns max. after write operation

MISCELLANEOUS	
Analog Section Modularity	The MUX-S/H-A/D module is socketed for function interchange.
Analog Section Adjustments	Offset and gain per channel for SSH on PC-414A,F,G. A single offset and gain pot is provided on PC-414B,C,D,E. Recommended recalibration interval is 90 days in stable conditions.
Analog Input Connectors	Four SMA miniature coaxial, mounted on rear slot. [Note 8]
Multipurpose Connector [Note 8]	5th SMA user-selectable for: 1. Pacer trigger input 2. Analog threshold comparator input 3. D/A output
Operating Temp. Range	0 to + 60°C
Storage Temp. Range	-25 to +85°C
Humidity	10% to 90%, non-condensing
Altitude	0 to 10,000 feet. Forced cooling is recommended.
Power Required	+5V dc @ 3.5A max. from AT bus.
Outline Dimensions (10.5" long 414 "dot")	4.5 x 13.31 x 0.625 inches, compatible to PC/AT bus.

TECHNICAL NOTES

1. Resistor-programmed gain from X1 to X100 is available on PC-414E with increased settling delay at higher gain. Fixed gains of X1 and X10 on 2 channels, offering 1V ranges, are selectable on the PC-414A.

2. Total throughput includes MUX settling time after changing the channel address, S/H acquisition time to rated specifications, A/D conversion, and FIFO transfer. Total throughput is not delayed by host software whenever the FIFO is not full.

3. THD test conditions are:
   1. Input freq. 500kHz (414A,F) 200kHz (414B,E) 300kHz (414C) 1MHz (414D) 100kHz (414G)
   2. Generator/filter THD is -90dB minimum.
   3. THD computed by FFT to 5th harmonic.

$$THD = 20 * \log 10 \frac{(V2^2 + V3^2 + V4^2 + V5^2)^{0.5}}{Vin}$$

   4. Inputs are 1/2 full scale. No channel advance.
   5. A/D trigger rate = 1.5MHz (414A), 500kHz (414B,C,E), 4MHz (414D), 2MHz (414F), 1MHz (414G)

4. The rates shown for sequential sampling are the maximum A/D converter start rates and include MUX sequencing and settling. For example, if four channels of the PC-414C were scanned, the maximum sample rate on any one channel would be 2µs X 4 channels = 8µs (125kHz per channel).

5. For fastest response on the analog comparator trigger, keep the reference voltage near the trip input voltage. To avoid overload recovery delays, do not let the trip input (or any other analog input) exceed ±10V.

6. The input impedance of 10MΩ minimum avoids attenuation errors from external input source resistance. For many applications, an in-line coaxial 50 Ohm shunt, inserted adjacent to the front connectors, is recommended to reduce reflections and standing wave errors.

7. Allow 20 minutes warmup time to rated specifications for models PC-414B, G.

8. A 25-pin DB-25S connector is used for the PC-414E.

9. 5MHz sampling on PC-414D requires an external clock. Maximum on-board sampling is 4MHz.

10. Input impedance is shown with power on. Impedance with power off is 1500 Ohms or less.

11. PC-414G acquisition time is 250ns to ±0.003% of FSR.

12. Digital I/O registers apply to PC-414 "dot" models only, BASE + 2 bits 15 through 8.

13. Refer to the PC-414 User's Manual for added PC-414 "dot" modes.

14. IRQ 12 is not available on PC-414 "dot" models.

FIFO DATA FORMAT

A/D data is delivered as a stream from the FIFO memory. For multichannel inputs, this means that data is multiplexed. For example, for 4-channel inputs, the output channel sequence is 0, 1, 2, 3, 0, 1, ... Some applications may need this data de-multiplexed by software so that each channel's data is placed in its own separate buffer.

PC-414 "dot" Series

Beginning in mid-1993, an alternate version of the PC-414 is available under special order. This version (the "dot" series), is fully downward compatible to the PC-414 but offers a separate digital I/O port, additional data port modes (including DT® Connect) and other minor changes. The PC-414 "dot" is 10.5 inches in length. Contact DATEL for details.

PC-414SET Setup/Configuration Software

- Automatically configures to the display adapter, CPU, and mouse.
- Sets the I/O base address.
- Initializes the interrupt and DMA systems and D/A output.
- Allocates base or extended memory.
- Performs self-test and A/D-D/A calibration.
- Configures A/D sample rate, frame rate, and sample counter.
- Selects trigger mode and DMA or I/O block transfer.
- Selects disk file output format to integer binary, float binary, or ASCII float.
- Saves data to base memory, extended memory, or disk.
- Full source code in "C" and assembly is available.
- MS-DOS or WINDOWS version (visual "C" interface).

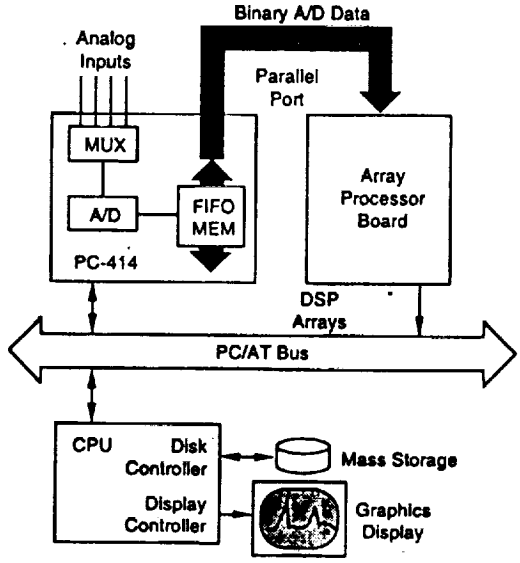

Figure 3. Array Preprocessing

I/O Register Memory Mapping [Note 13]

The base address may be selected anywhere up to 3F0h on 16-byte boundaries.

I/O Address (hex)	Direction	Description
Base + 0	Write	Command Register
Base + 0	Read	Status Register
Base + 2	Write	Channel Address/Digital Output [Note 12]
Base + 2	Read	Digital Input Register [Note 12]
Base + 4	Write	D/A Data Register
Base + 6	Write	FIFO Reset Register
Base + 6	Read	FIFO A/D Data Register
Base + 8	Read/Write	Counter #0 (82C54)
Base + 0Ah	Read/Write	Counter #1 (82C54)
Base + 0Ch	Read/Write	Counter #2 (82C54)
Base + 0Eh	Read/Write	Control Register (82C54)

At power-up or PC bus reset, all registers contain zeroes except the FIFO HF and FF bits. The registers may be programmed in any sequence as long as the command register is last. Use 16-bit I/O word operations.

Command Register (Write BASE + 0)

15 14	13 12 11	10 9	8 7	6	4	3	2	1	0
DMA Lvl	Intrpt Lvl	DMA Req	Intrpt Req	Prt/ Bus	Trg Pol	Aut Inc	Scn En	Cn En	Trg Src
1 0	2 1 0	1 0	1 0						

Bits not shown or "x" bits are not used or don't care.

Trigger Source [Bit 0]
0 = Sample from the internal trigger
1 = Sample from the external trigger

Internal triggers are generated from the 82C54 timer. Each internal trigger will enable sampling until the sample count is done or command 1 = 0. For continuous triggering, use timer mode 2. For a single trigger, set timer mode 5 and enable the A/D converter.

The external trigger may be from the analog threshold comparator or the digital TTL trigger.

Convert Enable [Bit 1]
0 = Disable A/D conversion (default)
1 = Enable A/D conversion

Scan Enable [Bit 2]
0 = One A/D conversion per A/D start clock
1 = Up to 16 A/D conversions per A/D start clock (set by the channel address register).

Channel Address Auto-increment [Bit 3]
0 = Single channel (no increment)
1 = Sequence channel address at A/D conversion (The address counter will wrap around from channel 15 to 0).

External Trigger Polarity [Bit 4]
0 = Trigger on falling edge (default)
1 = Trigger on rising edge

Bit 5
Not used. On PC-414 "dot" models,
0 = Internal 8MHz clock
1 = External A/D start clock

Select FIFO Output Data Steering [Bit 6]
0 = Select PC bus data register (Inhibit parallel port)
1 = Enable FIFO transfers to parallel port (Inhibit PC bus data access)

Interrupt Request Source — Bit 8 7
0 1 = Interrupt on FIFO full
1 0 = Interrupt on FIFO half full
0 0 = Interrupt on data Acquire flag
1 1 = Interrupt on terminal count of DMA completion (required for DMA).

DMA Request Source — Bit 10 9
0 1 = DMA request on FIFO full (block mode)
1 0 = DMA request on FIFO half full (block mode)
0 0 = DMA request on data Acquire flag (block mode)
1 1 = DMA request on FIFO not empty (demand mode)

On PC-414 "dot" models, DMA Request Source is connected to the FIFO empty flag for demand mode transfers.

Block Mode: After setting up the DMA controller registers, a DMA block transfer will occur on a DMA request. At the end of the transfer, the PC-414 will generate a terminal count interrupt.

Demand Mode: This is identical to the Block Mode except that the transfer will continue as long as the FIFO is not empty. The transfer will stop when the FIFO is empty or a terminal count occurred at the end of a 64k word transfer.

Interrupt Level Select — Bit 13 12 11
0 0 0 = Interrupt disable
0 0 1 = Interrupt request on IRQ 7
0 1 0 = Interrupt request on IRQ 9
0 1 1 = Interrupt request on IRQ 10
1 0 0 = Interrupt request on IRQ 11
1 0 1 = Interrupt request on IRQ 12
1 1 0 = Interrupt request on IRQ 15
1 1 1 = Not used

IRQ 12 is not available on the PC-414 "dot" models.

DMA Level Select — Bit 15 14
0 0 = DMA disable
0 1 = DMA request on DRQ 5
1 0 = DMA request on DRQ 6
1 1 = DMA request on DRQ 7

Channel Address Register (Write BASE + 2)

15 - 8	7 6 5 4	3 2 1 0
Digital I/O R/W [Note 12]	Scan Control	Channel Address
	3 2 1 0	3 2 1 0

Channel Address [Bits 3 - 0]
Only bits 1 and 0 are used for the 4-channel analog modules. All 4 counter bits are available at the A/D module.

Scan Control [Bits 7 - 4]
In the scan mode (command 2 = 1), each A/D start convert pulse will cause multiple A/D conversions as selected by these bits. Each scan starts from channel zero.

PC-414F,G Addressing:

Address (bits 7 - 0)	Channel Selected
00h	Channel 0 only
01h	Channel 1 only
02h	Both channels, simultaneously

Do not use autoincrement. Set BASE + 0, bit 3 = 0.

Status Register (Read BASE + 0)

15 - 8	7	6 5 4	3	2	1	0
Not Used	Xfr In Pro	FIFO Status FF HF EF	Ovr Smp Err	Ana Trg Lvl	EOC Sts	ACQ Sts

Acquisition Status [Bit 0]
0 = A/D scan not in progress or scan done (Counter 0 sample count was reached).
1 = A/D scan in progress (Counter 0 sample count not reached).

End of A/D Conversion Status (EOC) [Bit 1]
0 = A/D conversion in progress, data invalid
1 = A/D conversion done, data valid

Analog Trigger Comparator Output [Bit 2]
0 = Analog trigger input is below reference
1 = Analog trigger input is above reference

Oversample Error [Bit 3]
0 = No error
1 = A/D was triggered before EOC is done.

Bit 3 is cleared by disabling A/D conversions (write command 1=0).

FIFO Status Flags
Bit 4: 0=FIFO is empty, 1= FIFO not empty
Bit 5: 0=FIFO is half full or greater, 1=less than half full
Bit 6: 0=FIFO is full, 1=FIFO is not full

NOTE the negative true coding on these bits. The FIFO status bits are not latched

Transfer in Progress [Bit 7]
0 = Remote receiver is not ready for transfer
1 = Remote receiver is ready for transfer

Bit 7 displays parallel inport pin 2 (external Transfer Enable In) ANDed with command bit 6.

D/A Data Register (Write BASE + 4)

15-12	11	10	9	8	7	6	5	4	3	2	1	0
x-x	DA1 MSB	DA2	DA3	DA3	DA5	DA6	DA7	DA8	DA9	DA10	DA11	DA12 LSB

FIFO Reset Register (Write BASE + 6)

15	0
x	x

Any write to this register will clear the FIFO and set the empty flag true. If A/D conversion is still running, the FIFO will be not empty when the next A/D sample EOC occurs.

FIFO Data Register (Read BASE + 6)

15	14	13	12	11	00
S	S	S	S	MSB 12	LSB ALL

12-bit A/D data

15	14	13	00
S	S	MSB 14	LSB ALL

14-Bit A/D Data

"S" bits are sign-extended from either bit 11 (12 bit A/D's) or bit 13 (14-bit A/D's) in bipolar input range. For unipolar ranges, S = 0.

82C54 Programmable Interval Timer

Refer to the PC-414 User Manual for detailed programming information.

Counter Register
(Read/Write BASE + 8 - Counter #0)
(Read/Write BASE + 0Ah - Counter #1)
(Read/Write BASE + 0Ch - Counter #2)

15 8	7	6	5	4	3	2	1	0
x - x	C07	C06	C05	C04	C03	C02	C01	C00

Control Word Register (Read/Write BASE + 0Eh)

15 8	7	6	5	4	3	2	1	0
x - x	SC1	SC0	RL1	RL0	M2	M1	M0	BCD

Select Counter

SC1	SC0	
0	0	Select counter #0
0	1	Select counter #1
1	0	Select counter #2
1	1	Read back command

Read/Load

RL1	RL0	
0	0	Counter latch operation
0	1	Read/Load LSB only
1	0	Read/Load MSB only
1	1	Read/Load LSB then MSB

Mode

M2	M1	M0	
x	1	0	Rate generator
1	0	0	Software trigger
1	0	1	Hardware trigger

BCD

BCD	
0	16-bit binary count
1	4-decade binary coded decimal count

Transfer Speeds

PC/AT bus transfer rates are host dependent and should be determined by testing. For example, a 80386 Compaq operating at 33MHz achieved 800 nanoseconds instantaneous sample-to-sample timing using the REP INSW instruction. To optimize throughput, disable all possible interrupts. For higher speed continuous (non-stop) A/D sampling, consider using a parallel port.

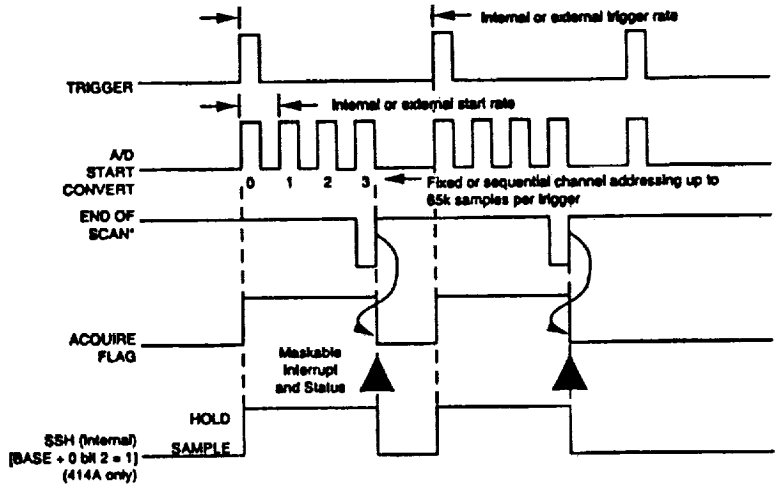

Figure 4. PC-414 Timing Diagram

ORDERING INFORMATION

MODEL NUMBERING PC-414 ___ ___

A/D Type, Channels, Speed Resolution	FIFO Memory Size
A = 4 SSH chans., 1.5MHz, 12-bit B = 4 chans., 500kHz, 14-bit C = 4 chans., 1MHz, 12-bit D = 1D chan., 4MHz, 12-bit E = 16S/8D chans., 250kHz (scan), 12-bit F = 2 simul. chans., 2MHz, 12-bit G = 2 simul. chans., 1MHz, 14-bit	1 = 1,024 A/D samples 2 = 4,096 A/D samples 3 = 16,384 A/D samples

Example: PC-414F3 Two simultaneous A/D's, 2 MHz, 12-bit resolution, 16,384 FIFO samples.
For PC-414 "dot" models, add a period after the model number.
Example: PC-414B2.

61-7342340	SMA male to BNC male coaxial cable, 1 meter length. (One cable required per channel)
PC-490B	DB-25 screw termination adapter, 25-pin for PC-414E

Each board is power-cycle burned-in, tested, and calibrated. All models include a user's manual. The warranty period is one year. A QuickBASIC source disk is available on request at no charge.

Software:

PC-414SET	Setup/configuration program. Includes executable files on both 3.5-inch and 5.25-inch 1.2M MS-DOS disks.
PC-414SRC	Source code to setup and configuration program on both 3.5-inch and 5.25-inch MS-DOS disks. Includes "C" and assembly source code and window driver library. Documentation is on disk.
PC-414WIN	Setup/configuration program for Microsoft WINDOWS. Executables only.
PC-414WINS	Source code for PC-414WIN.
PC-DADISP	Signal Display and Analysis worksheet software on 3.5-inch and 5.25-inch disks. Includes manuals. Accepts PC-414SET/WIN files.

DATEL, Inc. 11 CABOT BOULEVARD, MANSFIELD, MA 02048-1194 TEL (508) 339-3000 / FAX (508) 339-6356
INTERNATIONAL: DATEL (UNITED KINGDOM) Basingstoke Tel. (256) 880-444 • DATEL (FRANCE) Tel. (1) 3460.0101
DATEL (GERMANY) Tel. (89) 54 4334-0 • DATEL (JAPAN) Tokyo Tel. (3) 3779-1031 • Osaka Tel. (6) 354-2025

Appendix 6
Miscellaneous

Helicopter with Antenna Mounted

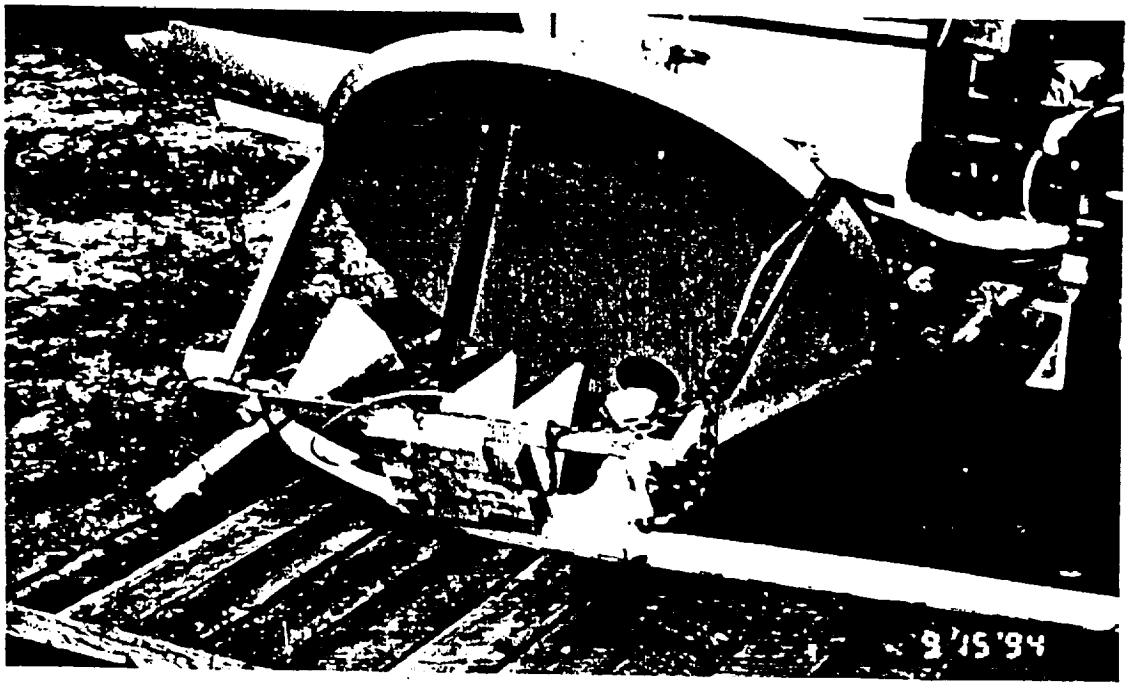

Antenna System During IFC-3

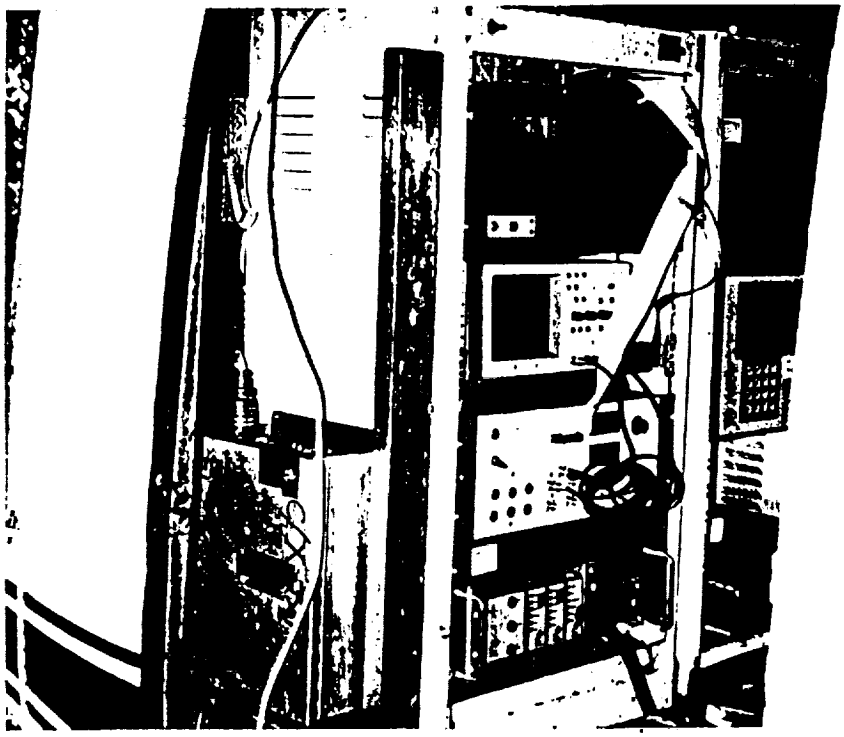

Radar System in Helicopter

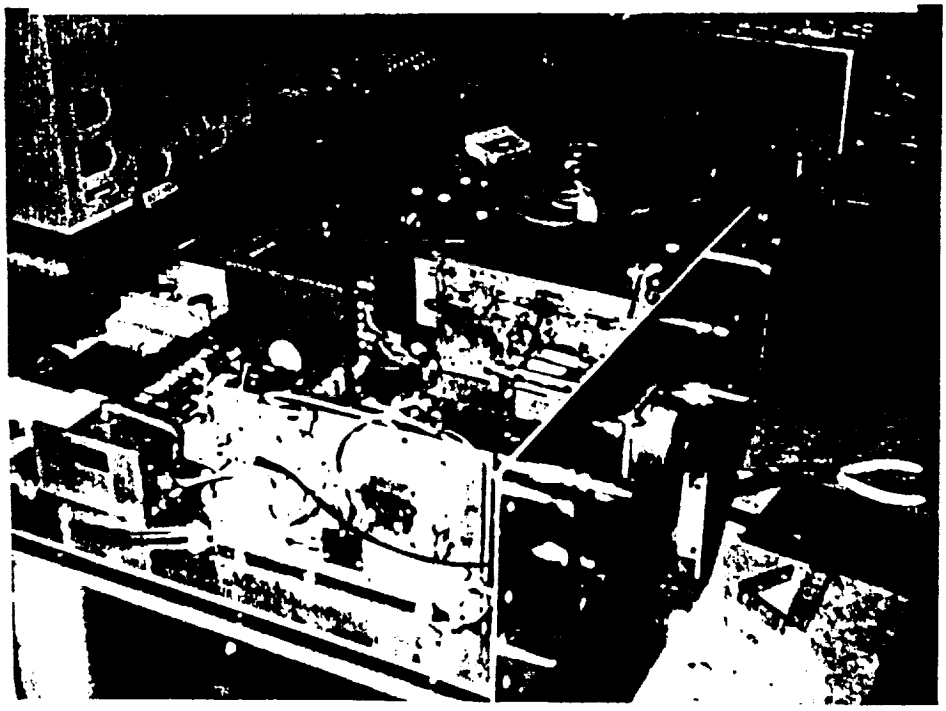

New RF Box

DG189/190/191
High-Speed Drivers with Dual SPDT JFET Switches

Siliconix incorporated

FEATURES

- Constant ON-Resistance Over Entire Analog Range
- Low Leakage
- Low Crosstalk

BENEFITS

- Low Distortion
- Eliminates Large Signal Errors
- High Bandwidth Capability

APPLICATIONS

- Audio Switching
- Video Switching
- Sample/Hold
- D/A Ladder Switches

DESCRIPTION

The DG189-191 are precision dual single-pole, double-throw (SPDT) analog switches designed to provide accurate switching of video and audio signals. This series, like the entire DG180 family, is ideally suited for applications requiring a constant ON-resistance over the entire analog range.

The major design difference is the ON-resistance, being 10, 30, and 75 Ω for the DG189, DG190, and DG191 respectively. Reduced switching errors are achieved through low leakage current ($I_{S(OFF)} < 1$ nA for the DG190/191). Applications which benefit from flat ON-resistance include audio switching, video switching, and sample and holds.

Each device comprises four n-channel JFET transistors and a bipolar driver (TTL compatible) to achieve fast and accurate switch performance. The driver is designed to achieve break-before-make switching action, eliminating the inadvertent shorting between channels and the crosstalk which would result. In the ON state, each switch conducts current equally well in either direction. In the OFF condition, the switches will block up to 20 V peak-to-peak, with feedthrough less than -60 dB at 10 MHz.

Packaging options for the DG189-191 include the 16-pin side braze, and the 14-pin flatpack. The flatpack version is only available for the DG190/191. Performance grades include both the military, A suffix (-55 to 125°C) and industrial, B suffix (-25 to 85°C) temperature ranges. The flatpack option is only available in the military grade.

PIN CONFIGURATION

Dual-In-Line Package

Top View

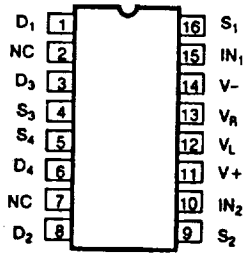

Order Numbers:

Side Braze:

DG189AP, DG189AP/883, DG189BP
DG190AP, DG190AP/883, DG190BP
DG191AP, DG191AP/883, DG191BP

Flat Package

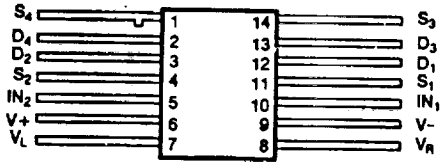

Top View

Order Numbers:

Refer to JAN38510 Information Chapter 1

FUNCTIONAL BLOCK DIAGRAM AND TRUTH TABLE

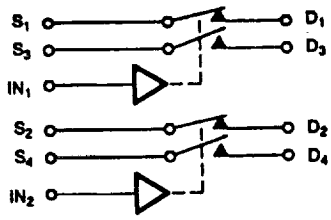

Two SPDT Switches per Package*

Truth Table*

Logic	SW 1 SW 2	SW 3 SW 4
0	OFF	ON
1	ON	OFF

Logic "0" $\leq$ 0.8 V
Logic "1" $\geq$ 2.0 V

*Switches Shown for Logic "1" Input

ABSOLUTE MAXIMUM RATINGS

V+ to V- ..... 36 V
V+ to V_D ..... 33 V
V_D to V- ..... 33 V
V_D to V_D ..... ±22 V
V_L to V- ..... 36 V
V_L to V_{IN} ..... 8 V
V_L to V_R ..... 8 V
V_{IN} to V_R ..... 8 V
V_R to V- ..... 27 V
V_R to V_{IN} ..... 2 V
Current (S or D) DG180 ..... 200 mA
Current (S or D) DG181, DG182 ..... 30 mA
Current (All Other Pins) ..... 30 mA
Storage Temperature ..... -65 to 150°C
Operating Temperature (A Suffix) ..... -55 to 125°C
(B Suffix) ..... -25 to 85°C
Power Dissipation*
16-Pin DIP** ..... 900 mW
Flat Pack*** ..... 900 mW

*All leads welded or soldered to PC board.
**Derate 12 mW/°C above 75°C.
***Derate 10 mW/°C above 75°C.

SPECIFICATIONS[a] (DG189)

PARAMETER	SYMBOL	TEST CONDITIONS Unless Otherwise Specified V+ = 15 V, V- = -15 V, V_L = 5 V, V_R = 0 V		TEMP[f]	TYP[d]	A SUFFIX -55 to 125°C MIN[b]	A SUFFIX -55 to 125°C MAX[b]	B SUFFIX -25 to 85 °C MIN[b]	B SUFFIX -25 to 85 °C MAX[b]	UNIT
ANALOG SWITCH										
Analog Signal Range[c]	V_{ANALOG}			Full		-7.5	15	-7.5	15	V
Drain-Source ON-Resistance	$r_{DS(ON)}$	V_{IN} = 0.8 V or 2 V[e]	I_S = -10 mA, V_D = -7.5	Room Full	7.5		10 20		15 25	Ω
Source OFF Leakage Current	$I_{S(OFF)}$		V_S = 10 V, V_D = -10 V V+ = 10 V, V- = -20 V	Room Hot	0.05		10 1000		15 300	nA
			V_S = 7.5 V, V_D = -7.5 V	Room Hot	0.05		10 1000		15 300	
Drain OFF Leakage Current	$I_{D(OFF)}$		V_S = -10 V, V_D = 10 V V+ = 10 V, V- = -20 V	Room Hot	0.04		10 1000		15 300	
			V_S = -7.5 V, V_D = 7.5 V	Room Hot	0.03		10 1000		15 300	
Channel ON Leakage Current	$I_{D(ON)}$ + $I_{S(ON)}$		V_D = V_S = -7.5 V	Room Hot	-0.1	-2 -200		-10 -200		
Saturation Drain Current	I_{DSS}	2 ms Pulse Duration		Room	300					mA

5

Siliconix incorporated

SPECIFICATIONS[a] (DG189)

PARAMETER	SYMBOL	TEST CONDITIONS Unless Otherwise Specified V+ = 15 V, V- = -15 V, V_L = 5 V, V_R = 0 V		TEMP[f]	TYP[d]	A SUFFIX -55 to 125°C MIN[b]	A SUFFIX -55 to 125°C MAX[b]	B SUFFIX -25 to 85 °C MIN[b]	B SUFFIX -25 to 85 °C MAX[b]	UNIT
DIGITAL INPUT										
Input Current with Input Voltage HIGH	I_{INH}	V_{IN} = 5 V		Room Hot	<0.01		10 20		10 20	µA
Input Current with Input Voltage LOW	I_{INL}	V_{IN} = 0 V		Full	-30	-250		-250		
DYNAMIC CHARACTERISTICS										
Turn-ON Time	t_{ON}	See Switching Time Test Circuit		Room	240		400		425	ns
Turn-OFF Time	t_{OFF}			Room	140		200		225	
Source-OFF Capacitance	$C_{S(OFF)}$	f = 1 MHz	V_S = -5 V, I_D = 0	Room	21					pF
Drain-OFF Capacitance	$C_{D(OFF)}$		V_D = -5 V, I_S = 0	Room	17					
Channel-ON Capacitance	$C_{D(ON)}$ + $C_{S(ON)}$		V_D = V_S = 0 V	Room	17					
OFF Isolation		f = 1 MHz, R_L = 75 Ω		Room	>55					dB
POWER SUPPLIES										
Positive Supply Current	I+	V_{IN} = 0 V, or 5 V		Room	0.6		1.5		1.5	mA
Negative Supply Current	I-			Room	-2.7	-5		-5		
Logic Supply Current	I_L			Room	3.1		4.5		4.5	
Reference Supply Current	I_R			Room	-1	-2		-2		

SPECIFICATIONS[a] (DG190)

PARAMETER	SYMBOL	TEST CONDITIONS Unless Otherwise Specified V+ = 15 V, V- = -15 V, V_L = 5 V, V_R = 0 V		TEMP[f]	TYP[d]	A SUFFIX -55 to 125°C MIN[b]	A SUFFIX -55 to 125°C MAX[b]	B SUFFIX -25 to 85 °C MIN[b]	B SUFFIX -25 to 85 °C MAX[b]	UNIT
ANALOG SWITCH										
Analog Signal Range[c]	V_{ANALOG}			Full		-7.5	15	-7.5	15	V
Drain-Source ON-Resistance	$r_{DS(ON)}$	V_{IN} = 0.8 V or 2 V[e]	I_S = -10 mA, V_D = -7.5	Room Full	18		30 60		50 75	Ω
Source OFF Leakage Current	$I_{S(OFF)}$		V_S = 10 V, V_D = -10 V V+ = 10 V, V- = -20 V	Room Hot	0.06		1 100		5 100	nA
			V_S = 7.5 V, V_D = -7.5 V	Room Hot	0.1		1 100		5 100	
Drain OFF Leakage Current	$I_{D(OFF)}$		V_S = -10 V, V_D = 10 V V+ = 10 V, V- = -20 V	Room Hot	0.05		1 100		5 100	
			V_S = -7.5 V, V_D = 7.5 V	Room Hot	0.06		1 100		5 100	

SPECIFICATIONS[a] (DG190)										
PARAMETER	SYMBOL	TEST CONDITIONS Unless Otherwise Specified V+ = 15 V, V- = -15 V, V_L = 5 V, V_R = 0 V		TEMP[f]	TYP[d]	A SUFFIX -55 to 125°C MIN[b]	A SUFFIX -55 to 125°C MAX[b]	B SUFFIX -25 to 85 °C MIN[b]	B SUFFIX -25 to 85 °C MAX[b]	UNIT
ANALOG SWITCH (Cont'd)										
Channel ON Leakage Current	$I_{D(ON)}$ + $I_{S(ON)}$	V_D = V_S = -7.5 V, V_{IN} = 0.8 V or 2 V[e]		Room Hot	-0.02	-2 -200		-10 -200		nA
DIGITAL INPUT										
Input Current with Input Voltage HIGH	I_{INH}	V_{IN} = 5 V		Room Hot	<0.01		10 20		10 20	µA
Input Current with Input Voltage LOW	I_{INL}	V_{IN} = 0 V		Full	-30	-250		-250		
DYNAMIC CHARACTERISTICS										
Turn-ON Time	t_{ON}	See Switching Time Test Circuit		Room	85		150		180	ns
Turn-OFF Time	t_{OFF}			Room	95		130		150	
Source-OFF Capacitance	$C_{S(OFF)}$	f = 1 MHz	V_S = -5 V, I_D = 0	Room	9					pF
Drain-OFF Capacitance	$C_{D(OFF)}$		V_D = -5 V, I_S = 0	Room	6					
Channel-ON Capacitance	$C_{D(ON)}$ + $C_{S(ON)}$		V_D = V_S = 0 V	Room	14					
OFF Isolation		f = 1 MHz, R_L = 75 Ω		Room	>50					dB
POWER SUPPLIES										
Positive Supply Current	I+	V_{IN} = 0 V, or 5 V		Room	0.6		1.5		1.5	mA
Negative Supply Current	I-			Room	-2.7	-5		-5		
Logic Supply Current	I_L			Room	3.1		4.5		4.5	
Reference Supply Current	I_R			Room	-1	-2		-2		

SPECIFICATIONS[a] (DG191)										
PARAMETER	SYMBOL	TEST CONDITIONS Unless Otherwise Specified V+ = 15 V, V- = -15 V, V_L = 5 V, V_R = 0 V		TEMP[f]	TYP[d]	A SUFFIX -55 to 125°C MIN[b]	A SUFFIX -55 to 125°C MAX[b]	B SUFFIX -25 to 85 °C MIN[b]	B SUFFIX -25 to 85 °C MAX[b]	UNIT
ANALOG SWITCH										
Analog Signal Range[c]	V_{ANALOG}			Full		-10	15	-10	15	V
Drain-Source ON-Resistance	$r_{DS(ON)}$	V_{IN} = 0.8 V or 2 V[e]	I_S = -10 mA, V_D = -7.5	Room Full	35		75 150		100 150	Ω
Source OFF Leakage Current	$I_{S(OFF)}$		V_S = 10 V, V_D = -10 V V+ = 10 V, V- = -20 V	Room Hot	0.05		1 100		5 100	nA
			V_S = 7.5 V, V_D = -7.5 V	Room Hot	0.07		1 100		5 100	

5

Siliconix incorporated

SPECIFICATIONS[a] (DG191)

PARAMETER	SYMBOL	TEST CONDITIONS Unless Otherwise Specified V+ = 15 V, V- = -15 V, V_L = 5 V, V_R = 0 V		TEMP[f]	TYP[d]	A SUFFIX -55 to 125°C MIN[b]	A SUFFIX -55 to 125°C MAX[b]	B SUFFIX -25 to 85 °C MIN[b]	B SUFFIX -25 to 85 °C MAX[b]	UNIT
ANALOG SWITCH										
Drain OFF Leakage Current	$I_{D(OFF)}$	V_{IN} = 0.8 V or 2 V[e]	V_S = -10 V, V_D = 10 V V+ = 10 V, V- = -20 V	Room Hot	0.04		1 100		5 100	nA
			V_S = -7.5 V, V_D = 7.5 V	Room Hot	0.05		1 100		5 100	
Channel ON Leakage Current	$I_{D(ON)}$ + $I_{S(ON)}$	V_D = V_S = -7.5 V, V_{IN} = 2 V		Room Hot	-0.03	-2 -200		-10 -200		
DIGITAL INPUT										
Input Current with Input Voltage HIGH	I_{INH}	V_{IN} = 5 V		Room Hot	<0.01		10 20		10 20	µA
Input Current with Input Voltage LOW	I_{INL}	V_{IN} = 0 V		Full	-30	-250		-250		
DYNAMIC CHARACTERISTICS										
Turn-ON Time	t_{ON}	See Switching Time Test Circuit		Room	120		250		300	ns
Turn-OFF Time	t_{OFF}			Room	100		130		150	
Source-OFF Capacitance	$C_{S(OFF)}$	f = 1 MHz	V_S = -5 V, I_D = 0	Room	9					pF
Drain-OFF Capacitance	$C_{D(OFF)}$		V_D = -5 V, I_S = 0	Room	6					
Channel-ON Capacitance	$C_{D(ON)}$ + $C_{S(ON)}$		V_D = V_S = 0 V	Room	14					
OFF Isolation		f = 1 MHz, R_L = 75 Ω		Room	>50					dB
POWER SUPPLIES										
Positive Supply Current	I+	V_{IN} = 0 V, or 5 V		Room	0.6		1.5		1.5	mA
Negative Supply Current	I-			Room	-2.7	-5		-5		
Logic Supply Current	I_L			Room	3.1		4.5		4.5	
Reference Supply Current	I_R			Room	-1	-2		-2		

NOTES:
a. Refer to PROCESS OPTION FLOWCHART for additional information.
b. The algebraic convention whereby the most negative value is a minimum and the most positive a maximum, is used in this data sheet.
c. Guaranteed by design, not subject to production test.
d. Typical values are for DESIGN AID ONLY, not guaranteed nor subject to production testing.
e. V_{IN} = Input voltage to perform proper function.
f. Room = 25°C, Hot and Full = as determined by the operating temperature suffix.